



**UCGE Reports  
Number 20288**

Department of Geomatics Engineering

**Design and Implementation Issues of a Portable  
Navigation System**

(URL: <http://www.geomatics.ucalgary.ca/research/publications>)

**by**

**Zainab Fatima Syed**

**FEBRAURY, 2009**



THE UNIVERSITY OF CALGARY

Design and Implementation Issues of a Portable Navigation System

by

Zainab Fatima Syed

A DISSERTATION

SUBMITTED TO THE FACULTY OF GRADUATE STUDIES

IN PARTIAL FULFILLMENT OF THE REQUIREMENTS FOR THE

DEGREE OF DOCTOR OF PHILOSOPHY

DEPARTMENT OF GEOMATICS ENGINEERING

CALGARY, ALBERTA, CANADA

FEBRAURY , 2009

© Zainab Syed 2009

## **Abstract**

Personal navigation is one of the fastest developing fields due to ever changing needs of consumers. Most recently, GPS-based systems have gained popularity in commercial navigation systems. However, a problem arises when the GPS is unable to provide positions due to interruptions in the signals. One way to solve this problem is by using inertial sensors that do not require any outside signals.

The thesis deals with the issues related to the design specifications for a completely portable navigation system (PNS). A PNS is defined as a navigation module that is completely transferable from vehicle to vehicle and from one mode of transit to the other and should be able to provide navigation information even for short GPS signal outages.

The PNS requires calibration and alignment before navigation can be started. These two topics require different implementation methods to accommodate for the special needs associated with portability. A new method was proposed that can perform calibration of the sensors without any requirement on the PNS shape. Alignment is not required if six sensors are part of the system, however, partial sensor system will require some alignment criteria.

For low-cost commercial system, signal sampling requirement is also important as the choice of micro processor, memory card and DAQ card are all cost defining factors. A frequency of 50Hz and timing errors of up to 1 ms did not degrade the navigation results, however, 10 bits resolution produced significant degradation. It was also determined that a heading gyro and a dual axis accelerometer in the horizontal plane with velocity aiding

produced comparable results to six sensors unit without any aiding, and hence can be used for low-cost navigation.

As a PNS can be used either by a person on-foot or in-vehicle, one of the important issues is to identify the correct mode of transit to apply the most appropriate navigation equations. Consequently, an algorithm was developed and tested to detect mode of transit when the system was attached on the belt of the user. A levelled ground walking scenario produced the best results and the average accuracies of other cases stayed over 90%.

## **Acknowledgements**

Today, as I am concluding this work, I will try to acknowledge all the people that have helped me during my studies. First I would like to thank Dr. Naser El-Sheimy for giving me this chance. He provided me with the guidance and opportunities that has changed me from an ordinary student to a strong research engineer. In addition to his usual supervisory role, he was also my true friend whom I could depend on without hesitation. I would also like to acknowledge the unconditional support from Dr. A. Noureldin during my thesis work. Dr. Noureldin was always there for a good technical discussion whenever I had a question or problem. I would also like to thank Dr. ME Cannon for all her input in improving this thesis.

Another big supporter when I started my PhD was Dr. X. Niu. He was always a source of knowledge and encouragement for me. I deeply thank him for his unlimited support and his technical expertise that turned me into an expert in the field of inertial navigation.

I would also like to thank Dr. D. Gu, Dr. Y. Yang, Ms. P. Aggarwal, Dr. C. Goodall, Dr. S. Nassar, Mr. X. Zhao, Mr. T. Hassan, Mr. Haiying Hou, Dr. Kaiwei Chiang, Dr. Walid Abd El-Hamid, Dr. El-Habiby and Dr. M. Youssef for their help in data collection and technical discussions. Also, my sincere thanks go to Mr. B. Wright for all his efforts in developing the hardware and teaching me the art of developing parsers for the newly developed hardware systems. Dr. E-H. Shin is also acknowledged in the partial development of the AINS EKF toolbox that was used for loosely coupled implementation.

This section will be incomplete if I do not mention Mr. H. Martell. He was my supervisor at NovAtel Inc. and the time that I have spent under his supervision was nothing short of best. I worked on different projects in the field of inertial navigation that I would have never explored on my own. The confidence that I have today in this field is partly related to Mr. Martell's, Dr. Cosandier's and Ms. S. Kennedy's projects.

Last but not least, I am indebted to my loving husband, Ahmad Najmy Ahmad, for his support, help and confidence in me. He made sure that he was there for me whether I needed his moral or technical support. There were times that I was stuck badly and his out-of-the-box thoughts gotten me out of my problem. To conclude, I would like to acknowledge the sacrifices and unconditional love of my parents.

This study was supported in part by research fund from the Natural Science and Engineering Research Council of Canada (NSERC) and Geomatics for Informed Decisions (GEOIDE), Network Centers of Excellence (NCE) to Dr. Naser El-Sheimy.

## Dedication

*To my best friend and mentor,*

*and to the most qualified engineer that I have known;*

*my father, Muhammad Ali Syed.*

# Table of Contents

<b>ABSTRACT .....</b>	<b>II</b>
<b>ACKNOWLEDGEMENTS.....</b>	<b>IV</b>
<b>DEDICATION.....</b>	<b>VI</b>
<b>LIST OF FIGURES .....</b>	<b>XII</b>
<b>LIST OF TABLES .....</b>	<b>XVIII</b>
<b>ACRONYMS .....</b>	<b>XIX</b>
<b>1. REFERENCE FRAMES .....</b>	<b>XXI</b>
1.1 INERTIAL FRAME .....	XXI
1.2 EARTH FIXED FRAME .....	XXI
1.3 GEODETIC REFERENCE FRAME .....	XXII
1.4 LOCAL LEVEL FRAME.....	XXIII
1.5 BODY FRAME .....	XXIV
<b>CHAPTER ONE: INTRODUCTION.....</b>	<b>1</b>
1.1 BACKGROUND .....	1
<i>1.1.1 In-Vehicle Navigation Systems.....</i>	<i>2</i>
<i>1.1.2 On-foot Navigation Systems.....</i>	<i>4</i>
1.2 THESIS OBJECTIVE.....	7
1.3 THESIS OUTLINE.....	9
<b>CHAPTER TWO: BACKGROUND .....</b>	<b>12</b>



2.1 SENSOR CALIBRATION AND ERROR MODELLING.....	15
2.2 ALIGNMENT.....	16
2.3 NAVIGATION EQUATIONS .....	19
2.4 GPS/INS INTEGRATION TECHNIQUES.....	24
2.4.1 Loosely Coupled Integration.....	25
2.4.2 Tightly Coupled Integration.....	26
2.5 EXTENDED KALMAN FILTER .....	28
2.5.1 Linearization.....	29
2.5.2 Prediction .....	33
2.5.3 Update Equations .....	35
2.5.4 A Note on Loosely and Tightly Coupled Simulations.....	39
2.6 VELOCITY CONSTRAINTS.....	42
2.6.1 Vehicle Body Frame.....	43
2.6.2 Velocity computation in the v-frame .....	44
<b>CHAPTER THREE: CALIBRATION.....</b>	<b>48</b>
3.1 INERTIAL MEASUREMENT UNIT SIGNAL.....	48
3.2 INS ERRORS .....	53
3.3 SIMPLE CALIBRATION SCHEME .....	55
3.4 CURRENT INS CALIBRATION METHODS .....	56
3.5 MULTI-POSITION CALIBRATION METHOD.....	60
3.5.1 General model.....	60
3.5.2 Inclusion of non-orthogonality .....	61
3.5.3 Inclusion of biases and scale factors .....	63
3.5.4 Least squares adjustment.....	64
3.5.5 Multi-position schemes .....	65
3.6 MODIFIED MULTI-POSITION CALIBRATION .....	66
3.7 RESULTS.....	69

3.7.1 Test Description.....	69
3.7.2 Effect of full gyro calibration using a turntable.....	73
3.7.3 Calibration Results Comparison.....	75
3.7.4 Navigation accuracy comparison .....	77
3.7.5 Calibration of an arbitrary shaped MEMS unit.....	81
3.8 SUMMARY .....	83
<b>CHAPTER FOUR: SIGNAL SAMPLING REQUIREMENTS FOR PORTABLE NAVIGATION ..</b>	<b>87</b>
4.1 METHODOLOGY .....	88
4.1.1 Description of Test data.....	88
4.1.2 Analysis Method.....	91
4.1.3 Determination of Minimum Sampling Frequency.....	92
4.1.4 Determination of Minimum Number of Bits.....	92
4.1.5 Determination of Time Synchronization Error Budget.....	93
4.1.6 DAQ Specifications.....	96
4.2 RESULTS.....	96
4.2.1 Low Sampling Frequencies Simulations .....	96
4.2.2 Number of Bits Reduction .....	98
4.2.3 Time Synchronization Effects on Drifts Errors.....	101
4.2.4 Results for Economical DAQ Cards .....	103
4.3 SUMMARY .....	105
<b>CHAPTER FIVE: ECONOMICAL INERTIAL SENSOR CONFIGURATION FOR PORTABLE</b>	
<b>NAVIGATION SYSTEM .....</b>	<b>107</b>
5.1 METHODOLOGY .....	111
5.1.1 Data Collection.....	111
5.1.2 Modification to AINST <sup>TM</sup> .....	112
5.2 RESULTS.....	116

5.2.1	<i>Drift Errors without NHC</i> .....	116
5.2.2	<i>Drift Errors with NHC</i> .....	118
5.3	SUMMARY .....	120
<b>CHAPTER SIX: REQUIRED ALIGNMENT OF A PORTABLE NAVIGATION SYSTEM .....</b>		<b>122</b>
6.1	CONSIDERATIONS FOR MEMS SENSORS NAVIGATION .....	122
6.1.1	<i>Portable Navigation System</i> .....	123
6.1.2	<i>Commercial Perspectives</i> .....	124
6.2	METHODOLOGY .....	125
6.2.1	<i>Simulation of Misalignment</i> .....	126
6.2.2	<i>Test Trajectories and Simulated GPS Outages</i> .....	127
6.2.3	<i>Analysis Strategy</i> .....	128
6.2.4	<i>Misalignment Estimation</i> .....	129
6.3	RESULTS .....	131
6.3.1	<i>Full IMU without NHC</i> .....	132
6.3.2	<i>Full IMU with NHC</i> .....	136
6.3.3	<i>1G2A without NHC</i> .....	138
6.3.4	<i>1G2A with NHC</i> .....	142
6.3.5	<i>Misalignment Estimation Algorithm</i> .....	145
6.4	SUMMARY .....	147
6.4.1	<i>Errors Due to Misalignments</i> .....	148
6.4.2	<i>Full IMU without NHC</i> .....	148
6.4.3	<i>Full IMU with NHC</i> .....	150
6.4.4	<i>Partial IMU without NHC</i> .....	150
6.4.5	<i>Partial IMU without NHC</i> .....	151
<b>CHAPTER SEVEN: DETECTION OF MODE OF TRANSIT .....</b>		<b>153</b>
7.1	METHODOLOGY .....	154

7.1.1	<i>Detection Algorithm for full Sensors (Six Sensors Module)</i> .....	156
7.1.2	<i>Detection Algorithm for Partial Sensors</i> .....	159
7.1.3	<i>Test Scenarios</i> .....	159
7.1.4	<i>Accuracy Analysis</i> .....	163
7.2	RESULTS .....	164
7.2.1	<i>On-foot Mode Detection</i> .....	164
7.2.2	<i>In-Vehicle Mode Detection</i> .....	168
7.2.3	<i>Combination Mode Detection</i> .....	173
7.2.4	<i>Mode Detection for LRT</i> .....	174
7.2.5	<i>Bike Mode Detection</i> .....	179
7.2.6	<i>Accuracy Results</i> .....	180
7.3	SUMMARY .....	182
<b>CHAPTER EIGHT: CONCLUSIONS AND RECOMMENDATIONS.....</b>		<b>183</b>
8.1	CONCLUSIONS .....	183
8.2	DEVELOPED METHODS AND PROGRAMS.....	187
8.3	RECOMMENDATIONS AND FUTURE WORK.....	188
	REFERENCES .....	190
<b>APPENDIX A .....</b>		<b>199</b>
<b>APPENDIX B.....</b>		<b>201</b>
	DENOISING OF THE DATA .....	201
	STEP DETECTION .....	203
	<i>Peak Identification via Differencing and Thresholds</i> .....	203
	<i>Absolute Value, Peak to Peak Time and Correlation</i> .....	203
	COMPARISON OF DR RESULTS WITH GPS POSITIONS.....	204

## List of Figures

Figure 0-1. The inertial frame .....	xxi
Figure 0-2. The Earth fixed reference frame and Geodetic reference frame .....	xxii
Figure 0-3. NED frame definition.....	xxiii
Figure 0-4. The <i>b</i> -frame related to NED frame .....	xxiv
Figure 1-1. Different categories of digital navigation systems.....	1
Figure 1-2. Thesis outline .....	11
Figure 2-2. Land vehicle dynamics using gyro signal .....	13
Figure 2-3. Walking dynamics using gyro signal .....	14
Figure 2-5. Mechanization Algorithm for in-vehicle navigation mode.....	22
Figure 2-6: Flow chart of on-foot dead reckoning.....	23
Figure 2-7. Loosely coupled integration. (PV refers to position and velocity, respectively) .....	25
Figure 2-8. Tightly coupled integration scheme. ....	26
Figure 2-9. Graphical user interface for the tightly coupled integration scheme .....	27
Figure 2-10. Linearization process for EKF .....	33
Figure 2-11. Extended Kalman Filter .....	38
Figure 2-12. Comparison between loosely and tightly coupled integration .....	40
Figure 2-13. Example of a dataset with simulated GPS signal degradation periods for two integration schemes.....	41
Figure 2-14. Definition of NHC.....	42
Figure 2-15. Schematics of the misalignment of the IMU with respect to the vehicle body frame (Images for the top most panels are taken from Google Images).....	44
Figure 2-16. Schematics of the lever arm involved for NHC .....	45
Figure 3-1. Flowchart for inertial sensor error compensation. (Picture of GPS satellite is taken from Google Images).....	50

Figure 3-2. Position errors due to residual errors in biases and horizontal misalignment.....	53
Figure 3-3. Comparison of Different Calibration Methods for a Typical Dataset.....	54
Figure 3-4. Misaligned orthogonal sensor triad with respect to the <i>l</i> -frame (After: Shin and El-Sheimy, 2002) .....	61
Figure 3-5. An example of IMU rotation scheme.....	66
Figure 3-6. Test vehicle setup.....	70
Figure 3-7. Trajectory for run 3 along with simulated GPS outages.....	71
Figure 3-8. Trajectory for PNS unit. The inertial trajectory shown is for MMPM. ....	72
Figure 3-9. Comparison of CIU sensor position drifts using multi-position (MPM) and Modified Multi-Position (MMPM) calibration methods for run 1 for 60s GPS outages .....	74
Figure 3-10. Velocity profile for the outages.....	75
Figure 3-11. Comparison of MMPM and SPM for three different runs using two different inertial systems.....	79
Figure 3-12. Position errors in GPS outages obtained by applying MMPM for CIU in Run 3.....	80
Figure 3-13. Position errors in GPS outages obtained by applying SPM for CIU. ....	80
Figure 3-14. The Portable Navigation System.....	81
Figure 3-15. Maximum position drifts for PNS unit.....	83
Figure 4-1. Trajectory for dataset 1 with simulated signal degradation periods .....	89
Figure 4-2. GPS signal degradation locations with respect to the signal availability and vehicle dynamics .....	90
Figure 4-3. Trajectory for dataset 2 with simulated signal degradation periods (some outages are overlapped) .....	90
Figure 4-4. GPS signal degradation locations for dataset 2 with respect to the signal availability and vehicle dynamics.....	91
Figure 4-5. Flowchart for Down-sampling Algorithm .....	92

Figure 4-6. Graphical user interface for the sampling requirement program developed for the thesis .....	95
Figure 4-7. Downsampling results .....	97
Figure 4-8. CPU times for various frequencies .....	98
Figure 4-9. Drift errors for 14 bits resolution .....	99
Figure 4-10. Drift errors for 12 bits resolution .....	100
Figure 4-11. Example of Bit degradation. A 16 bits resolution was degraded to 12 bits in this example. ....	101
Figure 4-12. A typical of example of time synchronization error of 1ms .....	103
Figure 4-13. Results for Economical DAQ Cards for Dataset1.....	104
Figure 5-1: Sensors with their respective measurements.....	108
Figure 5-2: The Five Sensor Configurations Studied (Red bars represent gyros while green bars represent accelerometers. The x-axis corresponds to the forward/backward direction of the moving vehicle).....	109
Figure 5-3: Inertial Sensor signals for a typical land vehicle trajectory .....	110
Figure 5-4: Trajectory for the dataset 1 .....	112
Figure 5-5: The Modified AINS™ User Interface showing the Dropdown Menu Options for the different IMU Configurations.....	113
Figure 5-6: Average drift errors for the different sensor configurations for dataset 1 and dataset 2.....	117
Figure 5-7: Estimated roll and pitch errors for full (top panel) and 1G2A (bottom panel).....	118
Figure 5-8: Roll and pitch misalignments for dataset 1 (top panel) and dataset 2 (bottom panel).....	119
Figure 5-9: Average drift errors for the different sensor configurations for dataset 1 and dataset 2 using NHC.....	120
Figure 6-1. Summary of Navigation process .....	123
Figure 6-2. Trajectory for dataset 1 with eight simulated GPS outages (some outages are overlapped).....	128

Figure 6-3. Drift errors for full IMU during GPS outages without NHC .....	132
Figure 6-4. Induced attitude errors due to roll misalignment (Solid lines for dataset 1 and dashed lines for dataset 2) .....	133
Figure 6-5. Induced attitude errors due to Pitch misalignment (Solid lines for dataset 1 and dashed lines for dataset 2.) .....	134
Figure 6-6. Induced attitude errors due to Azimuth misalignment (Solid lines for dataset 1 and dashed lines for dataset 2.) .....	135
Figure 6-7. Typical Position Drift errors for full IMU during GPS outages, with non-holonomic constraint.....	137
Figure 6-8. Typical induced attitude errors due to misalignment in azimuth.....	138
Figure 6-9. Position drifts for dataset 1 without NHC under different misalignments ..	139
Figure 6-10. Position drifts for dataset 2 without NHC under different misalignments	139
Figure 6-11. Typical roll misalignment results.....	141
Figure 6-12. Typical azimuth misalignment results .....	141
Figure 6-13: Position drift errors for partial IMU (with NHC) under different misalignments. ....	142
Figure 6-14. Typical attitude errors due to roll misalignment .....	143
Figure 6-15. Typical attitude errors due to pitch .....	144
Figure 6-16. Typical attitude errors due to azimuth .....	144
Figure 6-17. Misalignment estimation results for $v^l \geq 1\text{m/s}$ for full sensors .....	146
Figure 6-18. Misalignment estimation results for $v^l \geq 3\text{m/s}$ for 1G2A .....	147
Figure 7-1. Components of the navigation module .....	155
Figure 7-2. Mode detection algorithm .....	158
Figure 7-3. Possible user positions in an LRT. The direction of travel is into the page. Position 1 is when the user is facing the direction of travel; position 2 is the direction away from the travel direction. Positions 3 and 4 represent the positions when one of the user shoulders is facing the travel direction (Google Image).....	161
Figure 7-4. Example of a hardware switch with accuracy computation for full sensor .	163



Figure 7-5. User1 walk only data classification for full IMU.....	165
Figure 7-6. User1 walk only data classification with one vertical gyro and a tri-axial accelerometer .....	165
Figure7-7. User2 walk only data classification.....	166
Figure 7-8. User3 mixed walk dataset. The algorithm detected the walking motion for three different scenarios.....	167
Figure 7-9. User3 mixed walk dataset. The algorithm detected the walking motion for two different scenarios.....	168
Figure 7-10. User4 vehicle only datasets with mixed trajectory consisting of levelled road and inclined road.....	170
Figure 7-11. User4 dataset when partial sensors were used .....	170
Figure 7-12. User4 vehicle only dataset using equal weighting scheme for ZUPT detection .....	171
Figure 7-13. User5 vehicle only dataset with six sensors .....	172
Figure 7-14. User5 vehicle only dataset with one vertical gyro and tri-axial accelerometer .....	173
Figure 7-15. Dataset with vehicle and on-foot mode of navigation using six sensors algorithm .....	174
Figure 7-16. User6 mode of transit detection in position 1 using six sensors .....	175
Figure 7-17. User7 mode of transit detection for position 2 using partial sensors when the user stands by holding the handle .....	176
Figure 7-18. User7 mode of transit detection for LRT data in position 2 with support using 6 inertial sensors.....	177
Figure 7-19. User8 mode of transit detection for LRT data in position 3 using six inertial sensors .....	178
Figure 7-20. User9 mode of transit detection for LRT data in position 4 using one heading gyro and a tri-axial accelerometer .....	179
Figure 7-21. Bike dataset classified by six sensors algorithm .....	180
Figure 7-22. Absolute and relative accuracies .....	181

Figure 0-1: Denoising results.....	202
Figure 0-2: Step Detection Results .....	204
Figure 0-3: Initial Dead Reckoning Results.....	205

## List of Tables

Table 1-1: Example of available navigation systems (G: Gyros, A: Accelerometers, M: Magnetometers, and B: Barometer) .....	5
Table 3-1. Description of approximate position error terms.....	52
Table 3-2. Summary of available calibration methods. H = High grade system, L= Low grade system and R = Required .....	67
Table 3-3. Biases and scale factors computed by the MMPM and SPM for MotionPak II.....	76
Table 3-4. Biases and scale factors calculated by the MMPM and SPM for CIU.....	76
Table 3-5. Maximum position drift in simulated GPS outages in run 1.....	77
Table 3-6. Maximum position drifts in simulated GPS outages in run 2. ....	78
Table 3-7. Maximum position drifts in simulated GPS outages in run 3. ....	78
Table 3-8. Biases and scale factors calculated by the MMPM and SPM for PNS. ....	82
Table 5-1: Omitted sensor values for AINS™ for partial sensors configuration .....	116
Table 6-1. Degradations of full IMU(without NHC) under different misalignments.....	136
Table 6-2. Degradations of partial IMU (without NHC) under different misalignments. ....	140
Table 6-3: Actual and Converged Misalignment values.....	145
Table 6-4. Allowable misalignments with degradation less than 20% (as compared to a well aligned system).....	151
Table 0-1: Example of available in-vehicle navigation systems .....	199

## Acronyms

3D	Three dimensional
ADC	Analog to digital converter
AINS	Aided inertial navigation system
ARW	Angle random walk
<i>b</i> -frame	Body frame
BW	Bandwidth
CIU	Custom inertial unit
CPU	Central processing unit
DAQ card	Data Acquisition Card
DCM	Direction cosines matrix
DGPS	Differential Global Positioning System
DR	Dead Reckoning
EKF	Extended Kalman Filter
<i>i</i> -frame	Inertial frame
IMU	Inertial measurement unit
INS	Inertial navigation system
KF	Kalman Filter
Litton 200	LN200
LRT	Light Rail Transit
LSB	Least significant bit
MEMS	Micro Electro Mechanical Sensors

MMPM	Modified multi-position method
MMSE	Minimum mean-squared error
MPM	Multi-position method
NED	North, East and Down
<i>n</i> -frame	Navigation frame
NHC	Non-holonomic constraints
PDA	Personal digital assistant
PND	Portable Navigation Devices
PNS	Portable Navigation System
PPS	Pulse per second
PVA	Position, velocity and attitude
RW	Random walk
SPM	Six position static and rate method or test
SSE	Sum of squared errors
STD	Standard deviation
<i>v</i> -frame	Vehicle frame
VRW	Velocity random walk
ZUPT	Zero velocity update

# 1. Reference Frames

Five different frames are defined that are equally important to explain the navigation parameters of a land vehicle ([Titterton and Weston, 2007](#)).

## 1.1 Inertial Frame

The inertial (*i*) frame is a stationary reference frame (Figure 0-1) with the origin at the centre of the Earth. The *z*-axis is parallel to the Earth's polar axis or the axis of rotation of the reference ellipsoid. The *x*-axis pointing towards the mean vernal equinox and the *y*-axis completes the right-handed orthogonal coordinate system. The vernal equinox is the ascending node between the celestial equator and the ecliptic.

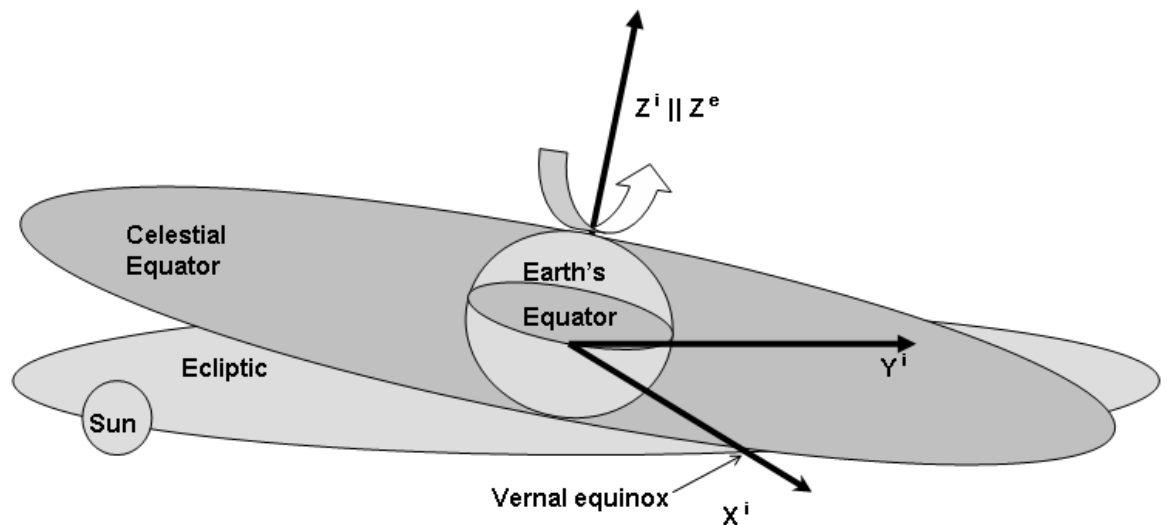


Figure 0-1. The inertial frame

## 1.2 Earth Fixed Frame

The Earth (*e*) fixed frame is a non-stationary frame which rotates with respect to the *i* frame at an angular rate ( $\omega^e$ ) of approximately  $15^\circ/\text{h}$  about the polar axis. The *x*-axis of

the  $e$ -frame ( $X^e$ ) points toward the Greenwich meridian in the equatorial plane; the  $y$ -axis ( $Y^e$ ) is  $90^\circ$  East of Greenwich meridian in the equatorial plane and the  $z$ -axis ( $Z^e$ ) is along the Earth's polar axis.

### 1.3 Geodetic Reference Frame

A geodetic reference frame (Figure 0-2) uses an ellipsoidal approximate for the shape of the Earth. A point on the surface of the Earth given in geodetic reference frame will consist of two angles, latitude ( $\phi$  or  $\varphi$ ) and longitude ( $\lambda$ ), and a Cartesian component, height ( $h$ ). The height is along the direction of the normal to the ellipsoid. The longitude is measured from the Greenwich meridian to the meridian that contains the pierce point of the user location,  $P$ . Latitude is measured from the equator to the normal to the ellipsoid. The positions on the Earth's surface are usually given in terms of the latitude, longitude and height of the user.

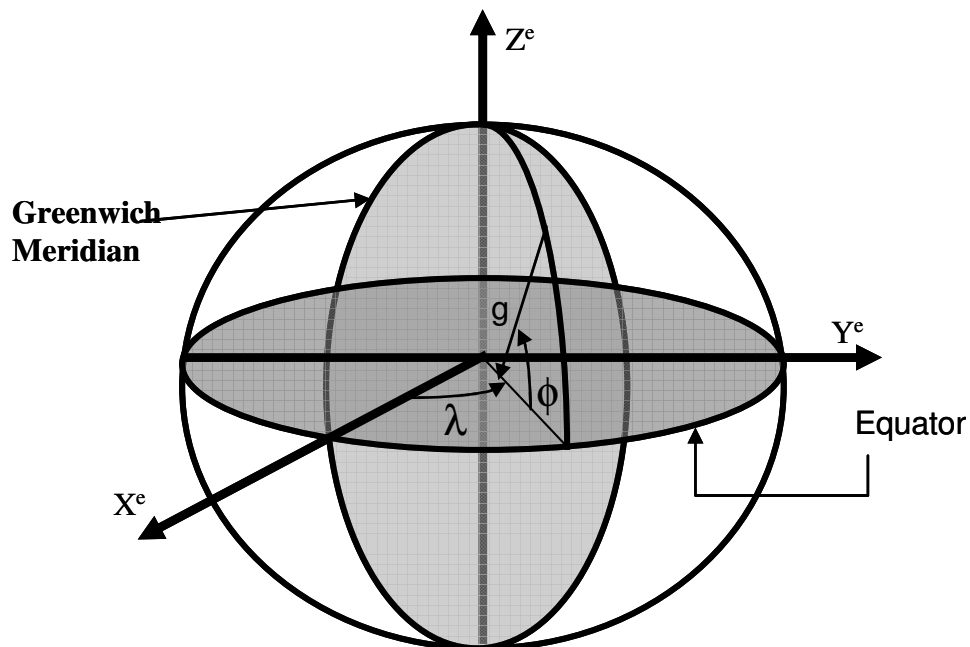
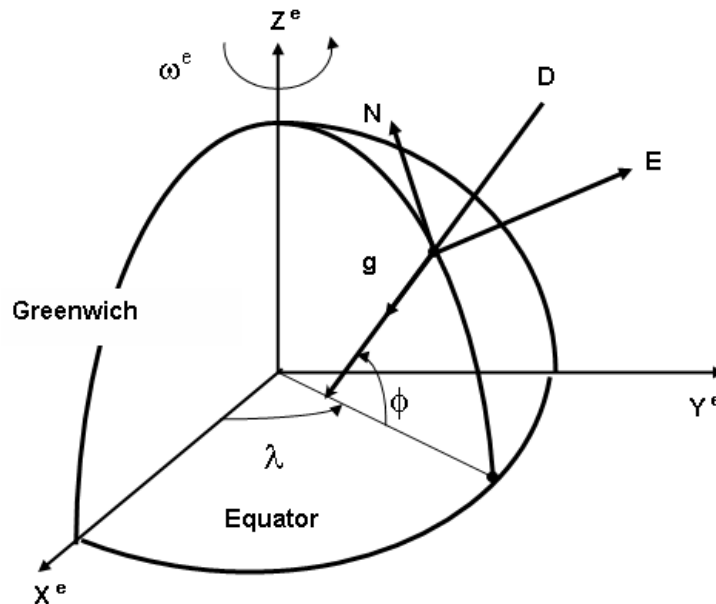


Figure 0-2. The Earth fixed reference frame and Geodetic reference frame

## 1.4 Local Level Frame

The local level frame (*l*-frame) is also known as the navigation frame (*n*-frame). The x-axis (N) points towards the ellipsoidal North (Figure 0-3), the z-axis is orthogonal to the reference ellipsoid and points downwards (D). The y-axis completes the right-handed orthogonal frame, thus pointing towards East (E). The *l*-frame can also refer to as NED. The major advantages of using this frame is that the axes coincide with moving body roll (*r*), pitch (*p*) and heading (*A*) when the body is heading North on a levelled road. The centre of NED is the origin of the navigation system.



**Figure 0-3. NED frame definition**

The roll angle takes positive values if the moving body is rolling towards right. The pitch angle is positive for uphill or nose up direction. Finally the azimuth is considered positive if calculated clockwise from the North direction.



### 1.5 Body Frame

The body frame (*b*-frame) is an orthogonal frame which is aligned with the roll, pitch and heading axes of the vehicle in some special way (Figure 0-4). For NED *l*-frame implementation, the *x*, *y* and *z* axes of the *b*-frame should be respectively along the forward, the transversal and the downward directions of the moving platform.

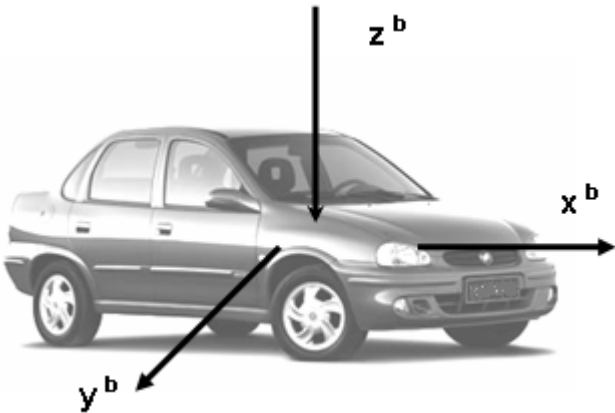
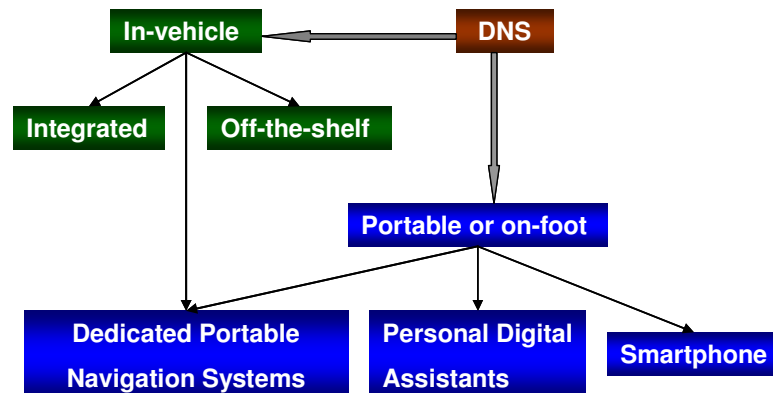


Figure 0-4. The *b*-frame related to NED frame

## Chapter One: Introduction

### 1.1 Background

The concept of navigation has evolved from paper maps to user friendly Global Positioning System (GPS) based digital navigation systems. With advancements in chip design, microprocessor speed and navigation algorithms, these systems are becoming more compact, inexpensive and robust. Consequently, the digital navigation market has seen an enormous growth in the last year which went up to 30.7million from 13.3 million units sold in 2006 ([Business Network, 2008](#)). Digital navigation systems (DNS) can be categorized as shown in the Figure 1-1.



**Figure 1-1. Different categories of digital navigation systems**

The GPS based navigation is quick, drift free and readily available most of the time. However, as GPS requires direct line of sight signals from at least four GPS satellites, navigation can be frequently interrupted in land based applications. For such situations when the GPS signals are not available, relative navigation can be performed using autonomous sensors. For example, the focus of the research for rescue personnel, such as fire fighters, is on developing inertial sensors embedded shoes and garments for their uninterrupted location information to the base station ([Foxlin, 2005](#)). The reason is

simply the unavailability of the GPS signals indoors. Use of an odometer ([GlobalWave, 2008](#)) along with GPS is also common for tracking of vehicles where seamless positioning information is compulsory. Seamless positioning is also significant for the general public as well. However, it is not convenient for the public to purchase specialized shoes/dresses or access their vehicles' odometers.

With the advancement in low cost inertial Micro Electro Mechanical Sensors (MEMS) design, it is now possible to integrate some of these sensors with GPS receivers. The concept is simple but the development of such a complete system requires well researched design specifications. Moreover, for a product to succeed, the end-user cost should be minimal without any compromise on the accuracy or robustness of the system. The next section will discuss the different types of digital navigation systems in detail.

### ***1.1.1 In-Vehicle Navigation Systems***

As shown in Figure 1-1, in-vehicle navigation systems can be divided into three basic categories. The first category consists of systems that are pre-installed by a manufacturer in a vehicle. The extents of the integration of these systems vary among vehicle manufacturers. Some integrated systems will only provide essential navigation information while others will integrate various systems with the navigation system, such as entertainment devices. It is also possible for the vehicle manufacturer to integrate the input from the vehicle's odometer for more robust positioning.

A variety of other systems can be installed in the vehicle's audio system compartment. The owner of the vehicle can choose the manufacturer from a wide variety of system

providers such as Alpine ([Alpine, 2008](#)), Clarion ([Clarion, 2008](#)) and Panasonic ([Engadget, 2008](#)) depending on the budget and needs of the user.

The third classification is the dedicated portable navigation devices (PNDs) ([TomTom, 2007](#); [Sony, 2007](#); [Garmin, 2007](#); [Navman, 2007](#)), which usually consist of a GPS chipset with the assumption that the GPS receiver will have four or more satellites available for navigation for most of the time. However, this assumption is unrealistic if the user's commute is concentrated in urban centres. The core of these systems, i.e. GPS positioning, fails to provide useful information due to many obstacles in the satellite's direct line of sight signals to the receiver. Similar problem exists, if the user decides to carry the system to navigate in an urban environment. A more detailed list of PND manufacturers is provided in Appendix A. It is also clear from Appendix A that most of these systems are basically similar in terms of functionality and the sensors used.

To get the competitive advantage, some of the manufacturers are integrating other useful features such as MP3 players, widescreen, traffic alerts, FM transmitters, hands free feature and integration of some inertial sensors for the seamless positioning. TomTom Go 940 ([TomTom Go 940, 2008](#)), for example, integrates a SiRFStar III GPS chipset, a gyro and a dual axis accelerometer to provide positioning information when the GPS signals are not available.

A similar product is developed by SiRF and known as SiRFDiRect (has not been released to date for commercial applications ([Niu and Han, 2008](#))). It is a chipset that can provide seamless positions by integrating different inertial and dead reckoning (DR) sensors for

in-vehicle mode. The module consists of SiRFStar III GPS chipset, one heading gyro and a tri axial accelerometer. In addition, the module is also capable of receiving input from the vehicle's odometer. In 2007, SiRF announced that this chipset will be incorporated into the Mio PDA cell phone A702 ([GPS Business News, 2008](#)), however, the official site of the Mio ([MiTAC Intl](#)) shows that only SiRFStar III GPS chipset was incorporated as a navigator.

### ***1.1.2 On-foot Navigation Systems***

The second category of personal navigation systems can be regarded as on-foot navigation devices. Some of the GPS-based portable devices can also be taken with the user, as the digital navigation system, for most outdoor activities. Probably, Honeywell's DRM 4000 module ([Honeywell, 2008](#)) is the only commercially available pedestrian navigation unit which is capable of GPS integration along with inertial sensor based positioning. Another sensor based navigation system is the NavShoe ([Foxlin, 2002](#); [Foxlin, 2005](#)). The NavShoe is designed to be placed on the shoes of the user to provide accurate DR but it is not available commercially. A complete list of pedestrian navigation systems currently available in the market is provided in Table 1-1.

**Table 1-1: Example of available navigation systems (G: Gyros, A: Accelerometers, M: Magnetometers, and B: Barometer)**

Manufacturer	Product	Sensors					Picture
		GPS/Map	G	A	M	B	
InterSense	Nav Shoe	X	x	x	x		
Honeywell	DRM® 4000	Can use GPS if available / yes	x	x	x	x	
Garmin	Garmin Mobile™	x/ yes					
Garmin	GPS-MAP® 76CSx	HSGPS/ optional			x	x	
Garmin	Rino 530HCx	x/ optional			x	x	
Garmin	Fore-runner® 405	x					
Garmin	GPS-MAP® 496	x/ yes					
TOMTOM	Naviga-tor 6	x / yes					

The pedestrian DR is a growing area of research covering all aspects including human body kinematics study to methods of estimating different DR parameters for improved navigation accuracies ([Bouten et al., 1997](#), [Lee and Mase, 2001](#); [Wagenaar and Beek, 1992](#), [Shin and Hong, 2005](#); [Jirawimut et al., 2001](#); [Levi and Judd, 1996](#), [Kwakkel, et al., 2008](#)). Most of this research implements systems on different body parts, especially feet, for a robust solution ([Grejner-Brzezinska, et al., 2007](#), [Kasameyer, et al., 2006](#), [Ojeda and Borenstein, 2007](#), [Bancroft, et al., 2008](#)). There is also research on systems that do not require a specific location on the body. One of such research project was presented in ([Kappi et al., 2001](#)).

Personal digital assistants (PDAs) and smart phones are also coming equipped with navigation capabilities where a GPS chip is integrated in to the system. These are quite popular as GPS is a free of charge service and most of the general public owns a PDA or mobile phone or both. The positions are shown on digital maps which are the same as other digital navigation system and most of these devices also provide search and route calculation capabilities as well.

All of the PNDs are designed in a way that they can only provide accurate navigation for a particular mode of transit, either in-vehicle or on-foot. None of these systems are capable of seamless positioning from one mode of transit to the next. The thesis investigates the issues related to a completely portable system that can be used from one mode of transit to the next.

## 1.2 Thesis Objective

The main objective of this thesis is to investigate the issues related to the development of an integrated GPS and inertial navigation system (INS) that will be completely transferable from on-foot mode to in-vehicle navigation mode and vice-versa. GPS and inertial navigation are well established fields but the concept of a PND capable of navigating in two different modes of transit has never been implemented before. It is important to note that different algorithms are required for the different transit modes, i.e., in-vehicle and on-foot, if GPS/INS integrated navigation is used. As this is a new idea ([El-Sheimy et al., 2007](#)) there are many issues and challenges in the designing of such a system. Such a system will consist of a real-time PND that can be used in any locomotion mode; however, to achieve this objective several important implementation, cost and operational issues need to be addressed.

- 1) Sensor calibration issues: A portable system will use off-the-shelf low cost inertial sensors. These sensors usually come with manufacturer provided calibration values. The use of manufacturer specifications is quite beneficial as they can save time and cost of sensor calibration. Therefore, the first issue is to investigate if the manufacturer-provided information about the calibration is consistent and sufficient for land navigation. If the manufacturer specifications are not sufficient, then what are the methods to calibrate a PNS? Also, the issue of which calibration method will be best suited for a commercial system will be addressed.



- 2) **Cost and Implementation Issue:** Data acquisition from low cost sensors will require a low cost data acquisition card (DAQ) to reduce the overall system cost. In addition, the processing speed needs to be improved for seamless computations of the navigation parameters regardless of the low cost of the system. These two topics raise certain issues such as what are the minimum signal sampling requirements for a PNS? What is the minimum sensor output frequency for land based applications? What kind of resolution and time synchronization is sufficient for such a system? What kinds of cost savings are viable in data acquisition?
- 3) **Cost Issue:** At least six inertial sensors are required to model the 3D motion of land navigation applications. However, each sensor will increase the cost of the system. This raises the issues of what is the minimum number of sensors required for an economical PNS and how the accuracy can be improved with the minimum number of sensors?
- 4) **Operational Issue:** Inertial sensors measure forces and angular rates of the moving body with respect to an i-frame of reference. Consequently, when inertial sensors are introduced in a navigation system, alignment of the system with respect to a reference frame becomes an important design aspect. In this regard, the following issue needs to be resolved: What is the alignment error budget to produce reasonable navigation results for a PNS?
- 5) **Implementation Issue:** A PNS should be completely transferable between the two modes of transit, i.e., on-foot and in-vehicle. For robust navigation, the two modes of transit will have different navigation algorithms. How different modes of

transit can be detected to switch between different navigation algorithms is another important issue that will be resolved here.

Complete answers to these questions and issues will be provided in this thesis as it is the first step towards the development of a PNS that can work on different modes. All the analysis is done using real field datasets to provide conclusions for realistic situations.

### **1.3 Thesis Outline**

This thesis covers the design and implementation issues of a PNS. Chapter 2 covers the necessary background information. Chapter 3 deals with the calibration issues and also introduces a new calibration method that is suitable for an arbitrary shaped integrated sensor module as the well developed calibration methods are only useful if the sensor system is a perfect cube. For a commercial system, it is likely that the corners and sides may be rounded for user comfort and overall ergonomics of the system.

After calibration, the navigation system should be aligned with a reference frame to start navigation. However, there is another issue that requires attention for a real-time integrated system before the alignment. Inertial sensors provide high data rates (up to 400Hz) and as a common practice, inertial based navigation is implemented at such high rates as well. However, such high data rates may not be necessary for civilian navigation. The frequencies of interest for land vehicle and on-foot navigation are low and therefore, the system design can benefit from a lower data rate. A low data rate will increase the online computation speed capabilities and decrease the data storage requirement at the system development stage. Similarly, data resolution and time delays among different

channels are also important factors in defining the cost of a commercial system. Chapter 4 investigates issues related to the signal requirement for a land navigation system.

Chapter 5 focuses on the issue of minimizing the system costs by reducing the number of inertial sensors. The chapter shows the results of using different sensor combinations. The main idea is to find a system that will require minimum number of sensors to reduce the costs to the user while providing reliable navigation during GPS signal outages. The simulation results from five sensor configurations, (a) three orthogonal accelerometers and three orthogonal gyros (Full IMU), (b) two gyros and three accelerometers (2G3A), (c) one gyro and three accelerometers (1G3A), (d) one gyro and two accelerometers (1G2A) and then with (e) one gyro and one accelerometer (1G1A), were used in the analyses.

Chapter 6 deals with the alignment issues of PNS. Alignment is one of the major requirements if inertial sensors are part of the navigation module. For portable system, it is important to determine alignment error budget for design specifications.

After alignment, the system needs to start navigation by implementing the appropriate navigation equations for the respective mode of transit. For portable system, two modes of transits are important which includes on-foot and in-vehicle modes. At this prototyping stage, the PNS contains a marker switch that can indicate the mode of transit if pressed by the user. For the complete product, this marker switch will be used as an automatic mode of transit detection switch after some modifications to the hardware of the PNS.

The hardware switch indication will be straight forward when it will indicate in-vehicle mode of transit by detecting the presence of in-vehicle holder. However, hardware switch will not be reliable for on-foot mode of transit. The user of the system can be riding in a motorized vehicle as a passenger instead of walking or running, and this will cause errors if the system tries to implement on-foot navigation equations. Chapter 7 discusses a software switch which is developed for mode detection issue when the hardware switch of the PNS will indicate on-foot transit. Figure 1-2 shows the outline of this thesis and functional classification of each topic according to the issues listed in section 1.3.

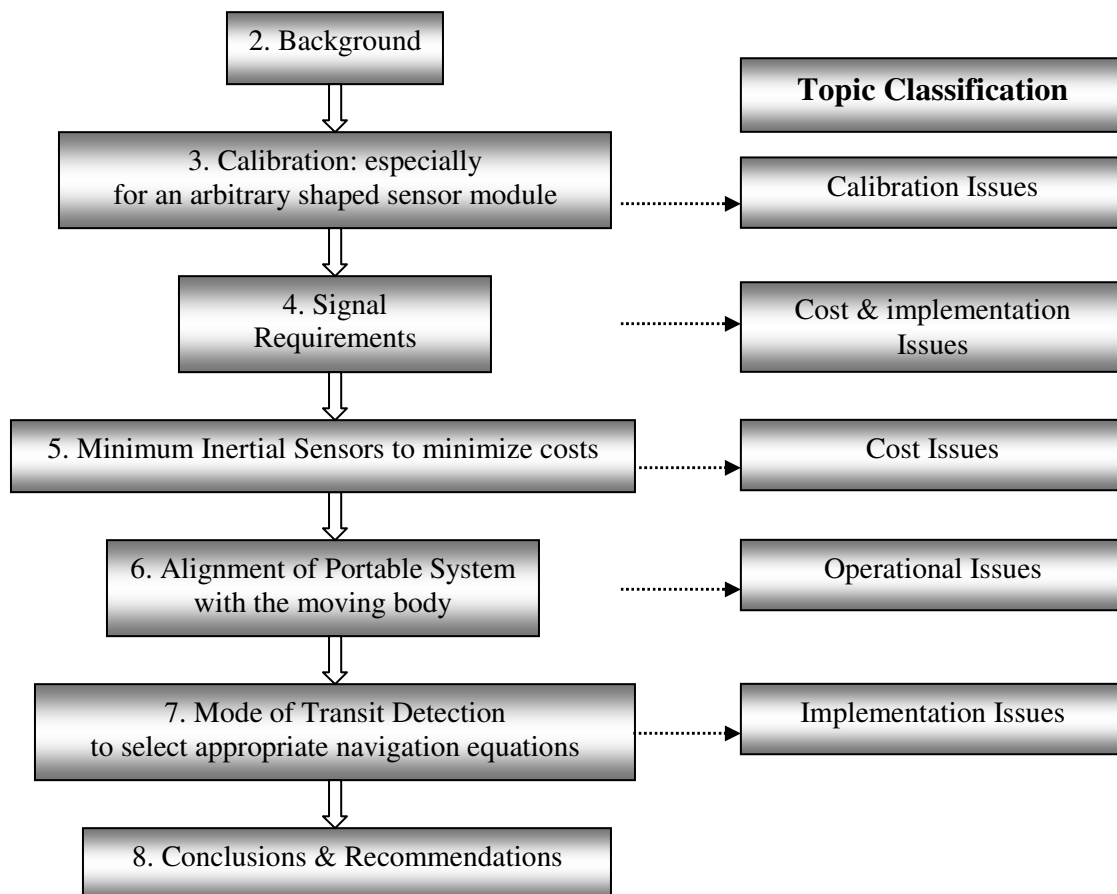


**Figure 1-2. Thesis outline**

## Chapter Two: Background

A PNS is a completely transferable system that can provide robust positioning information despite the user's mode of transit, i.e., in-vehicle or on-foot. From an implementation perspective, when a PNS consists of GPS and inertial sensors, these two modes of transit require different algorithms as shown in Figure 2-1.

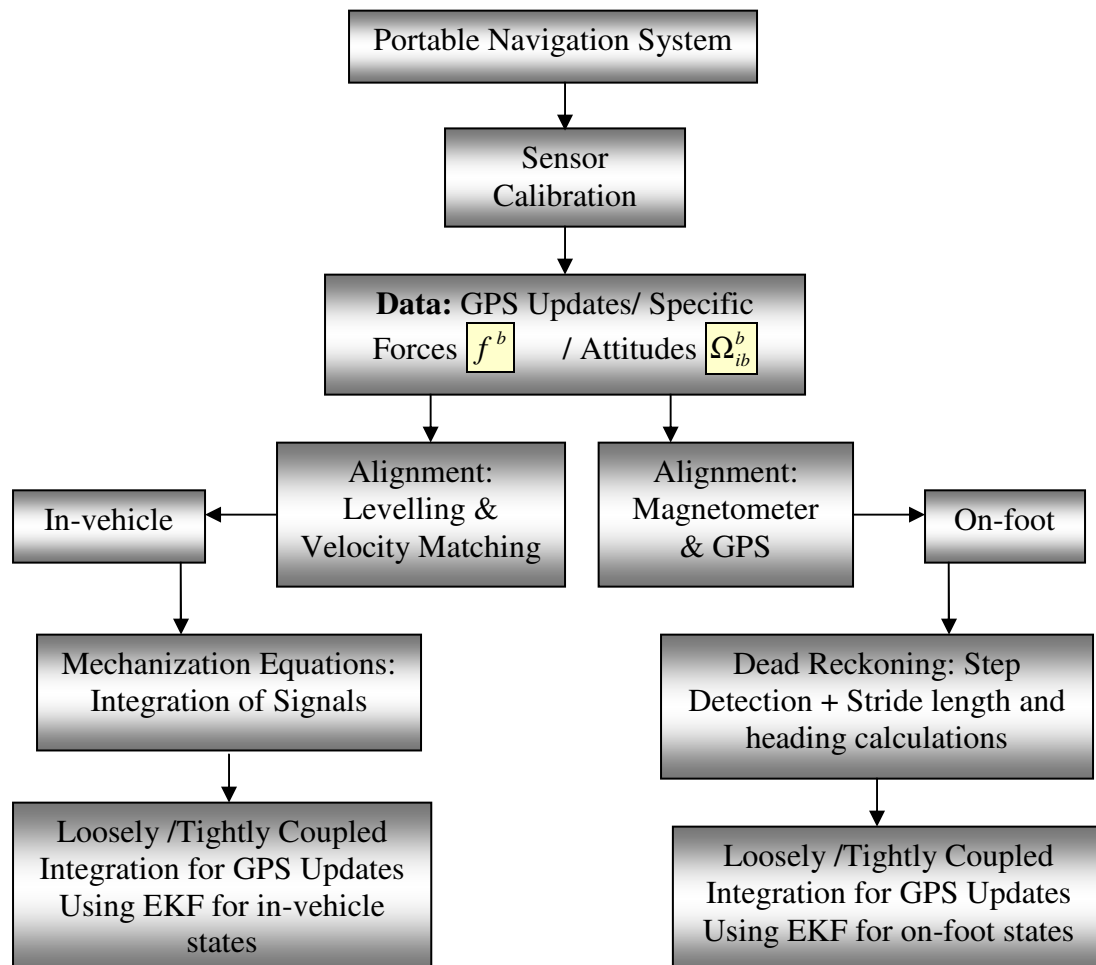


**Figure 2-1. Portable Navigation System**

In this thesis, issues related to in-vehicle mode of transit are explored in great detail due to the fact that both velocities and motion dynamics related to this mode are higher than

the on-foot navigation mode. The simple assumption is that if certain criteria (e.g. sampling rate, data resolution, etc.) work for a higher dynamic (0-8 Hz as shown in Figure 2-2) application, it should produce reasonable results for lower dynamics (0-4 Hz given in Figure 2-3) as well. However, this assumption needs to be verified.

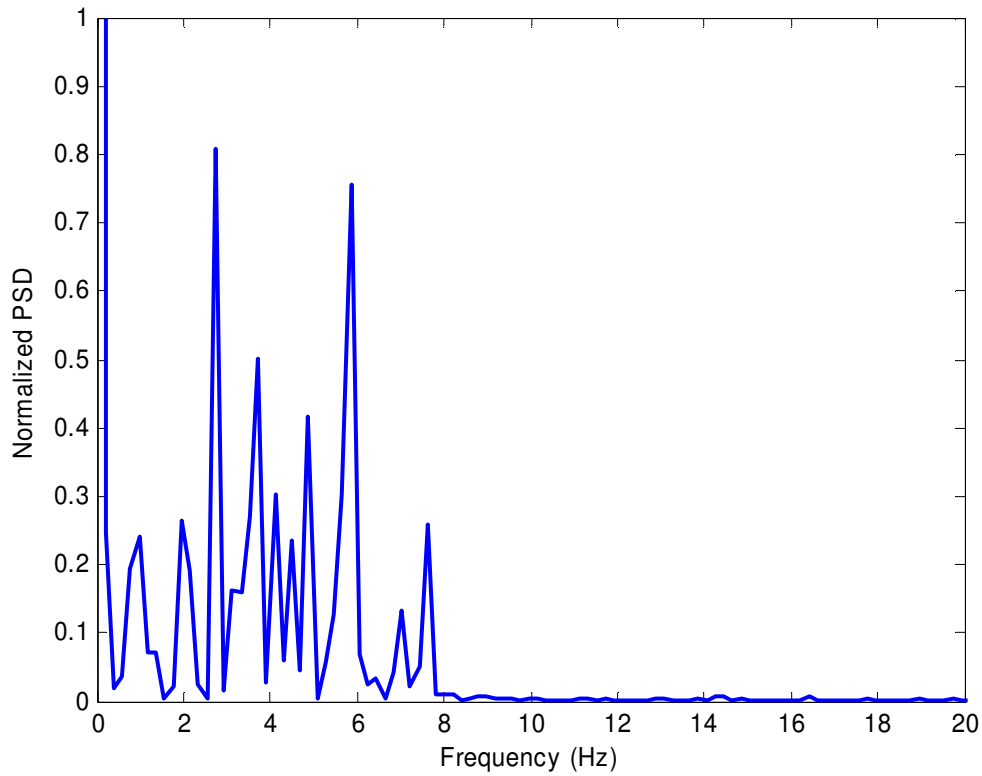


**Figure 2-2. Land vehicle dynamics using gyro signal**

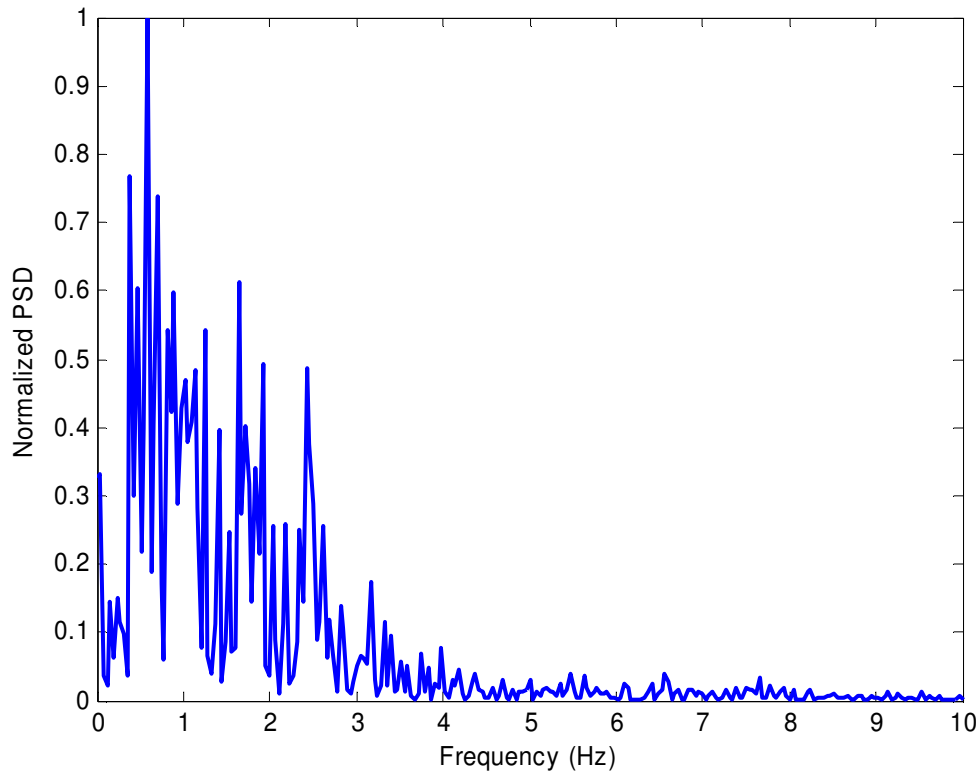


**Figure 2-3. Walking dynamics using gyro signal**

This chapter deals with the necessary background information required for GPS/INS integrated navigation systems. Starting from the calibration and error modelling of the inertial sensors to remove the manufacturing errors, the chapter then provides details of in-vehicle alignment, mechanization and filtering specific to in-vehicle navigation mode. For the on-foot navigation, the most important difference will be in the implementation of the navigation algorithm. Step detection and step length estimation along with the correct heading computation is required to propagate the user's position from one epoch to the next. The methods along with some results are provided in Appendix B. However, more data analysis is required to choose the algorithms that can provide the best accuracies for

on-foot navigation and hence, the decision on the most robust and efficient on-foot navigation equations are part of future work.

## 2.1 Sensor Calibration and Error Modelling

Inertial sensors, especially low-cost MEMS sensors, exhibit high biases, scale factor variations, axis non-orthogonalities, drifts and noise characteristics ([Hide et al., 2003](#); [Wang and Shen, 2005](#)). Any effect of the errors mentioned here will directly affect the position, velocity and attitude accuracies as a function of time and therefore, it is important to properly remove these errors before the start of navigation. A common way to estimate these errors is by simply comparing the raw signal with some reference. This type of comparison is known as calibration in which the sensors are subjected to known inputs. The output should correspond to input signal and any deviations from the known values are due to the sensor errors. Calibration will be discussed in detail in Chapter 3.

The stochastic noise errors of the sensors are usually modelled using first order Gauss Markov processes. In addition, the instantaneous random behaviour of the sensor signal is mostly modelled in terms of random walk (RW) which mimics the scenario when a person walks in random steps. RW for accelerometer signals is known as velocity RW (VRW) and for gyro signals it is called angle RW (ARW). The Allan variance method is used on the static sensors data to estimate the different stochastic errors such as RW, bias instability and exponentially correlated noise ([Hou, 2004](#)). Stochastic modeling is required to estimate the accuracy of the predicted positioning information. After sensor



calibration and error modelling, the next step is the alignment of the inertial sensors which is explained in the next section.

## 2.2 Alignment

Gyros and accelerometers measure the angular rates and specific forces, respectively, in  $b$ -frame but navigation is usually performed with respect to the  $l$ -frame ([Titterton and Weston, 1997](#)). Alignment requires computation of the orientation from the  $b$ -frame to the  $l$ -frame. There are different methods to perform alignment which are provided as follows:

- 1) Manual: Using orientation information provided by the user
- 2) Semi-automatic: Using accelerometer levelling for roll and pitch but the heading is provided by the user
- 3) Automatic: Using accelerometer levelling for roll and pitch, and velocity matching for heading.

Accelerometer levelling computes the roll and pitch of the sensor system by using the strong gravity signals ([El-Sheimy, 2006](#); [Titterton and Weston, 1997](#)). Consider an orthogonal triad of stationary accelerometers placed on a plane which is tilted by a small angle  $r$  with respect to the reference  $x$ -axis (generally called roll). Now due to this tilt, each accelerometer will measure a component of the gravity signal ( $g$ ). In the  $z$  direction, it will measure  $f_z = g \cos r$  and in  $y$  direction, it will measure  $f_y = g \sin r$ .

$$r = \text{sign}(f_z) \sin^{-1} \left( \frac{f_y}{g} \right) \quad \mathbf{2-1}$$

where  $f_y$  and  $f_z$  are y and z accelerometers signals.

A similar method can be used if the inertial measurement unit (IMU) or the vehicle is tilted by some angle with respect to the y-axis. This angular displacement is called pitch ( $p$ ) and can be derived as follows:

$$p = -\text{sign}(f_z) \sin^{-1} \left( \frac{f_x}{g} \right) \quad \mathbf{2-2}$$

A velocity matching technique is used to estimate the heading of the  $b$ -frame with respect to the North direction in the  $l$ -frame. GPS positions and velocities measurements can be used for the alignment of the IMU. The heading or azimuth of a vehicle can be determined by incorporating north and east velocity components from the GPS receiver. Along with the roll and pitch information calculated by using the accelerometer signals, the vehicle's attitude can be estimated by incorporating the GPS derived velocities. At every GPS update, the positions, velocities and heading can be updated to improve the navigation solution accuracy. Figure 2-4 shows the  $l$ -frame velocity vector and its relationship to the heading angle ( $A$ ).

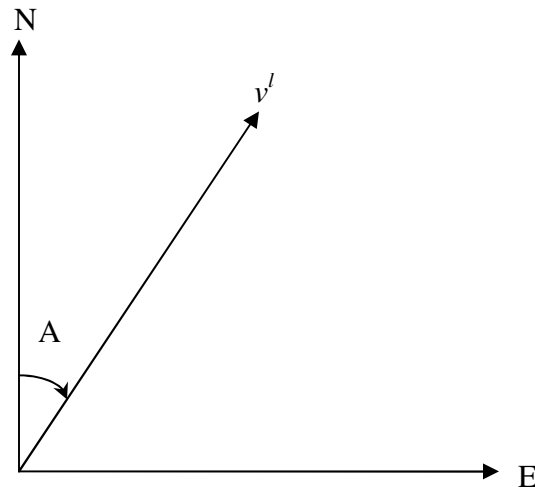


**Figure 2-4: Geometrical relationship between heading and  $l$ -frame velocity**

Heading is always measured from the North direction and therefore, can be written in terms of equation 2-3. However, care must be taken if there is any lever arm (LA) between the GPS receiver and the IMU. The LA must be compensated before GPS position update or attitude determination. Usually, a Kalman Filter (KF) is used to estimate the navigation parameters. The velocity from the GPS is fed back into the inertial navigation algorithm commonly known as the mechanization or navigation equations for the attitude at new time epochs. This method will require good manoeuvring and best results are obtained with velocities over 10m/s.

$$A = \tan^{-1}\left(\frac{V^E}{V^N}\right) \quad 2-3$$

## 2.3 Navigation Equations

After alignment, the next step is to estimate the relative position, velocity and attitude (PVA) information. Usually, an inertial sensors based navigation system consists of three gyros and three accelerometers. Gyros sense angular velocity  $\omega_{ib}^b$  ( $\Omega_{ib}^b = [\omega_{ib}^b \times]$ ) which is the rotation of the  $b$ -frame with respect to the  $i$ -frame, measured in the  $b$ -frame. Accelerometers measure the specific force  $f^b$  in the  $b$ -frame.

If the mode of transit is in-vehicle, the angular velocities  $\omega_{ib}^b$  are integrated in time to compute the angular displacements of the body relative to its initial orientation. The specific force measurements  $f^b$  are used to calculate body acceleration which is later used in estimating position differences after double integration with respect to time ([Titterton and Weston, 1997](#)). To summarize, all the navigation parameters can be estimated by solving 2-4 which uses specific force and angular velocity measurements.

$$\begin{pmatrix} \dot{r}^\ell \\ \dot{v}^\ell \\ \dot{R}_b^\ell \end{pmatrix} = \begin{pmatrix} D^{-1}v^\ell \\ R_b^\ell f^b - (2\Omega_{ie}^\ell + \Omega_{e\ell}^\ell)v^\ell + g^\ell \\ R_b^\ell (\Omega_{ib}^b - \Omega_{i\ell}^b) \end{pmatrix} \quad 2-4$$

where

$$\dot{r}^\ell = \begin{pmatrix} \dot{\phi} \\ \dot{\lambda} \\ \dot{h} \end{pmatrix} = \begin{pmatrix} \frac{1}{M+h} & 0 & 0 \\ 0 & \frac{1}{(N+h)\cos\phi} & 0 \\ 0 & 0 & -1 \end{pmatrix} \begin{pmatrix} V^n \\ V^e \\ V^d \end{pmatrix} = D^{-1}v^\ell \quad 2-5$$

$\varphi$ ,  $\lambda$  and  $h$  are latitude, longitude and height of the body;  $M$  and  $N$  are meridian and prime vertical radius of curvatures,  $v^l$  is the velocity in NED frame with the following components

$$v^l = \begin{pmatrix} V^n \\ V^e \\ V^d \end{pmatrix} \quad \mathbf{2-6}$$

and the scaling matrix is defined as

$$D^{-1} = \begin{pmatrix} \frac{1}{M+h} & 0 & 0 \\ 0 & \frac{1}{(N+h)\cos\varphi} & 0 \\ 0 & 0 & -1 \end{pmatrix} \quad \mathbf{2-7}$$

The rotation matrix from the  $b$ -frame to the  $l$ -frame is denoted as  $R_b^l$ . The rotation matrix at the start of navigation is obtained by utilizing the roll, pitch and heading information from the alignment phase.

$$R_b^l = R_3(-A)R_2(-p)R_1(-r) \quad \mathbf{2-8}$$

The angular velocities term,  $2\omega_{ie}^l + \omega_{el}^l$ , is explained as follows:

$$2\omega_{ie}^l + \omega_{el}^l = 2 \begin{pmatrix} \omega^e \cos\varphi \\ 0 \\ \omega^e \sin\varphi \end{pmatrix} + \begin{pmatrix} \frac{V^e}{N+h} \\ -\frac{V^n}{M+h} \\ \frac{V^e \tan\varphi}{N+h} \end{pmatrix} = \begin{pmatrix} \frac{V^e}{N+h} + 2\omega^e \cos\varphi \\ -\frac{V^n}{M+h} \\ -\frac{V^e \tan\varphi}{N+h} + 2\omega^e \sin\varphi \end{pmatrix} = \begin{pmatrix} \omega_x \\ \omega_y \\ \omega_z \end{pmatrix} \quad \mathbf{2-9}$$

where,  $\omega^e$  is the rotation rate of the Earth as mentioned before. The  $2\Omega_{ie}^l + \Omega_{el}^l$  used in equation 2-4 is the skew-symmetric representation of equation 2-9 which can be given as:

$$2\Omega_{ie}^l + \Omega_{el}^l = \begin{pmatrix} 0 & -\omega_z & \omega_y \\ \omega_z & 0 & -\omega_x \\ -\omega_y & \omega_x & 0 \end{pmatrix} \quad \mathbf{2-10}$$

$\Omega_{ie}^l$  is the angular velocity of the  $e$ -frame with respect to the  $i$ -frame as given in the  $l$ -frame and  $\Omega_{el}^l$  is the angular velocity of the  $l$ -frame with respect to the  $e$ -frame as measured in the  $l$ -frame.  $g^l$  is the normal gravity vector in the  $l$ -frame.  $\Omega_{il}^b$  is the skew symmetric representation of  $\omega_{il}^b$  which is the angular velocity of the  $l$ -frame with respect to the  $i$ -frame as represented in the  $b$ -frame.

$$\omega_{il}^b = R_l^b \begin{pmatrix} \frac{V^e}{N+h} + \omega^e \cos \varphi \\ -\frac{V^n}{M+h} \\ -\frac{V^e \tan \varphi}{N+h} + \omega^e \sin \varphi \end{pmatrix} \quad \mathbf{2-11}$$

The integration algorithm can be summarized using Figure 2-5. After obtaining the velocity in the NED frame, all the parameters requiring the velocity can be computed. As an example, equations **2-9** and **2-11** estimate two different angular velocity terms for the mechanization equations and both of them require velocity. The first rotation matrix  $R_b^l$  is estimated by the initial alignment of the system with respect to the  $l$ -frame.

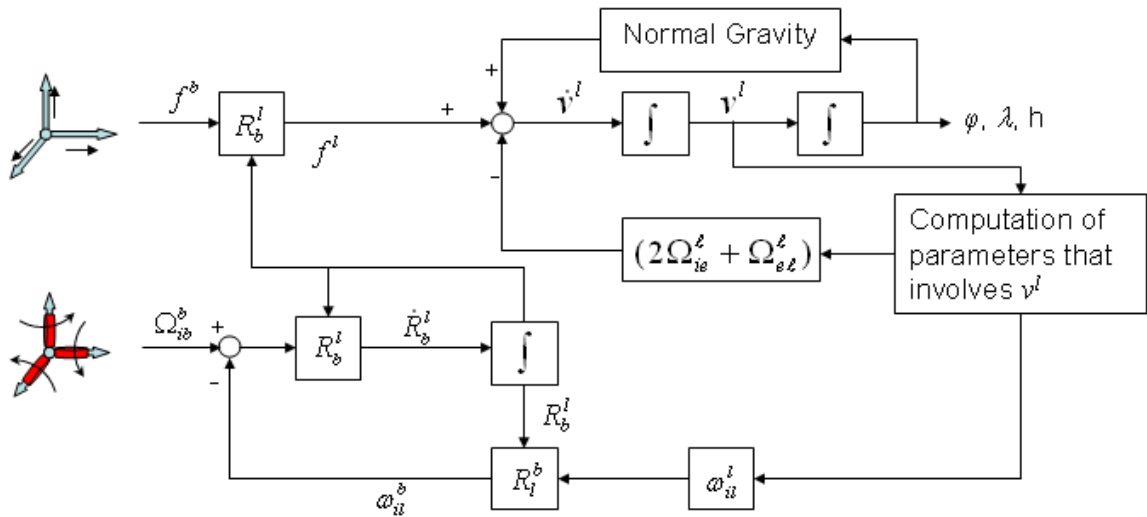


**Figure 2-5. Mechanization Algorithm for in-vehicle navigation mode**

Below is the summary of the required parameters to implement the mechanization algorithm for in-vehicle navigation.

**Table 2-1: Summary of required parameters for the mechanization equations**

Parameter	Obtained from
$f^b$	accelerometers
$\Omega_{ib}^b = [\omega_{ib}^b \times]$	gyros
$D^{-1}$	Reference ellipsoid and latitude at the epoch
$g^l$	Reference ellipsoid, gravity model and latitude at the epoch
M	Reference ellipsoid and latitude at the epoch
N	Reference ellipsoid and latitude at the epoch
$\omega^e$	Known
$R_b^l$	Alignment

The on-foot DR equations are different from the in-vehicle mechanization equations. The following is a flow chart along with the methods that were implemented for this project. However, more data analysis is required to deduce the best method. The preliminary results can be found in Appendix B.

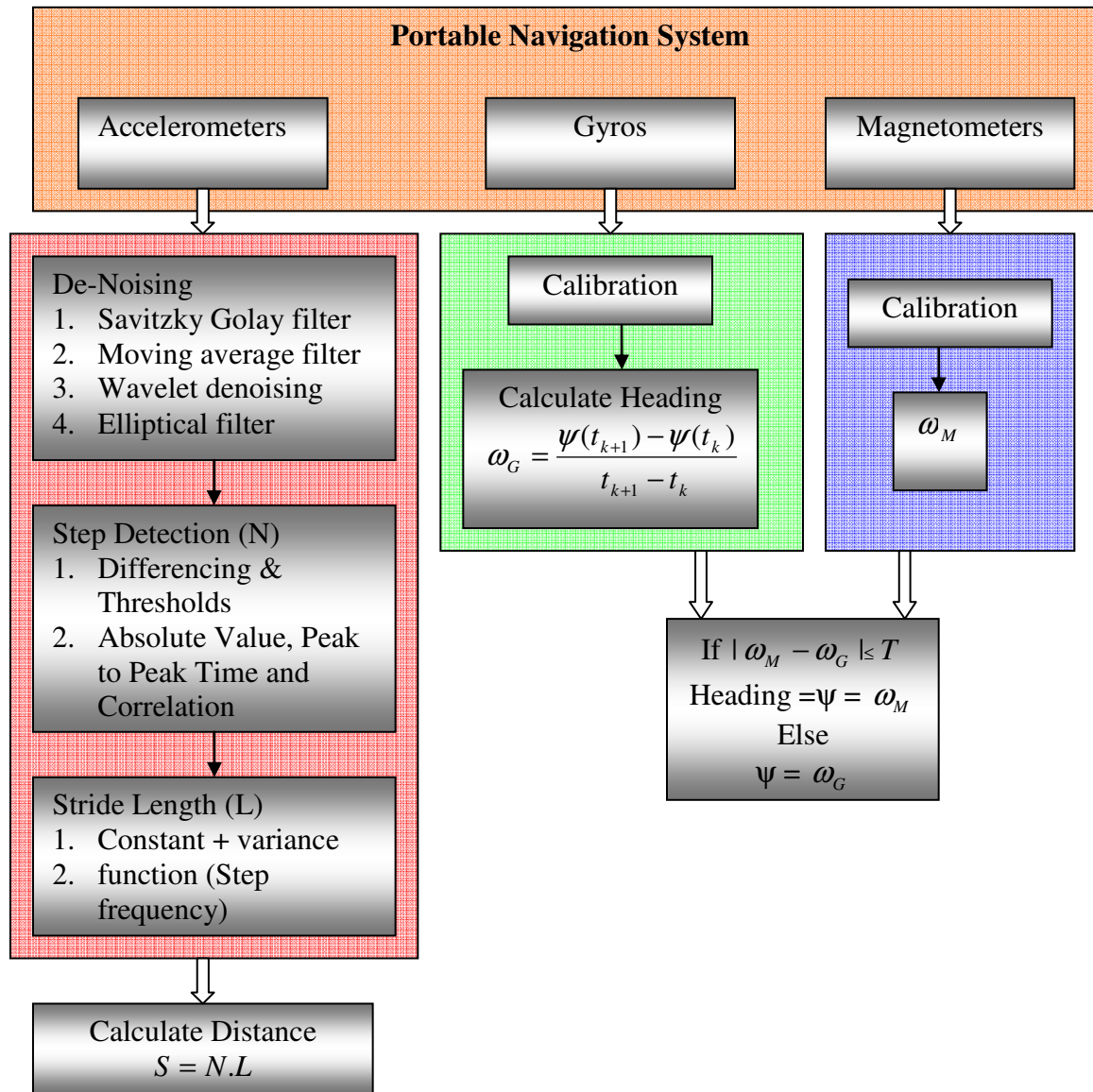


**Figure 2-6: Flow chart of on-foot dead reckoning**



DR does not drift as the distance is computed by multiplying the number of steps with the step length and therefore, it is desirable to use this method to reduce the errors. Furthermore, it is more likely that on-foot navigation may be indoors where GPS is not available for prolonged time periods and DR can be of real advantage ([Shin and Hong, 2005](#); [Jirawimut et al., 2001](#); [Levi and Judd, 1996](#)). The east ( $E_t$ ) and north ( $N_t$ ) position components at time  $t$  for DR can be propagated from the previous epoch  $t-1$  as follows:

$$\begin{aligned} E_t &= E_{t-1} + S_{[t-1,t]} \sin \psi_{t-1} \\ N_t &= N_{t-1} + S_{[t-1,t]} \cos \psi_{t-1} \end{aligned} \tag{2-12}$$

## 2.4 GPS/INS Integration Techniques

Theoretically, INS and GPS can both estimate navigation parameters for a body in motion. However, both systems have their own problems. For example, the time-dependent position errors can drift quickly due to the integration of the acceleration and angular rate data for in-vehicle navigation, and without updates the sensor errors and step length parameters can cause significant errors for on-foot navigation. GPS provided absolute and drift free positions are only possible when the receiver has a direct line of sight to four or more satellites.

The combination of the two systems can offer a number of advantages. The drift errors of the INS can be controlled by the GPS updates and for short GPS signal outages, the INS stand-alone navigation capabilities can be exploited for seamless navigation. Moreover, the combination of the two systems, i.e., INS and GPS, will provide redundant measurements and will result in improved reliability of the combined system.

A KF is used to optimally combine the redundant information in which the inertial state vector is regularly updated by GPS measurement. Two integration strategies can be implemented at the software level using the KF approach.

#### 2.4.1 Loosely Coupled Integration

The most commonly implemented integration scheme is called loosely coupled ([Grewal et al., 2001](#)) in which the GPS derived positions, velocities along with their accuracies from GPS KF are used as updates for the navigation KF. The error states include both the navigation errors and sensor errors. To further improve the accuracy of the navigation solution, the error states are fed back to the mechanization ([Kim et al., 2006](#)) subroutine as shown in Figure 2-7.

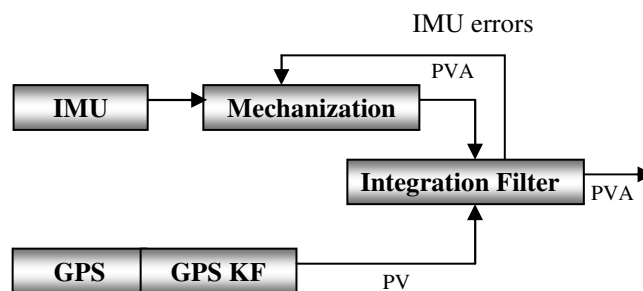


**Figure 2-7. Loosely coupled integration. (PV refers to position and velocity, respectively)**

There are certain advantages and disadvantages of using this integration scheme. For instance, one of the advantages is the smaller size of state vectors for both GPS and INS KF as compared to the state vector in the tightly coupled integration which results in the improved computation capabilities. A disadvantage of using such a system is the extra process noise due to the presence of two KFs which may decrease the signal to noise

ratio. Consequently, the probability that the integration filter will trust the predicted states more than the measurements will increase which is not desirable.

#### 2.4.2 Tightly Coupled Integration

Tightly coupled integration ([Grewal et al., 2001](#); [Knight, 1997](#); [Wendel and Trommer, 2004](#)) is also known as centralized KF approach. The major difference between the loosely coupled defined earlier and tightly coupled is the number of KFs present in the two schemes. The tightly coupled integration uses one centralized KF ([Hide et al., 2006](#); [Godha and Cannon, 2007](#)) that integrates the pseudorange ( $\rho$ ) and Doppler ( $f_{dopp}$ ) information from the GPS receiver and the PVA information from the mechanization of the inertial system.

The error states of the integration KF are composed of navigation errors, inertial sensor errors and GPS receiver clock errors. The inertial sensor errors and GPS receiver clock errors are then fed back to compensate for these errors for the next epoch PVA estimation. Figure 2-8 shows the summary of the tightly coupled integration. The  $\rho$  and  $f_{dopp}$  measurements from GPS, combined with the INS derived pseudorange and Doppler for every satellite  $i$ , are used as the observations for the integration KF.

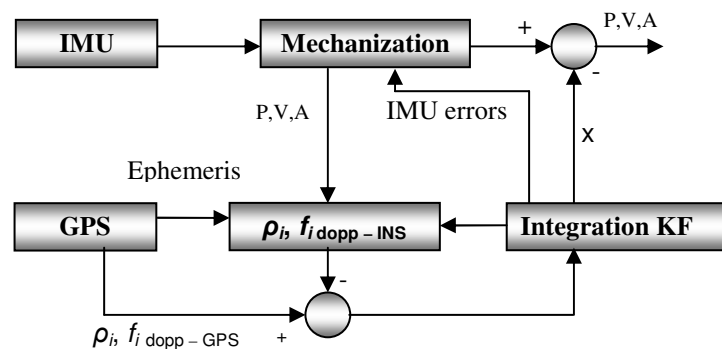


**Figure 2-8. Tightly coupled integration scheme.**

For this thesis, a tightly coupled integration filter was implemented. The graphical user interface for the software is provided in Figure 2-9.

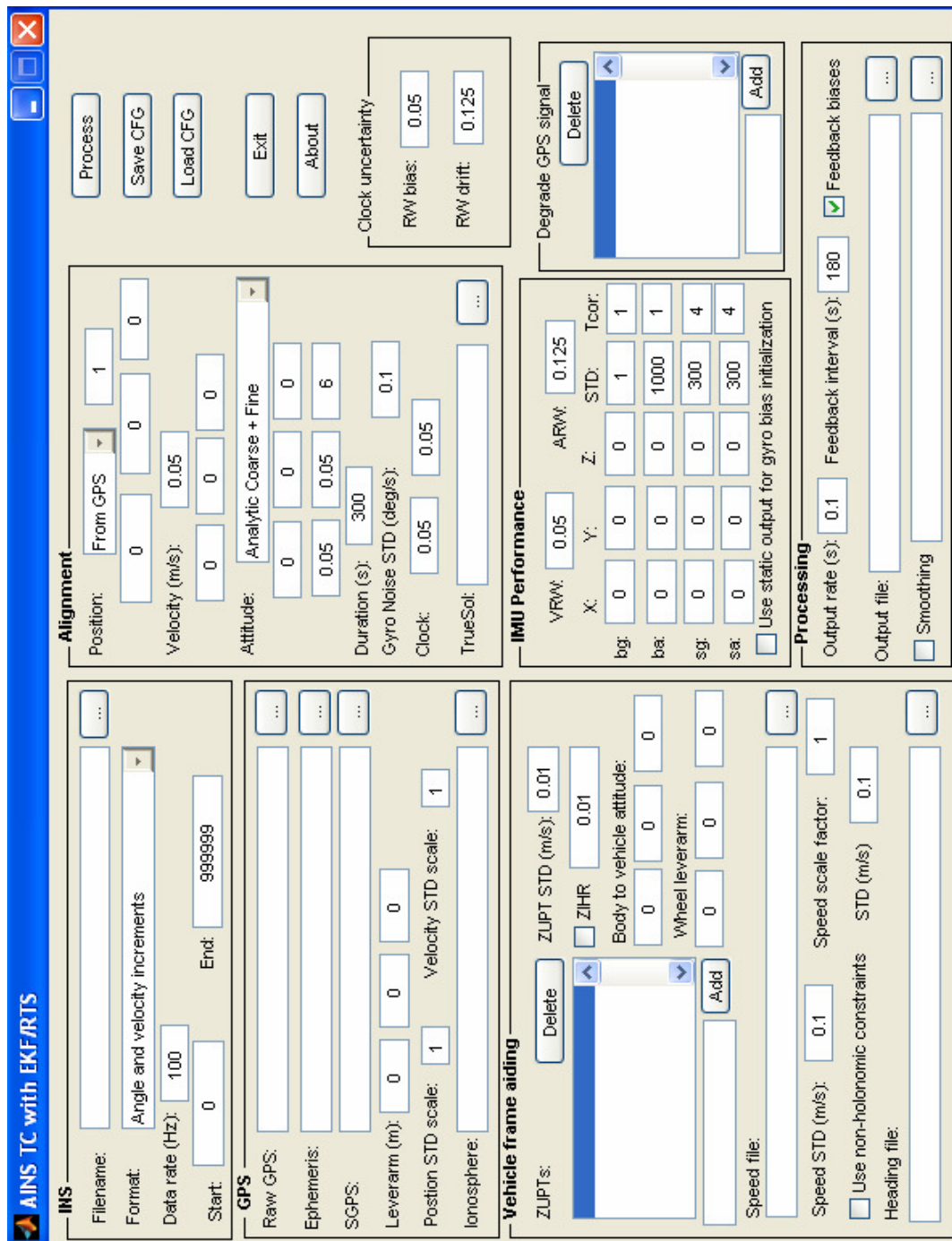


Figure 2-9. Graphical user interface for the tightly coupled integration scheme

The software takes the raw GPS ephemeris, raw GPS measurements and ionospheric corrections parameters file to perform the integration. If the user provides a true solution file, the program provides results in comparison with the true solution, otherwise, the result will be provided in comparison to the single point position file provided by the user. The software can also perform backward smoothing of the dataset using Rauch-Tung-Striebel (RTS) smoother. The user can also simulate GPS signal degradation period by specifying the number of satellites. In this case, the software will randomly select the required number of satellites from the available satellite list for particular epochs.

Moreover, it is also possible to perform certain aidings during the GPS signal outage periods. Non holonomic constraints (NHC), odometer aiding, heading and zero velocity updates (ZUPTs) are the examples of the available aiding options.

The loosely or tightly coupled integration scheme is realized by an extended KF (EKF). It is the method of choice for the blending of inertial data with GPS updates due to its optimal weighting schemes. As an EKF will be used throughout this thesis, it is explained in detail in the following section.

## **2.5 Extended Kalman Filter**

The KF estimates the state of a discrete-time controlled process governed by a *linear* stochastic difference equation. This condition of linearity cannot be satisfied all the time and for all applications. The integration of inertial data with GPS data using a KF is one of those cases when the system is non-linear due to the mechanization equations involved. It is however, not an isolated example and often the KF applications are non-

linear in nature. Despite the non-linear problems, the KF has shown remarkable success in those circumstances.

For the non-linear navigation cases, the system can be linearized about a nominal trajectory during the design phase of the KF. For a general non-linear case when the nominal trajectory is not available, the process can be linearized about the current state. In case of the inertial data integration, the current state can be obtained by integrating the sensor output with respect to time using the mechanization process. A KF that involves linearization about the current state is referred to as an EKF.

### **2.5.1 Linearization**

Navigation solution derived from the mechanization equations is a highly non-linear problem. This cannot be used directly in the KF unless linearization is performed to make the system linear. Hence, it is obvious that the most important step involving a non-linear difference equation is the linearization. A simple dynamic non-linear stochastic difference equation for the process with state  $x_k$  can be defined first. Here the subscript  $k$  refers to time epoch  $t$

$$x_k = f(x_{k-1}) + w_{k-1} \quad \mathbf{2-13}$$

The non-linear difference equation given by the function  $f$  relates the previous epoch state  $x_{k-1}$  to the current epoch state  $x_k$ . The random variable  $w_{k-1}$  is the dynamic process noise with

$$\begin{aligned} E[w_k] &= 0 \\ E[w_k w_j^T] &= Q_k \quad \text{for } k = j \end{aligned} \quad \mathbf{2-14}$$

where  $Q_k$  is the variance covariance matrix for the process noise. It can be estimated by computing the spectral density of the noise of different state vector components.

Equation 2-13 is the simplest form of the non-linear difference equation. Similarly, the best situation would be when only the measurement ( $z_k$ ) is related to the states with a non-linear functional relationship ( $h$ ) and the noise ( $v_k$ ) is uncorrelated and Gaussian distributed

$$z_k = h(x_k) + v_k \quad \mathbf{2-15}$$

$$\begin{aligned} E[v_k] &= 0 \\ E[v_k v_j^T] &= R_k \quad \text{for } k = j \end{aligned} \quad \mathbf{2-16}$$

where  $R_k$  is the variance covariance matrix for the measurement noise

For a highly non-linear model, the assumption of a linear measurement noise component may not be realistic. In this case, a better measurement model equation will be of the form

$$z_k = h(x_k, v_k) \quad \mathbf{2-17}$$

No matter if the noise is non-linear or linear, it cannot be estimated during the prediction step. Here it is assumed that the noise is Gaussian distributed, random with a zero mean.

Because of the zero mean condition, this term can be left out from the prediction stage.

After making the above changes, the state and measurement vector approximates,  $\tilde{x}_k$  and

$\tilde{z}_k$  are given as

$$\tilde{x}_k = f(\hat{x}_{k-1}) \quad \mathbf{2-18}$$

$$\tilde{z}_k = h(\tilde{x}_k) \quad \mathbf{2-19}$$

As mentioned earlier, for EKF, the linearization is performed at the most recent epoch or current state. In this case, the current state would be the last available state vector ( $\hat{x}_{k-1}^-$ ).

Taylor series expansion can be used for linearization as follows

$$x_k \approx f(\hat{x}_{k-1}^-) + \left. \frac{\partial f}{\partial x} \right|_{\hat{x}_{k-1}^-} (x_{k-1} - \hat{x}_{k-1}^-) + \frac{1}{2!} \left. \frac{\partial^2 f}{\partial x^2} \right|_{\hat{x}_{k-1}^-} (x_{k-1} - \hat{x}_{k-1}^-)^2 + \dots + \langle w_{k-1} \rangle \quad \mathbf{2-20}$$

The quantities  $x_k$  and  $x_{k-1}$  are the *true* state vectors. However, these quantities are not available directly as they can only be estimated. This kind of estimation will introduce errors, such as truncation errors. The Jacobian matrix  $\left. \frac{\partial f}{\partial x} \right|_{\hat{x}_{k-1}^-}$  that propagates a previous state vector to the current is the partial derivative of the non-linear process function  $f$  with respect to the elements of the state vector  $x$  evaluated about the estimate of the previous state ( $\hat{x}_{k-1}^-$ ). For simplicity this Jacobian matrix will be referred to as  $F_k$  for discrete time representation.

$$F_k = \left. \frac{\partial f}{\partial x} \right|_{\hat{x}_{k-1}^-} \quad \mathbf{2-21}$$

Another linearization is necessary if the measurement equation is also non-linear as discussed earlier.

$$z_k = \tilde{z}_k + \left. \frac{\partial h}{\partial x} \right|_{\tilde{x}_k} (x_k - \tilde{x}_k) + \frac{1}{2!} \left. \frac{\partial^2 h}{\partial x^2} \right|_{\tilde{x}_k} (x_k - \tilde{x}_k)^2 + \dots + v_k \quad \mathbf{2-22}$$

The measurement vector  $z_k$  is the *true* measurement that may be available from the GPS receiver or any other aiding source. Even a physical relationship can be used as the



measurement. For example, using the fact that a land vehicle cannot slide sideways and also it cannot jump up and down during its normal operation. These two physical constraints, commonly known as NHC, can be translated into measurements when no other source of aiding is present. In this case,  $z_k$  will consist of the two body frame velocity components in sideways and vertical direction of the vehicle.

The measurement equation is used to estimate the true value of the state vector  $x_k$ . The Jacobian matrix composed of the partial derivative of the measurement equation with respect to the state vector evaluated at the approximated current state  $\tilde{x}_k$  will be called  $H_k$ .

$$H_k = \left. \frac{\partial h}{\partial x} \right|_{\tilde{x}_k}$$

For the EKF implementation, the first order approximation of the linearized dynamic process and measurement equations are used.

$$x_k \approx f(\hat{x}_{k-1}^-) + F_k(x_{k-1} - \hat{x}_{k-1}^-) \quad \mathbf{2-23}$$

$$z_k = \tilde{z}_k + H_k(x_k - \tilde{x}_k) \quad \mathbf{2-24}$$

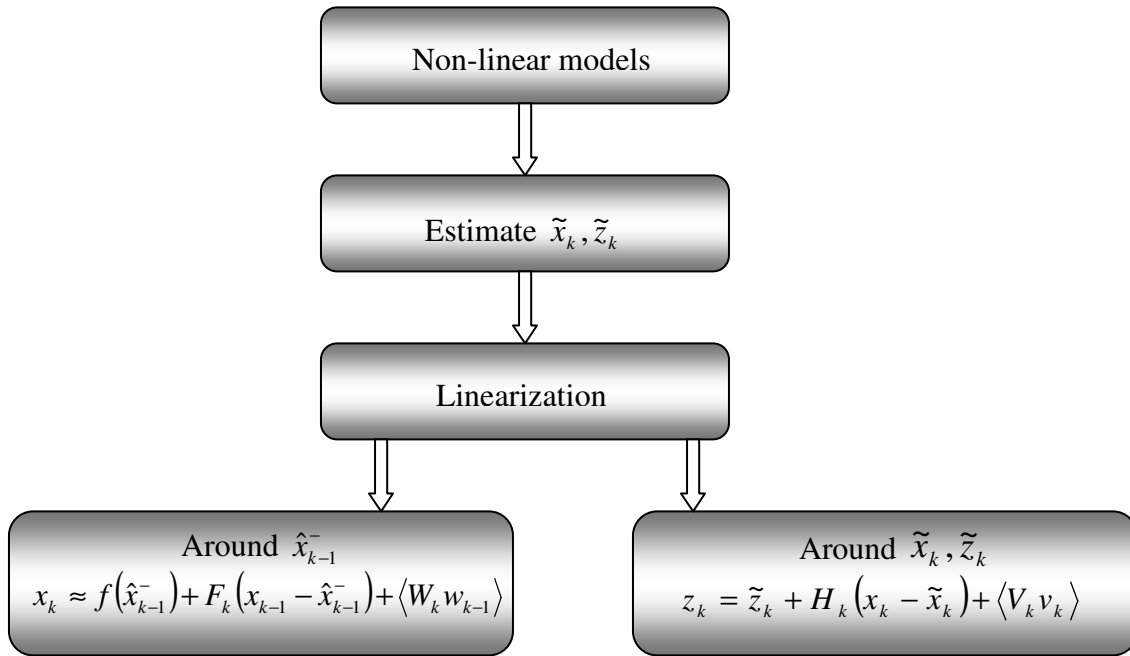


**Figure 2-10. Linearization process for EKF**

### 2.5.2 Prediction

The first part of the EKF is to predict the state vector when the update measurements are not available. The prediction equations are also known as time update equations. Prediction equations not only estimate the state for the current epoch but also the uncertainty or accuracy of the states.

The dynamic process and measurement in terms of their respective errors are defined since the true state vector is not available. The predicted errors will be used to get the corrected trajectory

$$\delta \tilde{x}_k = x_k - \tilde{x}_k \quad \mathbf{2-25}$$

$$\delta \tilde{z}_k = z_k - \tilde{z}_k \quad \mathbf{2-26}$$

Substituting equation 2-25 in equation 2-23 will give us the prediction equation for the error states ([Gelb, 1974](#)).

$$\delta\hat{x}_k^- = F_k(x_{k-1} - \hat{x}_{k-1}^-) \quad 2-27$$

The state error vector is given as follows:

$$\delta\hat{x}_k = \begin{matrix} \left. \begin{matrix} \text{Tightly} \\ \text{coupled} \end{matrix} \right\} & \begin{bmatrix} \delta r_x^l \\ \delta r_y^l \\ \delta r_z^l \\ \delta V^n \\ \delta V^e \\ \delta V^d \\ \varepsilon_x \\ \varepsilon_y \\ \varepsilon_z \\ b_a |_{3 \times 1} \\ b_g |_{3 \times 1} \\ sf_a |_{3 \times 1} \\ sf_g |_{3 \times 1} \\ b_c \\ d_c \end{bmatrix} & \left. \begin{matrix} \text{Loosely} \\ \text{coupled} \end{matrix} \right\} \end{matrix}$$

where  $\delta r_x^l, \delta r_y^l, \delta r_z^l$  are the position errors;  $\delta V^n, \delta V^e, \delta V^d$  are the velocity errors;  $\varepsilon_x, \varepsilon_y$  and  $\varepsilon_z$  are the errors in attitude;  $b$  and  $sf$  are the sensor bias and scale factor errors. The subscripts  $a$  and  $g$  represent the gyro and accelerometer, respectively. This comprises the loosely coupled state vector and if there are two additional states, clock bias ( $b_c$ ) and clock drift ( $d_c$ ), it will be the state vector for the tightly coupled integration scheme. Tightly coupled state vector may also include ambiguities terms for the available

satellites if the carrier phase measurements are implemented for some high accuracy application.

This is the first step in prediction and surely the second step is the propagation of the error covariance matrix ( $P$ ) to the next epoch. The estimate of the error  $\tilde{\delta x}_k$  can then be used after some manipulation to estimate the *true* state vector which was not directly available. The errors are also assumed to follow Gaussian probability density function, that is

$$E(\tilde{\delta x}_k) = 0 \text{ and}$$

$$E(\tilde{\delta x}_k \tilde{\delta x}_k^T) = P_k^-$$

From this basic expectation, a compact mathematical relationship to calculate the expected covariance of the error states can be derived. After substituting the value of the  $\tilde{\delta x}_k$  in the basic expectation equation and using mathematical identities, the a-priori covariance equation can be written as

$$P_k^- = F_k P_{k-1} F_k^T + Q_{k-1} \quad \mathbf{2-28}$$

### 2.5.3 Update Equations

Similarly, manipulation of the update equation given in equation 2-24 will yield to the measurement error equation.

$$\tilde{\delta z}_k = H_k \tilde{\delta x}_k^- + V_k v_k \quad \mathbf{2-29}$$

where for loosely coupled integration the values are defined as

$$\tilde{\mathcal{Z}}_k = \begin{bmatrix} (M+h)(\varphi_{INS} - \varphi_{GPS}) \\ (N+h)\cos\varphi(\lambda_{INS} - \lambda_{GPS}) \\ h_{INS} - h_{GPS} \\ v'_{INS} - v'_{GPS} \end{bmatrix} \quad \mathbf{2-30}$$

$$H_k = \begin{bmatrix} (M+h) & 0 & 0 & & \\ 0 & (N+h)\cos\varphi & 0 & \mathbf{0}_{3 \times 3} & \mathbf{0}_{3 \times 15} \\ 0 & 0 & 1 & & \\ & \mathbf{0}_{3 \times 3} & & \mathbf{I}_{3 \times 3} & \mathbf{0}_{3 \times 15} \end{bmatrix} \quad \mathbf{2-31}$$

where subscript INS and GPS refer to the parameters computed from INS and GPS respectively

The measurement equation for the tightly coupled integration can be written as:

$$\tilde{\mathcal{Z}}_k = \begin{bmatrix} \rho_{iIMU} - \rho_i \\ f_{idopp-IMU} - f_{idopp-GPS} \end{bmatrix}^T \quad \mathbf{2-32}$$

where  $\rho_{iIMU}$ ,  $f_{idopp-IMU}$  are IMU pseudorange and Doppler measurements for the  $i^{\text{th}}$  GPS satellite and  $\rho_i$ ,  $f_{idopp-GPS}$  are the GPS pseudorange and Doppler measurements for the  $i^{\text{th}}$  GPS satellite. The Doppler can be calculated using  $e$ -frame coordinates of the IMU and satellite position ( $rx$ ,  $ry$ ,  $rz$ ) and velocity ( $vx$ ,  $vy$ ,  $vz$ ) as

$$f_{idopp-IMU} = L(1)_i (vx_{IMU}^{ECEF} - vx_{GPS}^{ECEF}) + L(2)_i (vy_{IMU}^{ECEF} - vy_{GPS}^{ECEF}) + L(3)_i (vz_{IMU}^{ECEF} - vz_{GPS}^{ECEF}) \quad \mathbf{2-33}$$

where

$$L_i = \begin{bmatrix} \frac{rx_{IMU}^{ECEF} - rx_{GPS}^{ECEF}}{\rho_{iIMU}} \\ \frac{ry_{IMU}^{ECEF} - ry_{GPS}^{ECEF}}{\rho_{iIMU}} \\ \frac{rz_{IMU}^{ECEF} - rz_{GPS}^{ECEF}}{\rho_{iIMU}} \\ \rho_{iIMU} \end{bmatrix} \quad \mathbf{2-34}$$

The measurement matrix for the tightly coupled system is as follows:

$$H_k = \begin{bmatrix} (L_i^l)^T & 0_{1 \times 3} & 0_{1 \times 15} & 1 & 0 \\ 0_{1 \times 3} & (L_i^l)^T & 0_{1 \times 15} & 0 & 1 \end{bmatrix} \quad \mathbf{2-35}$$

where  $L_i^l$  is the  $L_i$  converted in the  $l$ -frame using the direction cosines matrix (DCM)

The Kalman gain yields the minimum mean-squared error (MMSE) estimate and is known as the *optimal Kalman gain*. If a linear blending factor  $K_k$  is used for a new measurement, the following relationship can be established between the predicted state and the measurement

$$\delta \hat{x}_k^+ = \delta \hat{x}_k^- + K_k (\delta z_k - H_k \delta \hat{x}_k^-) \quad \mathbf{2-36}$$

The a posteriori covariance for the state vector can now be estimated in a similar fashion as for the a-priori covariance.

$$P_k^+ = P_k^- - K_k H_k P_k^- - P_k^- H_k^T K_k^T + K_k (R_k + H_k P_k^- H_k^T) K_k^T \quad \mathbf{2-37}$$

The equation 2-37 is general equation for any arbitrary gain matrix. The optimal gain with MMSE of the covariance matrix can be obtained by minimizing the trace of

$P_k^+$  which is equivalent to taking the partial derivative of the matrix  $P_k^+$  with respect to the gain and setting it to zero.

$$\frac{\partial P_k^+}{\partial K_k} = -2(H_k P_k^-)^T + 2K_k(R_k + H_k P_k^- H_k^T) = 0 \Rightarrow P_k^- H_k^T = K_k(R_k + H_k P_k^- H_k^T) \text{ and}$$

$$K_k = P_k^- H_k^T (R_k + H_k P_k^- H_k^T)^{-1} \quad 2-38$$

Substitution of Kalman gain in equation 2-37 will reduce this equation as follows:

$$P_k^+ = P_k^- + \underbrace{P_k^- H_k^T (R_k + H_k P_k^- H_k^T)^{-1} H_k P_k^-}_{K_k} P_k^- \quad 2-39$$

$$P_k^+ = (I - K_k H_k) P_k^-$$

A summary of an EKF is given in the following flowchart.

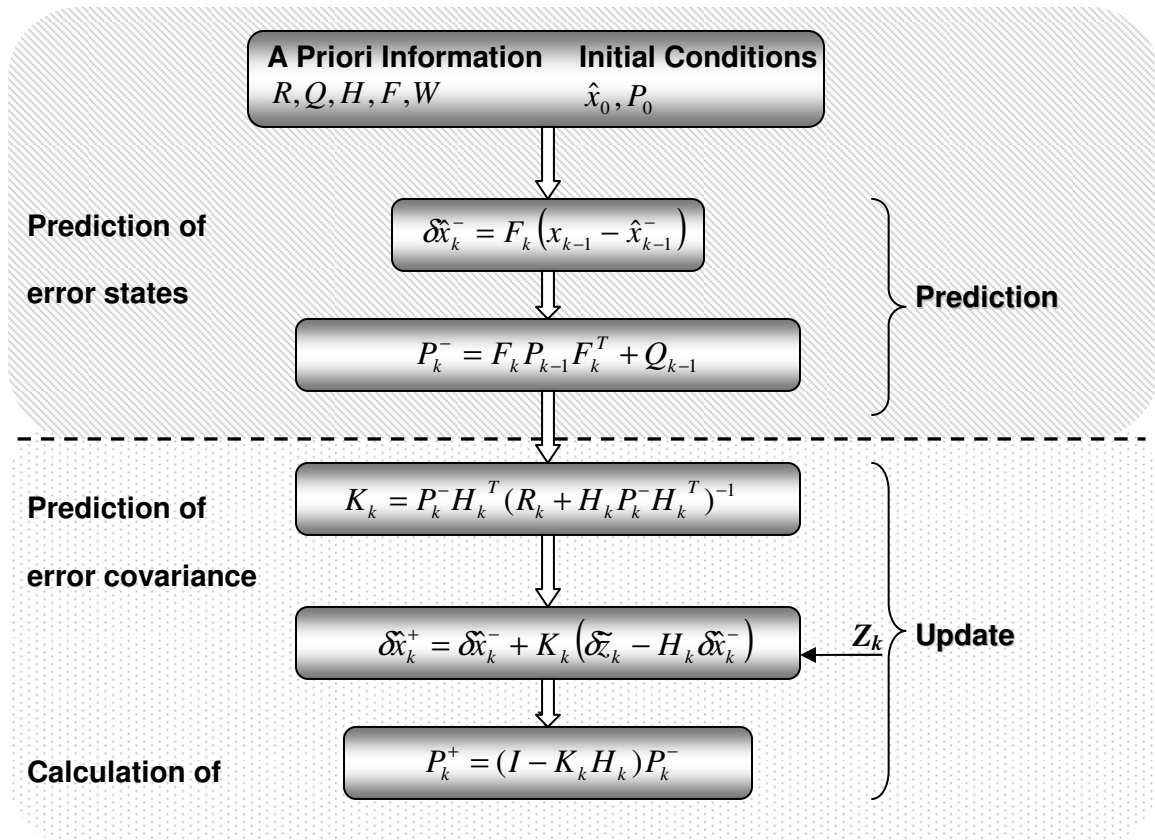


Figure 2-11. Extended Kalman Filter

#### ***2.5.4 A Note on Loosely and Tightly Coupled Simulations***

If GPS updates are available, the navigation accuracies for both loosely and tightly coupled integration strategies will be the same. The difference between the two strategies will be visible for the periods of time when less than four GPS satellites are available to the receiver. The time span representing less than four satellites will be referred to as signal degradation period. If a loosely coupled integration strategy is implemented, each GPS signal degradation period will have zero satellites. The reason is simply because the GPS KF needs a minimum of four satellites to produce position and velocity information. If less than four satellites are visible, the GPS KF cannot work due to its requirements of four satellites. Hence, for loosely coupled integration the navigation KF results for any degradation period will be the same as the results without any GPS signal availability.

On the contrary, the tightly coupled integration can take any number of GPS satellites during a GPS signal degradation period. For all the simulations shown in this thesis, the numbers of satellites available for the tightly coupled signal degradation periods were selected at random. Now consider an example from a dataset collected under open sky conditions. A first comparison was made for loosely and tightly coupled integration when four satellites were available as shown in Figure 2-12. The average drift for the two integration schemes were similar. The next simulation shows the result when three satellites were available. The tightly coupled integration drift errors were less than 50 m as it can use the information from any number of satellites. However, loosely coupled integration drift errors were close to 350 m since it needs minimum four satellites. Further reducing the number of satellites to 2, shows that tightly coupled results degraded



accordingly but stayed lower than loosely coupled results. For one and no satellites, the two integration strategies performed similarly.

Hence, if the same dataset is used in the thesis for loosely and tightly coupled integration, the results may look quite different for the same periods of satellite signal degradation periods depending on the number of available satellites.

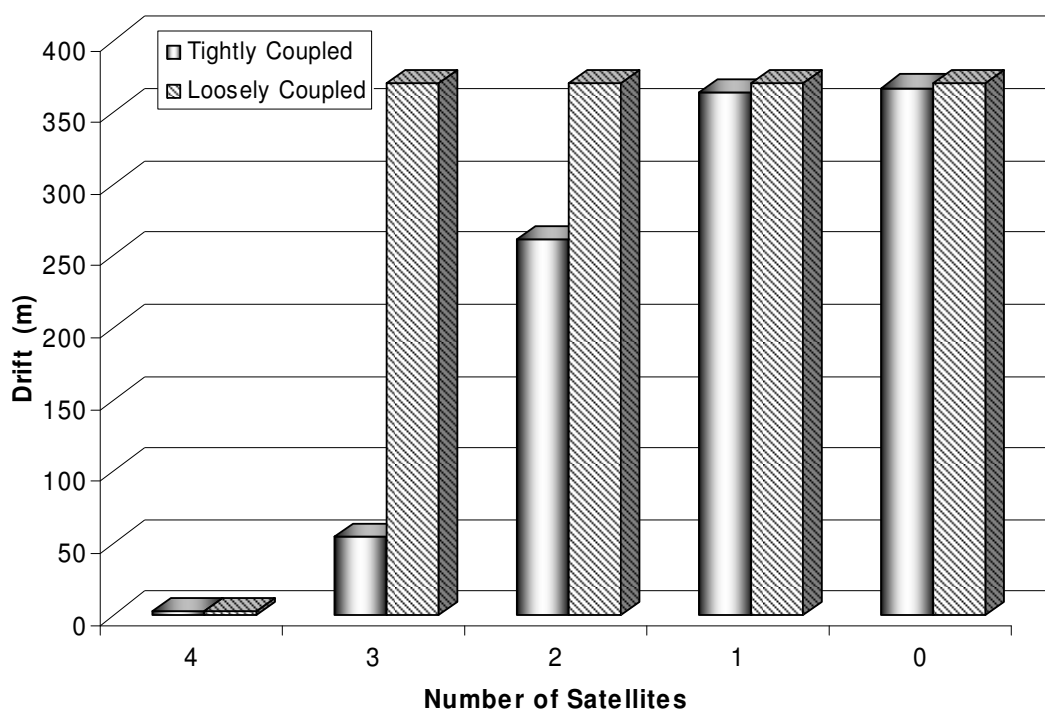


**Figure 2-12. Comparison between loosely and tightly coupled integration**

To mimic a real life situation, random numbers of satellites were selected for six signal degradation periods in the dataset used to obtain Figure 2-12. In this case, each degradation period was simulated for 60 seconds. For loosely coupled integration, the signal degradation period means stand-alone inertial navigation. For tightly coupled, however, any number of satellites can be used during the degradation period as long as they are less than four. Four satellites would mean that the GPS navigation is available.

The drift errors for the individual signal degradation period along with the mean drift error for the two integration schemes are provided in Figure 2-13.

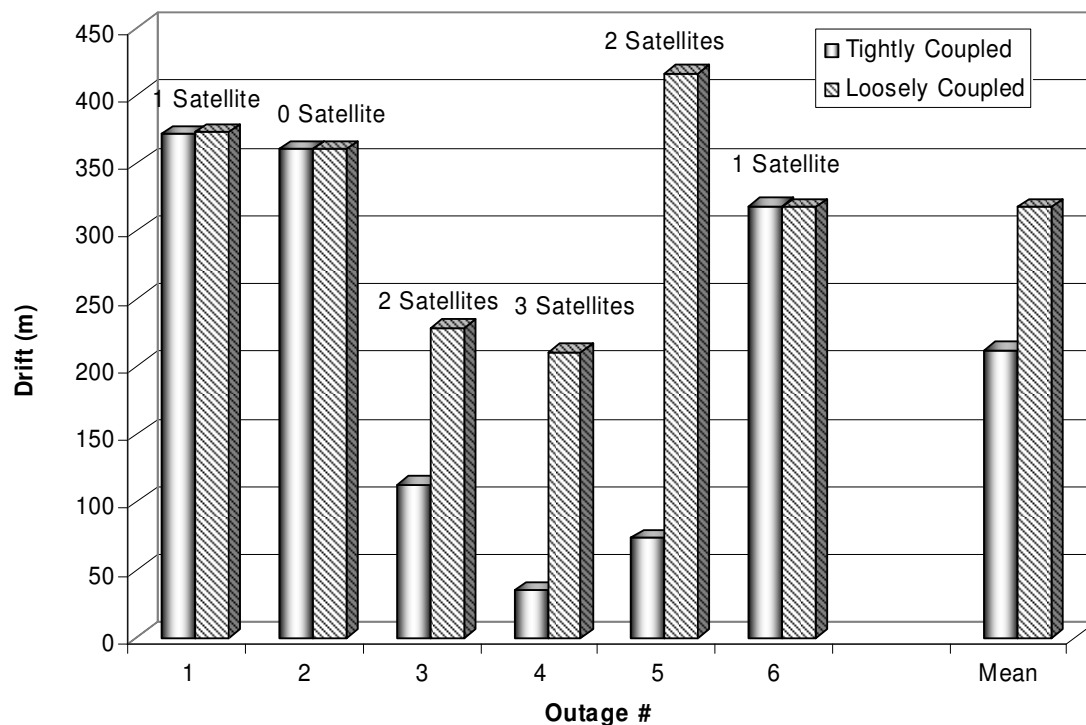


**Figure 2-13. Example of a dataset with simulated GPS signal degradation periods for two integration schemes**

For outages 1 (one satellite), 2 (0 satellites) and 6 (1 satellite), the performance for both loosely and tightly coupled integration was equivalent. However, the tightly coupled results are much better when two or more satellites were present. It is also clear from Figure 2-13 that the mean drift error for a dataset processed through loosely and tightly coupled may also be quite different depending on the number of satellites present during the degradation periods.

## 2.6 Velocity Constraints

Velocity constraints, also known as NHC can be used to further improve navigation parameters accuracy especially when GPS signal outages occur. NHC use the fact that a land vehicle cannot move sideways or vertically up or down and hence, these two velocity components should be zero. Hence, for NHC vehicle velocity components are required in vehicle body frame ( $v$ -frame) as compared to the  $l$ -frame.

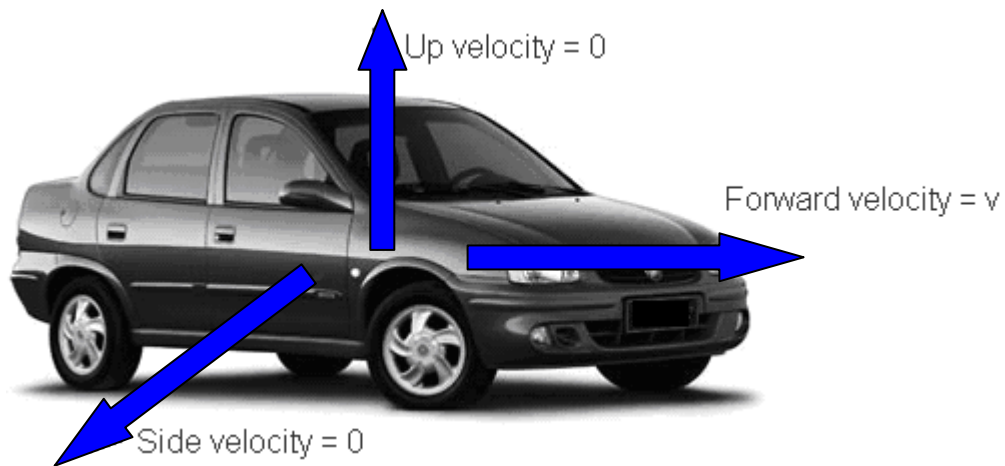


**Figure 2-14. Definition of NHC**

The NHC equations for the NED implementation of  $l$ -frame are as follows:

$$\left. \begin{array}{l} v_y^v \approx 0 \\ v_z^v \approx 0 \end{array} \right\} \quad \mathbf{2-40}$$

where

$y$  = sideways component of the velocity

$z$  = vertical component of the velocity

$v$  = vehicle body frame

Explanation of  $v$ -frame and the implementation of equation 2-40 for EKF are provided in the next two sections.

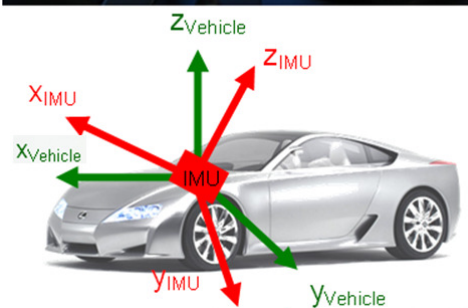
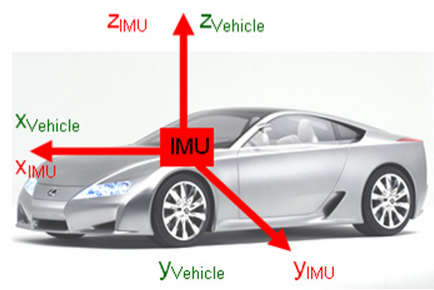
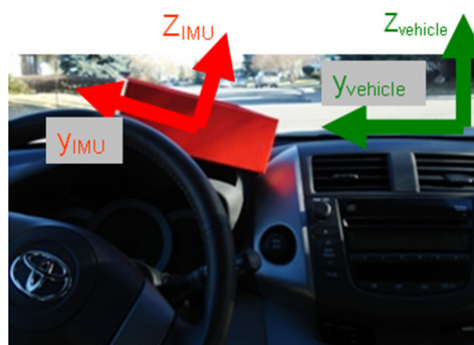
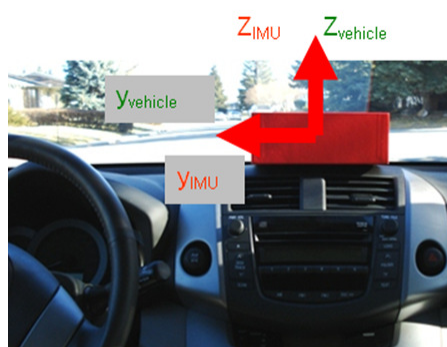
### 2.6.1 Vehicle Body Frame

Usually, an IMU frame is known as the  $b$ -frame. It is assumed that the  $b$ -frame is aligned with the  $v$ -frame, as shown in Figure 2-15A. However, this may not be the case and there may be some angular misalignment between the  $v$ -frame and the  $b$ -frame as illustrated in Figure 2-15B. This may be true for a PNS when the user is responsible for mounting the inertial system. More on this issue is covered in Chapter 6.

Assuming that the two frames have a roll angle  $\theta$ , pitch angle  $\phi$ , and azimuth angle  $\Psi$ , the DCM for these angles can be written as

$$\mathbf{R}_b^v = \begin{bmatrix} \cos \Psi \cos \phi & -\sin \Psi \cos \theta + \cos \Psi \sin \phi \sin \theta & \sin \Psi \sin \theta + \cos \Psi \sin \phi \cos \theta \\ \sin \Psi \cos \phi & \cos \Psi \cos \theta + \sin \Psi \sin \phi \sin \theta & -\cos \Psi \sin \theta + \sin \Psi \sin \phi \cos \theta \\ -\sin \phi & \cos \phi \sin \theta & \cos \phi \cos \theta \end{bmatrix}$$

**2-41**



A) A well aligned IMU with vehicle frame

B) Misaligned IMU and vehicle axes

**Figure 2-15. Schematics of the misalignment of the IMU with respect to the vehicle body frame (Images for the top most panels are taken from Google Images)**

### 2.6.2 Velocity computation in the $v$ -frame

Velocities from the navigation equations are given in the  $l$ -frame. These velocities can be converted into the  $v$ -frame after incorporating the appropriate rotations and the added

velocity due to the LA effect. The LA (Figure 2-16) is the distance from the point of contact of the vehicle to the ground with respect to the reference point which will be the centre of the GPS/INS unit.

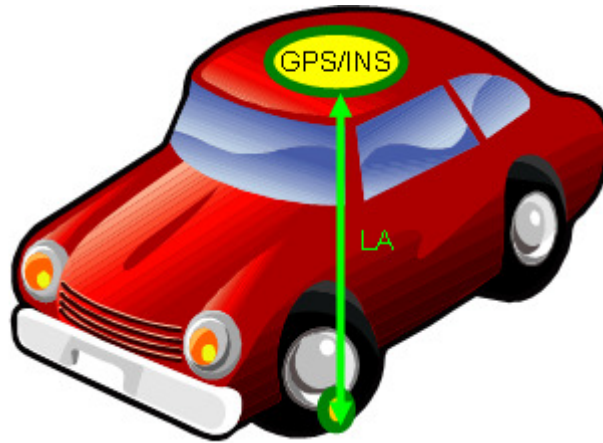


**Figure 2-16. Schematics of the lever arm involved for NHC**

In this case, everything needs to be represented in the  $v$ -frame as the velocity aiding of the vehicle is only possible in that frame. Therefore, the following equation can be written for an  $l$ -frame velocity represented in  $v$ -frame.

$$\tilde{v}^v = \tilde{R}_l^v \tilde{v}^l + R_b^v \tilde{\Omega}_{lb}^b LA_{wheel}^b \quad 2-42$$

where  $\tilde{R}_l^v = R_b^v \tilde{R}_l^b$

- $\tilde{\Omega}_{lb}^b$  is the rotation matrix that represents all the angular movement of the  $b$ -frame with respect to the  $l$ -frame and also contains the measurement errors  $\delta\Omega_{lb}^b$
- $LA_{wheel}^b$  is the lever arm in  $b$ -frame
- $\tilde{R}_l^b = R_l^b(I + E^l)$ , is the DCM from  $l$ -frame to  $b$ -frame which includes measurement errors  $E^l$

2-41 can be expanded by incorporating the error components ( $\delta$ ) as follows:

$$\begin{aligned}\tilde{v}^v &= R_b^v R_l^b (I + E^l) (v^l + \delta v^l) + R_b^v (\Omega_{lb}^b + \delta \Omega_{lb}^b) LA_{wheel}^b \\ \tilde{v}^v &= \underbrace{R_b^v R_l^b v^l + R_b^v \Omega_{lb}^b LA_{wheel}^b}_{v^v} + R_b^v R_l^b \delta v^l + R_b^v R_l^b E^l v^l + \underbrace{R_b^v R_l^b E^l \delta v^l}_{\approx 0} + R_b^v \delta \Omega_{lb}^b LA_{wheel}^b\end{aligned}\quad \mathbf{2-43}$$

where,  $\delta v^l$  is the measurement error in the velocity vector

Equation 2-43 shows the total velocity measured in the  $v$ -frame including the *true* velocity and the errors terms. The second order error terms will be small and therefore, can be ignored without degrading the estimated velocity for land based applications. The equation given above will be used in deriving the measurement equation in NED  $l$ -frame.

The two velocity component in this case will be the one measured in  $y$  and  $z$  axes of the  $v$ -frame. The NED implementation will take the 2<sup>nd</sup> and 3<sup>rd</sup> rows to make the measurement equation and measurement matrix as these two rows represents the two velocity components that we are after.

$$\delta z_k = \begin{bmatrix} \delta v_y^v \\ \delta v_z^v \end{bmatrix} \quad \mathbf{2-44}$$

$$H_k = \begin{bmatrix} \mathbf{0}_{1 \times 3} & r_{21} & r_{22} & r_{23} & -V^d r_{22} & V^d r_{21} & V^n r_{22} & la_{21} & la_{22} & la_{23} & \mathbf{0}_{1 \times 9} \\ \mathbf{0}_{1 \times 3} & r_{31} & r_{32} & r_{33} & -V^d r_{32} & -V^n r_{33} & -V^e r_{31} & la_{31} & la_{32} & la_{33} & \mathbf{0}_{1 \times 9} \\ & & & & +V^e r_{33} & +V^d r_{31} & +V^n r_{32} & & & & \end{bmatrix}$$

**2-45**

where the first three columns of the  $H_k$  matrix corresponds to the position errors in the state vector, the second set of three columns corresponds to the velocity errors, the third set of the three columns correspond to the angular displacements and the rest of the columns are for the sensor errors for loosely coupled integration. For tightly coupled integration, there will be two additional columns of zeros for clock bias and drift. Also, the  $r_{xx}$  are the elements of the matrix  $R_b^v R_l^b$

$$R_b^v R_l^b = \begin{bmatrix} r_{11} & r_{12} & r_{13} \\ r_{21} & r_{22} & r_{23} \\ r_{31} & r_{32} & r_{33} \end{bmatrix} \quad \mathbf{2-46}$$

and finally, the  $la_{xx}$  are the elements of the matrix  $R_b^v (LA_{wheel}^b)_{3 \times 3}$

$$R_b^v (LA_{wheel}^b)_{3 \times 3} = \begin{bmatrix} la_{11} & la_{12} & la_{13} \\ la_{21} & la_{22} & la_{23} \\ la_{31} & la_{32} & la_{33} \end{bmatrix}$$

Now that all the background information is provided, the actual contribution chapters of the thesis can be started. As described in Section 2.1, the first step towards the start of navigation is calibration of the inertial sensors and this is the first issue that will be explored for a PNS in the next chapter.



## Chapter Three: Calibration

MEMS inertial sensors are compact, inexpensive and most importantly, not controlled by governmental agencies due to their large error characteristics. Consequently, these sensors are the perfect candidate for PNDs. Usually, the manufacturer provides some calibration parameters that may be useful for navigation applications. The use of manufacturer specifications will also reduce the costs associated with large scale production of portable systems with inertial sensors. However, it is yet to be determined if the manufacturer specifications are sufficient. In the case that the manufacturer specifications are not sufficient, what are the parameters that are most important for navigation and what is the best strategy to obtain these parameters? The chapter provides the answers to the issues ([Syed et al., 2007-a](#)).

### 3.1 Inertial Measurement Unit Signal

The performance of an integrated INS/GPS system depends not only on signal quality from the GPS but also on the prediction quality of the IMU sensor errors. When the GPS signals are blocked for several seconds, or even minutes, the position predictions from the IMU drifts with respect to time since their errors are strongly time correlated due to the integration process as mentioned earlier. The drift rates depend largely on the minimization of the IMU residual errors. In the case of gyros, the following equation is typically used to describe the measured angular rate ([Schwarz and Wei, 2000](#)):

$$l_{\omega} = \omega + b_{\omega} + S\omega + N\omega + \varepsilon(\omega) \quad \mathbf{3-1}$$

$l_\omega$  is the measured angular rate,  $\omega$  is the true angular rate,  $b_\omega$  is the instrument bias,  $S$  is a matrix representing the scale factor,  $N$  is a matrix describing the non-orthogonality of the gyro triad and  $\varepsilon(\omega)$  represents the sensor noise. A similar equation can be used to describe the accelerometer observation ([Schwarz and Wei, 2000](#)):

$$l_f = f + b_f + S_1 f + S_2 f^2 + Nf + \delta g + \varepsilon(f) \quad \mathbf{3-2}$$

Similarly,  $l_f$  is the measured acceleration,  $f$  is the true specific force that we are after,  $b_f$  is the accelerometer instrument bias,  $S_1$  and  $S_2$  are the linear and nonlinear scale factor matrices,  $N$  is the non-orthogonality matrix,  $\delta g$  is the deviation from theoretical gravity and  $\varepsilon(f)$  represents the accelerometer noise.

From these two equations it is evident that bias, scale factor and non-orthogonality errors are the dominant deterministic elements. If these errors are minimized then their residual effects during navigation will in turn minimize the position drift of the navigation system. For example, an uncompensated accelerometer bias or scale factor will introduce an error in position proportional to the square of the elapsed time ( $t$ ). Similarly, an uncompensated gyro bias or scale factor will produce a position error proportional to time cubed ([El-Sheimy, 2006](#)).

During navigation these residual parameters are typically estimated as additional states of a filtering algorithm such as the KF. But convergence of the filter depends on the initial values. This means that initial estimates of these errors are needed for appropriate and timely online estimation. This is typically accomplished by performing calibration prior

to navigation. However, after the initial calibration a re-calibration is not required as the KF can update the bias and scale factor drifts.

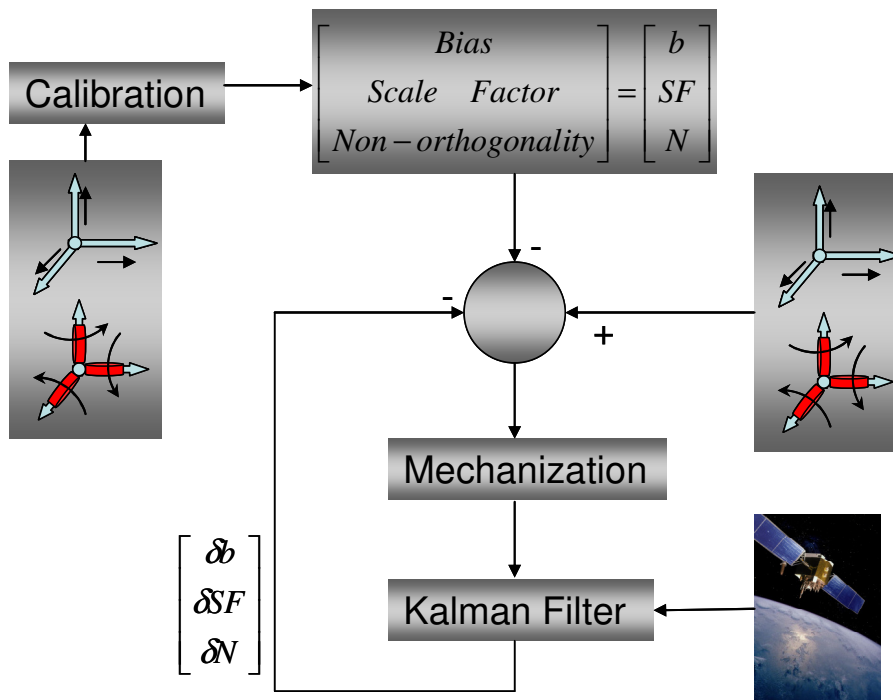


**Figure 3-1. Flowchart for inertial sensor error compensation. (Picture of GPS satellite is taken from Google Images)**

Factory-based sensor calibration of an INS is an expensive and time consuming process and is typically done for research specific high grade INSs. For very low-cost inertial sensors, such as MEMS sensors, a calibration is rarely performed in practice. For very high quantity and low-cost applications the sensors are often deployed without any calibration whatsoever. Yet there exist many applications that use MEMS sensors with GPS and require the maximum level of performance available. One such example would be the Attitude Heading Reference System (AHRS) for small airplanes ([Yuchnovicz et al., 1999](#)). Another example would be the use of inertial sensors in an integrated PNS.

For MEMS grade sensors the accelerometer and gyro bias instabilities can reach hundreds of micro-g and close to 150 deg/hr respectively ([Foxlin, 2002](#)). The linear scale factor errors can also be very large, in the thousands of parts per million. If these errors are unaccounted for the IMU stand-alone horizontal position estimate would drift. For example, this drift can be estimated using the following equation for all possible error sources for a single axis accelerometer in the horizontal plane:

$$\delta p(t) \approx \delta p_0 + \delta v_0 \Delta t + \delta b_{0a} \frac{\Delta t^2}{2} + \delta b_{0g} g \frac{\Delta t^3}{6} + \delta \theta_0 g \frac{\Delta t^2}{2} + \delta A_{0z} (V \Delta t) + SF_{0a} (f) \frac{\Delta t^2}{2} + SF_{0g} (\Delta A_z) (V \Delta t)$$

**3-3**

Table 3-1 lists all relevant terms in this equation. It can be seen that the dominant error sources are often due to the gyro and accelerometer biases, which result in errors proportional to time cubed and squared respectively as mentioned earlier. Also of interest are the roll/pitch misalignment angles and the scale factor errors as they introduce errors proportional to time squared.

Calibrations are particularly useful for the removal of misalignment errors since these should be relatively constant over time assuming a rigid body IMU platform. Unfortunately, for MEMS sensors the bias and scale factors can change over time or from power on to power off so a calibration strategy can only provide good initial estimates. It is unclear how important it is to start with a good estimate as compared to starting with any initial value and this issue will be explored first.

**Table 3-1. Description of approximate position error terms.**

<b>Term</b>	<b>Description</b>
$\delta p_0$	Position error at time $t_0$
$\delta v_0$	Velocity error at time $t_0$
$\Delta t$	Total elapsed time since last GPS update ( $\Delta t = t - t_0$ )
$\delta b_{0a}$	Residual accelerometer (uncompensated) bias at time $t_0$
$\delta b_{0g}$	Residual gyro (uncompensated) bias at time $t_0$
$\delta \theta_0$	Horizontal misalignment (uncompensated roll/pitch) angle error at time $t_0$
$\delta A_{0z} (V\Delta t)$	Azimuth misalignment multiplied by the approximate travel distance
$SF_{0a}$	Accelerometer residual scale factor error
$SF_{0g}$	Gyro residual scale factor error
$f$	Sensed acceleration
$g$	Acceleration due to gravity ( $\sim 9.81 \text{ m/s}^2$ )

To clearly visualize the effect of the residual errors, let us look at a simplified example. First, assume that an accelerometer bias of 0.5m/s/s is the only residual error for equation 3-3. The effect of this bias on the estimated position is shown in Figure 3-2. Next, error term that is of significant importance is the gyro bias. By assuming the other errors are zero, we can simulate the effect of this residual error on the position by using equation 3-3. For the residual gyro bias error of 0.005rad/s, the position error values are provided in Figure 3-2. Horizontal misalignment or non-orthogonalities in roll and pitch errors were used in the position error simulation next and are provided in Figure 3-2.

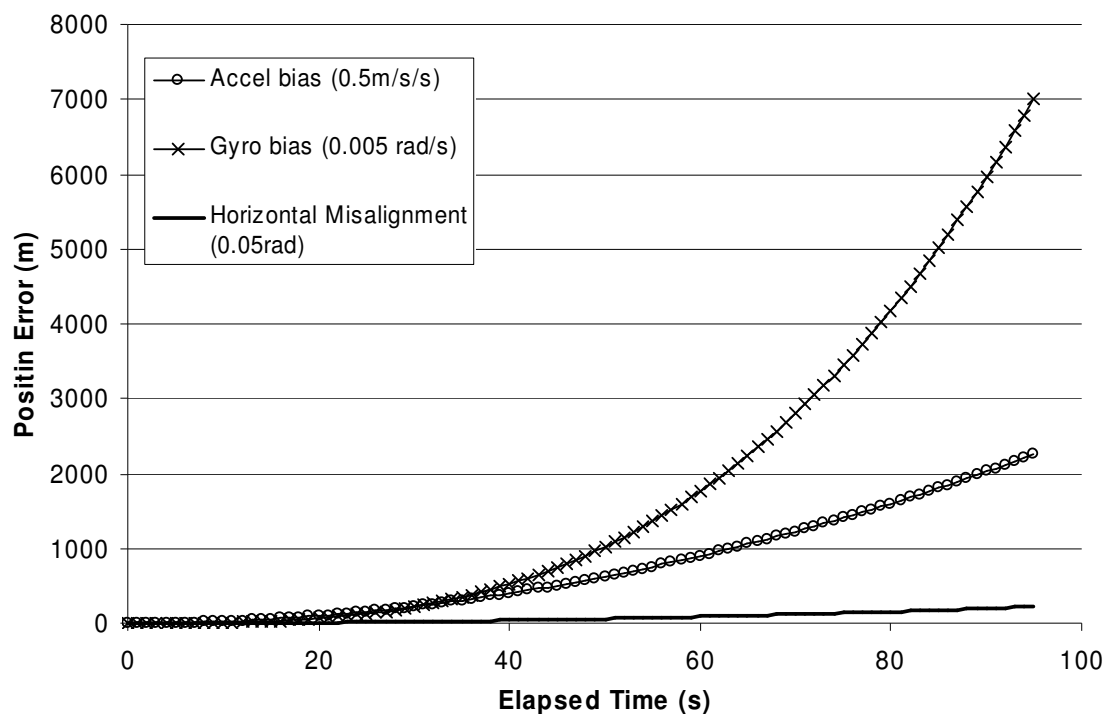


**Figure 3-2. Position errors due to residual errors in biases and horizontal misalignment**

### 3.2 INS Errors

Three different errors in the inertial sensors will be discussed here which are biases, linear scale factors and non-orthogonalities. There is usually a value for the bias and scale factor from the manufacturer provided specification sheet. As mentioned earlier, the importance of these values needed to be determined as they may be quite economical and time saving to use for a commercial system. Therefore, a thorough analysis was performed using the manufacturer specification on real datasets. The datasets consisted of three trajectories collected in Calgary from March to December 2005.

To test the manufacturer provided parameters, more than fifteen 30 seconds GPS signal outages were simulated. The outage simulation is simply performed by not using the GPS position updates during the specified time, thus letting the inertial sensors navigate in stand-alone mode. The maximum 3D position drift during each outage was taken for the analysis. Figure 3-3 presents the results when the specifications from the manufacturer datasheet were used. The average drift for this typical example is over 400 m (SpecSheet bar). For comparison, Figure 3-3 also provides the position drifts when three different calibration schemes were used before the start of navigation. The “Traditional Calib” and “New Calib” bars refer to the results when a traditional lab calibration and a newly developed calibration techniques were used. The last two bars in Figure 3-3 show the result of implementing a simple calibration scheme on gyros and accelerometer signals. The “SpecSheet” drift is too high for a navigation system and therefore, it is obvious that some other method is required to bring the errors to acceptable level.

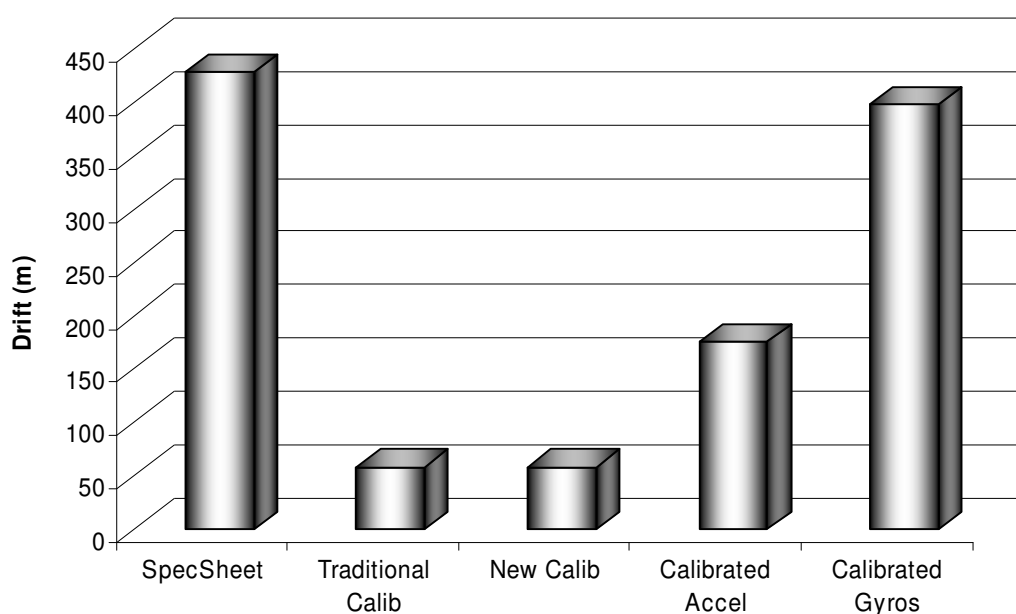


**Figure 3-3. Comparison of Different Calibration Methods for a Typical Dataset**

### 3.3 Simple Calibration Scheme

It is clear from Figure 3-2 that biases introduce significant position errors. One simple way to compensate for biases would be to take the average of the static period of a dataset and subtract it as a bias from the remaining data. In this case, the user needs to ensure that the first part of the navigation data consists of a stationary period. The gyro biases can be compensated using this method as the three gyros should be measuring zero for the angular rates when the system is static. However, the same is not true for accelerometer signals. The forward and lateral accelerometer signals for the static period are used to estimate the pitch and roll of the system. The vertical accelerometer bias may be corrected using the averaging technique. However, this technique will degrade the results if the bias error is small as compared to the sensor  $b$ -frame misalignment with  $l$ -frame.

This method was tested for both gyros and accelerometers. First, the improvement in the navigation solution due to the corrections in gyro signals were tested by keeping the accelerometer signals as constant. The constant accelerometer signals refer to well calibrated accelerometer signals. The raw gyro signals were corrected by using manufacturer specifications and then the static period of the gyro signals was subtracted as a bias. The resultant gyro signals were provided as input to the navigation equations and the drift errors for the GPS signal outage periods were computed. The results are shown in Figure 3-3 as “Calibrated Accel” bar with a magnitude of approximately 175m by using this simple technique.



Next the method was tested for the vertical accelerometer with the assumption that the system was aligned properly. In this case, the gyros signals were kept constant after full calibration. As the two horizontal accelerometers cannot be calibrated by this averaging method, the drift errors shown in Figure 3-3 as “Calibrated Gyros” bar has similar magnitude as specification sheet parameter results. This clearly indicates the need of performing some type of calibration before navigation.

### **3.4 Current INS Calibration Methods**

Calibration of inertial instruments is required to decrease the errors in the INS derived PVA of moving platforms. Calibration is the process of comparing instrument outputs with known reference information and determining the coefficients that force the output to agree with the reference information over a range of output values ([Chatfield, 1997](#)). To determine the error parameters given in equations 3-1 and 3-2, the first step in inertial navigation is to calibrate the sensors. Generally, calibration methods such as the *l*-frame method, the six-position static method and rate tests are used for this purpose.

The standard methods used for calibrating IMUs were primarily designed for in lab tests and high quality sensors, such as navigation or tactical grade IMUs. These tests often require the use of special references such as alignment to a given frame or specialized equipment. The six-position static and rate tests are among the most commonly used ([Titterton and Weston, 1997](#)) calibration methods. The six position method requires the inertial system to be mounted on a levelled surface with each sensitive axis of every sensor pointing alternately up and down. For a triad of orthogonal sensors this results in

a total of six positions. The bias and scale factors can then be calculated using the following equations:

$$b = \frac{l_f^{up} + l_f^{down}}{2} \quad 3-4$$

$$S = \frac{l_f^{up} - l_f^{down} - 2 \times K}{2 \times K} \quad 3-5$$

Where  $l_f^{up}$  is the sensor measurement when the sensitive axis is pointed upward,  $l_f^{down}$  is the measurement when the sensitive axis is pointed downwards and  $K$  is the known reference signal. For accelerometers  $K$  is the local gravity constant and for gyros  $K$  is the magnitude of the earth rotation rate projection to the vertical at a given latitude. However, the earth rotation rate can only be used for navigation and tactical grade gyros, since low grade gyros such as MEMS suffer from bias instability and noise levels that completely mask the earth's reference signal.

The six-position calibration accuracy depends on how well the axes are aligned with the vertical axes of the  $l$ -frame. For accurate results a perfect cube shaped mounting frame is required. This standard calibration method can be used to determine the bias and scale factors of the sensors, but cannot estimate the axes misalignments (non-orthogonalities). To estimate the non-orthogonalities, an improved six-position test can be performed which takes into account all three types of errors ([Niu, 2002](#)). In matrix form, the output of a triad of sensors (e.g. accelerometers) can be represented as:

$$\begin{bmatrix} l_{ax} \\ l_{ay} \\ l_{az} \end{bmatrix} = \begin{bmatrix} m_{xx} & m_{xy} & m_{xz} \\ m_{yx} & m_{yy} & m_{yz} \\ m_{zx} & m_{zy} & m_{zz} \end{bmatrix} \begin{bmatrix} a_x \\ a_y \\ a_z \end{bmatrix} + \begin{bmatrix} b_{ax} \\ b_{ay} \\ b_{az} \end{bmatrix} \quad \text{or} \quad \begin{bmatrix} l_{ax} \\ l_{ay} \\ l_{az} \end{bmatrix} = \underbrace{\begin{bmatrix} m_{xx} & m_{xy} & m_{xz} & b_{ax} \\ m_{yx} & m_{yy} & m_{yz} & b_{ay} \\ m_{zx} & m_{zy} & m_{zz} & b_{az} \end{bmatrix}}_M \underbrace{\begin{bmatrix} a_x \\ a_y \\ a_z \\ 1 \end{bmatrix}}_a \quad \mathbf{3-6}$$

The diagonal  $m$  elements represent the scale factors, the off-diagonal  $m$  elements are the non-orthogonalities and the  $b$  components are the biases. By aligning the IMU using the standard six-position method the ideal accelerations would be measured as:

$$a_1' = \begin{bmatrix} g \\ 0 \\ 0 \end{bmatrix}, a_2' = \begin{bmatrix} -g \\ 0 \\ 0 \end{bmatrix}, a_3' = \begin{bmatrix} 0 \\ g \\ 0 \end{bmatrix}, a_4' = \begin{bmatrix} 0 \\ -g \\ 0 \end{bmatrix}, a_5' = \begin{bmatrix} 0 \\ 0 \\ g \end{bmatrix}, a_6' = \begin{bmatrix} 0 \\ 0 \\ -g \end{bmatrix} \quad \mathbf{3-7}$$

Consequently, the design matrix for the least squares adjustment ( $A$ ) will be of the form:

$$A = \begin{bmatrix} a_1' & a_2' & a_3' & a_4' & a_5' & a_6' \\ 1 & 1 & 1 & 1 & 1 & 1 \end{bmatrix} \quad \mathbf{3-8}$$

and the raw output of the sensors in Volts would be measured as a matrix  $U$  as follows:

$$U = \begin{bmatrix} u_1 & u_2 & u_3 & u_4 & u_5 & u_6 \end{bmatrix} \quad \mathbf{3-9}$$

where  $u_1 = \begin{bmatrix} l_{ax} \\ l_{ay} \\ l_{az} \end{bmatrix}_{X\text{-axis pointing up}}$   $u_2 = \begin{bmatrix} l_{ax} \\ l_{ay} \\ l_{az} \end{bmatrix}_{X\text{-axis pointing down}}$  and so on.

The desire is to extract the components of the matrix  $M$  in equation 3-6. This can be done using the well-known solution of least squares:

$$M = U.A^T.(AA^T)^{-1} \quad \mathbf{3-10}$$

Similarly, the bias and scale factor of a superior quality gyro can be estimated when the average of the static value is used in equation 3-9 for at least 10 to 15 minutes ([Hou, 2004](#)). However, the six position static test cannot be used if a low quality gyro is part of the system as the earth rotation rate will be unobservable due to high noise and drift errors.

Angular rate tests are used for calibrating the biases, scale factors and non-orthogonalities of the gyros for lower grade navigation systems. If the rate tests and the improved six-position static method are used together, one can determine all the error components even for low cost sensors. Rate tests are typically done using a precise rate turntable. By rotating the unit through given turning rates and comparing the outputs of the IMU to these references, the biases, scale factors and non-orthogonalities can be estimated. This is typically accomplished by rotating the table through a defined angular rate in both the clockwise and counter clockwise directions. The improved six position static test along with the angular rate test will give the biases, scale factors and non-orthogonalities of the accelerometers and gyros. These two tests together will be referred to as SPM (six position method).

A third method of calibration uses precise alignment of a multi-axes turntable to the  $l$ -frame. The IMU is mounted on the aligned turntable and then the unit is rotated through a series of accurately known angles and positioned in different orientations with respect to the  $l$ -frame. This technique makes use of the gravity and earth rotation rates as references ([El-Sheimy, 2006](#)). Again similar to the SPM, precise alignment with the  $l$ -frame is the main requirement and therefore even small orientation errors will contaminate the error

estimates. Also, similar to the SPM,  $l$ -frame calibration for MEMS suffers from the fact that the earth rotation is a very weak signal and is typically buried within the sensor noise for low grade inertial sensors.

### 3.5 Multi-position Calibration Method

Multi-position calibration method (MPM) uses the combined three axes effect of the local gravity and earth rotation to generate the references needed for calibration regardless of the misalignment to the  $l$ -frame. Using a redundant number of IMU rotations, the IMU errors can then be estimated using a least squares adjustment.

#### 3.5.1 General model

According to ([Shin and El-Sheimy, 2002](#)) any measurement vector can be expressed by linear combinations of three-orthonormal vectors corresponding to the three orthogonal axes of the accelerometers or gyros. This characteristic holds even if the three axes are misaligned, which shows the usefulness of this method. If we start with a perfectly orthogonal and stationary triad of accelerometers then their relation to the  $l$ -frame gravity vector can be expressed as:

$$\left. \begin{aligned} gx &= -g \bullet \cos \alpha \\ gy &= -g \bullet \cos \beta \\ gz &= -g \bullet \cos \gamma \end{aligned} \right\} \quad \mathbf{3-11}$$

Where  $\alpha$ ,  $\beta$  and  $\gamma$  are the angles generated between the local gravity vector and the IMU  $x$ ,  $y$ ,  $z$  axes as shown in Figure 3-4.

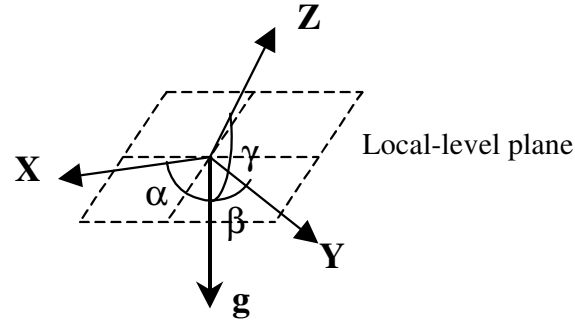


**Figure 3-4. Misaligned orthogonal sensor triad with respect to the  $l$ -frame (After: [Shin and El-Sheimy, 2002](#))**

Using these angles the following relationship forms the general model for this calibration method:

$$gx^2 + gy^2 + gz^2 = |g|^2 (\cos^2 \alpha + \cos^2 \beta + \cos^2 \gamma) = |g|^2 \quad 3-12$$

A similar model can be developed for the gyros using the earth rotation rate as the reference.

### ***3.5.2 Inclusion of non-orthogonality***

This method considers non-orthogonality by creating a series of rotation matrices that define the relationship of the misaligned axes to those of the perfectly orthogonal triad considered in the general model. Considering first the  $y$  axis, if it is misaligned about the  $z$  axis by  $\theta_{yz}$  then the rotation matrix needed to rotate back to the orthogonal  $y$  axis can be represented by:

$$y_1 = R_z y; \text{ where } R_z = \begin{bmatrix} \cos \theta_{yz} & -\sin \theta_{yz} & 0 \\ \sin \theta_{yz} & \cos \theta_{yz} & 0 \\ 0 & 0 & 1 \end{bmatrix} \quad \mathbf{3-13}$$

Similarly, a non-orthogonality of the z axis can be represented by two elementary rotations, one about x ( $\theta_{zx}$ ) and another about y ( $\theta_{zy}$ ). The forms of these two matrices would be:

$$R_x = \begin{bmatrix} 1 & 0 & 0 \\ 0 & \cos \theta_{zx} & -\sin \theta_{zx} \\ 0 & \sin \theta_{zx} & \cos \theta_{zx} \end{bmatrix} \text{ and } R_y = \begin{bmatrix} \cos \theta_{zy} & 0 & \sin \theta_{zy} \\ 0 & 1 & 0 \\ -\sin \theta_{zy} & 0 & \cos \theta_{zy} \end{bmatrix} \quad \mathbf{3-14}$$

In shorthand notation, all vectors in 3D space can be expressed as linear combinations of these three vectors for an accelerometer or gyro triad. Here it is considered that the x-axis is the reference axis and the above misalignments are given with respect to the x-axis:

$$\left. \begin{array}{l} x_1 : (1,0,0) \\ y_1 : (-\sin \theta_{yz}, \cos \theta_{yz}, 0) \\ z_1 : (\sin \theta_{zy}, -\sin \theta_{zx} \cos \theta_{zy}, \cos \theta_{zx} \cos \theta_{zy}) \end{array} \right\} \quad \mathbf{3-15}$$

Going back to the general model of the accelerometers, the values sensed by the non-orthogonal axes would be:

$$\left. \begin{array}{l} gx_1 = gx \\ gy_1 = -gx \cdot \sin \theta_{yz} + gy \cdot \cos \theta_{yz} \\ gz_1 = gx \cdot \sin \theta_{zy} - gy \cdot \sin \theta_{zx} \cdot \cos \theta_{zy} + gz \cdot \cos \theta_{zx} \cdot \cos \theta_{zy} \end{array} \right\} \quad \mathbf{3-16}$$

In matrix form, this system of equations can be more easily represented as:

$$\begin{bmatrix} gx_1 \\ gy_1 \\ gz_1 \end{bmatrix} = \begin{bmatrix} 1 & 0 & 0 \\ -\sin \theta_{gyz} & \cos \theta_{gyz} & 0 \\ \sin \theta_{gzy} & -\sin \theta_{gzx} \cos \theta_{gzy} & \cos \theta_{gzx} \cos \theta_{gzy} \end{bmatrix} \begin{bmatrix} gx \\ gy \\ gz \end{bmatrix} \quad 3-17$$

And assuming small misalignment angles it can be approximated by:

$$\begin{bmatrix} gx_1 \\ gy_1 \\ gz_1 \end{bmatrix} = \begin{bmatrix} 1 & 0 & 0 \\ -\theta_{gyz} & 1 & 0 \\ \theta_{gzy} & -\theta_{gzx} & 1 \end{bmatrix} \begin{bmatrix} gx \\ gy \\ gz \end{bmatrix} \quad 3-18$$

### 3.5.3 Inclusion of biases and scale factors

The introduction of bias and scale factor errors into the non-orthogonality model would constitute the major errors in equation 3-3. For the accelerometers, the sensed signals would be:

$$\left. \begin{aligned} l_{gx} &= b_{gx} + (I + s_{gx})gx \\ l_{gy} &= b_{gy} + (I + s_{gy})(-gx \cdot \sin \theta_{yz} + gy \cdot \cos \theta_{yz}) \\ l_{gz} &= b_{gz} + (I + s_{gz})(gx \cdot \sin \theta_{zy} - gy \cdot \sin \theta_{zx} \cdot \cos \theta_{zy} + gz \cdot \cos \theta_{zx} \cdot \cos \theta_{zy}) \end{aligned} \right\} \quad 3-19$$

By rearranging these equations we can solve for  $gx$ ,  $gy$  and  $gz$  as was done in ([Shin and El-Sheimy, 2002](#)). Or more directly, using the approximation in equation 3-18, we can solve the following system of equations:

$$\begin{bmatrix} l_{gx} \\ l_{gy} \\ l_{gz} \end{bmatrix} = \begin{bmatrix} 1 + s_{gx} & 0 & 0 \\ -\theta_{gyz} & 1 + s_{gy} & 0 \\ \theta_{gzy} & -\theta_{gzx} & 1 + s_{gz} \end{bmatrix} \begin{bmatrix} gx \\ gy \\ gz \end{bmatrix} + \begin{bmatrix} b_{gx} \\ b_{gy} \\ b_{gz} \end{bmatrix} \quad 3-20$$

Then, using the general model we can create an implicit form of the equations as follows:

$$gx^2 + gy^2 + gz^2 - |g|^2 = 0, \text{ for the accelerometers} \quad 3-21$$



$$\omega_x^2 + \omega_y^2 + \omega_z^2 - |\omega|^2 = 0, \text{ for the gyros} \quad 3-22$$

### 3.5.4 Least squares adjustment

Using these implicit mathematical models, a weighted least squares adjustment can be performed using a combined case with weighted parameters as described in ([Krakiwsky, 1990](#)). The adjustment aims to minimize the sum of squared errors (SSE) such that the linearized mathematical model is upheld:

Minimize

$$\hat{r}^T C_l^{-1} \hat{r} \quad 3-23$$

Such that

$$A_l \hat{\delta} + B \hat{r} + w = 0 \quad 3-24$$

Where  $w$  is the misclosure vector and,  $A_l$  and  $B$  are design matrices consisting of the partial derivatives with respect to the estimated states (sensor biases, scale factors, non-orthogonalities) and the measurements respectively and are provided as follows:

$$A_l = \begin{bmatrix} \frac{\partial \ddot{f}_g}{\partial b_{gx}} & \frac{\partial \ddot{f}_g}{\partial b_{gy}} & \frac{\partial \ddot{f}_g}{\partial b_{gz}} & \frac{\partial \ddot{f}_g}{\partial s_{gx}} & \frac{\partial \ddot{f}_g}{\partial s_{gy}} & \frac{\partial \ddot{f}_g}{\partial s_{gz}} & \frac{\partial \ddot{f}_g}{\partial \theta_{gyz}} & \frac{\partial \ddot{f}_g}{\partial \theta_{gzx}} & \frac{\partial \ddot{f}_g}{\partial \theta_{gzy}} \\ \dots & \dots & \dots & \dots & \dots & \dots & \dots & \dots & \dots \end{bmatrix}$$

$$B = \begin{bmatrix} \dots & \dots & \dots & \dots & \dots & \dots & \dots & \dots & \dots \\ & & \frac{\partial f_g}{\partial l_{gx}} & \frac{\partial f_g}{\partial l_{gy}} & \frac{\partial f_g}{\partial l_{gz}} & & & & \\ & & & & & \dots & \dots & \dots & \end{bmatrix}$$

$$w = (\dots f_g(x, l) \dots)^T$$

$\delta$ ,  $r$  and  $C_l^{-1}$  represent the corrections to the estimated states, observed measurements and the covariance of the observed measurements. The solution is as follows:

$$\hat{x} = x + \hat{\delta} \quad \mathbf{3-25}$$

$$\hat{l} = l + \hat{r} \quad \mathbf{3-26}$$

$$\hat{\delta} = -\left(A_1^T (BC_l B^T)^{-1} A_1 + C_x^{-1}\right)^{-1} A_1^T (BC_l B^T)^{-1} w \quad \mathbf{3-27}$$

$$C_{\hat{x}} = \left(A_1^T (BC_l B^T)^{-1} A_1 + C_x^{-1}\right)^{-1} = N^{-1} \quad \mathbf{3-28}$$

where  $C_x$  is the covariance matrix for the required solution

For further details please refer to ([Shin and El-Sheimy, 2002](#)) and ([Shin, 2001](#)). The termination criterion was set to 300 iterations for the least squares but the results typically converge in 10 to 30 iterations.

### **3.5.5 Multi-position schemes**

To avoid singularity when calculating the inverse of the normal matrix ( $N^{-1}$ ), it is required that as many attitudes are observed as parameters estimated. For a triad of accelerometers or gyros we would typically be estimating three biases, scale factors and non-orthogonalities, making a total of nine unknowns per triad. This means that a minimum of nine different attitudes would have to be used within the adjustment. But in reality, more positions that cover various attitudes are needed to get reliable results ([Shin and El-Sheimy, 2002](#)).

For the purpose of this analysis a total of 26 different attitudes were used (some attitudes are shown in Figure 3-5) within the adjustment. The first six positions consisted of each face down. Then each side of the IMU frame was put down for another 12 positions. Finally, each corner was placed down to generate another 8 positions. The exact alignments of these placements were not important, just that each position was significantly different from the others to avoid singularities. To avoid confusion with other calibration methods, Shin and El-Sheimy's method ([Shin and El-Sheimy, 2002](#)) will be referred to as MPM for the continuum of this chapter. Also, to note is that this method can only deal with small biases and will not work for systems with high bias errors.

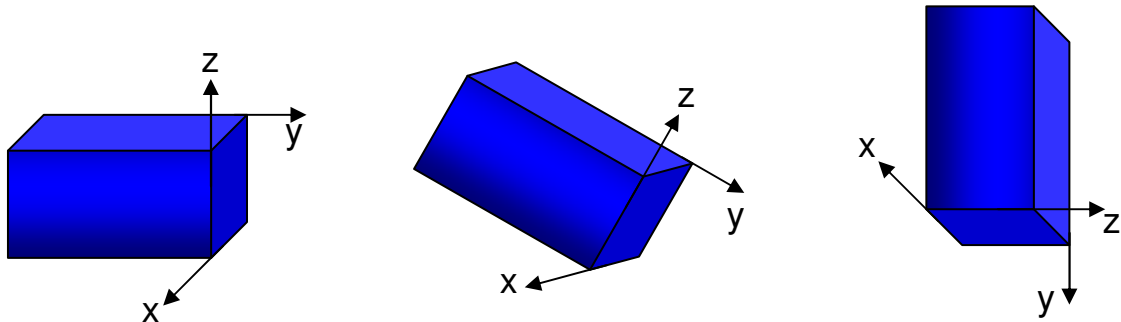


**Figure 3-5. An example of IMU rotation scheme**

### 3.6 Modified Multi-Position Calibration

The main drawback in using the MPM is that the gyro reference (earth rotation rate) is a weak signal which can result in observability problems when estimating the scale factors and non-orthogonalities. In ([Shin and El-Sheimy, 2002](#)) this problem was not addressed, however, it will be shown in the following sections that for MEMS sensors these errors can contribute largely to the overall position error during prediction periods. Instead of

using the earth rotation as a reference signal, this technique modifies the MPM by introducing a rotation rate table. Refer to Table 3-2 for a summary of the available calibration methods. The summary also contains the information about the proposed method, Modified Multi-Position Method (MMPM).

**Table 3-2. Summary of available calibration methods. H = High grade system, L= Low grade system and R = Required**

		Simple		SPM		MPM		MMPM	
Accelerometer	Bias			H	L	H		H	L
	Scale Factor			H	L	H		H	L
	Non-ortho			H	L	H		H	L
Gyro	Bias	H	L	H	L	H		H	L
	Scale Factor			H	L			H	L
	Non-ortho			H	L			H	L
	Turntable			R	R			R	R
	Special Alignment			R	R				

Another issue with the MPM for MEMS IMUs is that it is difficult to converge to reasonable bias and scale factor values for MEMS sensors without an initial rough estimate of these error values. This is due to the large parameter variation of these sensors. To provide approximate starting values for the biases and scale factors of the accelerometers, the positions closest to face up and face down configurations were used in the MMPM.

The reason these are only approximate values is due to the rough installation of these positions with respect to the vertical gravity vector; a perfect cube was not used as in the SPM. For the starting value of the gyros, any static output can be regarded as the gyro bias since the earth rotation is negligible compared to the original gyro biases.

In summary, the MMPM has the following two differences than the previously published paper by ([Shin and El-Sheimy, 2002](#)) for use with low cost MEMS inertial sensors:

- 1) Use of approximate up and down configurations to remove the large biases of low grade MEMS accelerometer sensors and use of an initial static period as bias for gyros sensor signals
- 2) Inclusion of a single axis turntable for the calculation of scale factor and non-orthogonalities of gyros. Here it is important to reiterate that any specialized alignment of the IMU is not required.

The intent of MMPM is to remove large deterministic MEMS sensor errors using as practical a method as possible. The current method in ([Shin and El-Sheimy, 2002](#)) does not estimate gyro scale factors and non-orthogonalities. Thus the first step will be to analyze the impact of neglecting these errors.

By using a rotation rate turntable, the gyro scale factors and non-orthogonalities errors computations can then be included into the MMPM. The calibration results of this MMPM are compared to those of SPM using a perfect cube. The calibration estimates are compared directly and are also applied in a real navigation field test to compare the positional error drifts during several induced GPS signal outages. During these outage

periods the IMU will provide the navigation parameters to the KF, however, the predicted position errors expected to increase as outlined in equation 3-3. Finally, since there is a wide variety of MEMS sensors, three very different MEMS units were used for comparison of these calibration methods. The new calibration procedure was run on a Pentium 4, 3.2 GHz CPU and took less than a minute to complete starting from raw measurements.

### **3.7 Results**

This section contains comparison between the commonly used calibration methods that requires a cube shaped system with a MPPM that does not require a specific shape for the system.

#### ***3.7.1 Test Description***

As mentioned before, the different calibration methods were compared not only by the calibrated sensor parameters, but also by the navigation performance in field tests using these compensated parameters. The two MEMS IMUs included in these tests were the BEI MotionPak II and the MEMS custom inertial unit (CIU). The MotionPak unit is a relatively high grade MEMS IMU while the CIU would be classified as a low grade MEMS IMU.

The CIU was developed by the Mobile Multi-Sensor Systems (MMSS) research group at the University of Calgary and more details can be found in ([Niu and El-Sheimy, 2005](#)). The CIU has Analog Devices Inc. inertial sensors. All equipments were setup in a 2003 Dodge Grand Caravan for testing on the same vehicle trajectories. Two NovAtel GPS

OEM4 antennas, a MotionPak II inertial measurement unit and a high end tactical grade inertial system were installed on the roof, as shown in Figure 3-6.



**Figure 3-6. Test vehicle setup.**

The CIU was installed in the cargo area of the van on a rigid platform along with the batteries and the laptops needed to record the data. The first dataset was collected around the University of Calgary research park area in mainly open sky conditions with several short (<10 seconds) real GPS blockage periods. Two separate loops were followed in clockwise and counter clockwise directions along the same trajectory. The first loop was short while the second was nearly twice the circumference of the first. Both loops involved stops for four to six minutes near the same open sky areas. This trajectory is a typical low speed scenario which mimics driving in residential areas. In the remainder of the paper this trajectory will be referred to as Run 1. In Run 1, eleven 60 second GPS signal outages were simulated by removing the GPS updates from the KF.

The second trajectory, called Run 2, started from the University campus and ended at the Calgary International Airport. This trajectory involved moderate turns and accelerations, along with natural GPS signal outages such as bridges and underpasses. Run 2 was a typical highway scenario. The final trajectory, Run 3, was simply the reverse direction of run 2. Runs 2 and 3 had six and ten 60 seconds GPS signal outages respectively. Figure 3-7 shows the trajectory for Run 3 along with the locations of some 60 seconds GPS signal outages.

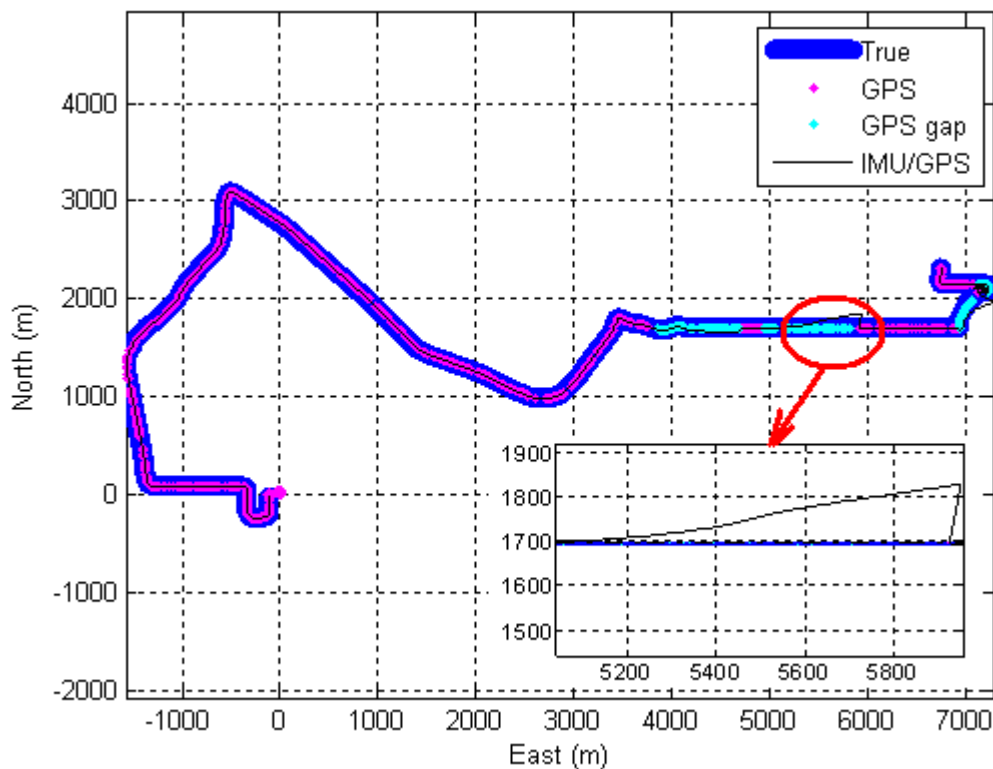


**Figure 3-7. Trajectory for run 3 along with simulated GPS outages.**

The CIU position errors during GPS signal outages were obtained and then compared with the reference solution. This true solution was acquired from a post-processed



smoothed best estimate of Litton 200 IMU (LN200) combined with differential GPS (DGPS) using POSPac™ software of Applanix Corporation.

In addition to the tests described above with proper reference trajectories and orientations of the unit in the vehicle, another test results will also be discussed. This test does not have a reference trajectory and the unit orientation was also approximate. Single point GPS was used as reference in this particular dataset. The unit was not properly fixed in the vehicle and was only left on the dashboard area to mimic a real life PND situation where the orientation and placement of the unit will be at the user's discretion. Three 30s GPS outages were simulated along with one 60 s outage for this dataset. The trajectory with the GPS outage locations is provided in Figure 3-8.

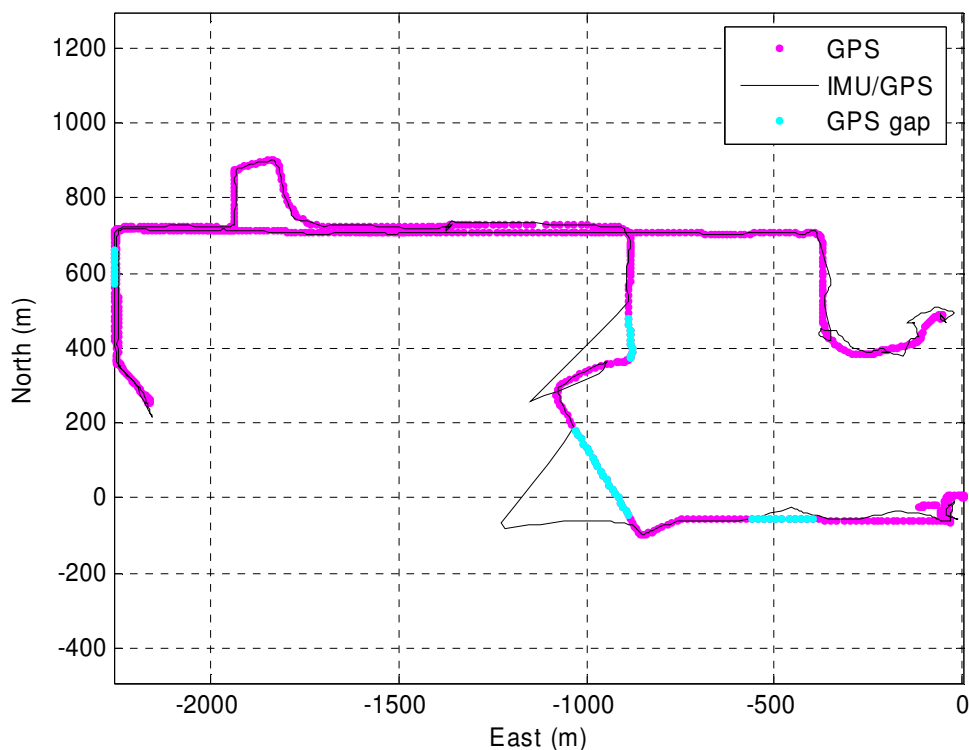


**Figure 3-8. Trajectory for PNS unit. The inertial trajectory shown is for MMPM.**

The results are divided into four sections. Section 3.7.2 provides motivation for including gyro scale factor and non-orthogonality calibration in the MMPM by comparing the navigation solution of the CIU with and without compensation of these calibration values. Section 3.7.3 includes comparisons between the bias and scale factors computed by the MMPM and the SPM. In the third section, position drifts during the simulated GPS outages for both MotionPak II and the CIU are shown to compare the navigation accuracies. The last section contains the results of PND that has very difficult shape (sides and corners are not straight) for standard calibration procedures.

### ***3.7.2 Effect of full gyro calibration using a turntable***

It is important to analyze if gyro scale factor and non-orthogonalities are important for navigation. If these two parameters are important, there is a need of MMPM. The effect of these errors will be analyzed for the CIU for a general idea of their importance for actual field datasets. Equation 3-3 can also be consulted where we find that these errors are typically proportional to time squared.

Figure 3-9 shows the maximum position drifts obtained without calibrating/compensating for scale factor (SF) errors and non-orthogonalities, i.e., using the MPM without the use of a turntable, and the drifts obtained by the MMPM. As the MPM cannot converge when the sensor errors are significantly large, the solution shown here was obtained by subtracting pre-calculated sensor biases. Similar results were obtained when run 2 and run 3 position drifts were analyzed for the two methods described above. The results in Figure 3-9, clearly indicates that MEMS sensors, SF errors and non-orthogonalities play

an important role in the overall navigation accuracy of the system which can only be estimated using a turntable.

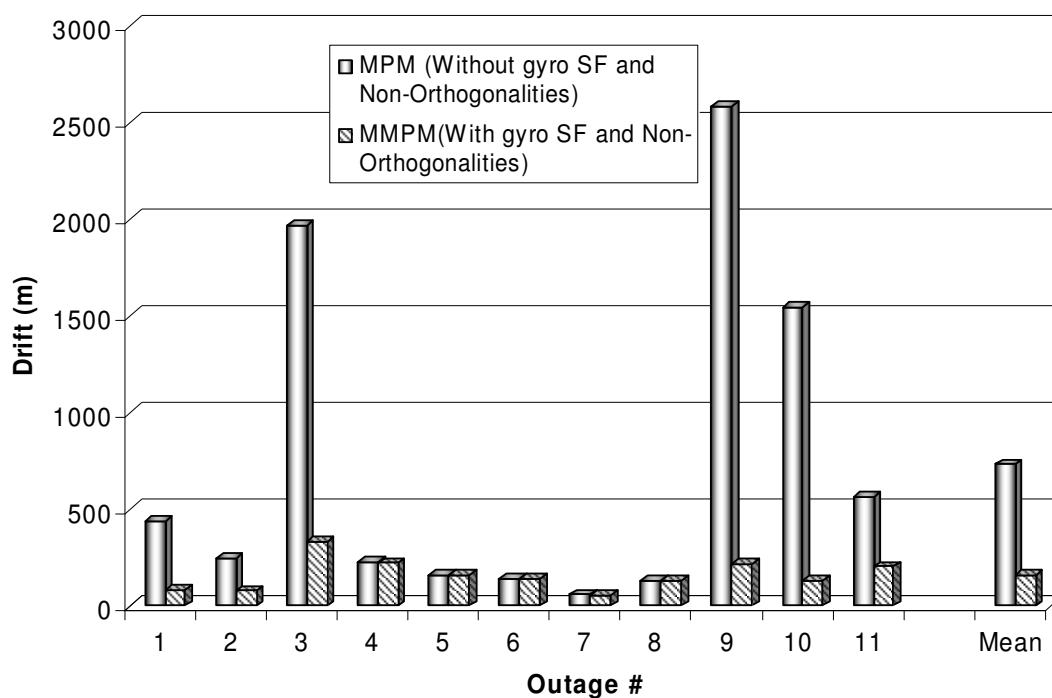


**Figure 3-9. Comparison of CIU sensor position drifts using multi-position (MPM) and Modified Multi-Position (MMPM) calibration methods for run 1 for 60s GPS outages**

The high drift values were observed when the outages included turns or high velocities showing that a good estimation of scale factors and non-orthogonalities are vital during these areas as shown in Figure 3-10. GPS outage 9 is an excellent example since it is simulated at a turn with high velocity profile (the north velocity is changing from negative to positive value) and the dataset without scale factor and non-orthogonalities corrections produced maximum drift.

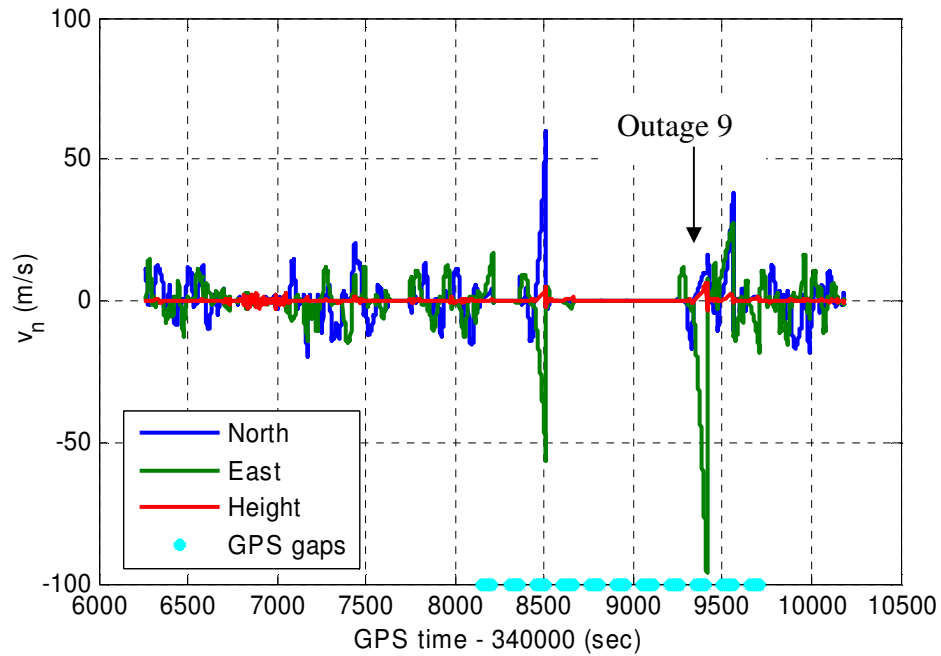


**Figure 3-10. Velocity profile for the outages**

### 3.7.3 Calibration Results Comparison

The biases and scale factors computed by the MMPM were also compared with the values obtained by SPM as shown in Table 3-3 and Table 3-4. The results of MMPM cannot be compared with MPM as the later cannot converge for low cost sensors. The values given in Table 3-3 correspond to the MotionPak II (MPII) unit which is considered a higher grade MEMS IMU. Here it is important to note that the biases and scale factors for the MMPM were calculated in two steps. The first step was the rough estimation of these values using face up and down configurations to provide a starting point for the least squares estimation. The second step was the computation of the residual errors using the least squares adjustment. For MPII, the SPM biases and scale factors were computed by other group members two years earlier.

**Table 3-3. Biases and scale factors computed by the MMPM and SPM for MotionPak II.**

		<b>MMPM Biases</b>	<b>SPM Biases</b>	<b>MMPM Scale Factor</b>	<b>SPM Scale Factor</b>
Accelerometers	X	-0.4770 m/s <sup>2</sup>	-0.4951 m/s <sup>2</sup>	0.9954 (unitless)	0.9967 (unitless)
	Y	-0.7233 m/s <sup>2</sup>	-0.7957 m/s <sup>2</sup>	0.9862 (unitless)	0.9875 (unitless)
	Z	-0.4210 m/s <sup>2</sup>	-0.5227 m/s <sup>2</sup>	0.9888 (unitless)	0.9875 (unitless)
Gyros	X	-0.8269 deg/s	-0.6521 deg/s	-0.9963 (unitless)	-0.9963 (unitless)
	Y	-0.5248 deg/s	-0.2905 deg/s	-1.0000 (unitless)	-1.0000 (unitless)
	Z	0.0107 deg/s	0.0318 deg/s	-1.0000 (unitless)	-1.0000 (unitless)

**Table 3-4. Biases and scale factors calculated by the MMPM and SPM for CIU.**

		<b>MMPM Biases</b>	<b>SPM Biases</b>	<b>MMPM Scale Factor</b>	<b>SPM Scale Factor</b>
Accelerometers	X	14.5950 m/s <sup>2</sup>	14.6331 m/s <sup>2</sup>	1.0289 (unitless)	1.0291 (unitless)
	Y	18.7237 m/s <sup>2</sup>	18.9774 m/s <sup>2</sup>	-1.0397 (unitless)	-1.0355 (unitless)
	Z	-12.7753 m/s <sup>2</sup>	-13.1699 m/s <sup>2</sup>	1.0579 (unitless)	1.0563 (unitless)
Gyros	X	8.8706 deg/s	8.9763 deg/s	1.0072 (unitless)	1.0066 (unitless)
	Y	7.6968 deg/s	7.5834 deg/s	-1.0168 (unitless)	-1.0160 (unitless)
	Z	9.1928 deg/s	9.1337 deg/s	0.9984 (unitless)	0.9968 (unitless)

Table 3-3 and Table 3-4 lists the computed biases and scale factors for the MotionPak II and the CIU sensors. The biases and scale factors estimated from the MMPM are similar to the commonly used SPM.

### 3.7.4 Navigation accuracy comparison

This section compares the effect of the two calibration methods in terms of the position drifts during simulated GPS outages for both the MotionPak II and CIU. Table 3-5 gives the maximum position drifts for run 1, evaluated using the IMU data calibrated by the MMPM and the commonly used SPM. The performance was evaluated with respect to the reference trajectory during the 60 second GPS outages when the CIU was working as a stand-alone navigation predictor. As can be seen from Table 3-5, for MotionPak II, a 9% decrease in position drift errors is achieved when using the MMPM while the drifts are increased by 5 % for the CIU.

The results for Runs 2 and 3 are given in Table 3-6 and Table 3-7 respectively. Both of the tables clearly indicate that the performance of the MMPM is comparable to the traditional SPM. However, it should be reiterated that the MMPM achieved these results without complicated alignment, which is the major advantage of this method. A summary of these tables is provided in Figure 3-11.

**Table 3-5. Maximum position drift in simulated GPS outages in run 1.**

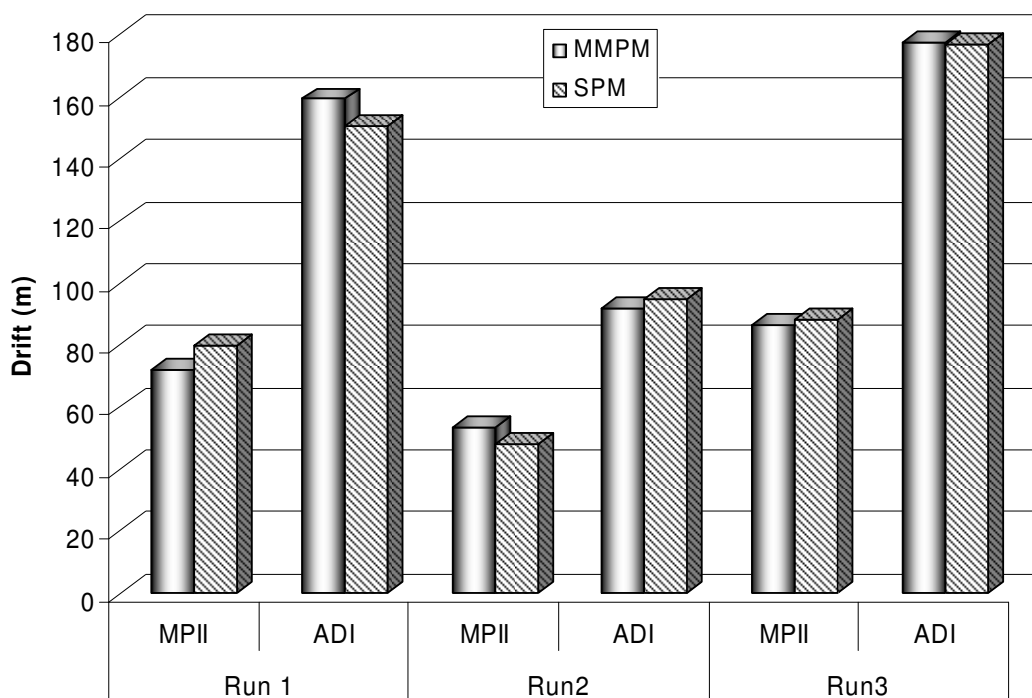
	MotionPakII		CIU	
	MMPM	SPM	MMPM	SPM
Maximum Drift Error (m)	226.11	256.68	85.14	82.84
	26.05	25.05	76.01	70.43
	66.56	59.32	327.74	296.64
	65.45	65.90	220.65	214.58
	92.19	91.88	161.32	161.27
	23.67	23.53	142.79	143.32
	40.94	40.83	53.26	53.58
	13.45	12.31	131.50	131.63
	55.82	52.95	219.76	182.70
	79.08	104.09	132.67	121.69
101.80	142.39	201.37	200.50	
Mean (m)	71.92	79.54	159.29	150.83

**Table 3-6. Maximum position drifts in simulated GPS outages in run 2.**

		MotionPakII		CIU	
		MMPM	SPM	MMPM	SPM
Maximum Drift Error (m)		119.13	63.00	46.62	47.23
		58.51	70.12	122.57	144.27
		55.65	61.55	140.31	136.79
		18.92	20.50	103.53	97.06
		18.76	18.65	89.00	89.08
		49.71	53.91	49.91	53.21
Mean (m)		53.45	47.95	91.99	94.61

**Table 3-7. Maximum position drifts in simulated GPS outages in run 3.**

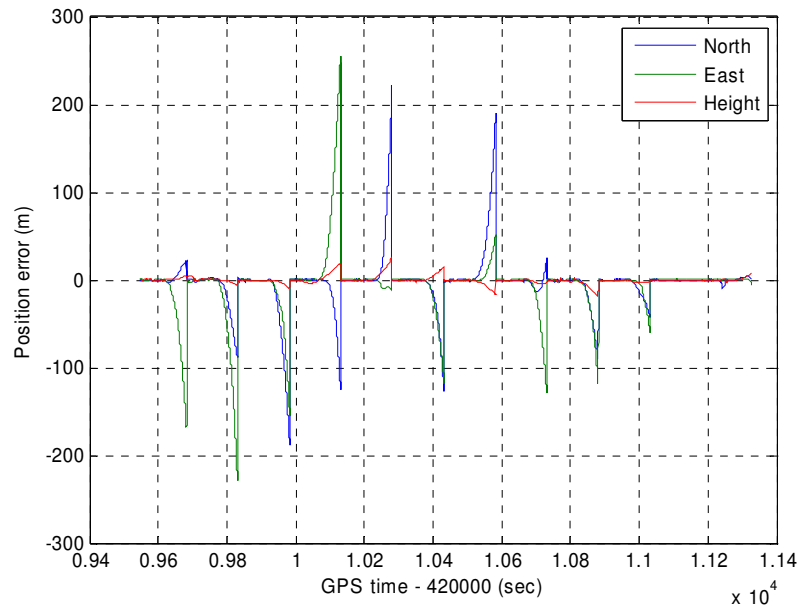
		MotionPakII		CIU	
		MMPM	SPM	MMPM	SPM
Maximum Drift Error (m)		52.66	51.78	156.64	159.51
		77.86	76.93	236.73	251.80
		76.87	80.18	215.36	222.97
		97.10	116.13	276.96	265.65
		145.99	146.84	213.77	195.69
		116.60	126.56	158.97	146.60
		51.18	47.39	175.96	184.59
		172.73	173.54	126.09	125.59
		35.42	22.10	144.81	153.61
		37.62	37.96	68.02	64.75
Mean (m)		86.21	87.94	177.33	177.08



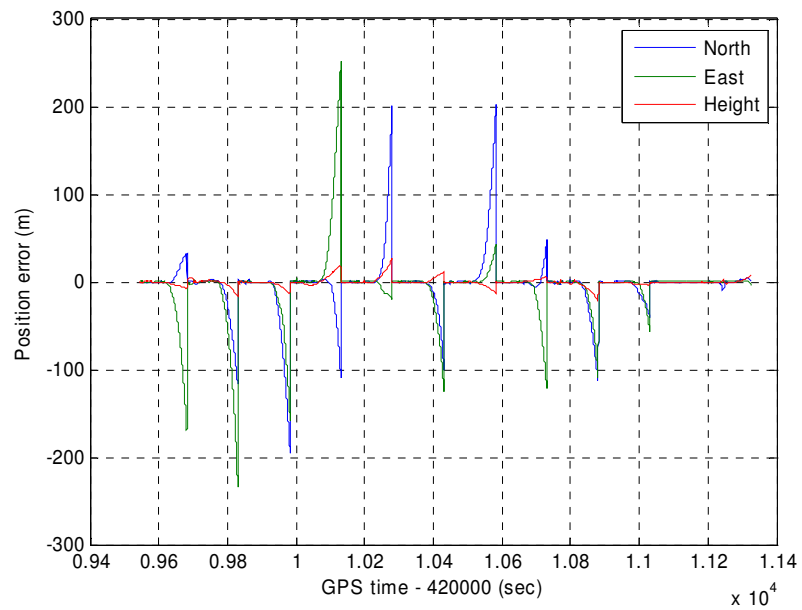
**Figure 3-11. Comparison of MPPM and SPM for three different runs using two different inertial systems**

Figure 3-12 and Figure 3-13 show the position drifts obtained during run 3 for the CIU using the two calibration methods of comparison. The drifts for the CIU were comparatively greater than the MotionPak II drifts which was expected due to the quality difference of the MEMS sensors. Again, the drift errors were consistent in each GPS outage for the two calibration methods. The drift errors can be reduced by tuning the KF for the particular systems, however, the main objective of this chapter was to show the similarities between the two calibration methods and hence the tuning was not performed.





**Figure 3-12. Position errors in GPS outages obtained by applying MPPM for CIU in Run 3.**



**Figure 3-13. Position errors in GPS outages obtained by applying SPM for CIU.**

### ***3.7.5 Calibration of an arbitrary shaped MEMS unit***

So far the results shown are from systems that can be oriented accurately in such a way that each axis can measure the gravity vector for the calibration. These systems were fixed to a perfect cube with the help of the screws to obtain accurate results. The main advantage of MMPM is that it can calibrate an arbitrary shaped system that cannot be oriented properly despite careful attempts.

Consequently, the results of a system are shown here that has rounded sides and protruding buttons and clips on five out of six sides and hence, the system is very difficult to orient.



**Figure 3-14. The Portable Navigation System**

Initially SPM was attempted on this system and after five trials, the best set of parameters was chosen for the comparison here. Next, the MMPM was used to obtain the same parameters. Following are the calibration parameters for the two methods.

**Table 3-8. Biases and scale factors calculated by the MMPM and SPM for PNS.**

		<b>MMPM Biases</b>	<b>SPM Biases</b>		<b>MMPM Scale Factor</b>	<b>SPM Scale Factor</b>
Accelerometers	X	3.3184 m/s <sup>2</sup>	3.8943 m/s <sup>2</sup>		1.3212 (unitless)	1.3182 (unitless)
	Y	3.3625 m/s <sup>2</sup>	3.9091 m/s <sup>2</sup>		1.3776 (unitless)	1.3818 (unitless)
	Z	3.2656 m/s <sup>2</sup>	2.7944 m/s <sup>2</sup>		1.3729 (unitless)	1.3727 (unitless)
Gyros	X	1.8496 deg/s	1.8700 deg/s		1.0991 (unitless)	1.1000 (unitless)
	Y	1.8374 deg/s	1.8400 deg/s		1.0783 (unitless)	1.0800 (unitless)
	Z	2.0510 deg/s	2.0572 deg/s		1.0702 (unitless)	1.0720 (unitless)

Both sets of parameters were used to compute the navigation results. The accuracy of calibration parameters were determined when the inertial system was operating in a standalone mode. To simulate the inertial only navigation, four GPS outages were simulated at random locations as shown in Figure 3-8. The results for the two calibration parameters are shown in Figure 3-15.

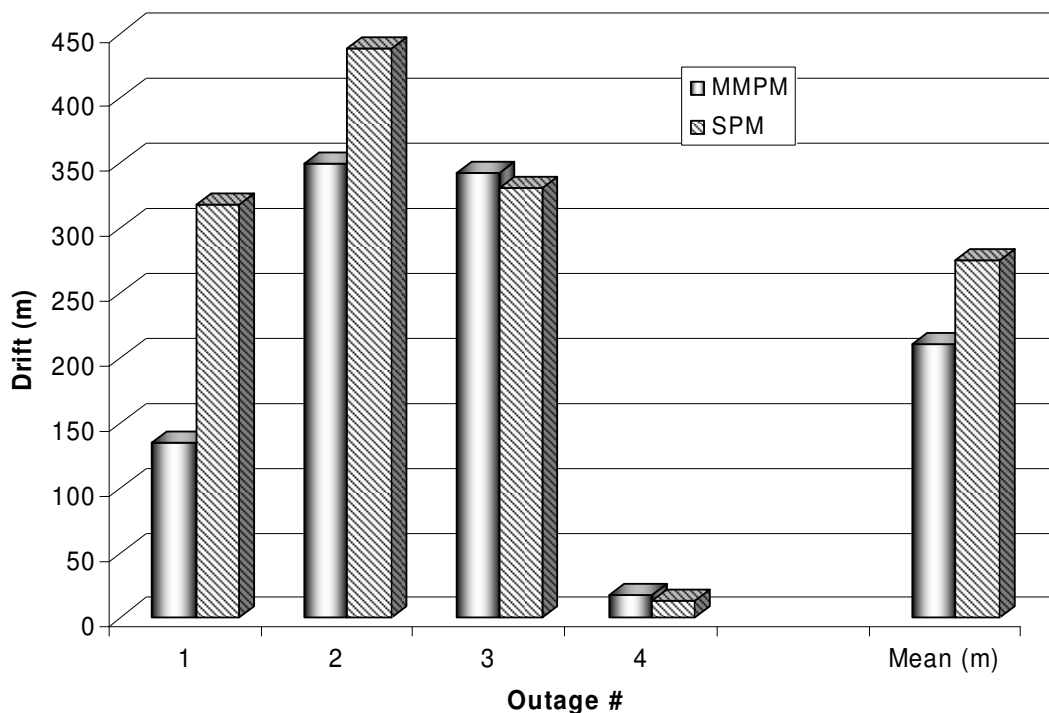


**Figure 3-15. Maximum position drifts for PNS unit**

### 3.8 Summary

IMUs provide an attractive solution to bridge GPS signal outages for land vehicle navigation. Although they are stand alone navigation systems, they still suffer from time related errors due to the integration of signals. As such, any residual deterministic error in the signals can significantly degrade the navigation accuracy. MEMS sensors are light weight and low-cost and hence, can be used in civilian navigation systems. However, these systems need calibration for an accurate navigation solution when the GPS is unavailable. Although it is not realistic to calibrate all MEMS sensors which will be used in portable navigation, the calibration of several sensors is very important to offer a better understanding of the performance characteristics. The calibration parameters for these

sensors can, in principle, be used for all the other sensors of the same category, as a good initial estimate is required to start the KF which refines the errors further.

There are several methods such as *l*-frame calibration, SPM, and MPM to calibrate the inertial sensors. The first two methods require precise alignment of the sensor with either the *l*-frame or to the vertical direction. Consequently, a perfect cube is required for SPM, which is commonly used for IMU calibration. On the contrary, the MPM does not require precise alignment. The drawbacks of the MPM calibration are redundant positions needed to observe the parameters and difficulties in dealing with the large biases and scale factor errors associated with MEMS IMUs.

This chapter provided a new tool for calibration of an arbitrary shaped inertial system based on MPM ([Shin and El-Sheimy, 2002](#)) for MEMS sensors. The results were compared with the commonly used SPM. First, modification to the MPM was done in order to provide a starting point for the least squares adjustment for bias and scale factor estimation. The second modification to the method was the inclusion of a turntable to provide a strong reference rotation rate for the high noise MEMS sensors that cannot use the weak earth rotation signal as a reference. The modified method produced similar results when compared to the well established SPM for a cube shaped system.

The use of the turntable was clearly justified by the results provided in Section 3.7.2. The results degraded significantly when the gyro scale factor and non-orthogonalities were not compensated using the same MPM principle. The mean deviation of drift errors was over 600 m as compared to only 79 m when these additional errors were compensated

with the turntable calibration. The maximum drift was as large as 2579.5 m, for the standard MPM, making this calibration nearly useless for MEMS IMUs without a reference rotation rate signal to calibrate the scale factor and non-orthogonalities of the gyros.

The computed biases and scale factors from the two methods were compared in Table 3-3. The similarity of the two sets of results show that the MMPM can be used to replace the well established SPM and thus can eliminate the need of perfect alignment of the IMU. The only remaining drawback would be the additional positions needed to perform the calibration.

A similar comparison for the non-orthogonalities of the IMU axes was not possible. The SPM estimates the non-orthogonalities in the frame of the perfect cube and hence, the scale factor and non-orthogonalities matrix in equation 3-19 would be fully populated and the misalignment between the accelerometer and gyro triads can also be calibrated out. The MMPM, on the contrary, performs the alignment of the accelerometer and gyro with respect to their x-axes. The x-axis is considered as the constant and the y and z axes are rotated to make them orthogonal to the x-axis. Furthermore, the MMPM still cannot estimate the inter-triad misalignments between the accelerometer and gyro triads.

The drift error comparisons using simulated GPS signal outages have demonstrated that the MMPM is as good as the SPM with the exception that the MMPM does not require a cube to ensure perfect alignment of the IMU during calibration. The results for all GPS outages were consistent for both calibration methods. Furthermore, the separate

components of the position (i.e., north, east and height) also showed similar trends for both methods.

The last section of the results shows the accuracy of the MMPM for a system that cannot be calibrated using traditional methods. The traditional SPM calibration parameters were obtained by repeating the test five times with as accurate alignment as possible and then choosing the best parameters on the basis of INS standalone navigation results. The results clearly indicate the advantage of using this method for such a system.

After calibration, the sensors are ready to be aligned for implementing the navigation algorithm. However, an extra step is taken in the design process to maximize the economical benefits of a PNS. This extra step is to evaluate the minimum requirement for signal sampling, signal resolution and time synchronization errors without compromising the navigation accuracies beyond a threshold. The focus of the next chapter is on the sampling requirements for a commercially compatible PNS. The vehicle datasets are used in this analysis as their frequencies are over two orders of magnitude higher than the on-foot frequencies, and hence if certain signal requirement is good for vehicle, in theory, it will be better for on-foot mode. However, this is an assumption and it needs to be evaluated.

## Chapter Four: Signal Sampling Requirements for Portable Navigation

Inertial systems are usually capable of providing a higher data rate than GPS. In most inertial navigation applications, this high frequency data is used to get continuous positioning information. However, when it comes to high noise and low cost sensors, the benefit of using a high sampling frequency becomes unclear. Similar questions can be raised about the signal resolution for sensors exhibiting high noise characteristics. In the MEMS INS/GPS integrated navigation system, the bit resolution of the DAQ card usually defines its price ([National Instrument, 2007](#)).

Another factor that affects the price of the DAQ card is the sampling rate among channels. If a cost effective solution is required, the data for different sensors coming through individual channels may not be simultaneous. Depending on the sensors used in the INS, the subsequent channels to be scanned will be delayed according to the quality of the DAQ card. How the navigation accuracies degrade due to the time synchronization error is still unknown.

For land vehicle applications, the frequencies of interest are typically from 0 to 8 Hz ([Barak, 1991](#)) and for on-foot walking scenarios, the frequencies of interest are even lower and fall in the range of 0 to 4 Hz ([Bouten et al., 1997](#)), also shown in Figure 2-2 and Figure 2-3. Consequently, land vehicle data sets were used in this study with the assumption that there will be more degradation in a higher frequency application due to



the degradation in signal sampling in the case an inexpensive Analog to digital converter (ADC) is utilized.

## **4.1 Methodology**

Real field datasets are used in the study which will be described in Subsection 4.1.1. All the datasets were recorded with NI DAQ 6036 that has a 16 bits resolution and a sampling rate of 1.27 MS/s (Mega Samples per seconds). The output frequency of the data was 100 Hz and due to the high sample rate of the DAQ card, the recorded data can be regarded as simultaneously sampled without any inter channel delays. The original bandwidth (BW) at the data collection phase was set at 40 Hz. This chapter will investigate various issues about the sampling needs for land vehicle navigation to search for the minimum requirements for an inexpensive DAQ card and improved computation capabilities. The DAQ card used in the data collection cannot be utilized for commercial systems as it is approximately 20 times the cost of the entire system.

This section will also provide the algorithms used in the simulation of down sampling, resolution degradation and time synchronization errors for the field datasets. In addition, the last section will give the specification of two low cost ADCs that may be desirable for commercial system.

### ***4.1.1 Description of Test data***

As the focus of the thesis is on low cost inertial sensors, the CIU described in Section 3.7.1 will be used in these tests. The results and analysis are based on the integration of CIU with the NovAtel's OEM4 receiver using two different integration schemes (loosely

and tightly coupled integration). An LN200 with higher accuracy was integrated with DGPS to produce the reference trajectory. The OEM4 GPS antenna and the LN200 were mounted on the roof of the vehicle and the CIU was installed inside the van. Position drift errors were used to test the CIU performance with various sampling scenarios. The position errors were obtained by comparing the corresponding solution to the reference trajectory. The position errors showed the performance of the CIU as a stand-alone system. Comparison of the degradation due to sampling configurations was done on the basis of these position drift errors.

Two different trajectories with a wide range of GPS signal qualities as shown in Figure 4-1, Figure 4-2, Figure 4-3 and Figure 4-4 were used in the test. The vehicle dynamics, the location of the simulated GPS degradation and the number of GPS satellites available during the simulated GPS degradation periods are also shown in the figures. For loosely coupled, the same degradation periods were used for complete GPS signal outages as partial outages were not possible.

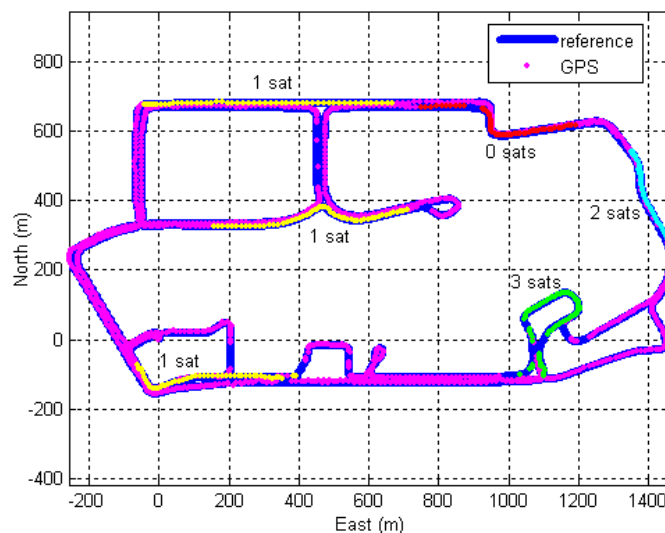


**Figure 4-1. Trajectory for dataset 1 with simulated signal degradation periods**

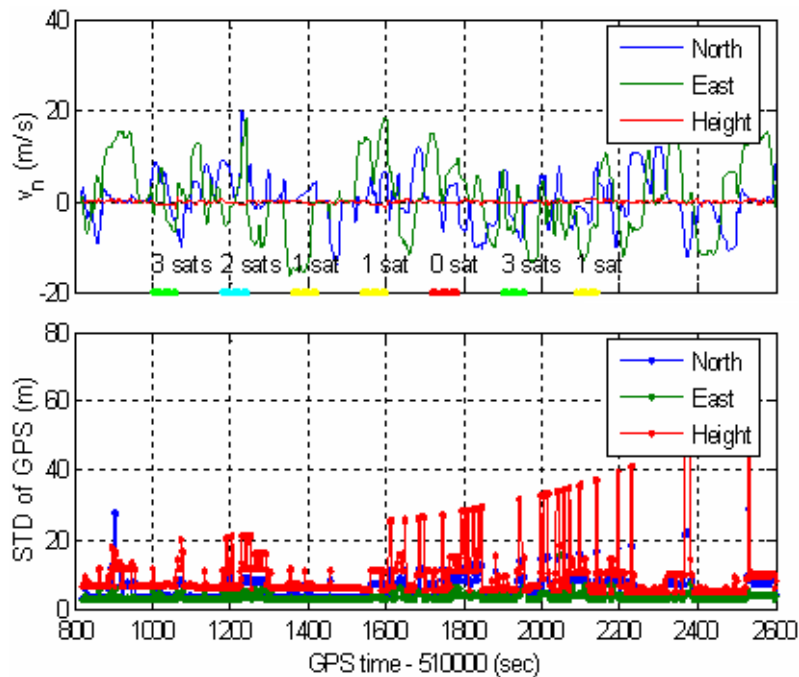


**Figure 4-2. GPS signal degradation locations with respect to the signal availability and vehicle dynamics**

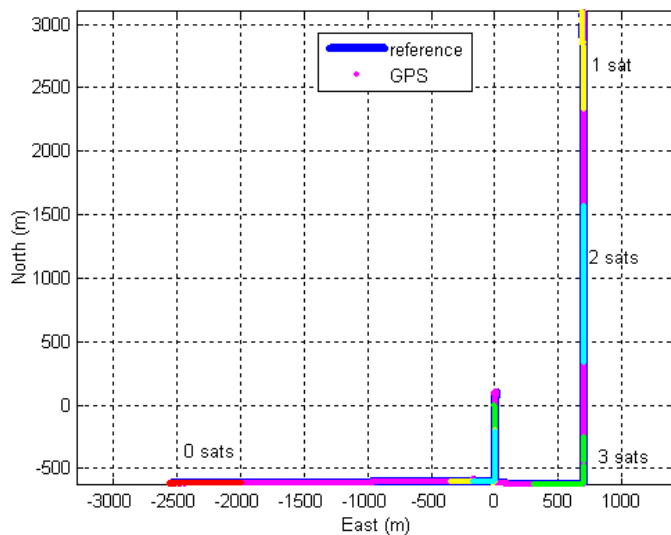


**Figure 4-3. Trajectory for dataset 2 with simulated signal degradation periods (some outages are overlapped)**

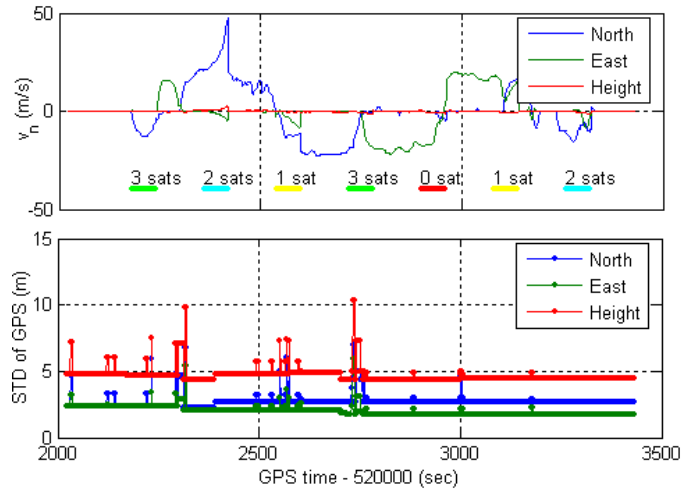


**Figure 4-4. GPS signal degradation locations for dataset 2 with respect to the signal availability and vehicle dynamics**

#### ***4.1.2 Analysis Method***

All the results were given in terms of drift errors in metres with respect to the reference trajectory. The comparison for this study was based on the drift errors obtained using the originally recorded data. The original data was recorded at 100 Hz, in a 16 bit resolution with virtually no time delay. The rest of the comparisons used these drift errors as base errors. Therefore, the percentage degradation in the drift errors is given with respect to the base errors.

The drift errors were calculated as a square root of the SSE in north ( $r_n$ ), east ( $r_e$ ) and down ( $r_d$ ) coordinates during the GPS signal degradation periods as shown below.

$$drift = \sqrt{(r_n^{ref} - r_n^{test})^2 + (r_e^{ref} - r_e^{test})^2 + (r_d^{ref} - r_d^{test})^2} \quad \mathbf{4-1}$$

where *ref* is reference value from reference trajectory (the true value) and *test* is CIU navigation values during GPS signal degradation periods.

#### 4.1.3 Determination of Minimum Sampling Frequency

The first step in downsampling is to reduce the BW of the data in such a way that the new frequency will satisfy the Nyquist theorem ([Mitra and Kaiser, 1993](#)).

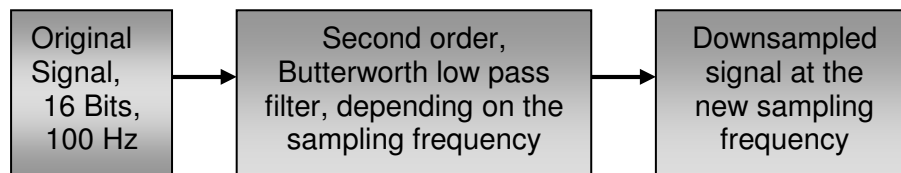


**Figure 4-5. Flowchart for Down-sampling Algorithm**

A second order Butterworth low pass filter ([Mitra and Kaiser, 1993](#)) is implemented to reduce the BW of the signal as per the new frequency requirements (Figure 4-5). First the data are downsampled to 50Hz and then to 20Hz. Finally the data was fed into EKF for drift error estimation during the GPS signal outages. These results were compared with the original 100 Hz dataset results for the same GPS signal outage periods.

#### 4.1.4 Determination of Minimum Number of Bits

In these simulations, the MEMS signals were pre-processed to mimic the case of low resolution DAQ cards. The resolution was reduced from 16 bits to 14 and 12 bits and the results were processed with both loosely and tightly coupled integration.

To reduce the resolution of a data point, the first step was to find a small value known as the least significant bit (LSB). In theory the data will become integer if it is divided by this LSB. However, because of the machine precision this number needed to be rounded to get the integer. The degraded resolution can be determined by simply multiplying the

data with the LSB scaled according to the new bit values. Following are the steps to obtain a lower resolution.

1. Compute the recording range

$$Range = \frac{ADC_{Range}}{SF} \quad 4-2$$

where  $ADC_{Range}$  = Originally recorded signal range

and  $SF$  = scale factor of the sensor

2. Calculate the LSB

$$LSB = \frac{Range}{2^n} \quad 4-3$$

where  $n$  = Original ADC bit number

3. Finally determine the degraded value

$$x = round\left(\frac{x_0}{LSB \cdot 2^{(n-m)}}\right) \cdot LSB \cdot 2^{(n-m)} \quad 4-4$$

where

$x$  is the degraded signal

$x_0$  is the original inertial signal

$m$  is the degraded ADC bit number

#### ***4.1.5 Determination of Time Synchronization Error Budget***

The last part of the degradation study included the time synchronization errors among the different channels. The original sampling rate would allow a virtually simultaneous recording of the channels. A one millisecond mismatch was introduced for 16, 14 and 12 bit resolutions at 100, 50 and 20 Hz sampling frequencies.

Linear interpolation was used to obtain the new values of the signal at the required timings. The mismatch was simulated by interpolating (equation 4-5) the value of the second gyro (gy) at 1 ms, the third gyro (gz) at 2 ms and consequently for the last accelerometer (az) at 5 ms. The interpolated data set was used in the EKF for INS/GPS integration and the drifts for the simulated GPS signal outages were computed and compared with the reference data set.

$$s_t = s_{t_1} + \left( \frac{t - t_1}{t_2 - t_1} \right) (s_{t_2} - s_{t_1}) \quad \mathbf{4-5}$$

where  $s_t$  = signal value at the desired time  $t$ .

The graphical user interface for the program is provided in Figure 4-6. The program gives the user the option to browse for the raw inertial measurements file. Next section requires input from the user about the original signal sampling specifications. For the simulations, there are three options for the user. First option is for down sampling the original dataset to a new frequency. If the user chooses a frequency that is less than twice the vehicle dynamics, i.e., if  $\text{frequency}_{\text{new}} < 2 \times 8\text{Hz}$ , the program will warn the user that some of the vehicle dynamics may be lost due to the chosen frequency. If the user chose to continue, the program will produce the required file.

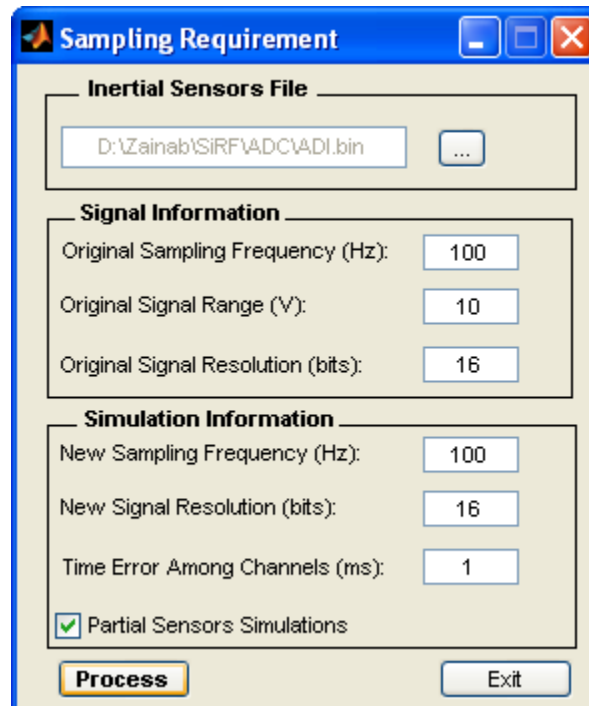


**Figure 4-6. Graphical user interface for the sampling requirement program developed for the thesis**

The next option for simulation is to degrade the data resolution. If the user tries to enter a resolution better than the original resolution of the signal, the program will produce a message and exit. A time synchronization error can be entered in milliseconds (ms) in the next dialog box. The final option is for partial sensor simulation. The program can only simulate the time mismatch if 1 vertical gyro and 2 horizontal accelerometers are part of the partial inertial system. More information about the partial sensors is provided in the next chapter.

If the user wants to do the three kinds of signal degradation simulations at once, the program will first down sample the data, then the resolution of the newly sampled data will be reduced to the provided resolution and finally the inter-channel delay will be



introduced in the dataset. To do one simulation at a time, the rest of the simulation options should be set to the original signal value and the time error should be set to 0 ms.

#### ***4.1.6 DAQ Specifications***

The AD7997 and AD7998 specifications will be used in the simulations as the cost of these cards are only \$2.13 and \$3.54 respectively. Both cards have 8 channels and a sampling rate of 79kS/s (kilo samples per second), which will translate into 0.1ms delay among subsequent channels. The only difference between the two cards is the resolution. The AD7997 has 10 bits resolution while AD7998 has a resolution of 12 bits. The resolution and time mismatch errors will be simulated in the original dataset and the results will be shown for these two cases.

## **4.2 Results**

Sections 4.2.1, 4.2.2 and 4.2.3 will provide the sampling, resolution and time synchronization error results. The last subsection will provide an example for the signal sampling simulation of a very low cost DAQ card.

### ***4.2.1 Low Sampling Frequencies Simulations***

Figure 4-7 shows the results when the data recorded at 100 Hz sampling frequency were downsampled to 50 Hz and then 20 Hz. The downsampled CIU data were then integrated with GPS using loosely and tightly coupled integration schemes in EKF. For loosely coupled integration, complete GPS signal outages was simulated at the exact locations where GPS signal degradation is shown in Figure 4-1 and Figure 4-3. The maximum

degradation of 6.18% was recorded at 20 Hz sampling frequency for loosely coupled integration. The tightly coupled integration also showed slight degradation in the results. For dataset 2 in tightly coupled integration, there was an improvement in the drift error results but this is not significant as the mean drift error stayed approximately 17 m for all the three cases.

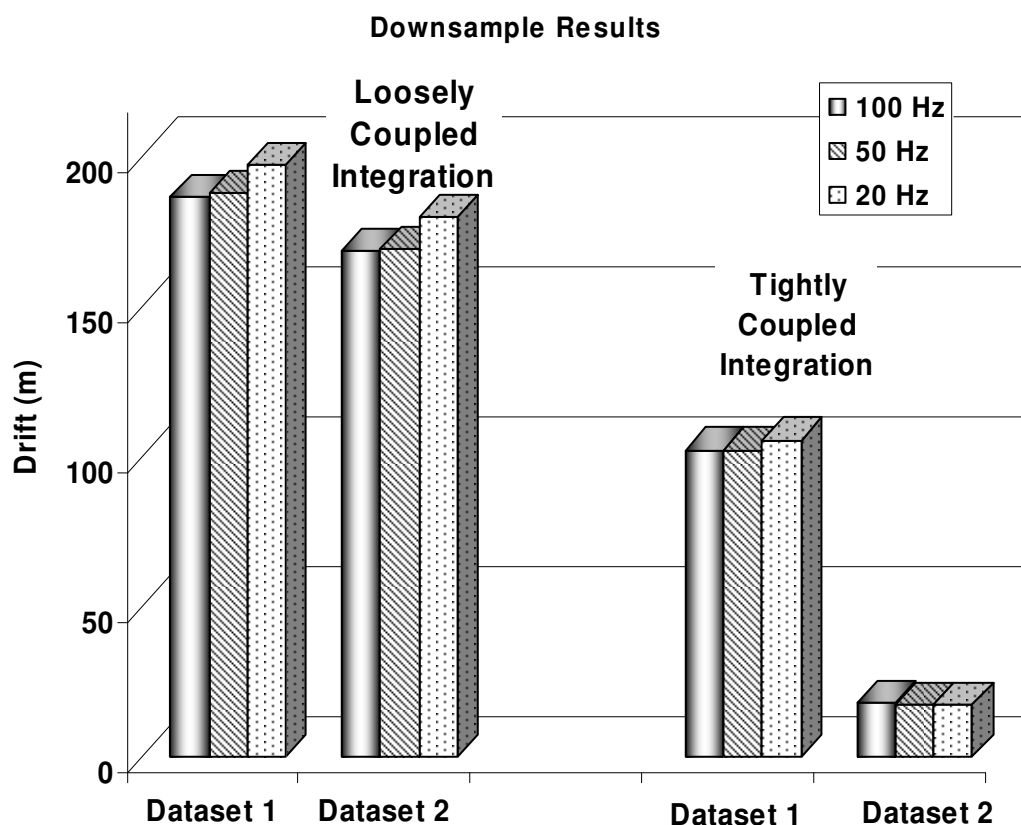


**Figure 4-7. Downsampling results**

Figure 4-8 showed the central processing unit (CPU) time consumption for various sampling frequencies. Both datasets showed a 52% reduction in CPU time at 50 Hz as compared to 100 Hz case. The CPU time was further reduced when 20 Hz datasets were processed and compared with the original 100 Hz datasets. In this case, the computer

took only 23% of the CPU time as compared to the original 100 Hz case. The downsampling not only reduced the CPU computation time but also decreased the memory storage requirements by the same percentages. Computation load is an important design consideration for a real time cost-effective vehicle navigation system and storage requirement is crucial at the design phase when post-processing is required. If 10% degradation is considered as threshold, a 20 Hz sampling frequency can be considered as an attractive option for online navigation algorithms involving low cost MEMS based IMU.

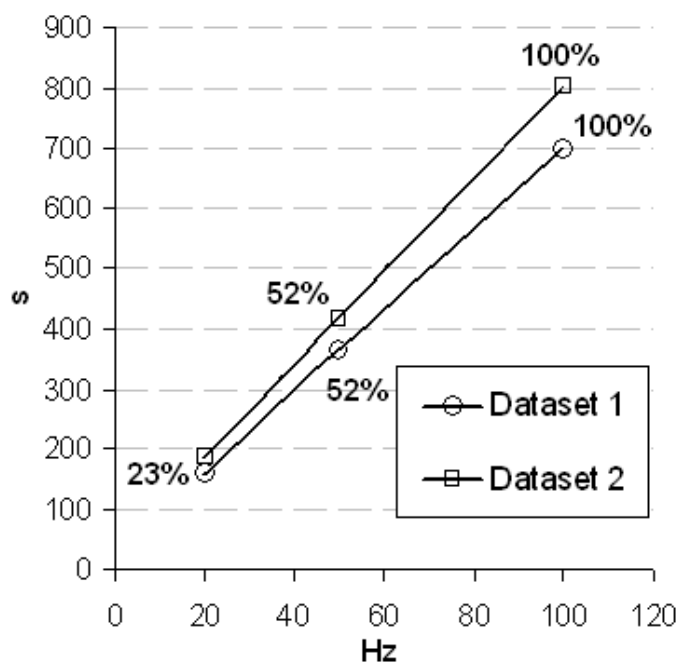


**Figure 4-8. CPU times for various frequencies**

#### ***4.2.2 Number of Bits Reduction***

Figure 4-9 showed the results of using loosely and tightly coupled integration schemes when the number of bits was reduced from 16 bits to 14 bits. The signal resolution was further reduced to 12 bits and the results were given in Figure 4-10. The reduction in bit

number would result in increased noise in the dataset. Low cost system used in this study itself had a high level of noise. Therefore, the increased noise resulted from bit reduction should not significantly affect the results.

Compared to Figure 4-7, the results in Figure 4-9 clearly indicated that a lower resolution of 14 bits instead of 16 bits would not degrade the results. The degradation percentages in both Figure 4-7 and Figure 4-9 were comparable to each other. The maximum degradation of 5.52% was observed for dataset 2 for loosely coupled integration.

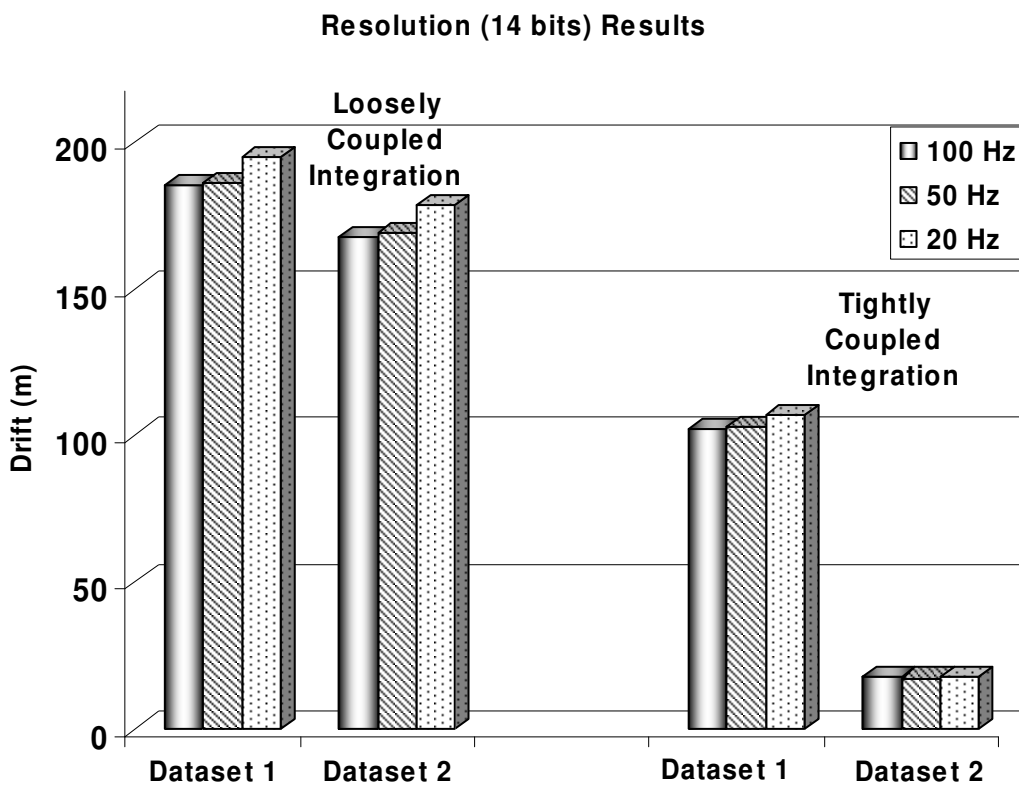


**Figure 4-9. Drift errors for 14 bits resolution**

As depicted in Figure 4-10, a maximum degradation of 10.64% was observed when the resolution was degraded to 12 bits for the 20 Hz dataset with loosely coupled integration. The tightly coupled performed similar to 16 bits case at each sampling frequency. This showed that tightly coupled integration scheme is more robust to signal quality and a lower sampling rate and lower resolution would not degrade the navigation results. On the other hand, the results of dataset 2 with loosely coupled integration indicated that if higher vehicle dynamics were involved, the signal resolution should be at least 14 bits for 20 Hz sampling frequency if the 10% degradation threshold was taken as the cut off criterion.

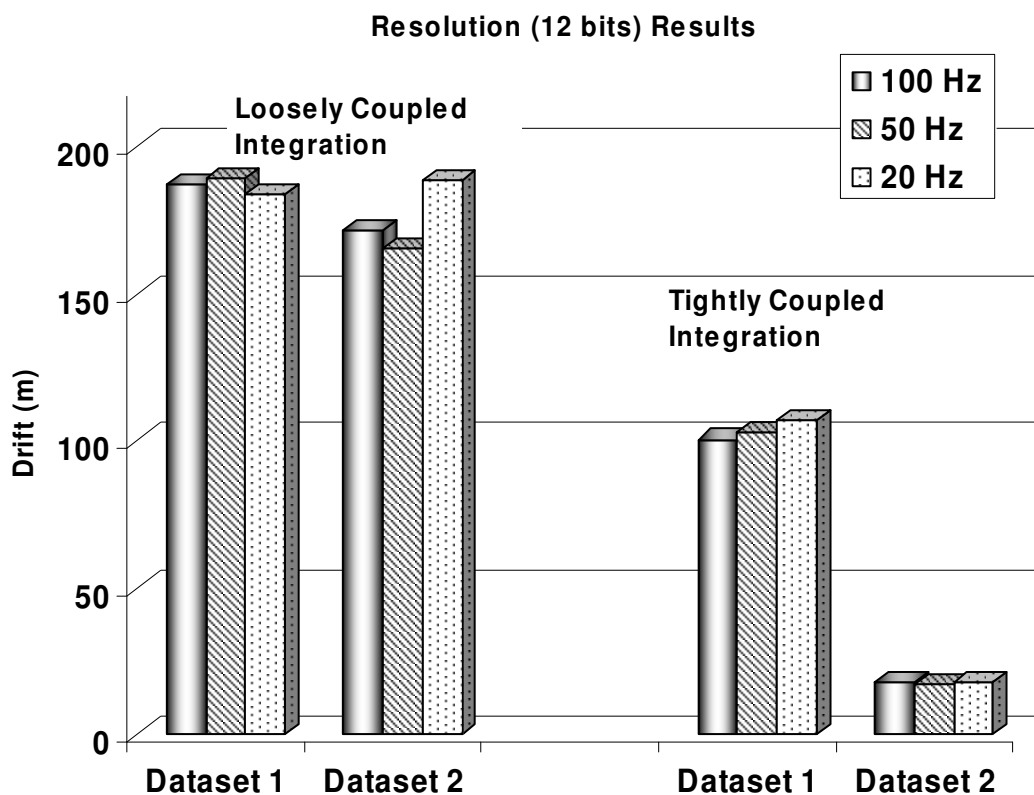


**Figure 4-10. Drift errors for 12 bits resolution**

Note that the resolution of the ADC (i.e. the LSB) is not only determined by the number of bits, but also related to the measurement range for a certain ADC as shown in 4-2. The larger the measurement range is, the coarser the resolution. In the field test data used in this study, the ADC input range was set to  $\pm 5V$ , which corresponds to  $\pm 20 g$  for accelerometers and  $\pm 400 \text{ deg/s}$  for gyros. These measurement ranges might be too wide for a land vehicle, and can be reduced by 5 to 10 times to save 2 to 3 ADC bits. Signal resolution degradation increases the data noise as shown in Figure 4-11.

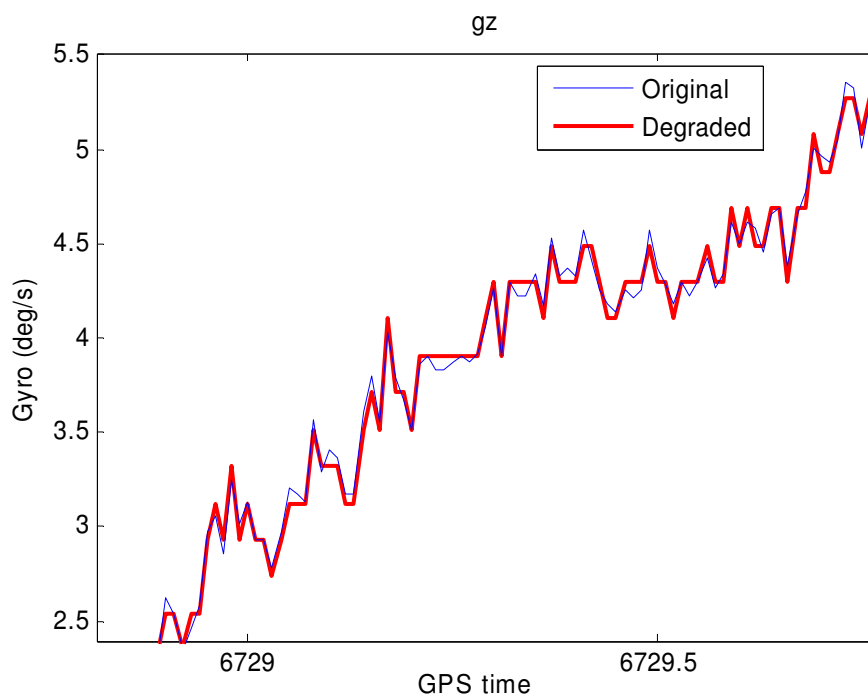


**Figure 4-11. Example of Bit degradation. A 16 bits resolution was degraded to 12 bits in this example.**

#### ***4.2.3 Time Synchronization Effects on Drifts Errors***

The sample rate per channel for DAQ cards is calculated as the overall sample rate divided by the number of scanned channels. The cost of the DAQ card is directly

proportional to its data rate capabilities ([National Instruments, 2007](#)). For land vehicle navigation applications, the ultimate goal is to provide the optimal results with the least expensive sensors and systems to reduce the consumer costs.

The effects of recording delays among the CIU channels were simulated in order to quantify the error budget for a less expensive DAQ card. As mentioned earlier, the recording for these datasets were conducted with NI DAQ 6036 with 16 bits at 200 kS/s data rate (among channels), which ensured almost simultaneous recording from each channel at a high cost.

The results of introducing 1 ms time delay in all channels for data at 100, 50 and 20 Hz sampling frequencies were quite similar and therefore a typical example is provided in Figure 4-12. The results clearly indicated that a cheaper DAQ card would not change the final results. Therefore, time synchronization issue among channels for low cost MEMS inertial sensors is not vital.

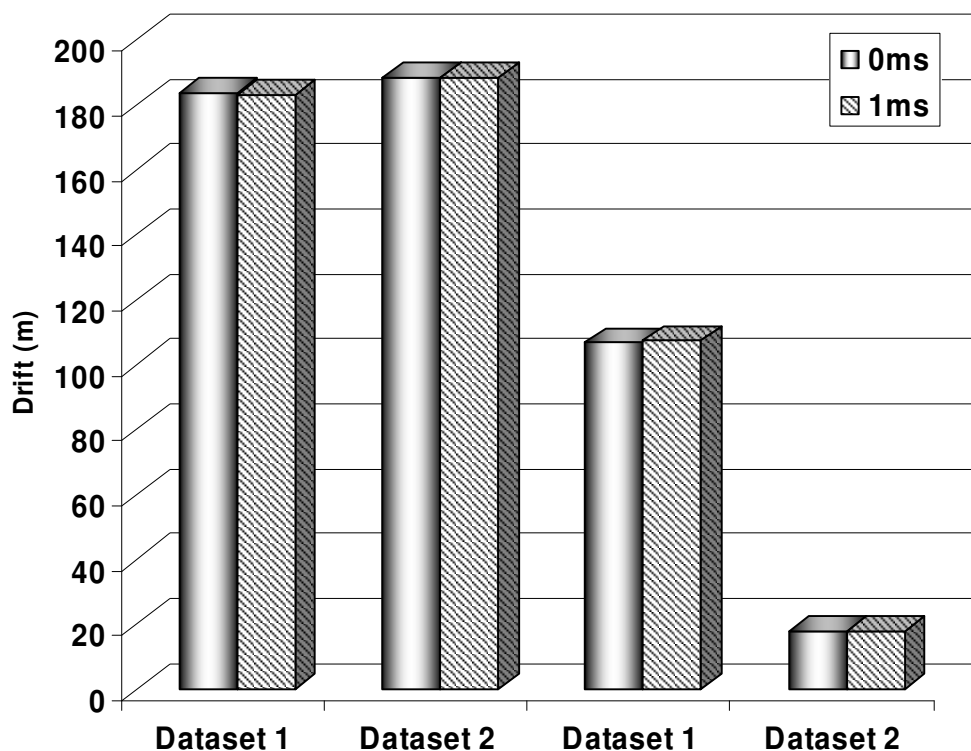


**Figure 4-12. A typical of example of time synchronization error of 1ms**

An extreme case of the delay is also considered here. In this case, it was assumed that half a second delay between first and consecutive channels was introduced due to the GPS measurement at 1Hz. In this case, the average drift was 257.86 m for dataset 1 for loosely coupled integration. Similar degradation was observed for tightly coupled integration. This shows that time synchronization is required for the GPS interrupt to improve the result qualities in both loosely and tightly coupled integration strategies.

#### ***4.2.4 Results for Economical DAQ Cards***

The results provided here are simulating the specifications for the DAQ cards described in Section 4.1.6. Both loosely and tightly coupled integration strategies were



implemented as before. The original dataset resolution was degraded to 10 bits for the first simulation, while for the second case the original resolution was degraded to 12 bits. In both cases, after the resolution degradation, an inter-channel delay of 0.1 ms was introduced.

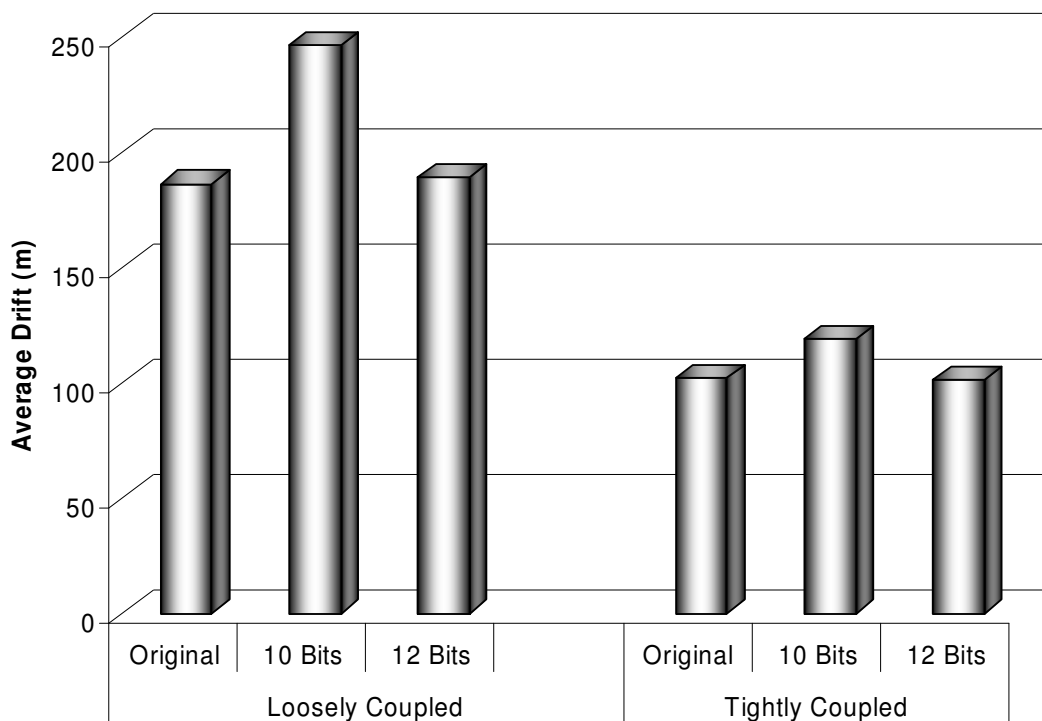


**Figure 4-13. Results for Economical DAQ Cards for Dataset1**

Here the results for dataset 1 are provided as similar trend was observed for dataset 2. The results clearly indicate that a resolution of 10 bits will significantly compromise the navigation accuracies. It is especially true when loosely coupled integration was used. The results degraded more than 24% as compared to the non-simulated original dataset. The tightly coupled integration also showed degradation but the magnitude was 14%.

However, both of the results are unacceptable if the degradation is set to maximum 10% as compared to the original.

### **4.3 Summary**

The worst drift errors with maximum degradation of 6.18% were observed when the data sampling frequency was reduced to 20 Hz in loosely coupled integration. The tightly coupled integration results showed a degradation of approximately 3%. The results were comparable for 50 Hz downsampled data indicating that a higher rate of 100 Hz is unnecessary for land vehicle navigation with frequencies of interest in the range of 0 to 8 Hz. Degradation in resolution to 12 bits and time delays up to 1ms among channels did not compromise the results accuracies significantly. The results of these simulations clearly indicate that a slower processor with a low quality DAQ card can be used as part of a PNS for land navigation. However, time synchronization is required, if the microprocessor is not dealing with the GPS interrupts properly and causing significant delays.

From the analysis of two different cost effective DAQ cards, it is clear that a DAQ card with at least 12 bit resolution is required for data acquisition. The time synchronization error was introduced in the dataset but since it was only 0.1 ms, it is unlikely that it caused any degradation. This statement can also be supported by the results for 12 bits resolution which did not show any degradation (the results were within +/- 0.5% of the original results).

Another important factor in the development of a commercial portable system is the production costs. In the next chapter, a detailed simulation study is conducted to find out

the minimum number of sensors for in-vehicle navigation. More work is required for the minimum number of sensors for on-foot navigation which is part of the future recommendations of this thesis.

## **Chapter Five: Economical Inertial Sensor Configuration for Portable Navigation System**

A typical IMU is composed of three orthogonal gyros and three orthogonal accelerometers which are necessary for determining the 3D trajectory of a vehicle. This configuration is specially required for air or marine navigations systems where roll, pitch and azimuth changes are significant. However, the nature of the ground vehicle operation is constrained mainly to two dimensions. Consequently, the issue arises regarding which sensors are the most important for land navigation applications. This chapter presents and compares different sensor configurations that can be used for this application, taking into consideration the robustness and hardware cost of IMU.

Theoretically heading information is of utmost importance for land navigation applications and therefore, a heading rate sensor must be included in any sensor configuration. Similar to the heading rate sensor, a vehicle moves along its longitudinal axis and thus, an accelerometer in this direction, i.e., the forward/backward direction, is also very important for the land navigation applications. If a heading gyro and a forward/backward sensing accelerometer are present in a land vehicle inertial system, it should be able to provide the required information. This topic will be discussed later in this section. Figure 5-1 shows measurements that each of the inertial sensors can record. Minimum number of sensors will reduce the unit cost which is one of the success factors for a commercial product.

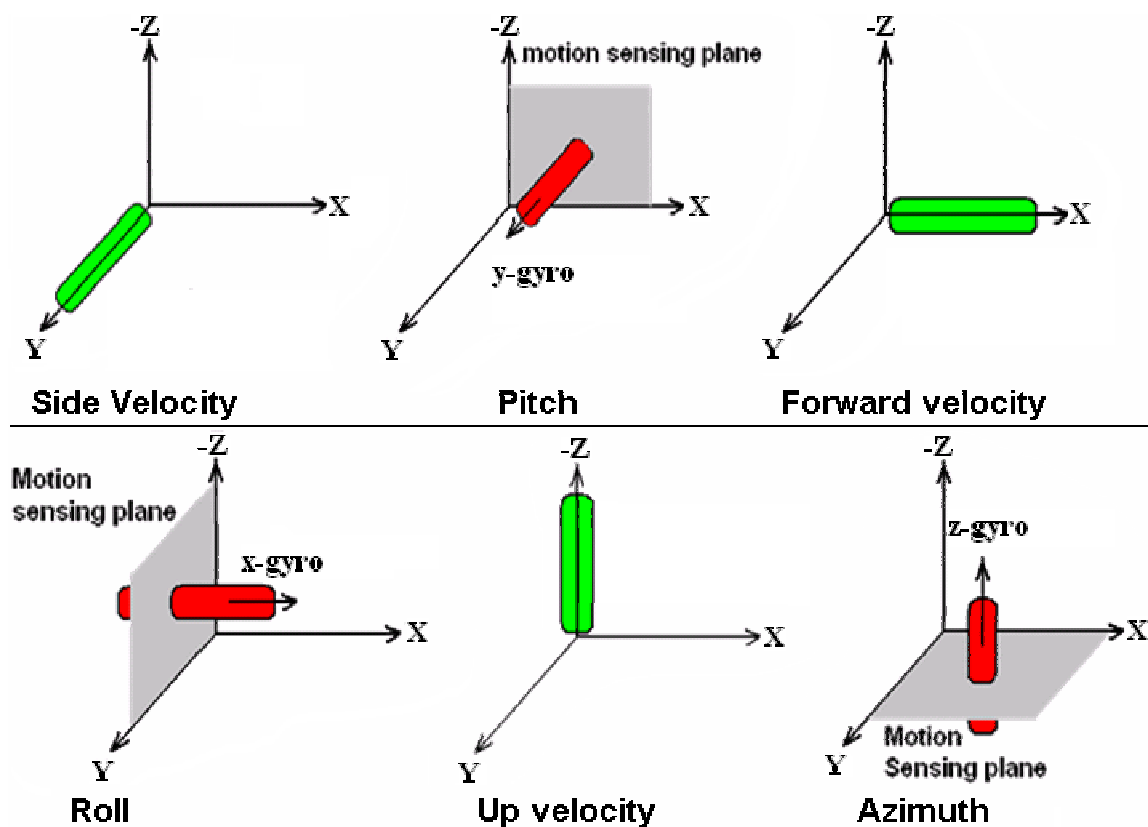


**Figure 5-1: Sensors with their respective measurements**

Five different sensor configurations were considered in total for this study as shown in Figure 5-2. The first set of results consists of position drift errors when a full IMU was used. This configuration is the most expensive as six sensors are part of the system; however, it should be able to provide details about any kind of motion. The second configuration considered in this chapter consists of two gyros and three accelerometers (2G3A). The reason of studying two gyros configuration is the recent development of dual axis MEMS gyros ([InvenSense, 2008](#)). The dual axis gyro module can be utilized in the system in a way that one gyro senses the heading rate while the second gyro provides

the pitch rate. All three accelerometers are kept orthogonal to each other to detect the three dimensional motion.

The third set of results consists of the drift errors when one heading rate gyro is used with the three orthogonal accelerometers (1G3A). Next, one gyro and two horizontal accelerometers (1G2A) followed by one gyro and one forward/backward sensing accelerometer (1G1A) are used.

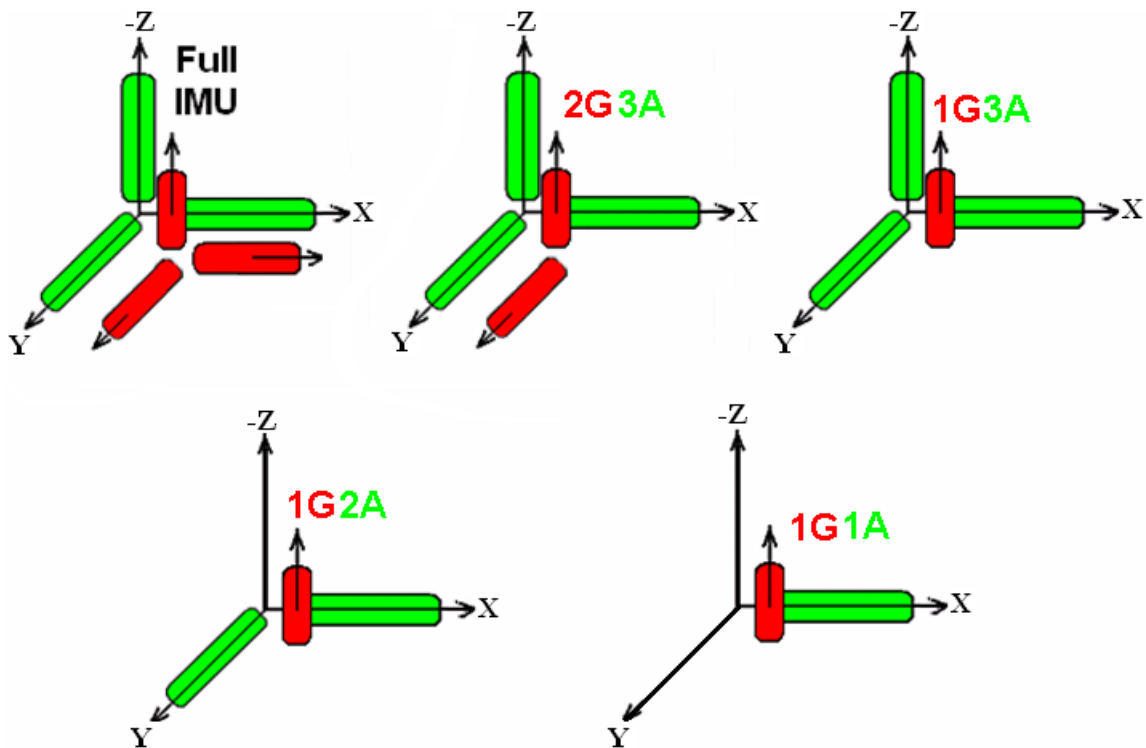


**Figure 5-2: The Five Sensor Configurations Studied (Red bars represent gyros while green bars represent accelerometers. The x-axis corresponds to the forward/backward direction of the moving vehicle)**

Certain assumptions are made when it is considered that land vehicle navigation is mostly constrained to two dimensions. The basic assumption is probably navigation on a well

levelled road, as the roll, pitch angles and vertical velocities on a levelled road will be negligible as shown in Figure 5-3. The forward or backward accelerometer is a compulsory sensor as most of the accelerations will be along this direction which is clear from this figure. What is also obvious is the information embedded in the lateral accelerometer. This accelerometer will measure the centripetal accelerations during turning. A vertical gyro is also necessary to measure the heading of the vehicle. Hence, for a well paved and levelled road, the roll and pitch gyros, i.e., gyros in forward and lateral directions, and vertical accelerometer will provide minimal information. Consequently, they will add to the overall system cost and computation load.

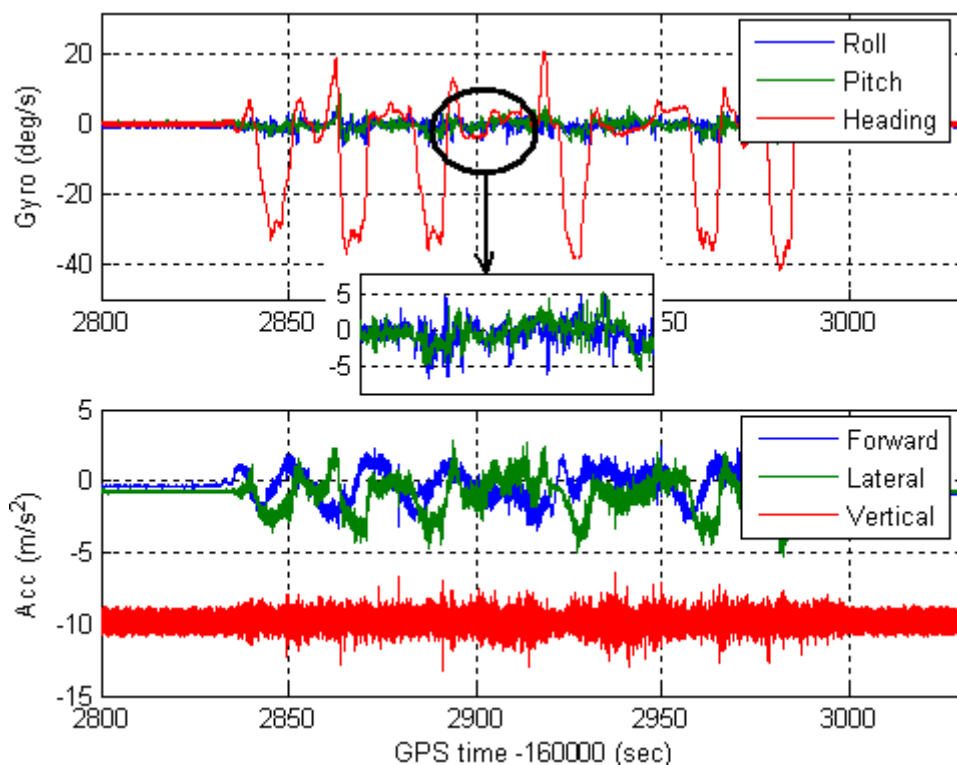


**Figure 5-3: Inertial Sensor signals for a typical land vehicle trajectory**

Also, application of NHC can significantly improve the drift errors in any sensor configurations. The chapter will conclude with the best compromised options for civilian vehicle navigation system in terms of robustness and cost effectiveness ([Syed et al. 2007-c](#)).

## **5.1 Methodology**

The methodology section can be divided in two subsections. The first subsection discusses the data collection strategies and the information about the trajectories used and the second subsection contains the necessary modifications in the EKF to accommodate the omitted inertial sensors.

### ***5.1.1 Data Collection***

Two land-vehicle INS/DGPS kinematic tests conducted in Calgary on April 2004 and December 2005 were used to investigate the performance analyses of the different sensor configurations. The results of the five configurations were compared based on IMU-only navigation and therefore, five (5) GPS signal outages were simulated for the first dataset and eleven (11) GPS signal outages were simulated for the second dataset. The duration of each outage was sixty seconds (60s). The trajectory of dataset 1 and the corresponding locations of simulated GPS outages are shown in Figure 5-4. The dataset 2 is the same as given in Figure 4-3. Both tests include the custom-made CIU as discussed previously in Section 3.7.1 and the LN200 was used to provide the reference trajectory. For both tests, NovAtel OEM4 GPS receivers were used for single point and DGPS solutions.



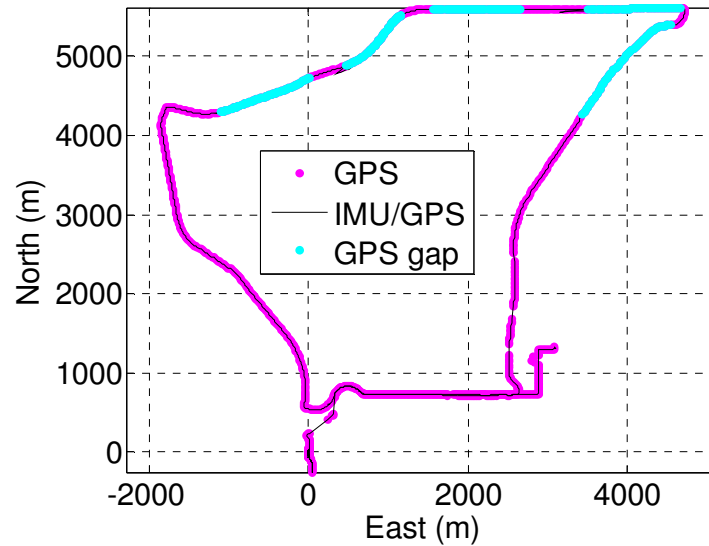


**Figure 5-4: Trajectory for the dataset 1**

In both tests, the CIU was used as the test IMU. The reference solution is obtained by combining LN200 data with DGPS solution providing centimetre-level accuracy.

### **5.1.2 Modification to AINS™**

There are two possibilities for processing partial sensor data. The first method will be to simplify the navigation equations and then process the data in the EKF. The second method can use the same navigation equations by implementing some pseudo signals for the omitted sensors.

The aided inertial navigation system (AINS™) Toolbox is a set of libraries written in MatLab®, a standard scientific computing environment, each of the libraries can be called separately. It also provides estimation tools to optimally combine the data files from an IMU together with information from other aiding sensors, such as the GPS,

odometers, heading, and NHC. For this study, AINS™ was modified such that a user can select the number of sensors to use during the inertial data processing. The selection is provided via a dropdown menu as shown in Figure 5-5.

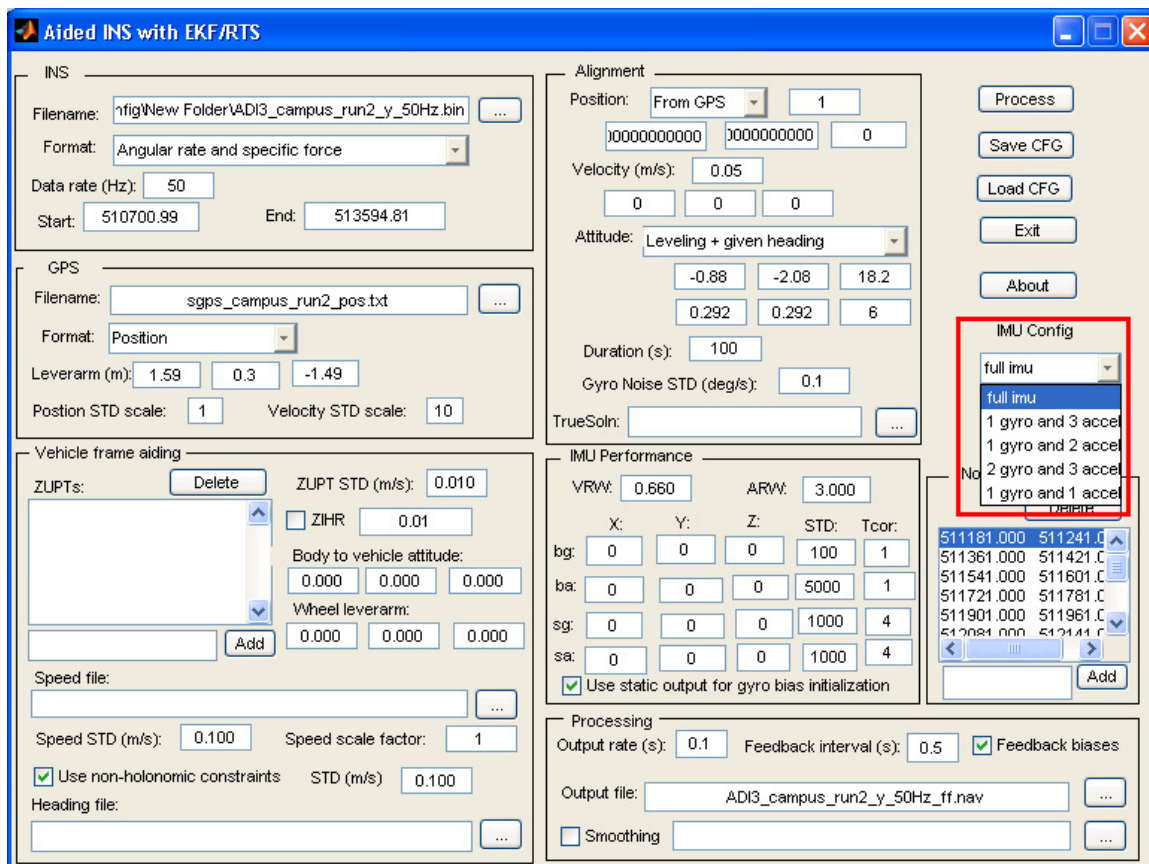


**Figure 5-5: The Modified AINS™ User Interface showing the Dropdown Menu Options for the different IMU Configurations**

The original version of AINS™ had processing capabilities for the full IMU data consisting of six sensors outputs, i.e., three (3) accelerometers and three (3) gyros signal output. In the modified version, the ARW and the VRW of the omitted sensors were

increased, the corresponding signals were assigned to pseudo signals and their weights (inverse of the variance covariance matrix) were set to zero.

The concept of pseudo signals is straight forward but there are certain requirements on using the pseudo signal. The new signal should satisfy the Gaussian white noise requirements for the KF. The systematic method to compute the pseudo signal Gaussian noise is by taking the spectral density,  $q$ , of the original signal. The  $q$  values are used to design the  $Q_k$  matrix of the EKF as provided in equation 2-14. The spectral density is a function of the standard deviation (STD) of the signal and the BW of the IMU.

$$\sqrt{q} = \frac{STD_{sensor}}{\sqrt{BW_{IMU}}} \quad 5-1$$

The corresponding noise values for the accelerometer and gyros that needed to be removed can be computed for the  $Q_k$  matrix. This matrix predicts the measurements depending on the quality of the signals and thus it is important to satisfy the Gaussian white noise requirements. The accelerometer and gyros used in this thesis are from the CIU which have signal standard deviations of  $0.084\text{m/s}^2$  and  $0.0035\text{deg/s}$  (static portion of Figure 5-3). Using these two values the spectral densities can be estimated as follows:

$$\sqrt{q_{accel}} = \frac{0.084}{\sqrt{40}} = 0.013\text{m/s} / \sqrt{s} \text{ and}$$

$$\sqrt{q_{gyro}} = \frac{0.0035}{\sqrt{40}} = 5.5e^{-4} \text{deg} / \sqrt{s}$$

The KF may diverge if the actual errors of the pseudo signals are not mainly white noise. To avoid such a problem, the noise spectral density is set to a much higher value to ensure that the filter does not provide any weight to the omitted sensors.

For the 2G3A configuration, the roll gyro was removed from the full IMU. As the data is from a full IMU, a pseudo signal of 0.0 was assigned to the roll gyro and the corresponding weight ( $\text{Variance}^{-1}$ ) value was also set to zero. In addition to that, the ARW value for the roll gyro was increased. Refer to the row which corresponds to Gyro-X in Table 5-1. This is to ensure that the AINS<sup>TM</sup> navigation filter will not use the measurement from this sensor and is equivalent to physically removing the sensor from the full IMU at the data processing level.

1G3A configuration only has a heading gyro and similar to the first case, pseudo signals of 0.0 magnitudes were assigned to both roll and pitch gyros and the signal weights were set to 0.0. The corresponding ARW values were also increased for the two sensors as shown in Table 5-1 (Gyro-X and Gyro-Y rows). The next set of simulations is for 1G2A sensor configuration. In this case, the vertical accelerometer signal was also removed by assigning it a pseudo signal value of -9.81 m/s/s. This was in addition to removal of the roll and pitch gyros as mentioned in 1G3A case. The corresponding weights of the omitted sensors were set to zeros and the RW values were also increased to ensure that the sensors are not used in the navigation KF (Table 5-1 – rows correspond to Accel-Z, Gyro-X and Gyro-Y).

The final configuration contains just one gyro, the heading gyro, and one accelerometer. In this case, pseudo signals of magnitude 0.0 replaced the original signals for roll gyro, pitch gyro and lateral accelerometer. The vertical accelerometer was assigned the pseudo signal of -9.81m/s/s as mentioned earlier. Also the weights of the omitted sensors were reduced to zero and the corresponding RW values were increased as shown in Table 5-1.

**Table 5-1: Omitted sensor values for AINS™ for partial sensors configuration**

	Original Values			Assigned Values		
	Signal	Variance <sup>-1</sup> (Weight)	RW	Signal	Variance <sup>-1</sup> (Weight)	RW
Accel-Y	From file	Bias & SF variance from calibration	VRW <sub>Y</sub> from calibration	0.0	0.0	12.25x VRW <sub>Y</sub>
Accel-Z	From file	Bias & SF variance from calibration	VRW <sub>Z</sub> from calibration	-9.81 m/s <sup>2</sup>	0.0	12.25x VRW <sub>Z</sub>
Gyro-X	From file	Bias & SF variance from calibration	ARW <sub>X</sub> from calibration	0.0	0.0	25xARW <sub>X</sub>
Gyro-Y	From file	Bias & SF variance from calibration	ARW <sub>Y</sub> from calibration	0.0	0.0	25xARW <sub>Y</sub>

## 5.2 Results

This section is divided into two subsections. The first subsection presents the position drift errors with respect to the reference solution without the use of any extra aiding sources (e.g. NHC). The second subsection presents the same results but after NHCs were applied during the test data processing.

### 5.2.1 Drift Errors without NHC

The position drift errors without NHC for datasets 1 and 2 are given in Figure 5-6. The figure clearly demonstrates that the mean of the drift errors will increase as the sensors are removed from the inertial unit, despite the fact that a land vehicle motion is constrained. Irrespective of the different magnitude for the mean drift errors the trend for the two datasets is similar.

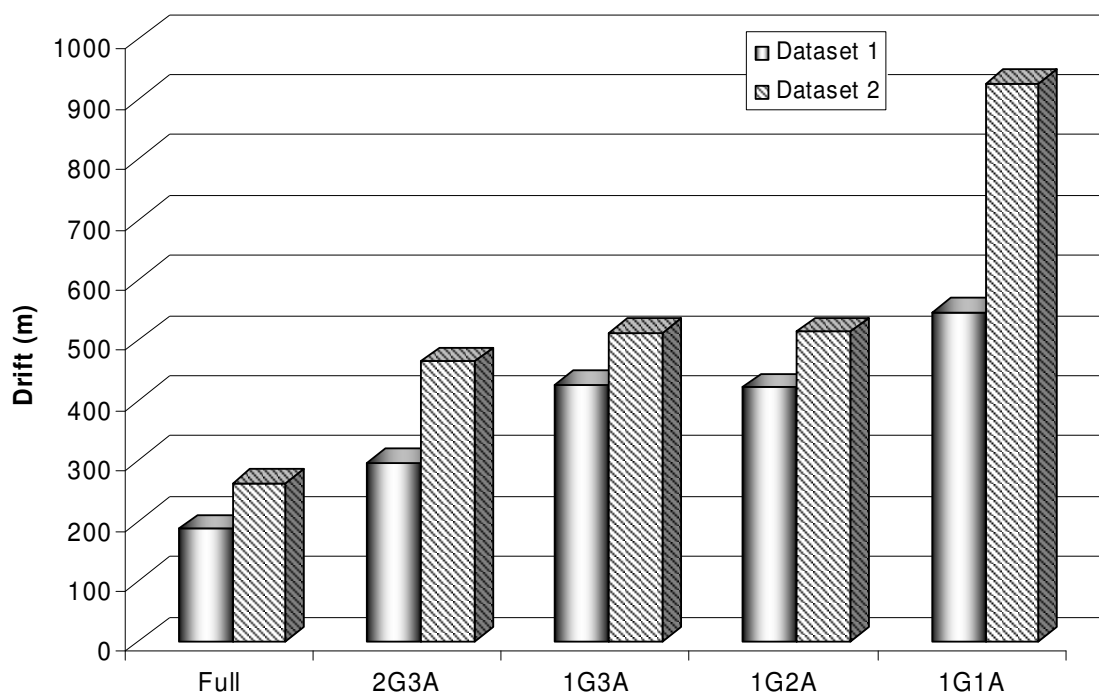


**Figure 5-6: Average drift errors for the different sensor configurations for dataset 1 and dataset 2.**

Figure 5-7 shows an example of the estimated roll and pitch with their standard deviations for full and partial (1G2A) sensor configurations. The KF estimates the errors in roll and pitch but the error is much more random with higher amplitude than the full sensor case. This is due to the higher RW values that were used in the simulations.

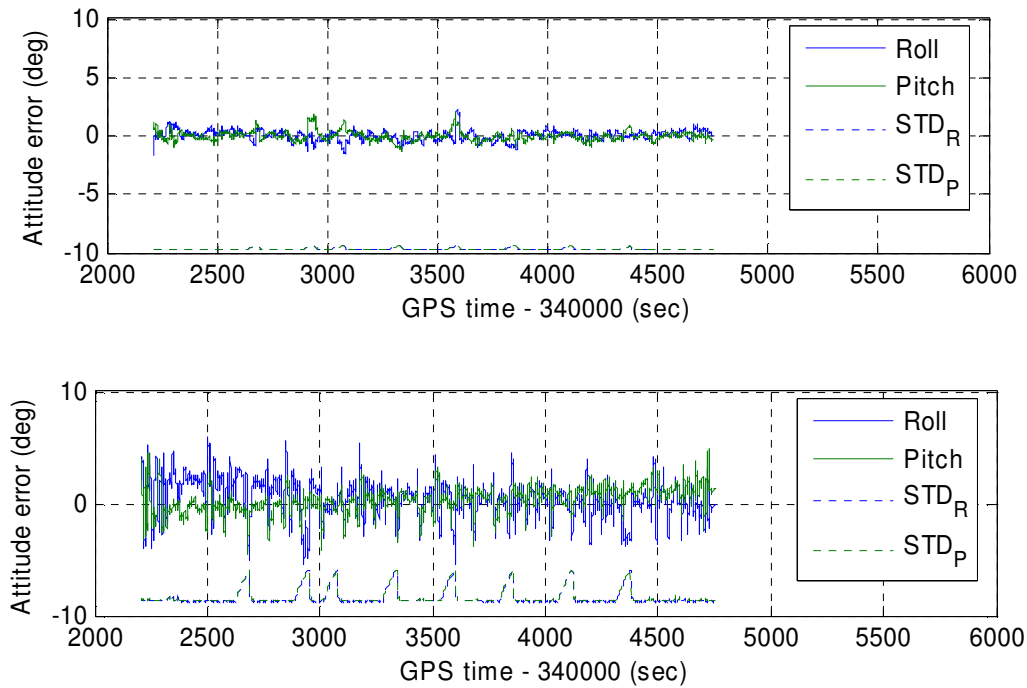


**Figure 5-7: Estimated roll and pitch errors for full (top panel) and 1G2A (bottom panel)**

### 5.2.2 Drift Errors with NHC

The NHC were applied to both datasets and the mean drift errors are given in Figure 5-9. It is evident that the application of the NHC reduced the overall drift errors and therefore, application of these constraints is desirable for an accurate navigation system. Recall that NHC make assumptions about the vehicle's velocity and therefore, a good alignment between  $b$ -frame and  $v$ -frame is required.

The dataset 1 has roll and pitch misalignments between  $b$ -frame and  $v$ -frame, while dataset 2 has virtually no misalignment between the two frames as shown in Figure 5-8. Theoretically, the NHC for dataset 1 should not decrease the drift errors as effectively as

for dataset 2 due to the underlying misalignment angles. More discussion on the misalignment is provided in Chapter 6.

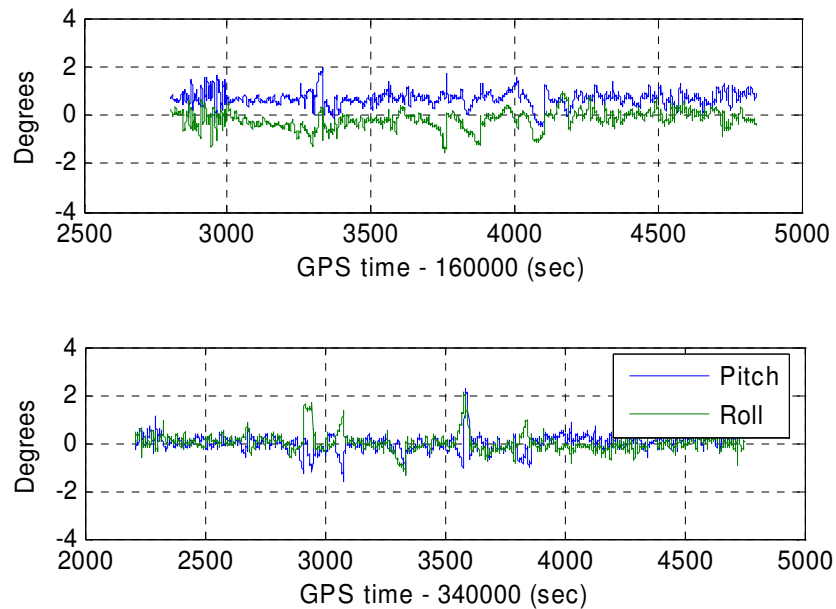


**Figure 5-8: Roll and pitch misalignments for dataset 1 (top panel) and dataset 2 (bottom panel)**

Consequently, the NHC decrease the drift errors by only 37.62% for dataset 1 (dataset with small misalignments) and 81.13% for dataset 2 (with no misalignment). Full IMU outperformed any other partial sensor configuration but it is interesting to note that 1G2A sensor configuration produced better overall results as compared to the other partial sensor configurations. For dataset 1 the mean drift errors for 1G2A is close to the full IMU, however, the 2G3A results are exhibiting slight degradation. For dataset 2, the mean drift errors for 2G3A, 1G3A and 1G2A are similar to each other ([Syed et al., 2007-c](#)).



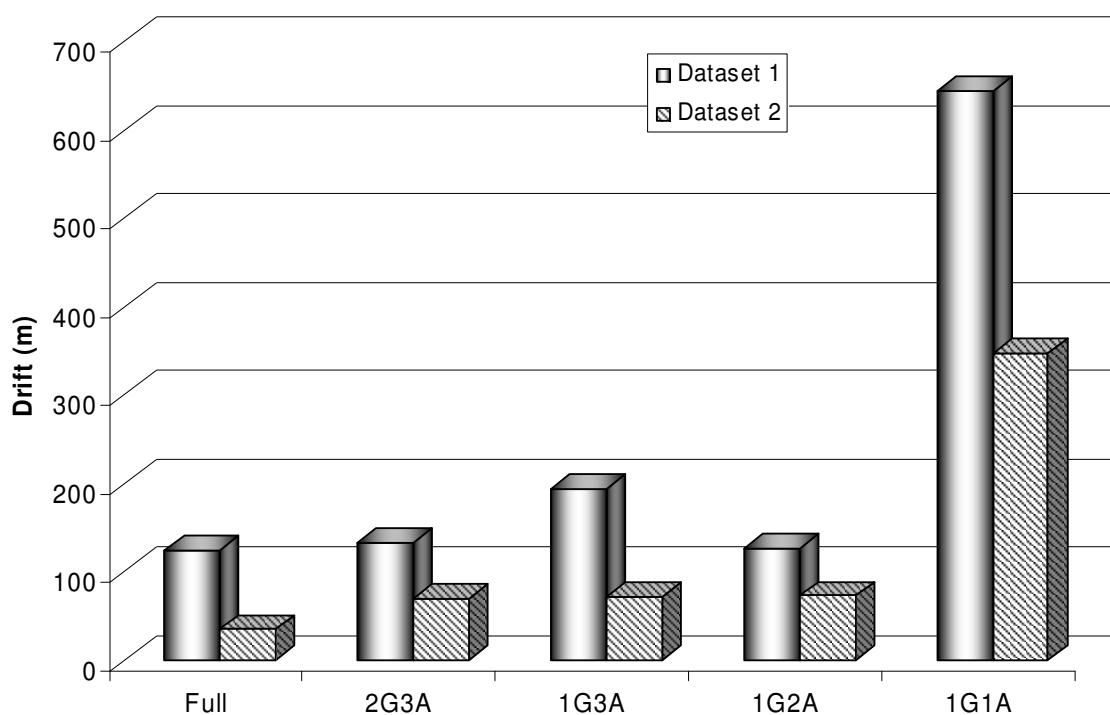


**Figure 5-9: Average drift errors for the different sensor configurations for dataset 1 and dataset 2 using NHC.**

### 5.3 Summary

The results of 2G3A are better than 1G3A or 1G2A without NHC. Without this constraint, the system is free to use its orientation information with no restrictions on the velocities depending on the sensor outputs. The presence of pitch gyro, therefore, was actually used in the navigation which resulted in the improved performance of a system with both heading and pitch gyros as compared to systems with only heading gyros.

The performance of 1G3A and 1G2A were quite similar mainly because the vertical accelerometer does not add significantly in land vehicle navigation. 1G1A degraded the results accuracy even further due to the inability of the system to measure centripetal accelerations that occur during turns.

NHC actually disregards the orientation information and constraints the land vehicle to a well levelled horizontal plane. For most of the applications, these constraints improve the accuracies as shown in Figure 5-9. However, it is clear that if NHC are applied, the best sensor combination is 1G2A where an ideal signal was assigned to the vertical accelerometer. Also, it is evident from the results that any misalignment between  $b$ - and  $v$ -frame will actually reduce the benefits of NHC. From this point onwards, two different kinds of results will be discussed in the upcoming chapters. The first set of results relate to full six sensors system (full IMU) while the second set will have 1G2A configuration for in-vehicle and 1G3A for on-foot navigation where physical dynamics of leg movements are captured by the vertical accelerometer.

So far, a PNS's major issues have been addressed and the thesis can now focus on the next issue of portability. An integrated system needs alignment and this issue becomes a major design issue when a portable system is required.

## Chapter Six: Required Alignment of a Portable Navigation System

Inertial systems require alignment whereby the orientation of the axes of an inertial system ( $b$ -frame), which should follow the axes of the  $v$ -frame as shown in Figure 2-15 (left panel), is determined with respect to a reference frame such as the  $l$ -frame or the  $n$ -frame. The alignment can be achieved by levelling and velocity matching. For MEMS sensors, the strong gravity signals from accelerometers can be used to determine the angular displacements in the roll and pitch of the inertial system the  $b$ -frame with respect to the reference frame. However, the basic assumption in this alignment is that the inertial system the  $b$ -frame is perfectly aligned with the  $v$ -frame. It means that the first set of accelerometer and gyro is pointing in the forward/backward direction, second set associate to the sides of the vehicle and finally, the third set is in the vertical direction ([Syed et al., 2008](#)).

For a PNS, the alignment of the system with the vehicle may not be guaranteed. Consequently, two issues arise: 1) what are the effects of misalignment on the navigation accuracies and 2) what can be done to mitigate the misalignment effects?

### 6.1 Considerations for MEMS Sensors Navigation

There are two types of alignment that are required before the navigation parameters can be estimated. The first alignment is the alignment of the IMU the  $b$ -frame with respect to the vehicle axes, i.e., making the  $b$ -frame coincides with the  $v$ -frame. Once they are

aligned then the next stage is aligning the  $b$ -frame with respect to the  $l$ -frame. Please refer to Figure 6-1 for a summary of navigation process. The alignment of the  $b$ -frame with the  $l$ -frame is a well researched area and can be found in any standard navigation book ([Titterton and Weston, 1997](#)). However, there is no discussion on the topic of the  $b$ -frame and the  $v$ -frame alignment which is important for a PNS.

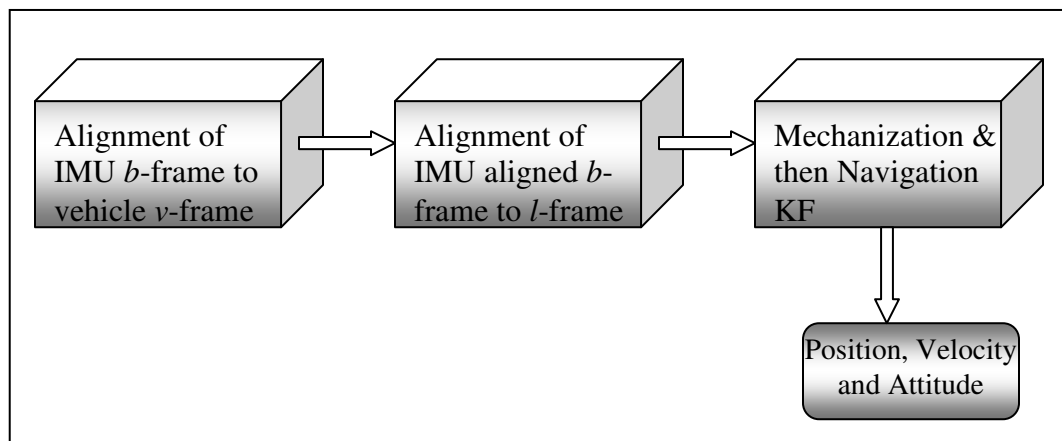


**Figure 6-1. Summary of Navigation process**

### **6.1.1 Portable Navigation System**

Two strategies can be implemented to align a PNS ( $b$ -frame) with the  $v$ -frame

- 1) Start navigation from a good GPS availability area and use the initial attitude errors from the navigation KF as the orientation parameters.
- 2) Restrict the orientation of the PNS to allowable limits.

There are pros and cons of both methods. For the first case, the user does not require orienting the PNS and therefore, the system can be considered user friendly. But to make the inertial sensors work, the system should have a GPS signal lock and also the user has

to stay under open sky conditions until the KF converges. These restrictions are not realistic as it is quite likely that the system will be initialized in a situation of denied GPS signal, such as a vehicle parked in an underground parking lot. Therefore, it is suffice to say that the condition of GPS availability may not be satisfied for all the common usage scenarios.

The second strategy is about limiting the orientation errors. In this case, the user requires aligning the PNS such that the IMU  $b$ -frame and  $v$ -frame are in good agreement. The orientation accuracy will totally depend on the user and it is quite easy to assume that even a careful user cannot align the system properly at every use.

An easy way to solve this problem is the introduction of a holder inside the vehicle that is aligned with the vehicle and provides the user an easy way to align the system at every use. The introduction of such a holder means that the user needs an extra component. On the plus side, if using such an aligned portable system, the navigation can be started without the condition of GPS lock. The user still needs to orient the holder at the first usage or when transferring the unit between vehicles and this will require the error budget on the alignment.

### ***6.1.2 Commercial Perspectives***

To reduce the cost of a PNS, a partial system is more attractive from a commercial perspective. The consideration of a partial system with minimum number of sensors, however, will require even more accurate alignment, especially in the roll and pitch direction. Any angular displacement of the system will not be able to resolve the correct

heading due to lack of information available. Therefore, to design a cost effective PNS, the following issues are important and are answered in this chapter.

- 1) What kind of sensor/vehicle alignment accuracy is required to obtain meaningful navigation results?
- 2) What is the required accuracy for the  $b$ -frame to the  $v$ -frame alignment if a partial IMU is used?
- 3) Can NHC improve the navigation results? What kind of alignment accuracy is required for these constraints to benefit the overall results?

To summarize, the purpose of this chapter is to estimate the effects of misalignment errors between the IMU  $b$ -frame and the vehicle  $v$ -frame (Figure 2-15). This misalignment will produce errors in initial alignment of the system and thus will result in erroneous navigation solution. Full IMU and partial IMU are studied and allowable misalignment limits for meaningful navigation solution is deduced.

## 6.2 Methodology

The methodology section is divided into four components to clearly differentiate different methods used to obtain the results. Section 6.2.1 provides a method to simulate misalignment errors in the field datasets that were collected with good alignment with the  $v$ -frame. The next two subsections give the information about the collected datasets and the analysis method. The last subsection contains an algorithm that can estimate the misalignments.

### 6.2.1 Simulation of Misalignment

To study the effect of misalignment, a Matlab® script was developed that converts the well aligned inertial signals from full IMU to the specified misaligned signals. The desired misalignment angles are first converted into the DCM and then multiplied with the well aligned inertial signals.

1) Calculating the DCM matrix:

Given below are the sequences of rotations from the  $v$ -frame to the IMU  $b$ -frame to obtain the DCM matrix when desired misalignment angles are introduced.

- a. A rotation about z-axis through the heading misalignment angle ( $\psi$ )
- b. A rotation about y-axis through the pitch misalignment angle ( $\theta$ )
- c. A rotation about x-axis through the roll misalignment angle ( $\phi$ )

$$DCM = \begin{bmatrix} 1 & 0 & 0 \\ 0 & \cos \phi & \sin \phi \\ 0 & -\sin \phi & \cos \phi \end{bmatrix} \begin{bmatrix} \cos \theta & 0 & -\sin \theta \\ 0 & 1 & 0 \\ \sin \theta & 0 & \cos \theta \end{bmatrix} \begin{bmatrix} \cos \psi & \sin \psi & 0 \\ -\sin \psi & \cos \psi & 0 \\ 0 & 0 & 1 \end{bmatrix} \quad \mathbf{6-1}$$

2) Multiplying the DCM with IMU signals:

Next the DCM is multiplied to the well aligned IMU data to obtain misaligned simulated signal values as given in equation 6-2.

$$\begin{bmatrix} x_{misaligned} \\ y_{misaligned} \\ z_{misaligned} \end{bmatrix} = DCM \begin{bmatrix} x_{aligned} \\ y_{aligned} \\ z_{aligned} \end{bmatrix} \quad \mathbf{6-2}$$

In this chapter, both accelerometer and gyro data are misaligned using the above formula. This will ensure that the analysis is unbiased and only represents the simulated misalignment. The range of simulated misalignments for the attitude varied from  $-45^\circ$  to  $45^\circ$ .

### ***6.2.2 Test Trajectories and Simulated GPS Outages***

Data from two test trajectories are being studied in this chapter. Dataset 1 was collected in August 2004 and dataset 2 is the same as dataset 1 of Chapter 5. For dataset 1, both test CIU and LN200 were installed inside the test vehicle while the NovAtel's OEM4 receiver was installed on the roof. Another OEM4 receiver was used to provide a DGPS solution for the reference trajectory at the base station (Roof of University of Calgary Engineering building).

The dataset 1 trajectory as shown in Figure 6-2 started from medium GPS signal quality where the number of observed satellites were 5 to 6 and then covered good quality GPS (7 or more satellites) on a highway.

To evaluate the performance of the CIU, the position drift of the test IMU during GPS signal blockages is used as the key indicator. In this chapter, 60 second long GPS signal outages were simulated that cover different parts of the trajectory as shown in Figure 6-2 and Figure 5-4. The IMU position errors during GPS signal outages are obtained by comparing the corresponding solution to the reference trajectory. The position errors showed the performance of the CIU as a stand-alone system and the comparison of the degradation due to misalignment was made on the basis of these position drift errors. The



attitude errors were also considered as a supplementary analysis tool to draw the conclusions.

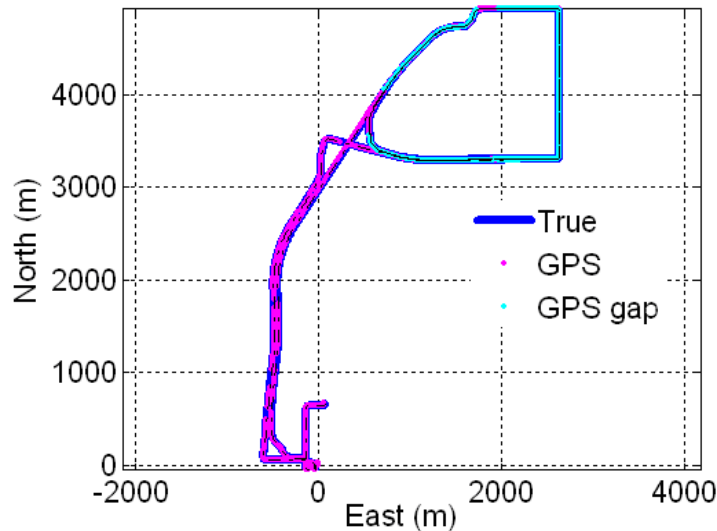


**Figure 6-2. Trajectory for dataset 1 with eight simulated GPS outages (some outages are overlapped)**

### 6.2.3 Analysis Strategy

As this study is to evaluate the limits for the misalignment of the IMU  $b$ -frame to the  $\nu$ -frame without any knowledge of the presence of this error to the integration tool, the analysis will always be provided with respect to the drift errors of a well aligned test CIU. These drift errors are given for GPS signal outage periods with respect to the reference trajectory. Two different analysis criteria were used as given below:

- 1) Comparison of the maximum position drift errors during GPS signal outages between a misaligned (the  $\nu$ -frame to the IMU  $b$ -frame) and a properly aligned the IMU  $b$ -frame
- 2) Comparison of the estimated attitude errors during GPS signal outages between a misaligned (the  $\nu$ -frame to the IMU  $b$ -frame) and a properly aligned IMU

### 6.2.4 Misalignment Estimation

Misalignment from  $\nu$ -frame to the  $b$ -frame can be estimated by velocity aiding using a similar method as described in Section 2.6. Hence, this section will also discuss the structure of a simple KF that can be implemented for the misalignment estimation. As the updates to the KF will be the vehicle's velocity in the  $\nu$ -frame, the misalignment estimation will be in the  $\nu$ -frame as well. Recall that equation 2-41 provides a DCM  $R_b^\nu$  consisting of the misalignment angles between the two frames. For misalignment estimation, we can start from this matrix and write it in terms of its components as:

$$(R_b^\nu)^T = R_\nu^b = \hat{R}_\nu^b (I - [\boldsymbol{\varepsilon}^\nu \times]) \quad \mathbf{6-3}$$

where  $\tilde{R}_\nu^b$  is the estimated DCM and  $[\boldsymbol{\varepsilon}^\nu \times]$  is the skew symmetric representation of the misalignment vector

$$[\boldsymbol{\varepsilon}^\nu \times] = \begin{bmatrix} 0 & -\delta\Psi & \delta\phi \\ \delta\Psi & 0 & -\delta\theta \\ -\delta\phi & \delta\theta & 0 \end{bmatrix} \quad \mathbf{6-4}$$

where  $\boldsymbol{\varepsilon}^\nu$  is a vector of misalignments between  $\nu$ -frame and  $b$ -frame represented in  $\nu$ -frame,  $\delta\theta$  is the roll misalignment,  $\delta\phi$  is the pitch misalignment and  $\delta\Psi$  is the misalignment in the azimuth direction.

The state vector for this simplified KF will consist of misalignment error vector as given in equation 6-5. These errors are random constants as it is assumed that the misalignment will not change during the estimation which will be utilized in the derivation of dynamic model for the KF.

$$\delta \mathbf{x} = \boldsymbol{\varepsilon}^v = \begin{bmatrix} \delta \theta \\ \delta \phi \\ \delta \Psi \end{bmatrix} \quad \mathbf{6-5}$$

And the dynamic model can be written simply as

$$\delta \dot{\mathbf{x}} = 0 \quad \mathbf{6-6}$$

The measurement equation should relate the  $v$ -frame velocities with the misalignment errors and the covariance matrix for the measurements. As the misalignment is between  $b$ -frame and  $v$ -frame, the following relationship will be used for the derivations.

$$\mathbf{v}^b = \mathbf{R}_v^b \mathbf{v}^v \quad \mathbf{6-7}$$

However, the velocities computed in the  $b$ -frame will have some errors ( $e$ ) and a complete equation will be the one that will account for the errors.

$$\hat{\mathbf{v}}^b = \mathbf{R}_v^b \mathbf{v}^v + e \quad \mathbf{6-8}$$

Substitution of equation 6-3 in equation 6-8 and then by conducting some manipulation of the terms, will provide the required measurement equation as follows:

$$\begin{aligned} \hat{\mathbf{v}}^b &= \hat{\mathbf{R}}_v^b \left( \mathbf{I} - [\boldsymbol{\varepsilon}^v \times] \right) \mathbf{v}^v + e \\ \hat{\mathbf{v}}^b &= \hat{\mathbf{R}}_v^b \mathbf{v}^v - \hat{\mathbf{R}}_v^b [\boldsymbol{\varepsilon}^v \times] \mathbf{v}^v + e \\ \underbrace{\hat{\mathbf{v}}^b - \hat{\mathbf{R}}_v^b \mathbf{v}^v}_{\delta \hat{\mathbf{x}}_k} &= \underbrace{\hat{\mathbf{R}}_v^b}_{H_k} [\mathbf{v}^v \times] \underbrace{[\boldsymbol{\varepsilon}^v]}_{\delta \hat{\mathbf{x}}_k} + e \end{aligned} \quad \mathbf{6-9}$$

where  $\mathbf{v}^v \times$  is the skew-symmetric representation of the velocity vector in  $v$ -frame

The computation of the variance covariance matrix, which is an indication of the accuracies, for the measurement model is also required. This computation needs some a-priori information about the velocities used in the derivation. As the velocities and their respected accuracies are calculated in  $l$ -frame in the navigation KF we can exploit this information by using the following relationship.

$$\hat{v}^b = \hat{R}_l^b \hat{v}^l \quad \mathbf{6-10}$$

The expanded form of this equation will be

$$v^b + \delta v^b = R_l^b (I + E^l) (v^l + \delta v^l) \quad \mathbf{6-11}$$

where  $\delta$  and  $E$  terms represent the errors in velocities and angular measurements

Collecting the first order error terms from the above equation will provide the relationship for the  $b$ -frame velocity error with the  $l$ -frame measurements.

$$\begin{aligned} \delta v^b &= R_l^b \delta v^l + R_l^b E^l v^l \\ \delta v^b &= R_l^b \delta v^l + R_l^b (\epsilon^l \times) v^l \\ \delta v^b &= R_l^b \delta v^l - R_l^b (v^l \times) \epsilon^l \end{aligned} \quad \mathbf{6-12}$$

The variance covariance matrix ( $R$ ) can be computed by using the expectations on the square of the above vectors.

$$\begin{aligned} R &= E \left\{ \delta v^b (\delta v^b)^T \right\} \\ R &= E \left\{ \left( R_l^b \delta v^l - R_l^b (v^l \times) \epsilon^l \right) \left( R_l^b \delta v^l - R_l^b (v^l \times) \epsilon^l \right)^T \right\} \\ R &= E \left\{ R_l^b \delta v^l (\delta v^l)^T R_b^l \right\} + E \left\{ R_l^b (v^l \times) \epsilon^l (\epsilon^l)^T (v^l \times)^T R_b^l \right\} \\ &\quad - 2E \left\{ R_l^b \delta v^l (\epsilon^l)^T (v^l \times)^T R_b^l \right\} \\ R &= R_l^b E \left\{ \delta v^l (\delta v^l)^T \right\} R_b^l + R_l^b (v^l \times) E \left\{ \epsilon^l (\epsilon^l)^T \right\} (v^l \times)^T R_b^l \\ &\quad - 2R_l^b E \left\{ \delta v^l (\epsilon^l)^T \right\} (v^l \times)^T R_b^l \end{aligned} \quad \mathbf{6-13}$$

where  $E \left\{ \delta v^l (\delta v^l)^T \right\}$  and  $E \left\{ \epsilon^l (\epsilon^l)^T \right\}$  are the standard deviations of the velocity and attitude from the navigation KF and  $E \left\{ \delta v^l (\epsilon^l)^T \right\}$  is the portion of the  $P$  matrix that corresponds to the correlation of velocity and attitude error.

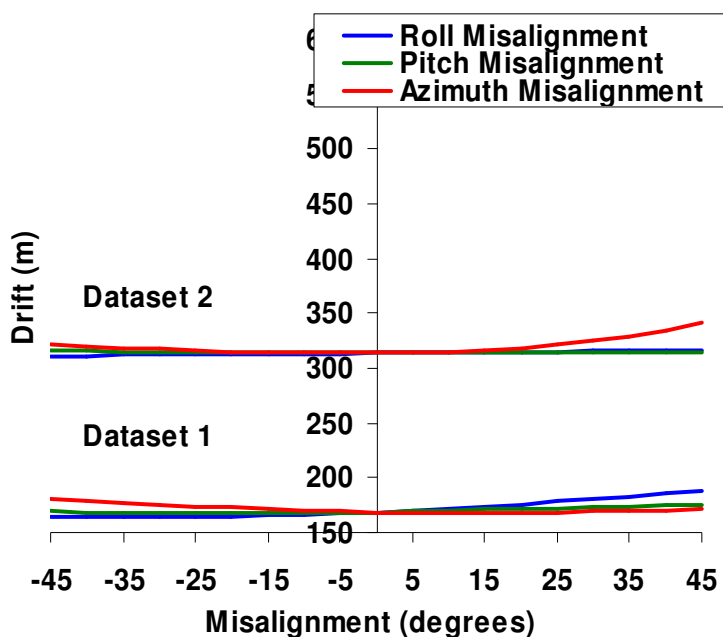
### 6.3 Results

The results section is divided into two subsections. The first subsection consists of the simulation results for the full IMU and the second subsection comprises of partial IMU

results. Each of the subsection is further divided into two parts to show the results with and without NHC.

### 6.3.1 Full IMU without NHC

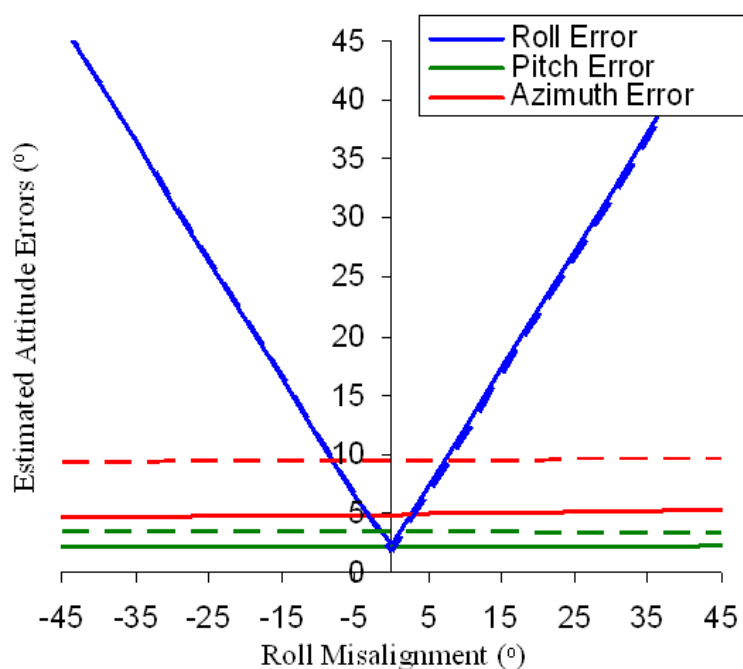
The results in Figure 6-3 show the maximum position drift errors for simulated misalignments in three axes for the two data sets. The blue lines represent the mean position drift when the roll misalignment is varied from  $-45^\circ$  to  $+45^\circ$ . The green lines show the results for simulated pitch misalignments with respect to the no misalignment case. The red line demonstrates the position drift results with azimuth misalignment. In all cases, the average drift stayed within 2% of the perfectly aligned dataset drift errors.



**Figure 6-3. Drift errors for full IMU during GPS outages without NHC**

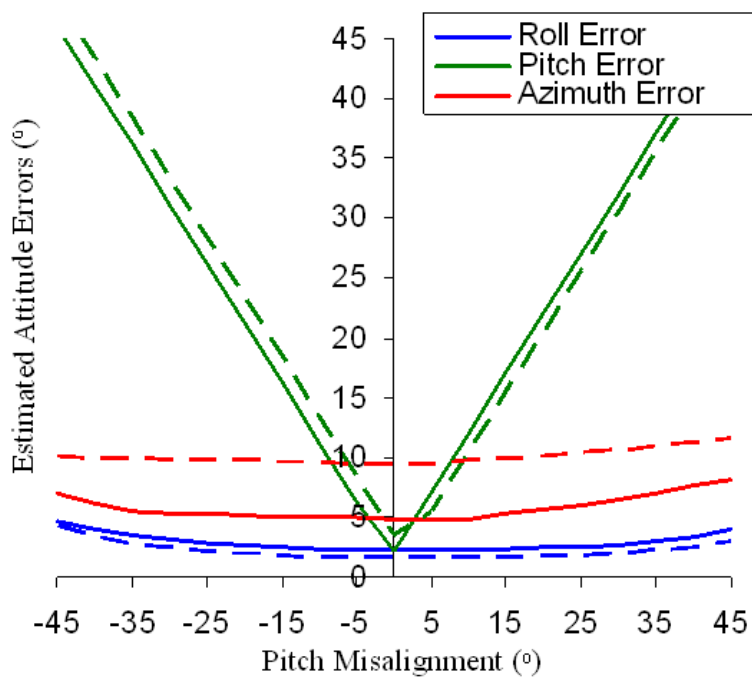
The next set of results shows the ability of the EKF to estimate the induced attitude errors due to the misalignment along each axis. First, misalignments from  $-45^\circ$  to  $+45^\circ$  were simulated in the roll angle and the maximum error estimated by the EKF in roll, pitch and

azimuth attitude was investigated in Figure 6-4 for the two data sets. The EKF showed an induced error of approximately  $\pm 45^\circ$  in roll angle (blue lines) when the roll was misaligned to  $\pm 45^\circ$ . As this roll error is calculated with respect to a well aligned inertial system roll angles, therefore it shows the ability of the full IMU to determine the simulated misalignment. The green and red lines show the estimated errors in pitch and azimuth when the roll angle was misaligned.



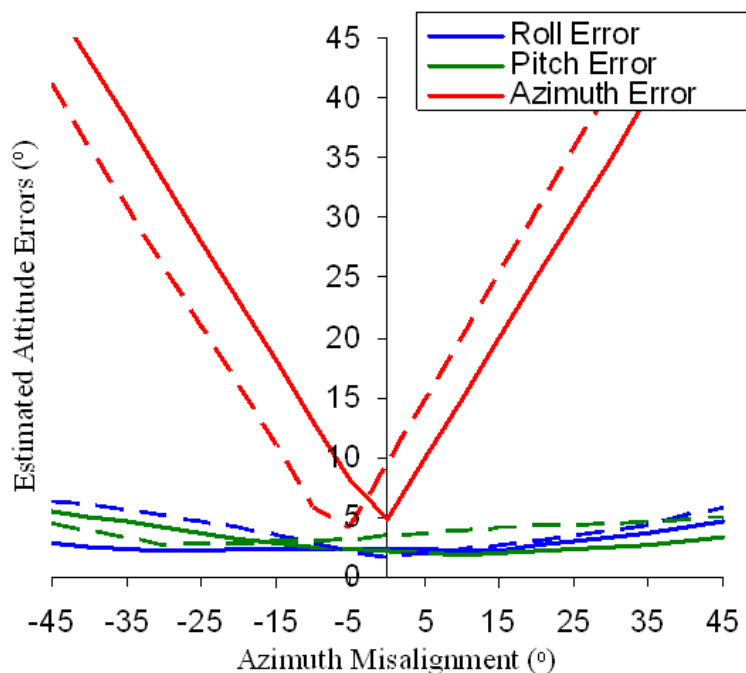
**Figure 6-4. Induced attitude errors due to roll misalignment (Solid lines for dataset 1 and dashed lines for dataset 2)**

Figure 6-5 shows the result for the two datasets when pitch misalignment was simulated. The result indicates that a misalignment in pitch will induce larger errors in roll and azimuth estimation as compared to the roll misalignment case. The EKF was also able to estimate the induced misalignment in pitch that was simulated in the datasets (green lines Figure 6-5). Again, the misalignment errors are provided with respect to a well aligned IMU in the same vehicle.



**Figure 6-5. Induced attitude errors due to Pitch misalignment (Solid lines for dataset 1 and dashed lines for dataset 2.)**

Simulated azimuth misalignments are given in Figure 6-6 with respect to a well aligned IMU navigation results. The navigation EKF estimation for the induced errors in roll, pitch and azimuth show that roll and pitch are also exhibiting degradation when the azimuth was misaligned from -45 to +45 degrees.



**Figure 6-6. Induced attitude errors due to Azimuth misalignment (Solid lines for dataset 1 and dashed lines for dataset 2.)**

The average induced errors for the two data sets due to simulated misalignments in roll, pitch and azimuth are given in Table 6-1.

Even though the specific values are different which is mainly due to road conditions since both datasets were collected on different trajectories with different roll and pitch angles, the results can be summarized together. A misalignment in roll angle will affect the estimation of the other two attitude angles minimally as pitch and azimuth are the important attitude angles for land vehicle navigation.

Misalignments in pitch will affect both roll and azimuth estimation. Similarly, roll and pitch attitude angles will be affected for any misalignment in azimuth angle. Moreover, the average drift errors remain within 2% of the perfectly aligned system for any misalignment case. As it is evident that both datasets show similar trend for a particular



misalignment simulation, therefore, for simplicity only typical results will be shown from this point forward.

**Table 6-1. Degradations of full IMU(without NHC) under different misalignments**

<b>Dataset 1</b>				
Due to misalignment in	Estimated induced average error in			
	Roll %	Pitch %	Azimuth %	Drift %
Roll	Misalign	0.57	0.75	1.61
Pitch	17.43	Misalign	13.62	0.86
Azimuth	11.14	21.20	Misalign	1.64
<b>Dataset 2</b>				
Due to misalignment in	Estimated induced average error in			
	Roll %	Pitch %	Azimuth %	Drift %
Roll	Misalign	0.06	0.02	0.03
Pitch	22.56	Misalign	5.93	0.18
Azimuth	52.07	5.76	Misalign	1.91

### 6.3.2 Full IMU with NHC

The next set of simulations is conducted with NHC. Position drift errors and induced errors in the attitude angles due to misalignment in any of the axes are investigated. The application of these constraints for perfectly aligned case significantly reduces the position drift errors when compared to the results without the constraints.

Figure 6-7 shows typical position drifts when misalignment along roll (blue line), pitch (green line) or azimuth (red line) axis was simulated. Figure 6-8 depicts a typical

example when misalignment was simulated in azimuth axis and it induced significant errors in all attitude angles. The blue, green and red lines for Figure 6-8 show the estimated attitude errors by the EKF in roll, pitch and azimuth when azimuth axis was misaligned with respect to the  $v$ -frame. This is in accordance with our previous analysis that NHC strictly depends on the alignment of the IMU and therefore, can only improve the navigation solution when the IMU is perfectly aligned with the  $v$ -frame as discussed in Section 5.2.2 as well.

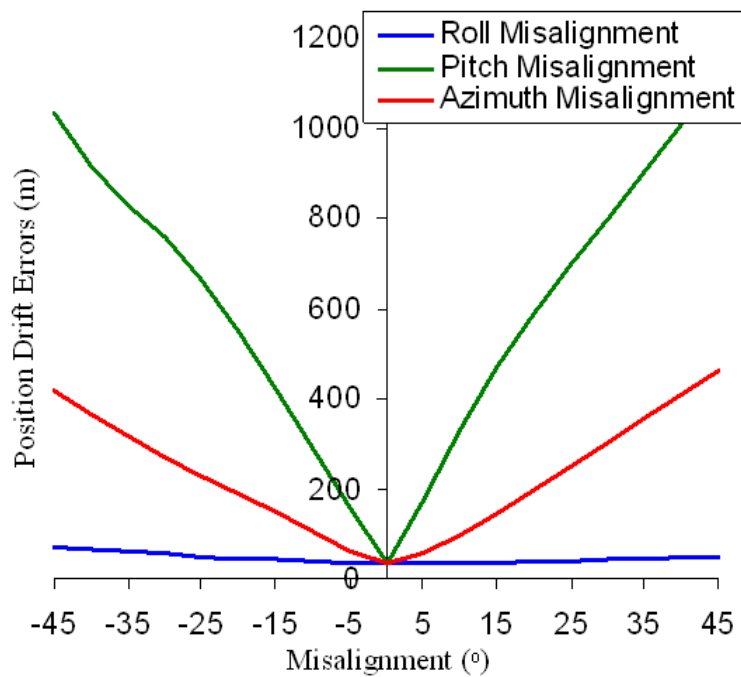


**Figure 6-7. Typical Position Drift errors for full IMU during GPS outages, with non-holonomic constraint**



**Figure 6-8. Typical induced attitude errors due to misalignment in azimuth**

### 6.3.3 IG2A without NHC

The first set of results show the position drift errors after simulating misalignment in roll, pitch and azimuth angles individually. Here it is important to note that the position drift error for perfectly aligned case of the partial IMU is larger than the position drift for any arbitrary case of the full IMU, mainly because of the missing sensors. An average of 50% increase in position drifts were observed for both datasets for the roll and pitch misalignment cases. The azimuth misalignment, on the contrary, only degraded the average position drift error less than 10% (Figure 6-9 and Figure 6-10).

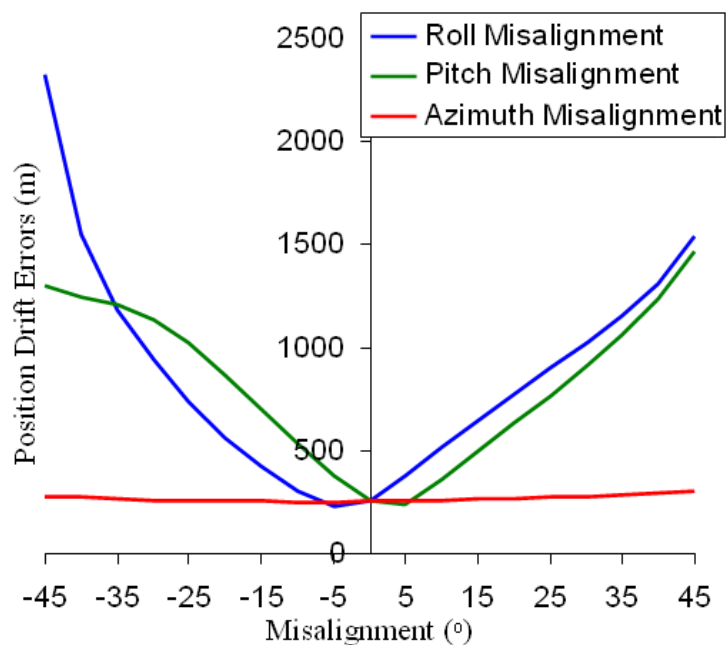


Figure 6-9. Position drifts for dataset 1 without NHC under different misalignments

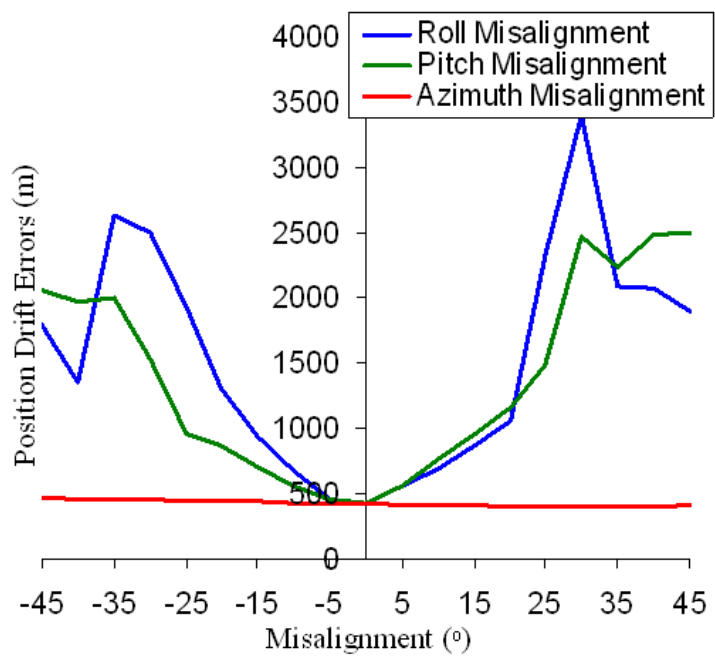


Figure 6-10. Position drifts for dataset 2 without NHC under different misalignments

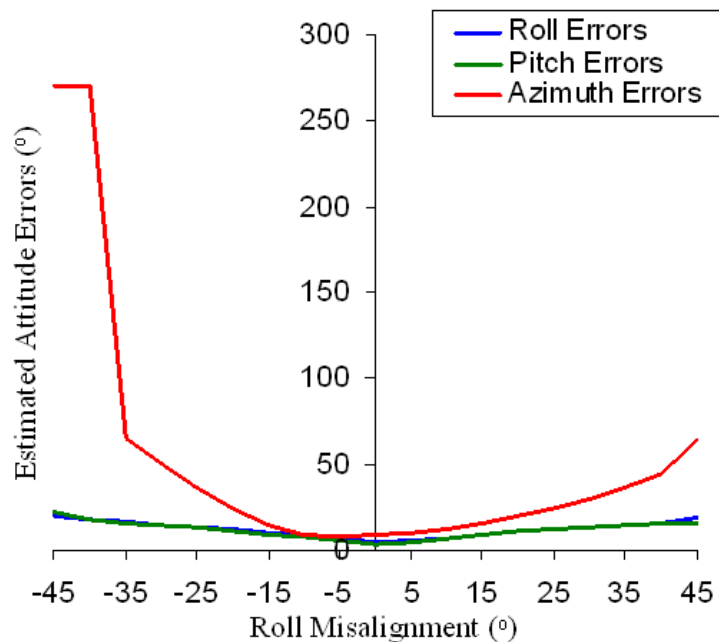
The average percent increase in position drift errors are summarized in Table 6-2. Also in the same table, the averages of the percent increase in attitude errors are provided. The table clearly indicates that only simulated misalignment in azimuth can be closely estimated as partial IMU only contains an azimuth sensing gyro. Moreover, the effect of azimuth misalignment on roll and pitch angles is minimal as the EKF is able to detect the respective error in the azimuth properly.

**Table 6-2. Degradations of partial IMU (without NHC) under different misalignments.**

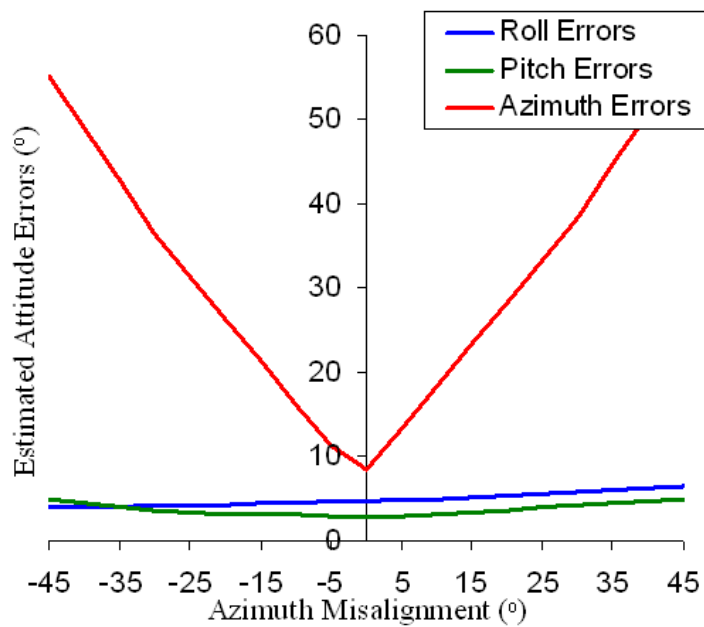
<b>Dataset 1</b>			
Due to Misalignment in			
	Roll	Pitch	Azimuth
Average Position Drift Errors increase	57.46 %	59.08 %	5.10%
Average Attitude Error increase	61.87 %	51.06 %	22.96 %
<b>Dataset 2</b>			
Due to Misalignment in			
	Roll	Pitch	Azimuth
Average Position Drift Errors increase	60.01 %	56.93 %	0.80%
Average Attitude Error increase	32.17 %	23.15 %	0.04%

Figure 6-11 shows typical induced errors in all three attitude angles when roll was misaligned, while Figure 6-12 has typical resultant attitude angles errors when misalignments were simulated in azimuth. The average values given in Table 6-2 can be

easily interpreted from these two figures. The non-symmetry of Figure 6-11 shows the inability of the partial sensors to estimate the roll misalignment errors properly.



**Figure 6-11. Typical roll misalignment results**

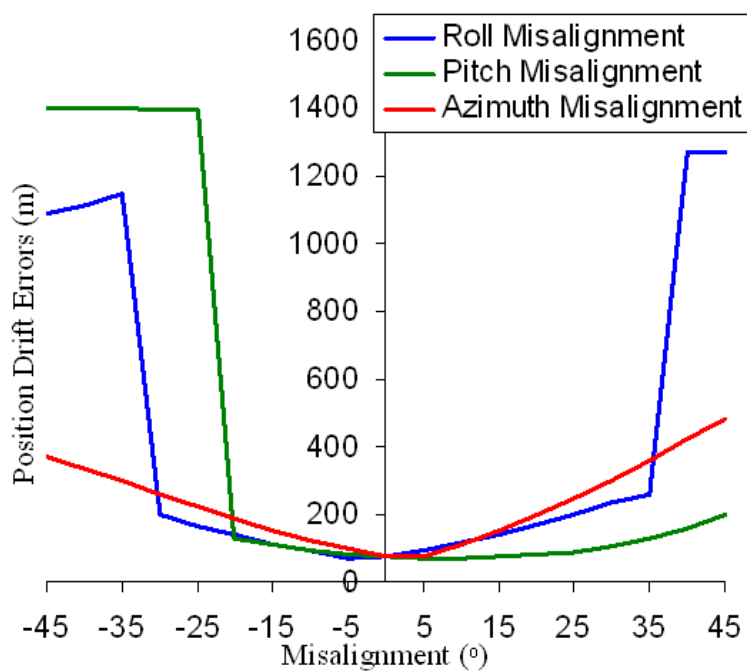


**Figure 6-12. Typical azimuth misalignment results**

### 6.3.4 IG2A with NHC

As mentioned earlier, NHC require the correct knowledge of  $v$ -frame to apply the physical constraints to the vehicle motion. The application of these constraints improved the position drift errors from 254m to 76m for dataset 1 and from 421m to 127m for dataset 2 for perfectly aligned cases, which showed that it is important to use these constraints if a partial IMU is considered for cost factors.

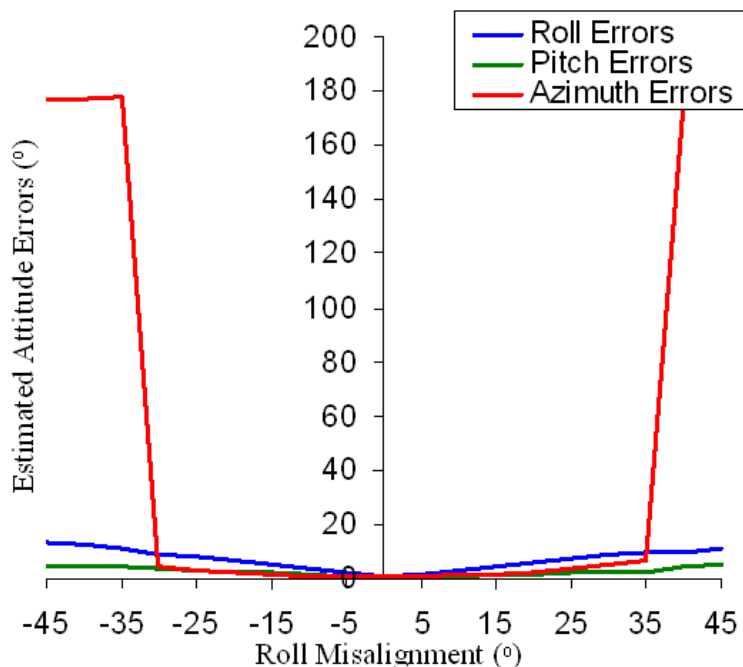
The first set of results (Figure 6-13) show typical position drift errors when misalignments were simulated in roll (blue lines), pitch (green lines) and azimuth (red lines) angles.



**Figure 6-13: Position drift errors for partial IMU (with NHC) under different misalignments.**

Figure 6-14, Figure 6-15 and Figure 6-16 have the typical induced attitude errors due to misalignments in roll, pitch and azimuth. Blue line in Figure 6-14 represents the range of

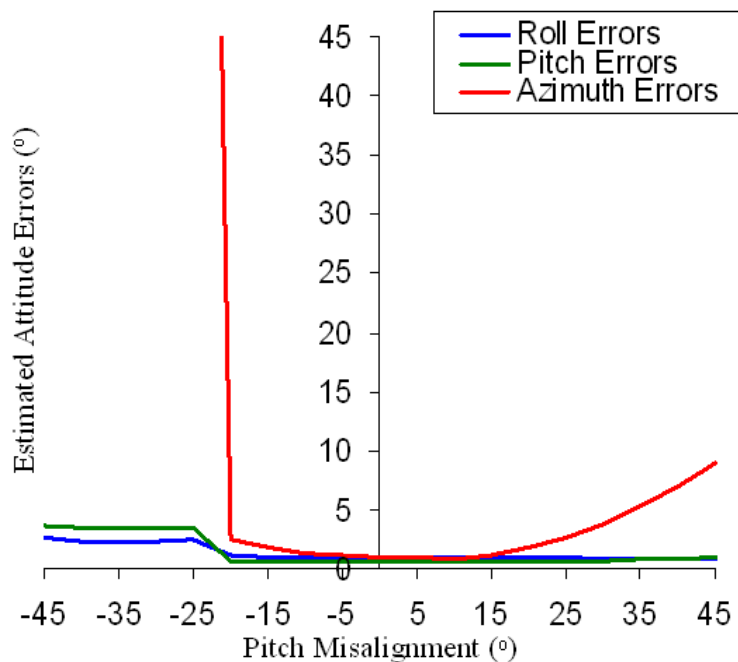
estimated roll errors due to misalignment simulation in roll. The error variation is small as the EKF cannot estimate the errors in the direction of the missing sensor. Green and red lines show the resulting attitude errors in pitch and azimuth due to the misalignment in roll.



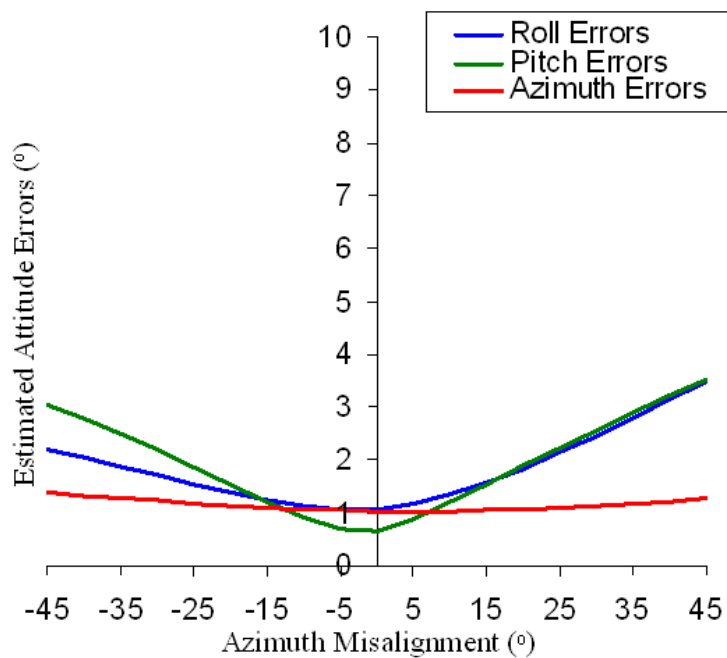
**Figure 6-14. Typical attitude errors due to roll misalignment**

Figure 6-15 and Figure 6-16 show the resulting attitude errors when misalignments were simulated in pitch and azimuth. Overall attitude errors due to the misalignment in each of roll and pitch axes grossly degraded the errors in other attitude angles mainly due to the lack of roll and pitch gyros. Consequently, the results are totally random for larger misalignment values in roll and pitch as partial sensors cannot determine these misalignments.





**Figure 6-15. Typical attitude errors due to pitch**



**Figure 6-16. Typical attitude errors due to azimuth**

The results for NHC show that  $\pm 15^\circ$  misalignment in any of the attitude angle will increase the errors under 20% and can be considered towards the system design.

### 6.3.5 Misalignment Estimation Algorithm

This section contains the result of misalignment estimation algorithm. As described earlier, this algorithm is based on the velocities and therefore, estimation accuracy and convergence to the right values also depend on the velocity and its quality. The first set of results was obtained when the velocities with magnitude 1m/s and more were utilized in the processing. The second set relates to the velocities of over 3m/s. The actual and converged values are shown in Table 6-3 and the results for 1m/s velocity estimation are shown in Figure 6-17. Also to note is the inability of this method to estimate roll misalignment as it is not observable.

**Table 6-3: Actual and Converged Misalignment values**

Angle	Actual Misalignment (degrees)	Estimated Misalignment (degrees)	
		$v' \geq 1\text{m/s}$	$v' \geq 3\text{m/s}$
Roll	0.25	-0.60	0.722
Pitch	-12.20	-12.89	-12.82
Heading	-1.10	-0.75	-0.90

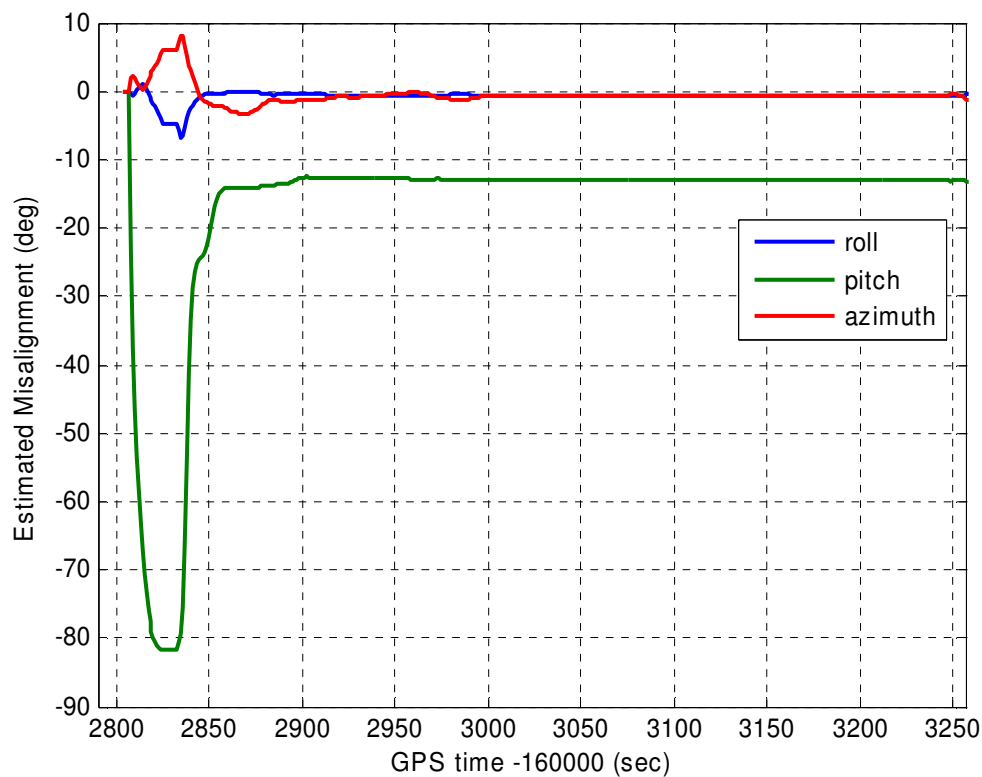


**Figure 6-17. Misalignment estimation results for  $v^l \geq 1\text{m/s}$  for full sensors**

The algorithm was used on both full IMU and 1G2A configuration and similar to the results shown in sections 6.3.3 and 6.3.4, was not able to properly estimate the errors for the reduced sensors. The results for the 1G2A are provided where the estimation KF tried to distribute the attitude errors in other attitudes.

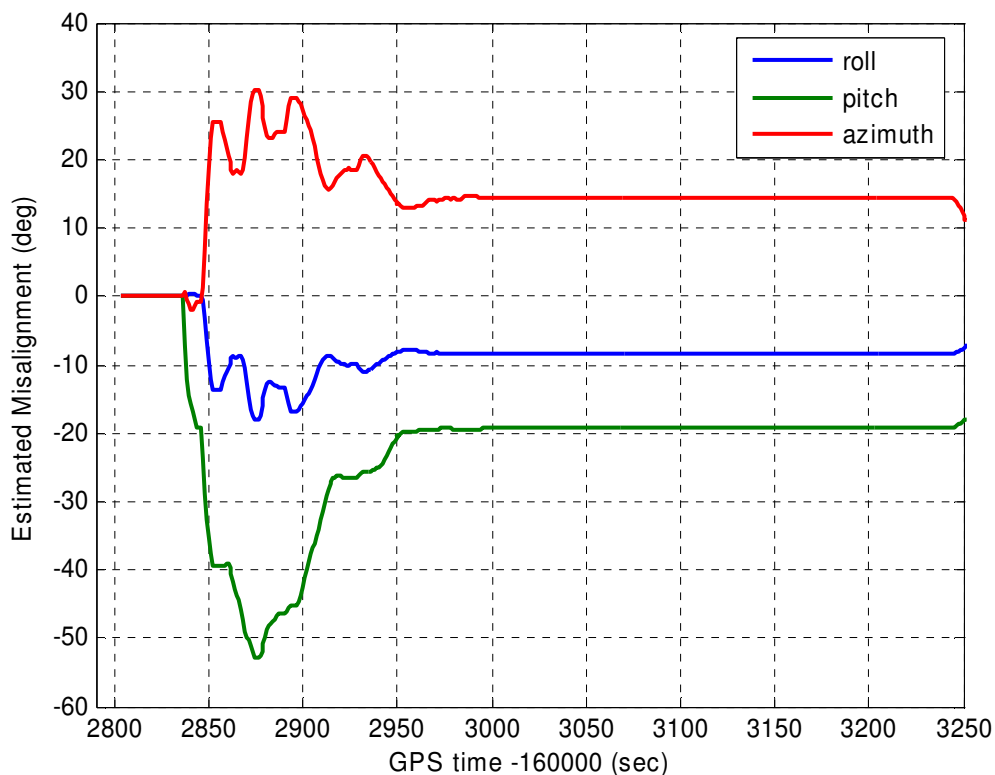


**Figure 6-18. Misalignment estimation results for  $v^l \geq 3\text{m/s}$  for 1G2A**

## 6.4 Summary

The development of integrated GPS/IMU systems for civilian vehicle navigation is a challenging area where cost, reliability, and ease of implementations are all important design aspects. This study focuses on the requirement of alignment of a PND with respect to the vehicle to produce reasonable navigation results for the most flexible settings for the end user. Full and partial IMU with and without NHC are investigated in the analysis. The analysis is performed during the GPS signal outages where the inertial system works in stand-alone mode.

In addition to the estimation of position drift errors, the errors induced in the other attitude angles due to the simulated misalignment are also studied in great detail. The comparisons for position drift errors and attitude angle errors are based on the results from a well aligned CIU navigation results. The results and analysis given in this study consisted of two datasets. Both datasets were collected on different roads with small but different roll and pitch angles.

#### ***6.4.1 Errors Due to Misalignments***

This study utilizes an EKF since KF is considered as a preferred method for GPS/INS integration. The results obtained by using different sensor orientations (Figure 2-15B) are compared with the results when the sensors were oriented exactly along the  $\nu$ -frame (Figure 2-15A). This chapter is analyzing the errors due to the erroneous information coming from the sensor due to misalignment and not the optimality of the EKF. Therefore, the same EKF is used to obtain the reference results with no misalignment case.

The study deals with the design of a system that can be used from one vehicle to the next without making special modifications to the vehicle. In this kind of scenario, the orientation cannot always be guaranteed at every installation. The focus of this chapter is to find the system design specifications for an approximate orientation for vehicle navigation.

#### ***6.4.2 Full IMU without NHC***

The misalignment in roll showed least impact on the pitch and azimuth estimation as roll is least important in navigation. It clearly indicates that for full IMU, roll can be allowed

to freely orient without any significant effect on the position drift. From design perspective of a user friendly civilian grade integrated GPS/IMU navigation system such as CIU, it is sufficed to say that roll can be arbitrarily oriented.

Pitch angle was misaligned next and the errors on position and other attitude angles were analyzed in detail. The maximum position drift error as compared to a perfectly aligned IMU was less than 5%, however, the pitch misalignment showed an average increase of 20% in errors for other attitude angles estimation. The maximum errors were in roll estimation for pitch misalignments of greater than 25°. The pitch misalignment showed less impact on the azimuth estimation errors. However, the average in azimuth estimation error was significantly greater than the case when roll angle was misaligned. The results indicate that if position drifts are the major requirement, the pitch alignment is also not an important factor and therefore, the consumer does not require aligning the pitch angle if full IMU is available. If the correct attitude angles are required, pitch angle should be constrained to  $\pm 25^\circ$ .

The last set of results consisted of azimuth misalignment simulations. The maximum position drift increment stayed well under 10% of the no misalignment case. However, roll and pitch estimated errors showed serious degradations. A quick examination of Figure 6-6 reveals that if correct attitude angles are required, azimuth angle need to be properly aligned. The navigation EKF was successfully able to determine the misalignment error in the azimuth and most importantly was able to estimate the position drift of the vehicle during GPS signal outages for azimuth misalignment. Consequently, a

full IMU can be used without any limit on the azimuth if roll and pitch accuracies is not important, which is the case for civilian navigation.

#### ***6.4.3 Full IMU with NHC***

NHC required the knowledge of the vehicle directions of motion, which in turn involved a well aligned inertial system with respect to  $v$ -frame. The application of NHC improved the position estimate for perfect alignment case. However, any grossly misaligned attitude angle caused serious degradation in position drift errors and other attitude estimation. Therefore, for the best navigation results in civilian vehicle navigation, a well aligned full IMU with NHC is the only choice. This kind of system is suited for a built-in navigation system in the vehicle but cannot be implemented in a PND.

#### ***6.4.4 Partial IMU without NHC***

Any misalignment in roll and pitch angles significantly degraded the results of the partial IMU. The azimuth misalignments, on the contrary, showed less than 10% increase in the position drift errors, if NHC is not applied. The results presented here shows that only azimuth misalignment can be estimated and tolerated if a partial IMU is used. The partial IMU only have an azimuth sensing gyro and therefore, it is estimating the azimuth misalignments properly without inducing significant errors in roll and pitch angles estimations. No error tolerance for misalignments in roll and pitch can also be explained on the basis of only one gyro of the system that cannot estimate roll or pitch. This will also affect the estimation of pitch errors due to mountainous terrain.

#### 6.4.5 Partial IMU without NHC

The position drift errors of the partial IMU are significantly larger as compare to the full IMU and therefore, NHC should be used to get better navigation accuracies. In terms of misalignment, the results from Figure 6-13, Figure 6-14, Figure 6-15 and Figure 6-16 show that  $\pm 15^\circ$  misalignments will cause less than 20% degradation as compared to the perfectly aligned partial IMU and can be considered towards the system design.

The results of this study can be summarized using Table 6-4. It is important to reiterate that the issue of misalignment of the IMU with respect to the vehicle (Figure 2-15) only arises if the navigation system is portable and the end-user is responsible for mounting it properly.

**Table 6-4. Allowable misalignments with degradation less than 20% (as compared to a well aligned system)**

Allowed Maximum Misalignment		Ease for the User
Full IMU	$\pm 45^\circ$ (for all axis)	No restrictions for users
Full IMU + Non-Holonomic	Require good alignment	Very Difficult for users
Partial IMU	$\pm 45^\circ$ (for azimuth only)	Difficult as roll and pitch angles should be well aligned with vehicle's roll and pitch
Partial IMU + Non-Holonomic	$\pm 15^\circ$ (for all axis)	Reasonable requirements to be implemented by users



A KF to estimate the misalignment was defined and implemented and it also confirmed that partial sensors misalignment cannot be properly estimated. Consequently, certain limits in design are required to obtain the desired accuracies as discussed earlier in Table 6-4.

After alignment, the integrated system is ready to start navigation. However, a PNS needs to determine the mode of transit with great accuracy to choose the correct navigation algorithm for the respective mode of transit. The focus of the next chapter is development and testing of a software switch or indicator for the detection of the mode of transit of the user.

## **Chapter Seven: Detection of Mode of Transit**

The main contribution of this thesis is to evaluate and design a completely transferable integrated navigation module that can work in the two most common modes of transit. The system should be able to produce navigation results for in-vehicle and on-foot navigation modes. In-vehicle navigation computes relative PVA of a moving platform by utilizing specialized mechanization equations that integrate the accelerometers and gyros signals. On the contrary, it is best to use step detection and step length method for relative position estimation if the user is on-foot as this method minimizes integration errors and drifts. Therefore, it is the first requirement of the system to detect the correct mode of transit of the user to implement the appropriate navigation algorithm.

Most recently GPS based navigation systems are commercially available for in-vehicle and outdoor on-foot navigation. These systems are designed in a way that they integrate the computed GPS positions on a digital map for user interpretation. The systems are useful as long as the GPS receiver has a direct line of sight to four or more satellites. Most of the urban navigation scenarios will seriously limit the GPS signal availability due to a variety of reasons. For example, a tunnel will completely stop the GPS based navigation while a typical downtown area with tall buildings will significantly limit the visibility of the number of satellites.

For these situations, it is only necessary to integrate the GPS based systems with some form of autonomous positioning system. MEMS inertial sensors can be the solution as they are self-contained and compact enough that they can be easily integrated in a

commercial GPS navigation product. There are some issues with these sensors as we discussed earlier. This chapter deals with another unique topic of a portable system.

For the best navigation accuracies, the inertial sensors output can be converted into the navigation parameters using two different strategies for the two modes of transit. A hardware switch is recommended for the system to roughly indicate the position of the system, i.e. either the system is placed on a dashboard or a waist belt. However, there are scenarios where the hardware switch will not provide the correct information. This is especially true, when the user is wearing the system on the waist belt and takes a bus or train or ride as a passenger inside a vehicle. In all of these situations, the hardware switch will tell that the mode of transit should be on-foot which needs to be corrected. Therefore, a software switch is required to recognize the mode of transit in addition to the hardware switch.

## **7.1 Methodology**

A PND consisting of four gyros, five accelerometers, temperature sensors, GPS receiver, barometer and magnetometer is used in the testing. The system was designed by the members of the Mobile Multi-sensor Group at the University of Calgary. In addition to a set of orthogonal gyros and accelerometers that are the minimum requirement to accurately capture the 3D motion, there is a dual axis gyro that covers roll and pitch angles and there are also redundant x and y accelerometers. The redundant information was not used in the detection of mode of transit as for commercial systems there will be

only minimum number of sensors for economical reasons. The system is shown in Figure 3-14 and Figure 7-1.

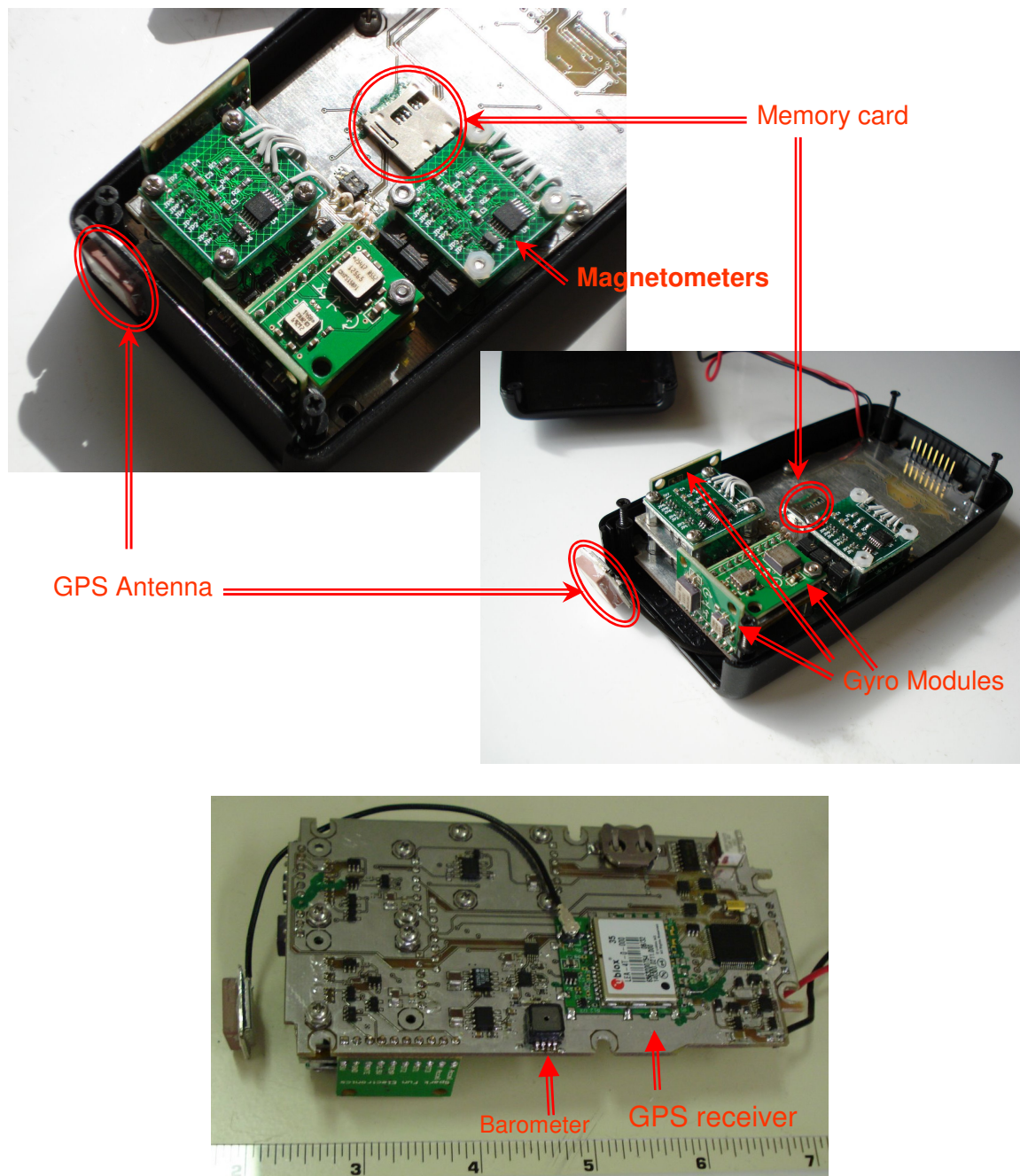


**Figure 7-1. Components of the navigation module**

### 7.1.1 Detection Algorithm for full Sensors (Six Sensors Module)

If six sensors are part of the sensor module, there is more redundancy available for algorithm development. The first algorithm utilizes the three orthogonal accelerometers and three orthogonal gyros in the mode detection. The following are the steps taken to estimate the mode of transit.

1. Align the sensors data with the GPS time using the GPS Pulse per second (PPS) as follows:

$$t^k = GPS^{PPS} + \frac{C^{PPS}}{T} \quad 7-1$$

where

$t^k$  = the GPS referenced time for the  $k^{\text{th}}$  epoch

$GPS^{PPS}$  = the GPS time that was related to the most recent PPS

$C^{PPS}$  = micro processor clock counts since the last PPS

$T = 16 \times 10^6$ , the processor speed

2. Add the absolute values of accelerometers signals together for the  $k^{\text{th}}$  epoch

$$a^k = |ax^k| + |ay^k| + |az^k| \quad 7-2$$

3. Add the absolute values of gyros signals together for the  $k^{\text{th}}$  epoch

$$g^k = |gx^k| + |gy^k| + |gz^k| \quad 7-3$$

4. Determine the frequency of the signals to choose the number of samples for the STD computation of the signal. For example, if the frequency is 50Hz, the STD will be calculated for the 50 samples at a time, i.e. the signal STD ( $std_x$ ) per second.

$$f^k = \frac{1}{t^k - t^{k-1}} \quad 7-4$$

$$std_x = \sqrt{f^k \sum_{i=1}^{f^k} (x_i - \bar{x})^2} \quad 7-5$$

where  $x$  = absolute value of the accelerometer or gyro signal at epoch  $k$

5. Determine a threshold by analyzing the dataset as shown in the following equations

$$[th_{accel}^{walk}] = c * mean(a^{1 \rightarrow k}) \quad 7-6$$

$$th_{accel}^{motion} = d * (std_a) \quad 7-7$$

$$[th_{gyro}^{walk}] = c * mean(g^{1 \rightarrow k}) \quad 7-8$$

$$th_{gyro}^{motion} = d * (std_g) \quad 7-9$$

where  $c$  is a constant with a value of 4 to accommodate for different walk styles by different people and  $d$  has a constant value of 3 to detect the motion periods. The two constants are the weighting factors that were tuned using a variety of datasets. This method is adaptive and the two constants were determined by analyzing known datasets.

6. If the gyro threshold indicates that the mode of transit is walk, cross reference the signal with the classification of the accelerometer signals at the same epoch using equation 7-6. A simplified algorithm is provided in Figure 7-2.

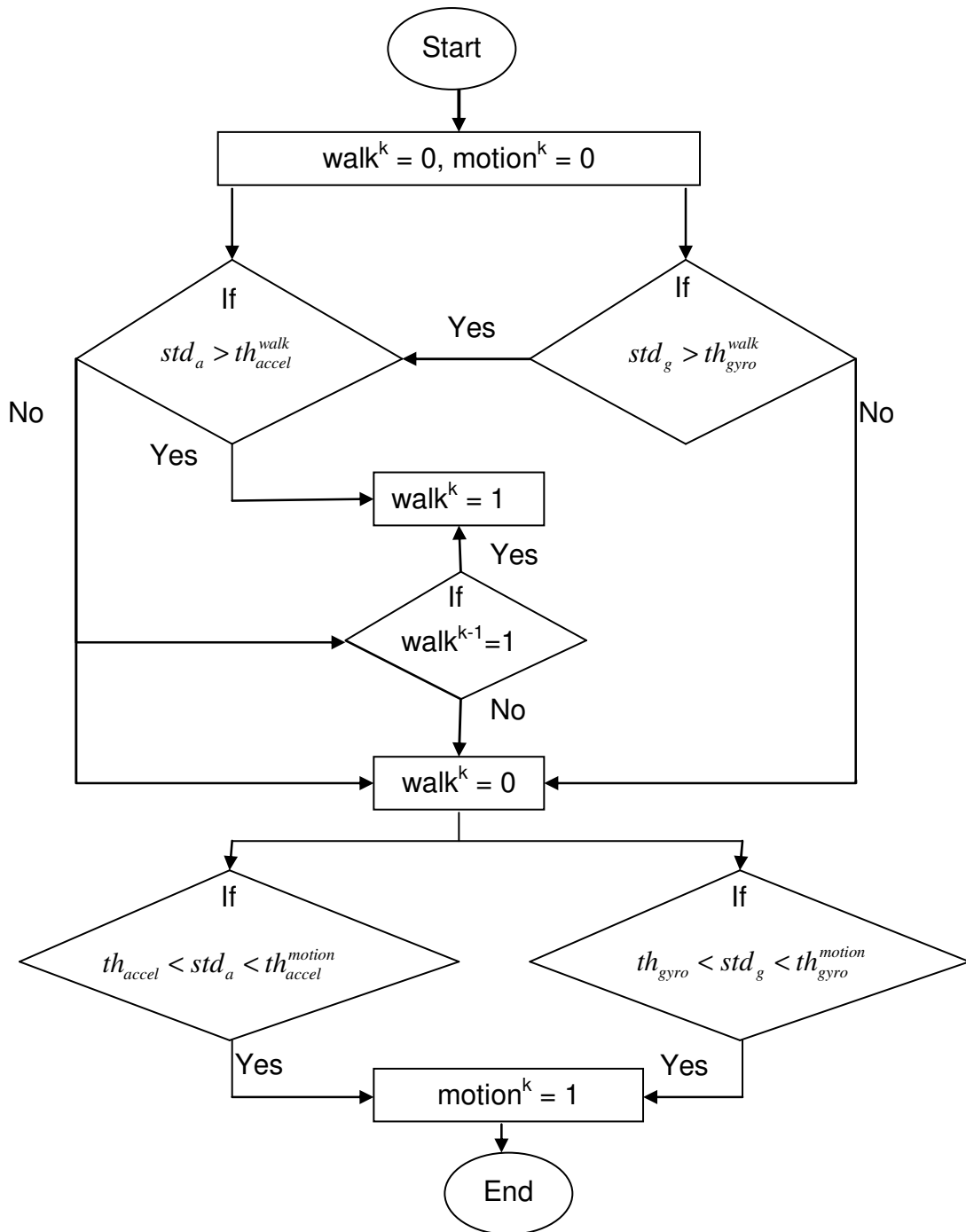


**Figure 7-2. Mode detection algorithm**

### ***7.1.2 Detection Algorithm for Partial Sensors***

A navigation module can have any number of partial sensors. The most obvious case would be a heading gyro and a bi or tri-axial accelerometer but there could be other options available as discussed in detail earlier.

The second set of results will assume that a heading gyro is part of the inertial module in addition to a tri-axial accelerometer. In this case, we will repeat the steps from 1 to 6 with the following difference. The signals from the roll and pitch gyros will not be used and equation 7-3 will become

$$g^k = |gz^k| \quad \mathbf{7-10}$$

### ***7.1.3 Test Scenarios***

There are two possible ways the system is designed to work. The first one is the case when the system is placed on the dashboard of a vehicle in its specialized holder and the hardware switch is indicating this mode. This is a straight forward situation and the software detection is not as important. In the second case, the sensor module is on the belt of a user and the user is free to choose the method of transit. It is likely that the user may use a combination of mode of transits. Therefore, it is important to test all the possible combination for the mode of transit.

The first set of tests consists of combined navigation, i.e., walk, and in-vehicle navigation. Eleven different people volunteered in the data collection for different modes of transit. Each volunteer was assigned a day on which the volunteer was required to carefully orient and fix the sensor module on their belt when they leave their office. The



volunteer collected another dataset on their way back to office the next morning. The volunteers also mark the data when they switch their mode of transit to provide reference for the software detection.

The next testing was to determine the feasibility of the algorithm in a LRT system which has different accelerations and decelerations profiles than road vehicles. Three people volunteered to take LRT for the data collection on three different days. Different positions were tried to test the algorithm for a variety of possible scenarios.

The first position is when the user is facing the same direction as the forward direction of the train. In the ideal case for this user position, the x-axis sensor should follow the acceleration of the train and the z-axis gyro should give the heading of the train. This position will be referred to as position 1 from this point onwards.

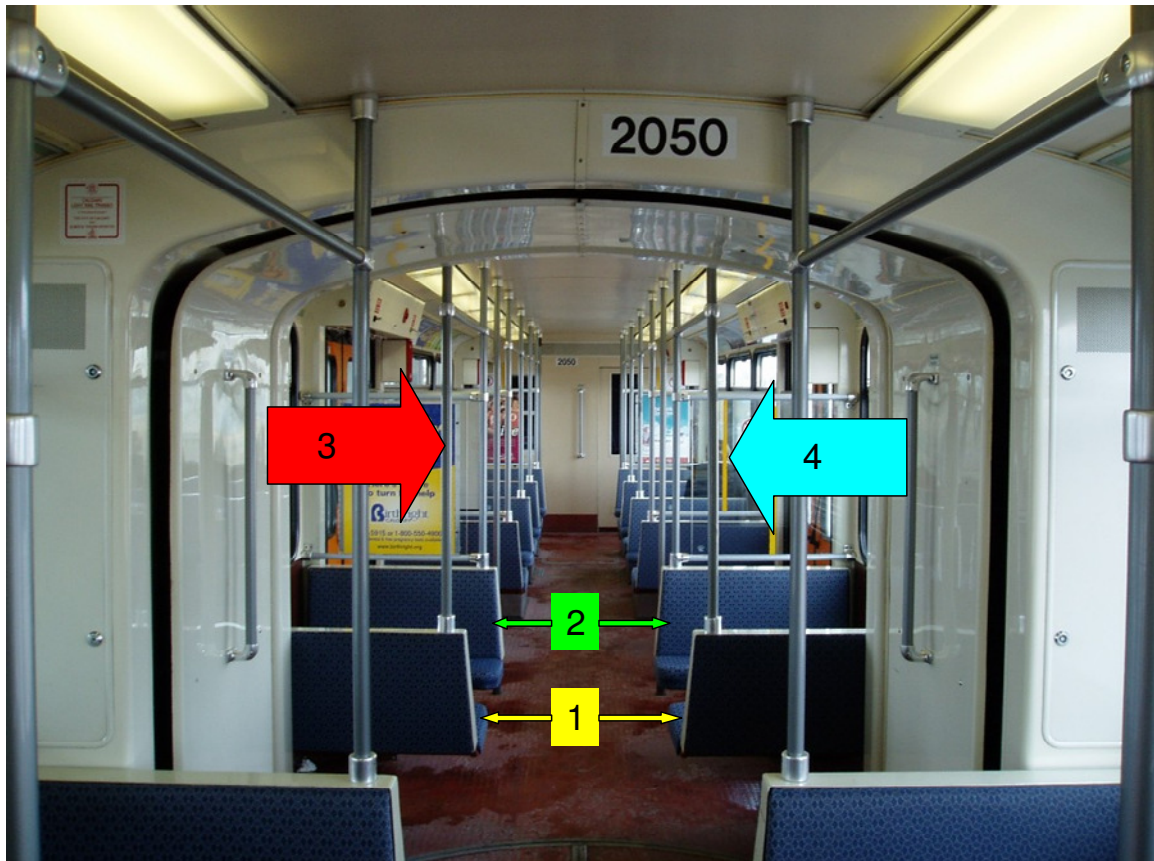


**Figure 7-3. Possible user positions in an LRT. The direction of travel is into the page. Position 1 is when the user is facing the direction of travel; position 2 is the direction away from the travel direction. Positions 3 and 4 represent the positions when one of the user shoulders is facing the travel direction (Google Image).**

Position 2 corresponds to the situation when the user in the train is facing away from the direction of travel. If the system is perfectly aligned with the user, ideally the x-axis accelerometer should be able to measure all the accelerations in the opposite direction. Similarly, the z-axis gyro will produce the angular displacement that relates to the heading of the moving platform.

There are times when the x-axis of sensor module that corresponds to the forward direction of the user may not be aligned with the axis of motion of the train. Although

many possibilities exist but for this chapter a common situation will be considered in which the user finds a seat or stands while facing one of the train's door. Two different ways are possible if the user is facing the door as represented by positions 3 and 4. In either of the position, the y-axis accelerometer should sense the acceleration of the train while the vertical gyro, i.e., z-axis gyro will measure the heading of the train.

These positions are the most common cases as the seating arrangement can follow any of the four positions defined here. The position of a user can change arbitrarily as the user move around for different stops during rush hour commute. In addition to the full IMU or six sensors mode detection, the results will also discuss the effectiveness of using partial sensors for mode detection in the above cases.

Another common situation for navigation is when a user uses a bike with the unit on his or her belt. Considering the unit is aligned with the user, the software will have to decide which kind of navigation mode the user is in. Most commonly, the user will either paddle to gain speed or the user will let the bike cruise once the bike reaches a certain speed. In the first case, the algorithm for mode detection should classify the motion as on-foot navigation and thus implement the appropriate navigation equations. For the cruising case, the algorithm will find smoother accelerations and in theory should start the in-vehicle navigation mode. The data was collected for different bike cases and the analysis is given in the next section.

### 7.1.4 Accuracy Analysis

There are two different accuracy analyses shown in the result section. The first analysis is based on the detection of mode of transit based on a full sensors result. This software detection was compared against the known locations of the mode of transit. The known locations were marked at the time of data collection as shown in Figure 7-4. Accuracy in percentage was computed as one less percentage point for every false positive after the hardware mode detection switch indication. In the simplified example given in Figure 7-4, five data points were below the threshold after the hardware detection and therefore, the accuracy of this detection will be given as 95%. Note that this is a simplified example but the principle is the same for experimental data analysis. This accuracy is termed as absolute accuracy.

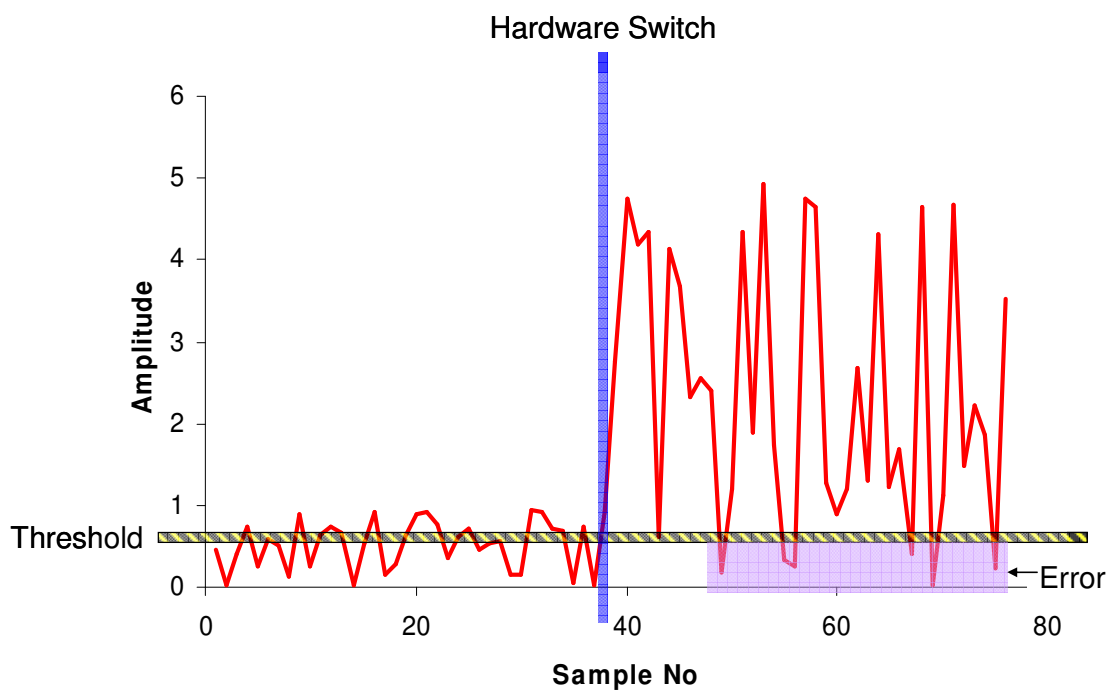


**Figure 7-4. Example of a hardware switch with accuracy computation for full sensor**

The next accuracy analysis was conducted among full and partial sensors IMU results. In this case, the full sensors results were considered as the reference despite their accuracies with respect to the hardware result (Figure 7-4). The main idea was to compare the accuracy degradation when partial sensors are used. The accuracy results are given in Section 7.2.6 and this is termed as relative accuracy.

## **7.2 Results**

The results are divided into six subsections and the first five subsections will discuss the results of utilizing six sensors versus partial sensor combination for the mode detection. The last subsection will show the absolute and relative accuracies of the two algorithms.

### ***7.2.1 On-foot Mode Detection***

On-foot mode detection refers to the case when the unit is attached to the user's belt. In this case, the hardware switch will indicate that the unit is in "On-foot navigation mode", however, the mode of transit for the user may not be pure walk. The first set of results consists of all six sensor signal analysis and shown in Figure 7-5 for a dataset containing pure walking. The results indicate the accuracy of the algorithm for a walk on a relatively levelled surface with respect to *l*-frame since the user route consisted of a well levelled and paved sidewalk. Figure 7-6 shows the results when partial sensors were used in the mode detection algorithm. The top panels of both figures show the accelerometer data while the bottom panel contains the gyro data.

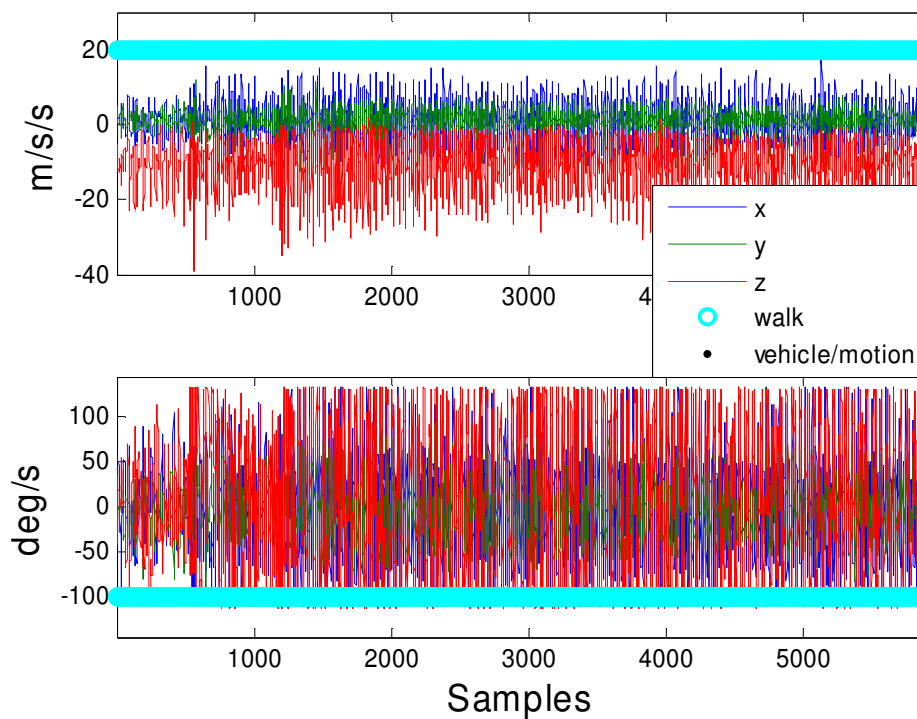


**Figure 7-5. User1 walk only data classification for full IMU**

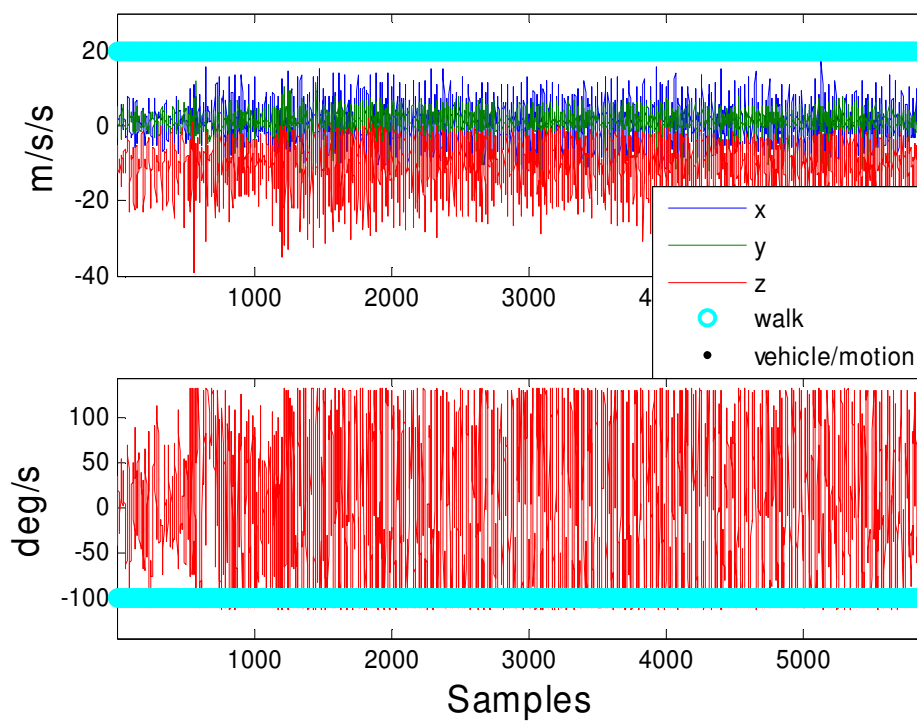


**Figure 7-6. User1 walk only data classification with one vertical gyro and a tri-axial accelerometer**

The next set of data is also from a levelled trajectory but corresponds to a different user. Both six sensors and partial sensors results were the same as in the case of user 1 and therefore are not shown here. The algorithm was clearly able to detect the walk periods of user 2, showing the effectiveness of the proposed method for on-foot mode detection on a levelled surface with respect to  $l$ -frame.

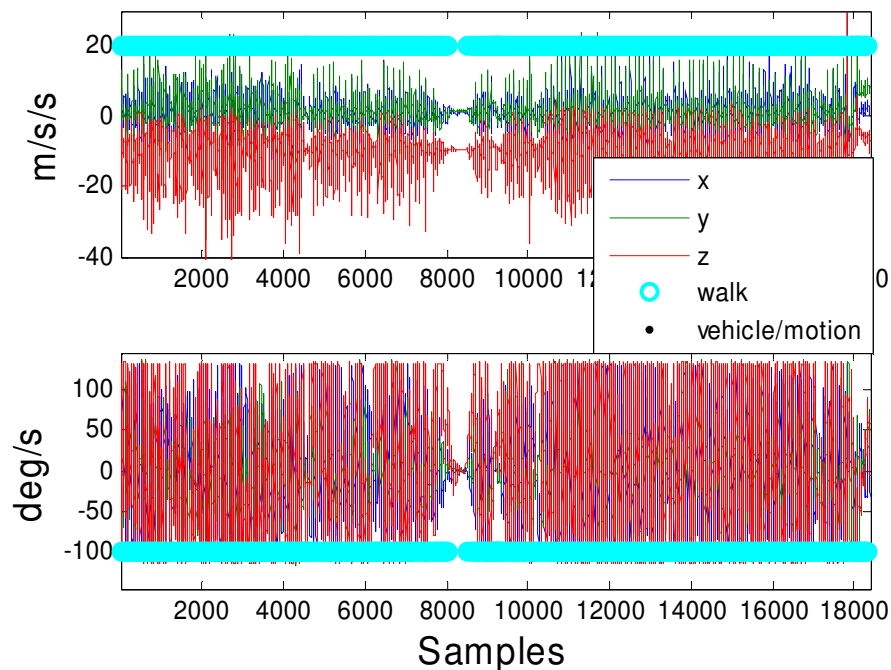


**Figure7-7. User2 walk only data classification**

The algorithm was further tested for on-foot mode that included mixed walk including levelled ground, inclined ground and stairs. The algorithm for six sensors and partial sensors were applied for detection. Both algorithms produced similar results and therefore, only one result is provided in Figure 7-8. The user started from a level area, and then the user entered an inclined route. The final part of the trajectory consisted of taking the stairs all the way from ground to third floor.

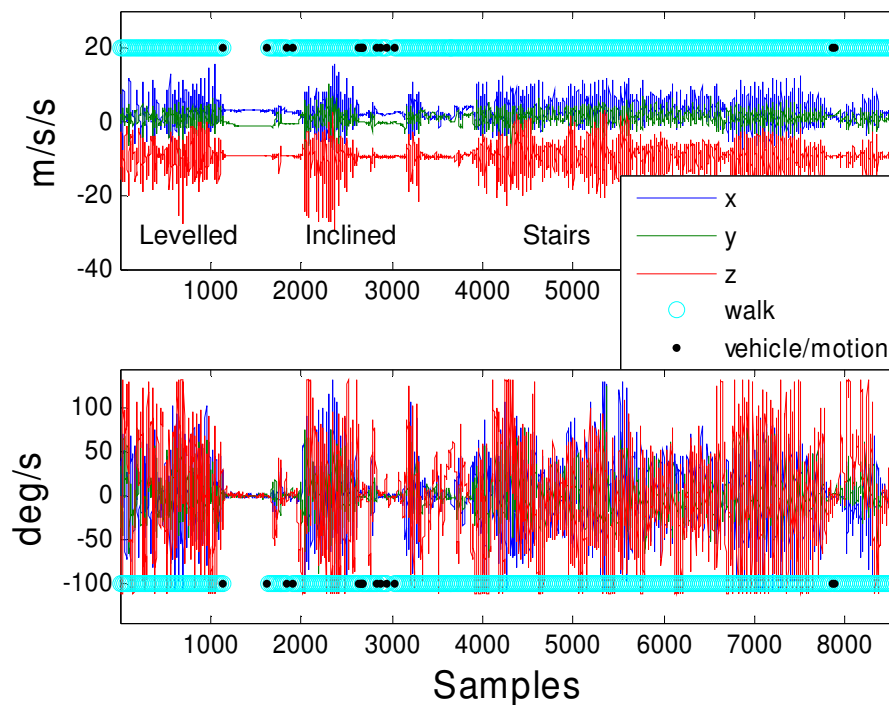


**Figure 7-8. User3 mixed walk dataset. The algorithm detected the walking motion for three different scenarios.**

The user of Figure 7-9 followed a trajectory that was initially a levelled area followed by stairs. In this case, the user took the stairs to go from third to first floor. The partial sensor algorithm detection accuracy was also quite close to the full sensors and therefore, only one set of results are provided. Both Figure 7-8 and Figure 7-9 show some misdetection, and therefore, for the switch of navigation algorithm, the mode detection switch should continuously detect the respective mode for at least 3 minutes.



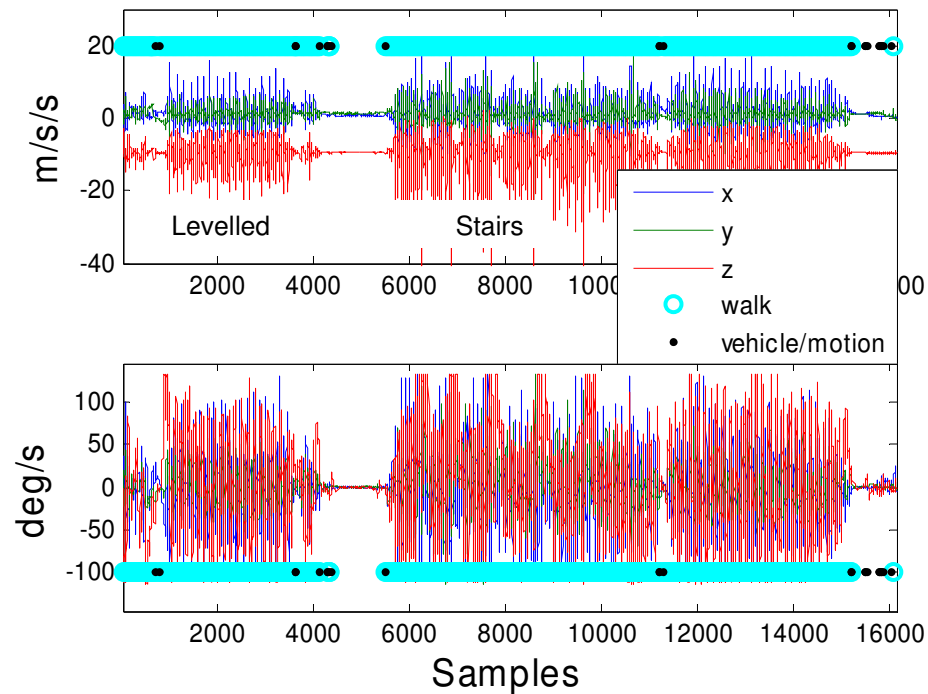


**Figure 7-9. User3 mixed walk dataset. The algorithm detected the walking motion for two different scenarios.**

### *7.2.2 In-Vehicle Mode Detection*

This section consists of vehicle only datasets in which the user took his or her own private vehicle for the data collection and therefore, this section shows the effectiveness of the detection algorithm for different vehicles. As mentioned earlier, this chapter will discuss methods for transit mode detection when the inertial sensor module is attached to the user's belt and the hardware switch is indicating that on-foot navigation mode should be implemented. However, it is important to see if the same algorithm is appropriate for in-vehicle navigation mode in which the system is fixed in its assigned place inside the vehicle.

In this case, the algorithm can be used to detect zero velocity regions. For low-cost MEMS based navigation, zero velocity updates (ZUPTs) are a useful method to improve the navigation accuracies. If the navigation is for civilian sector, it is more likely that the vehicles will make frequent stops during tough GPS situations. In fact, in urban centres where there will be more high-rises resulting in either very few lines of sights or no line of sight to the GPS satellites, the vehicle will more likely to stop at every intersection. The correct ZUPT detection in this scenario can be quite helpful as the high MEMS sensor errors can be minimized. ZUPT updates use the fact that every drift error should be zero if the vehicle is stationary. ZUPT is a well documented and researched area and will not be discussed further.

The dataset for ZUPT detection covers levelled road driving and then steep downhill and finally steep uphill driving. Initially, all six sensors were used to detect the mode of transit and the results are shown in Figure 7-10. Next partial sensors were used in the detection where data from heading gyro along with the tri-axial accelerometer data was used in the mode detection (Figure 7-11). Contrary to the on-foot navigation mode, the algorithm for partial sensors was not successful in identifying the periods of motion in the vehicle as shown by a very low relative accuracy of 19.68%.

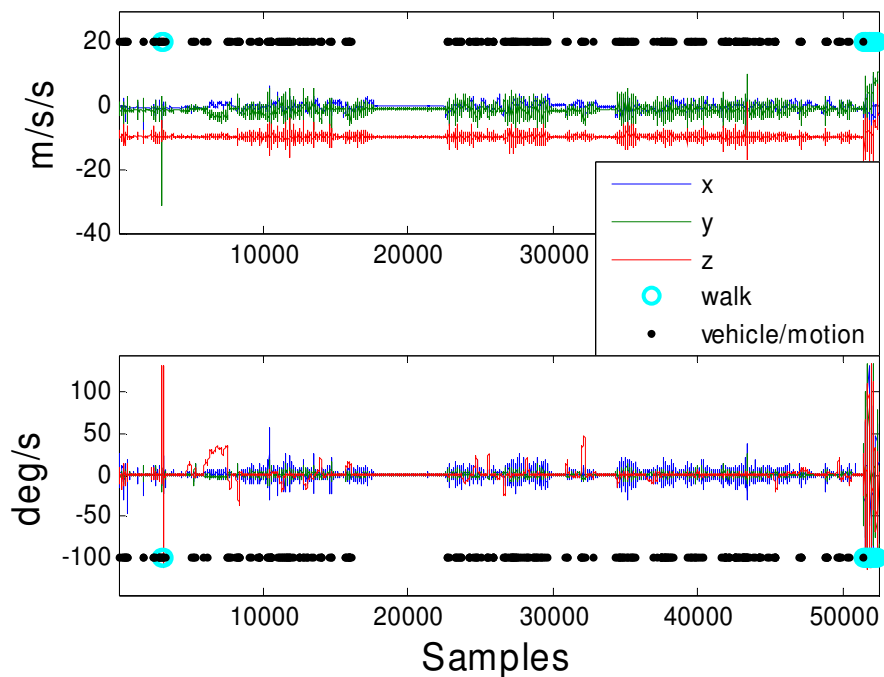


**Figure 7-10. User4 vehicle only datasets with mixed trajectory consisting of levelled road and inclined road**

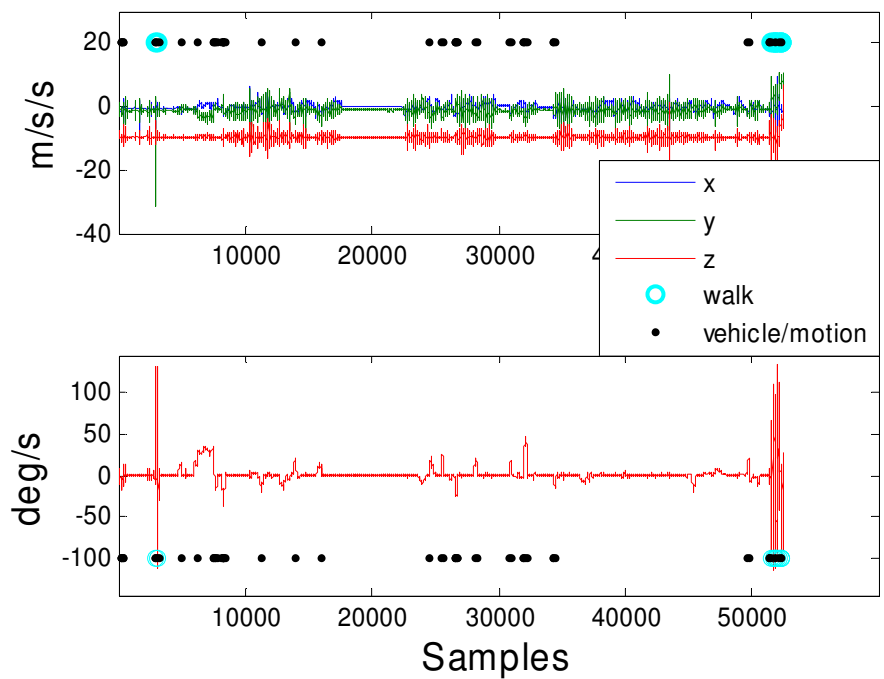


**Figure 7-11. User4 dataset when partial sensors were used**

Further analysis of the data indicated that the reason was due to the weighting scheme of different sensors output. Initially, higher weight is assigned to the gyro which did not work when two of the gyros were removed for in-vehicle navigation mode. To prove this point, equal weights were assigned to all the signals and the results were analyzed. It was obvious from Figure 7-12 that if partial sensors are used and the hardware switch indicates in-vehicle navigation mode, an equal weighting scheme should be implemented to detect stationary periods.

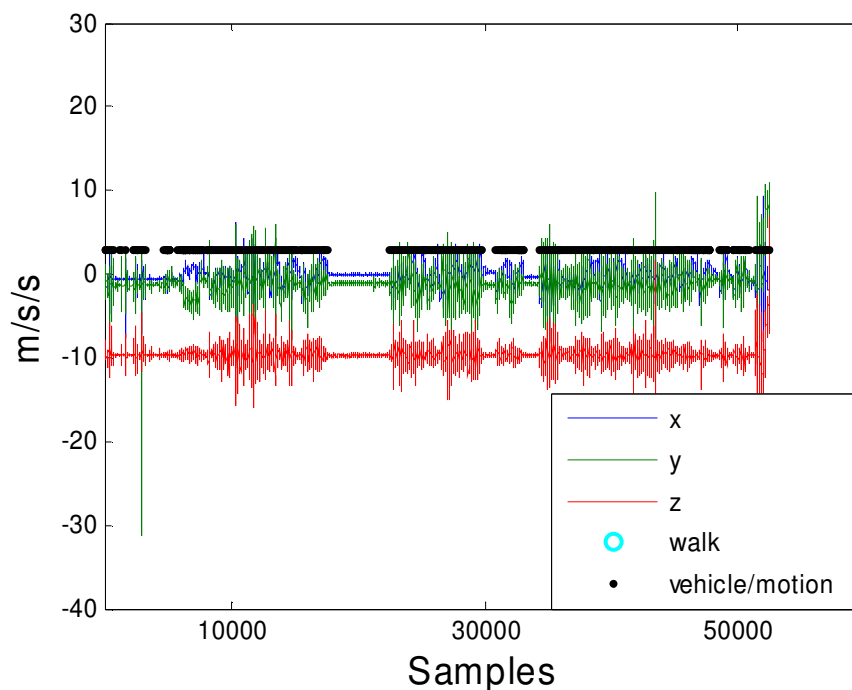


**Figure 7-12. User4 vehicle only dataset using equal weighting scheme for ZUPT detection**

The second situation is when a user enters a private vehicle and the system is attached to the belt of the user, i.e., the hardware switch is indicating on-foot navigation mode.

Initially, all the six sensors were used as mentioned earlier for the transit mode detection as given in Figure 7-13. The partial sensors results are shown in Figure 7-14.

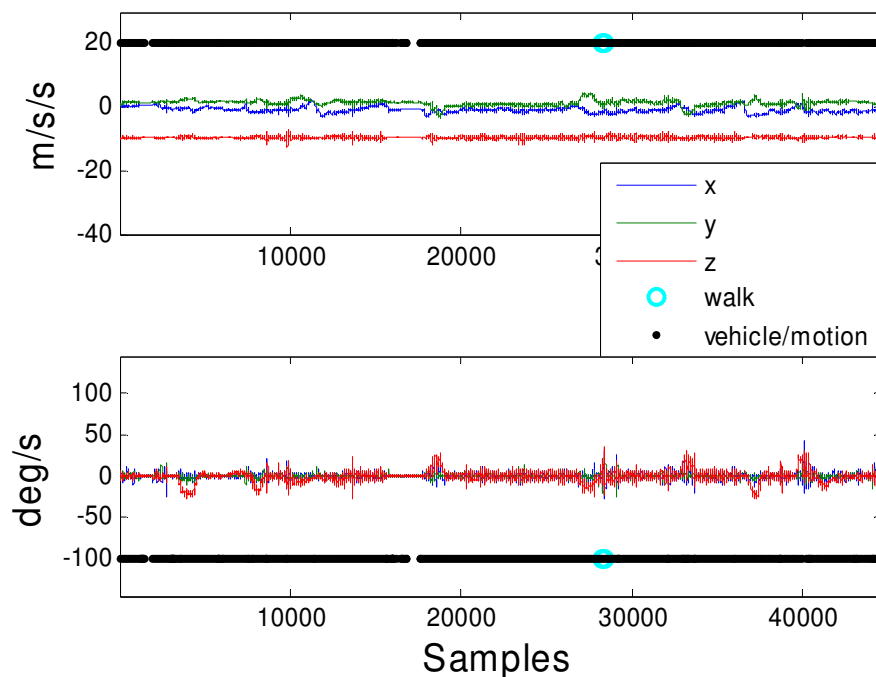


**Figure 7-13. User5 vehicle only dataset with six sensors**

The partial sensors in the case when the system is on a belt detected the in-vehicle motion better than the previous case. One reason of this might be the optimization of the algorithm for the on-foot mode. The on-foot mode will have higher signal dynamics than the system that is fixed to a more stable platform.

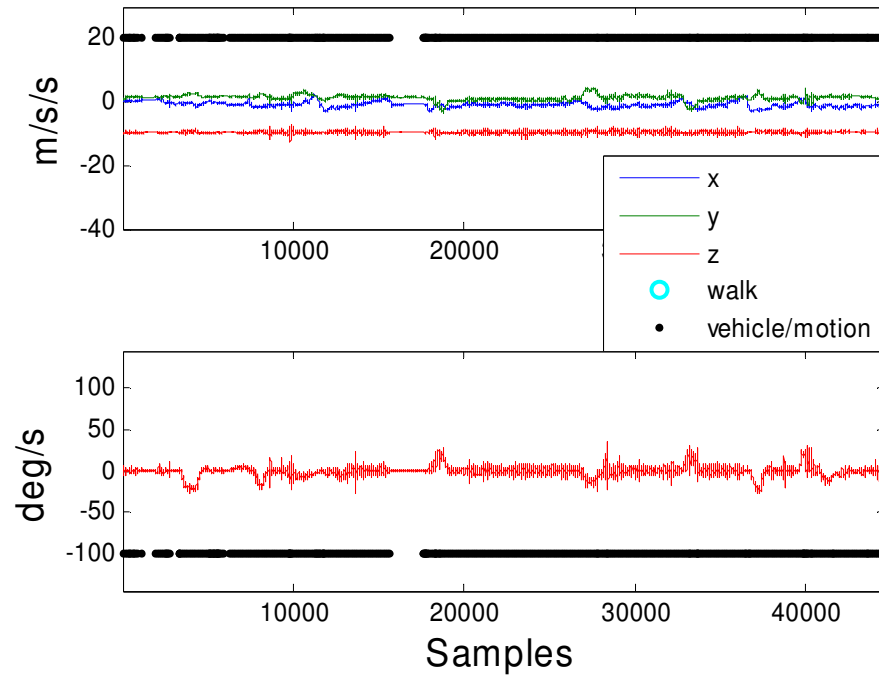


**Figure 7-14. User5 vehicle only dataset with one vertical gyro and tri-axial accelerometer**

Four more datasets were analyzed when the user was a passenger in a vehicle and the average absolute and partial accuracies were computed.

### ***7.2.3 Combination Mode Detection***

Three datasets were analyzed when the user either started the data acquisition inside a vehicle or the user initiated the system during on-foot navigation and then switched to the different mode. Both full and partial sensor algorithms were used and a typical example is shown below where the user started the navigation inside a vehicle and concluded the dataset with on-foot mode of transit.

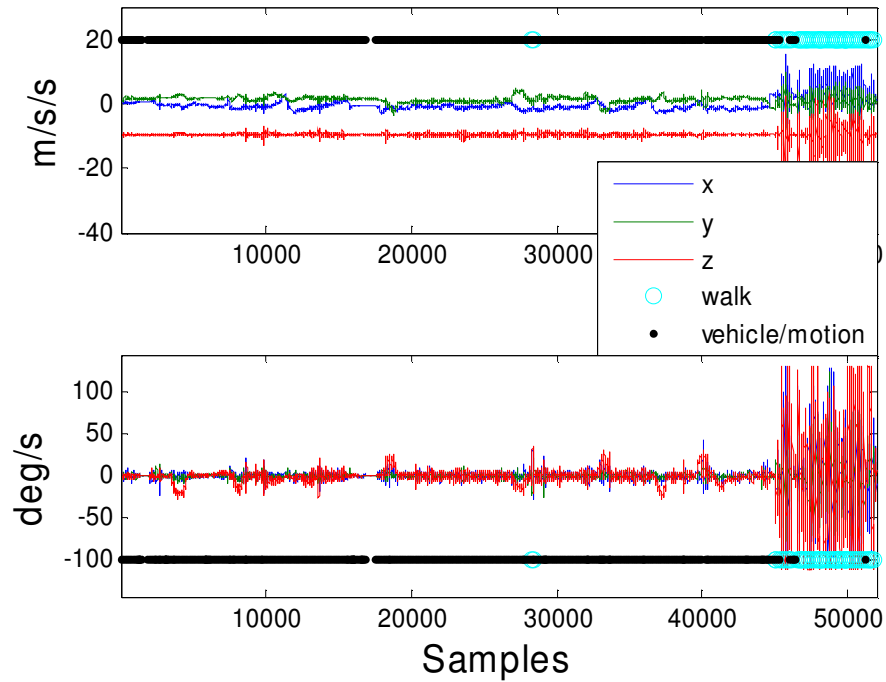


**Figure 7-15. Dataset with vehicle and on-foot mode of navigation using six sensors algorithm**

#### ***7.2.4 Mode Detection for LRT***

A LRT is usually part of big cities transit systems. If a user takes the train as part of a daily commute, it is important for the algorithm to identify this mode with good accuracy. However, as the train is usually a smoother ride due to even (levelled) tracks than other land transportations, it is important to study the datasets collected in an LRT.

If the user is taking a public transit that includes an LRT, the data can be in any kind of orientation as discussed in detail in Section 7.2.3. In addition to those well defined seating scenarios, the user may be standing during rush hour. In this case, it is important to check if the software switch can estimate this mode of transit.

If the user is in position 1 and sitting on a seat, the x-axis of the system will be in the direction of travel of the LRT as mentioned earlier. If the mode detection switch indicates in-vehicle mode of transit, the appropriate navigation equations can be applied. Application of the navigation equations is well developed area for in-vehicle or on-foot navigation and therefore, only mode detection is discussed here.

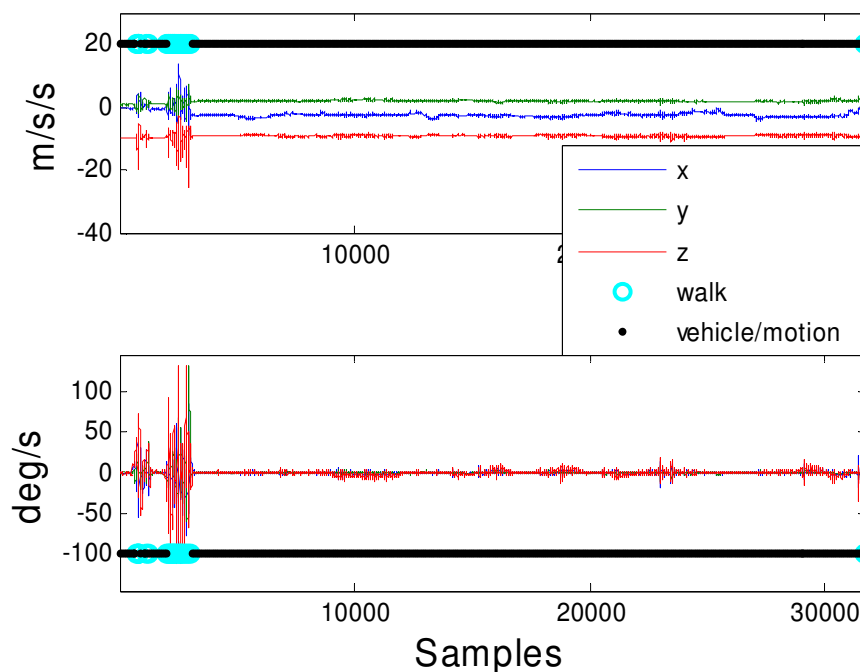


**Figure 7-16. User6 mode of transit detection in position 1 using six sensors**

Position 2 shows similar trends when the user was facing away from the direction of travel. The next set of results show the algorithm accuracy for full and partial configurations when a user was sitting and standing in position 2. Two different scenarios for the standing position will be discussed which include a user standing while holding a hanging-handle and the second scenario is when the user is resting along a wall of the



LRT. The scenarios are different as there may be more physical movements associated with acceleration and deceleration when the user is holding a hanging-handle.

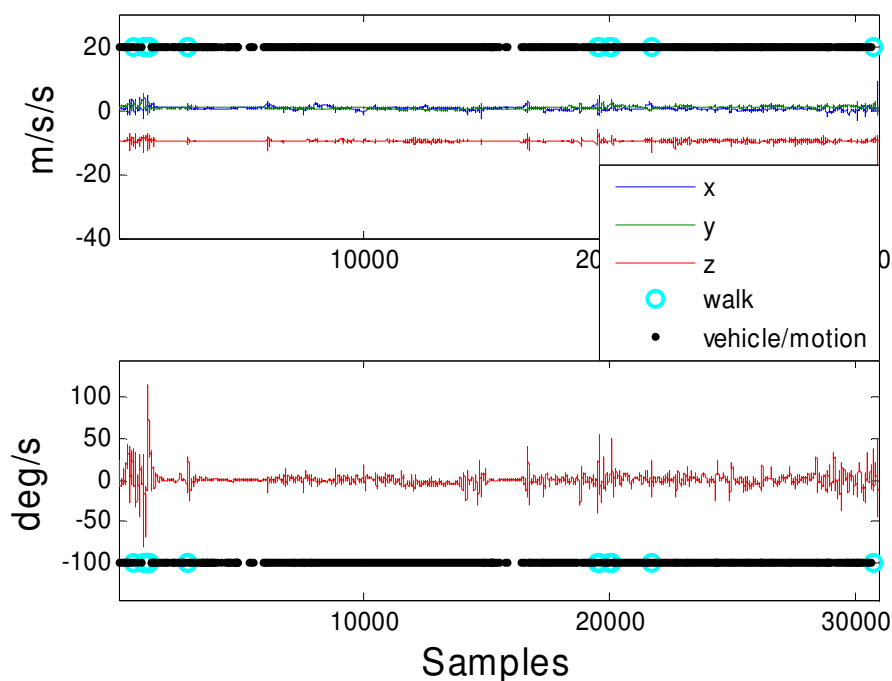


**Figure 7-17. User7 mode of transit detection for position 2 using partial sensors when the user stands by holding the handle**

Figure 7-17 shows the results of using partial sensors for the mode of transit detection. The partial sensors were 96.64% accurate (relative accuracy) as compared to the full sensor mode detection for this case. The accuracy was 90.92% for the partial sensors detection as compared to the full sensor detection algorithm when the user leans against one of the walls. Absolute accuracy values are provided in section 7.2.6.

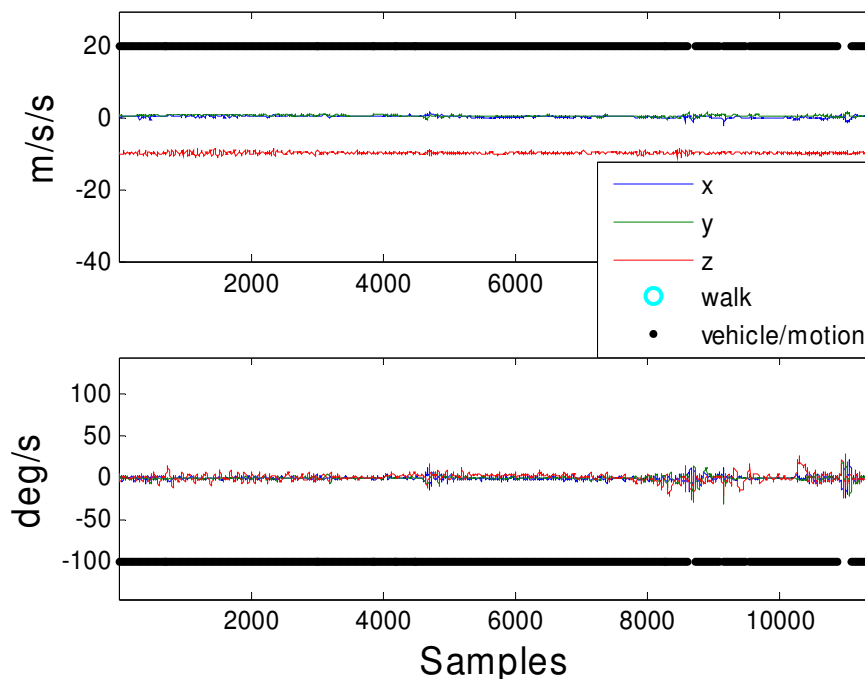


**Figure 7-18. User7 mode of transit detection for LRT data in position 2 with support using 6 inertial sensors**

Next, the two algorithms absolute and relative accuracies for positions 3 and 4 are evaluated. The different positions are used to actually establish the robustness of the mode detection algorithms. It is mainly because the motion dynamics for a typical land vehicle is mostly predictable and constant, and therefore, changing positions in a particular vehicle only shows that under any circumstances the algorithm can detect the correct mode of transit for the user. Again, this case is when the user is wearing the system on his or her belt and the hardware switch indicates on-foot navigation mode.

Position 3 results for full sensors are given in Figure 7-19. Two different datasets were used in the transit mode detection analysis for this position but due to the similarity in the results, only the first dataset is shown.

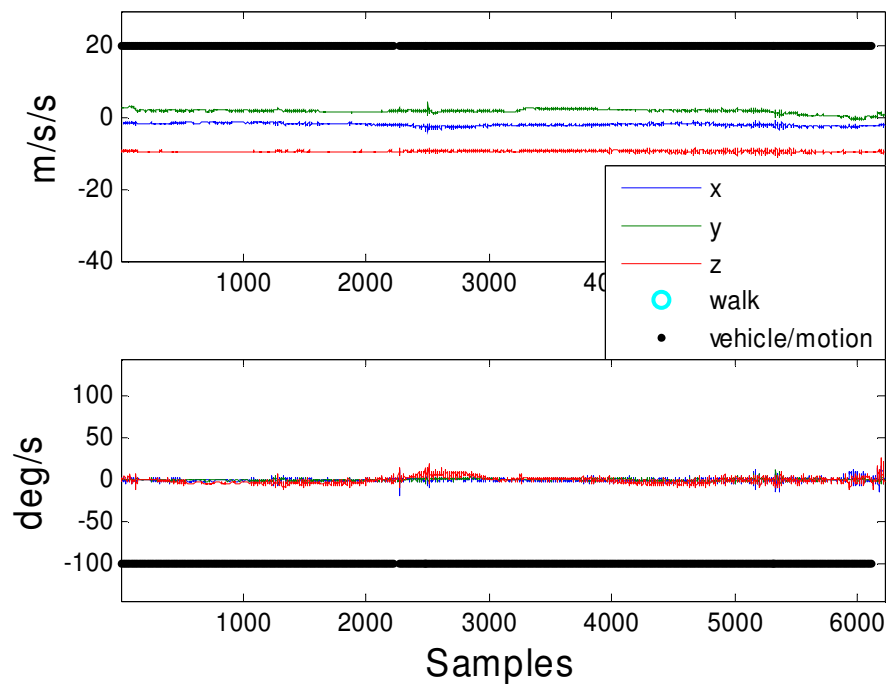


**Figure 7-19. User8 mode of transit detection for LRT data in position 3 using six inertial sensors**

Next the analysis was done on the dataset collected in position 4. The results for the partial sensors algorithm for one of the dataset are provided in Figure 7-20. The algorithm was also able to isolate the physical movement of the user which is at the end of the dataset shown in Figure 7-20.

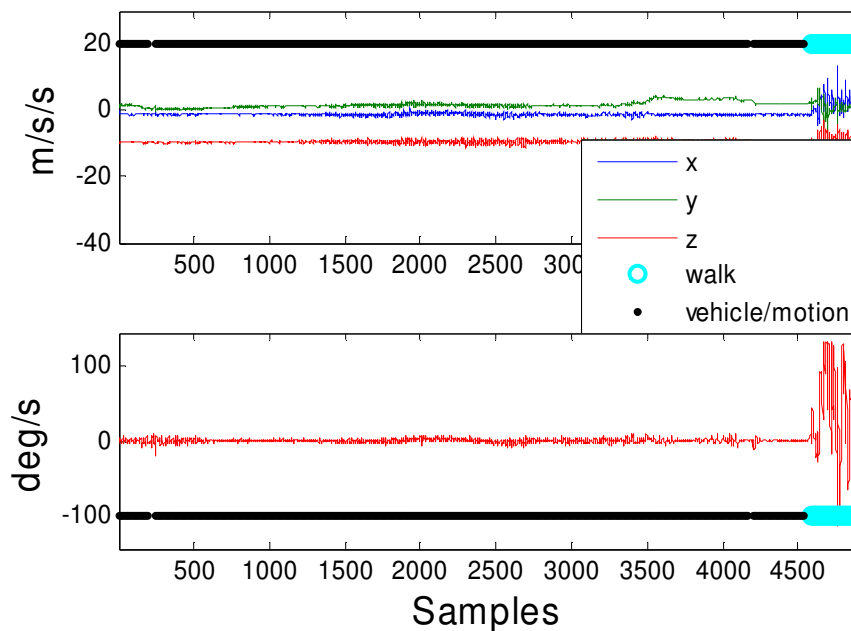


**Figure 7-20. User9 mode of transit detection for LRT data in position 4 using one heading gyro and a tri-axial accelerometer**

### ***7.2.5 Bike Mode Detection***

Another common scenario is when the user wearing the system rides on a bike. It will consist of two different kinds of dynamics. The first set of dynamics can be associated with periods when the user is accelerating, i.e., pedaling, while the second set is smoother and consists of the constant velocity (no pedaling) periods. Both algorithms performed equally well and therefore, only full sensor algorithm results are provided.

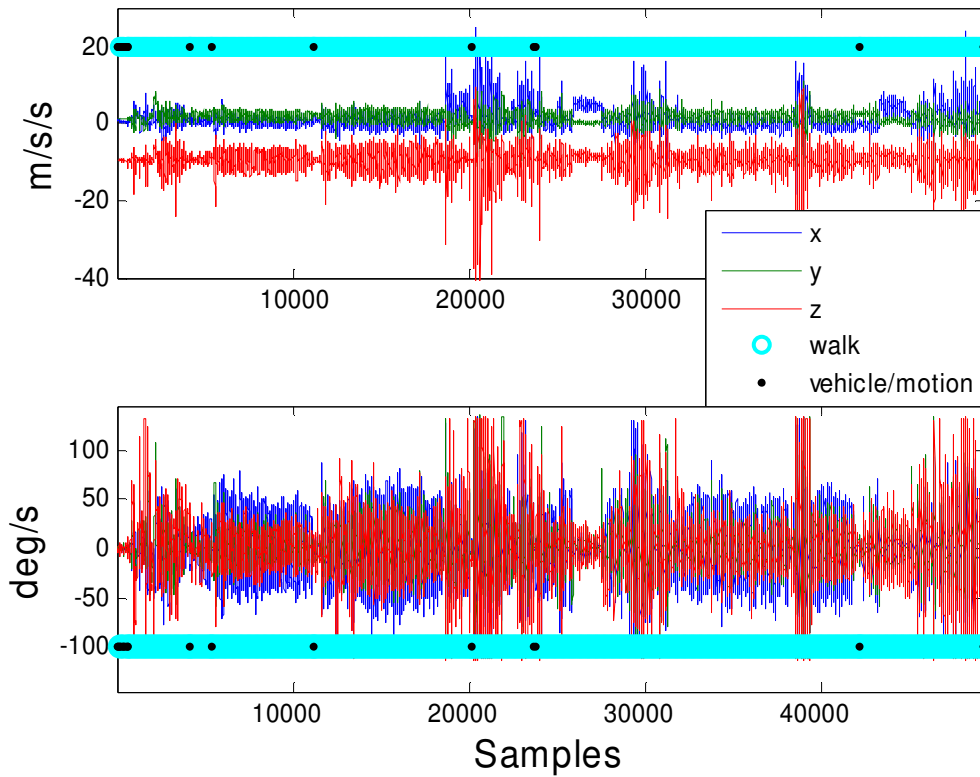


**Figure 7-21. Bike dataset classified by six sensors algorithm**

### 7.2.6 Accuracy Results

As mentioned earlier in the methodology that two different types of accuracies will be measured and discussed for each scenario. The first is absolute accuracy that compares the full sensors algorithm results with the hardware mark at the time of data collection. The best accuracies were noted for the levelled-ground walk scenarios. Both absolute and relative accuracies were higher than 97% as shown in Figure 7-22. The average absolute accuracy for the mixed walk situation was close to 90%, however, the relative accuracy between the two algorithms, was better. For both the LRT and in-vehicle case, the relative accuracies for the partial sensors algorithm was not as good as the previous two

cases showing that the missing information from roll and pitch gyros, actually degrade the results as discussed in detail in Chapter 5.

The relative accuracies improved again for the last two cases in which physical motions were significantly higher than in-vehicle or LRT cases. The absolute and relative accuracies of mixed walk and bike dataset are similar, which can be explained on the basis of different dynamics during various walking routes and bike's pedalling and no-pedalling cases. The best accuracies are observed for the levelled walk scenario in which both absolute and relative accuracies were over 95% for all the volunteers. The absolute accuracies of the mixed walk and the bike cases were both close to 90%. The relative accuracies of LRT and in-vehicle cases are lower than their absolute accuracies showing that the partial sensors detection algorithm is not very effective for lower dynamics.

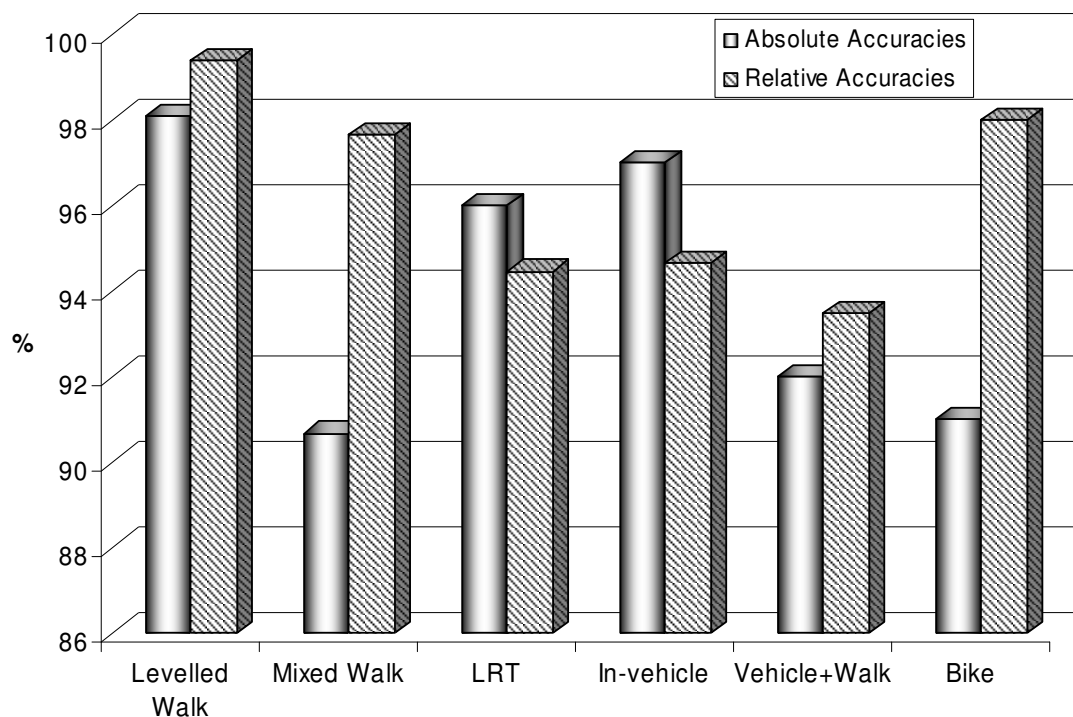


**Figure 7-22. Absolute and relative accuracies**

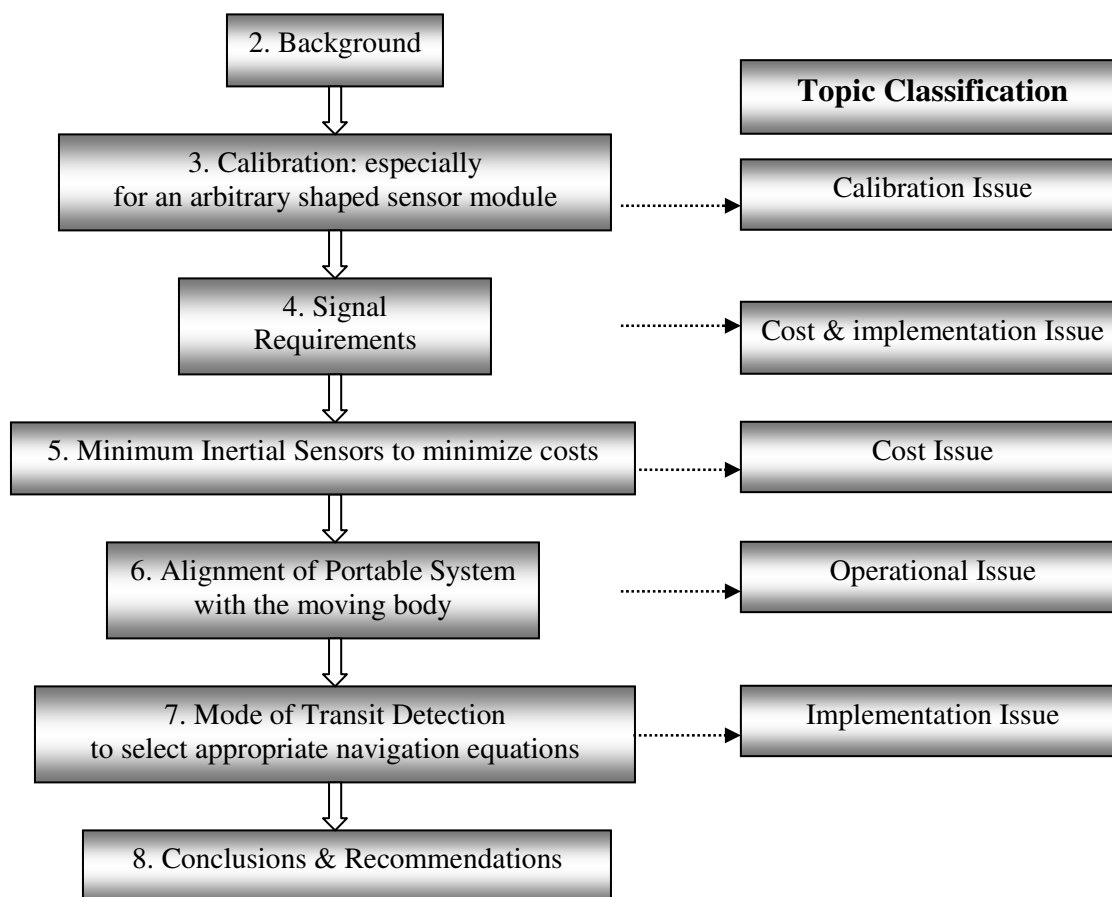
### **7.3 Summary**

This chapter constitutes the results of mode of transit detection algorithm for two different scenarios. The first scenario shows the situation where six sensors are part of navigation module and the second scenario is the case where partial sensors are used in the mode detection. The algorithms performed best when the person took a walk on a levelled ground. The accuracies are similar for mixed walk and bike datasets as the same logic applies for the two scenarios. Similarly, in-vehicle and LRT modes also performed in a comparable fashion. The same algorithm was also tested to detect ZUPTs for in-vehicle navigation mode. The accuracy was improved by changing the weighting scheme for in-vehicle navigation case.

## Chapter Eight: Conclusions and Recommendations

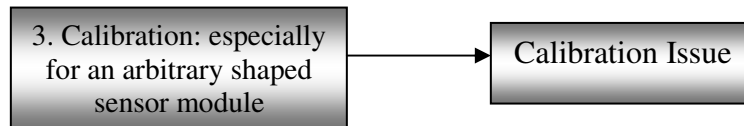
### 8.1 Conclusions

The thesis investigates the design issues related to a completely portable and integrated navigation system. Except for the fact that navigation or mechanization equations are the same as traditional inertial sensor system, a portable system is different in all the other aspects. From calibration to implementation of the navigation equations, the portable system needs special methods to account for the portability and ergonomics. Recall the outline of the thesis provided in Chapter 1.



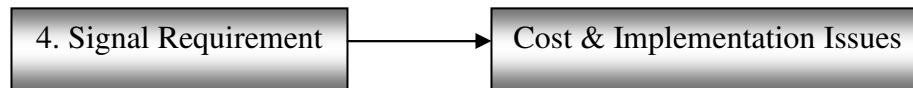


For systematic summary, we will take one block at a time and provide the conclusions for the topic and its issues.



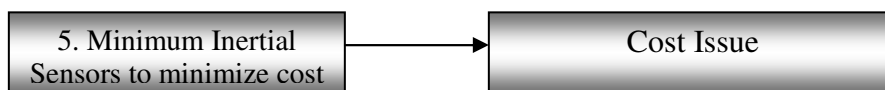
**Chapter 3** dealt with the calibration issues related to a PNS. It was established that manufacturer specifications for the deterministic errors are not sufficient and some sort of calibration scheme is required to produce reasonable results. Next MMPM was developed specifically for MEMS IMU of an arbitrary shape. The improvements include a coarse pre-calibration and the inclusion of gyro scale factor and non-orthogonality estimation by including a rotation reference input from a turntable. The results shown in this chapter clearly indicate that the proposed MMPM developed for MEMS sensors can replace the traditional SPM. The main advantage of the new method is that it uses multiple positions without any special alignment requirements to estimate the sensor bias, scale factors, and non-orthogonalities. This method is less costly as it only needs a single axis turntable and does not require special alignment equipment such as perfect cubes, etc. The orientation of the IMU in different positions is less time consuming since only the approximate positions are required.

The only remaining problem of using this method arises when the accelerometer and gyroscope triads have significant misalignment from each other. This method calibrates both sensors to one unique reference frame, and hence this misalignment between triads cannot be detected and in turn will cause errors during navigation.

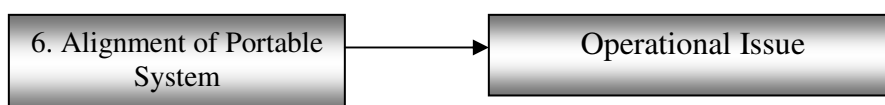


Issues related to signal sampling requirements were explored in **Chapter 4**. A signal sampling simulation program was developed for this chapter. The effects of sampling frequency, bit resolution and time synchronization error on the navigation result were explored in detail in Chapter 4 and the results were compared with a high frequency, high resolution and simultaneously sampled data. The results show that data recorded at a 20 Hz frequency are sufficient if tightly coupled integration is used. In loosely coupled integration, a degradation of about 6% was observed in a high dynamics dataset when a 20 Hz sampling frequency was used.

For tightly coupled integration, even 12 bits resolution did not produce significant degradation in the results. However, high dynamics navigation results in dataset 2 were deteriorated even further when 12 bits were used with a 20 Hz sampling frequency for loosely coupled integration. Time synchronization for low cost sensors is not as essential as signal resolution as depicted by the simulation results. Therefore, timing should not be a high priority when choosing an economical DAQ card for low cost and PNSs. On the other hand, the hardware and software should be able to properly handle the GPS interrupt because a delay caused by an interrupt may significantly reduce the results accuracies. Simulations for two inexpensive DAQ cards were also provided as an example to reduce the cost.

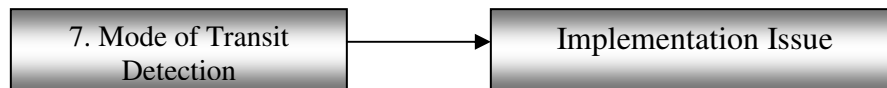


Civilian navigation requires robust, accurate but inexpensive systems. The main focus of **Chapter 5** was to determine the most economical navigation system that should be able to effectively deal with the difficult civilian vehicle navigation environment. Five different sensor configurations ranging from six sensors to only two sensors were studied in detail. As the land vehicle motion is physically constrained, NHC were also applied to improve the accuracy of the results. Full sensors configuration gave the best results with minimum average drift errors but is not cost effective. 1G2A sensors with NHC showed better results than full sensor configuration without NHC.



Another big issue with PNS is alignment with respect to the moving body. For the design process, a complete range of acceptable alignments is required. The results in **Chapter 6** show that a full IMU without any NHC can deal with any kind of alignment error and therefore, if the ease of implementation from a user's perspective is the most important criteria, a full IMU should be the system of choice. Partial IMUs show degradations when roll and pitch angles were not aligned with the vehicle. The azimuth misalignment did not degrade the navigation accuracy for a partial IMU. NHC can improve the navigation accuracy; however, these constraints cannot be applied if the IMU is not properly aligned with the vehicle. A full IMU is very sensitive to the misalignment once NHC is applied. On the contrary, a partial IMU with non-holonomic constraint can tolerate misalignment

of up to 15 degrees, if degradation of 20% is allowed. Considering the overall trade-off between performance, cost, and ease of use, the partial IMU with a non-holonomic constraints offer a promising solution to low-cost navigation.



There are two types of navigation equations for two different modes of transit. Both of these equations have certain advantages when implemented in a typical transit mode. Consequently, it is desirable to use both equations for their respective modes and this starts the issue of detecting the transit mode. The main topic of **Chapter 7** was to develop a software switch for the mode of transit when the user of a PNS is wearing the system on his or her belt. Two different algorithms were discussed which are important from a commercialization perspective. The first algorithm will detect the mode of transit by analyzing six different sensors outputs while the second algorithm utilizes the outputs from a heading gyro and a tri-axial accelerometer. The two algorithms performed exceptionally well for on-foot navigation on a levelled ground. Similar dynamics produced similar results, for example, the results for in-vehicle and LRT datasets were comparable, and the results of bike mode detection were like mixed walk results. For in-vehicle ZUPT detection, it was established that a different output weighting scheme produced better results.

## 8.2 Developed Methods and Programs

Following is a list of methods and programs developed for this thesis.

1. A Matlab based Tightly coupled integration KF for GPS and INS integration

2. A modified multi-position calibration method for the calibration of arbitrary shaped PND (Chapter 3)
3. Signal sampling degradation simulation program (Chapter 4)
4. Add partial sensors computation subroutines to AINS™ (Chapter 5)
5. A program that can simulate a range of misalignments in a well aligned dataset and produce the comparison results with respect to the well aligned dataset. Also made a KF that can estimate the misalignments (Chapter 6)
6. A mode detection program that can detect in-vehicle and on-foot navigation mode of transit (Chapter 7)

### **8.3 Recommendations and Future Work**

The following are the future works that are needed to realize a completely portable system. They are provided in terms of their importance

- 1) Implementation of the most robust DR algorithm for the completion of on-foot navigation. This will include the appropriate changes in the KF states, prediction and update equations.
- 2) Issues related to the data sampling for land vehicle case were discussed in detail with the assumption that on-foot navigation should produce similar or better results. This theory needs to be verified by using different on-foot scenarios. Walking slow and fast, and running are just few cases that will be required from different volunteers for the analysis.
- 3) Next issue that is very important is the alignment requirements for on-foot navigation mode. What kinds of accuracies are required and what are the best

alignment methods? If partial sensors are desired, what will be the error budget that can produce reasonable results are some of the issues that require proper investigation.

- 4) As the most economical system is desired, a simplified KF needs to be developed for the partial sensors.
- 5) This thesis is the part of the work towards development of a completely portable and integrated navigation system for robust positioning ([El-Sheimy, 2007](#)). Till now all the developments and studies are in post-processing mode. For the final prototype, a real time system will be developed and the algorithms will be optimized for the real time applications.
- 6) Last but not least, the real time portable system needs to be tested thoroughly for a variety of scenarios. This will be another big step towards the realization of this portable system.

## References

Alpine Electronics of America, Inc., <http://www.alpine-usa.com/US-en/>, visited November 3<sup>rd</sup>, 2008

Bancroft, J, Lachapelle, G., Cannon, ME, Petovello, M, “Twin IMU-HSGPS Integration for Pedestrian Navigation”, ION GNSS, September 16-19<sup>th</sup>, 2008, Savannah, Georgia

Barak, P., “Magic Numbers in Design of Suspension for Passenger Cars”, SAE Technical Chapters Series, n. 878, pp.53-88, July 1991.

Bossler, JD; Goad, CC and Bender, PL; “Using the Global Positioning System (GPS) for geodetic positioning”, Volume 54, Number 4, December, 1980, pp. 553-563

Bouten, CVC., Koekkoek, KTM., Verduin, M., Kodde, R. and Janssen, J.D., "A Triaxial Accelerometer and Portable Data Processing Unit for the Assessment of Daily Physical Activity," IEEE Transactions on Biomedical Engineering, vol. 44, pp. 136 - 147, 1997.

Business Network,

[http://findarticles.com/p/articles/mi\\_m0EIN/is\\_2008\\_June\\_25/ai\\_n27507984](http://findarticles.com/p/articles/mi_m0EIN/is_2008_June_25/ai_n27507984), visited October 31<sup>st</sup>, 2008

Chatfield AB, 1997. Fundamentals of High Accuracy Inertial Navigation. American Institute of Aeronautics and Astronautics, Inc.

Clarion, [http://www.clarion.com/jp/en/newsttopics/index\\_2008/080924\\_02/index.html](http://www.clarion.com/jp/en/newsttopics/index_2008/080924_02/index.html),  
visited November 2008

El-Sheimy, N. (2006), ENGO 623 Lecture Notes: Inertial Techniques and INS/DGPS  
Integration, Department of Geomatics Engineering, The University of Calgary, Winter  
2006.

El-Sheimy, N., Wright, B., Syed, Z.F., Hunter, A., Goodall, C., “Portable Navigation  
System”, Patent (038231-009 RO Prov) filed July 18, 2007 (2007)

Engadget, [http://www.engadget.com/2007/05/09/panasonic-launches-its-first-us-in-car-  
navigation-unit/](http://www.engadget.com/2007/05/09/panasonic-launches-its-first-us-in-car-navigation-unit/), visited November 2008

Foxlin E, 2002, InterSense, Inc. “Extended draft version of Chapter 8 in Handbook of  
Virtual Environment Technology”, Kay Stanney, Editor, Lawrence Erlbaum Associates

Foxlin, E., 2005, “Pedestrian tracking with shoe-mounted inertial sensors”, Computer  
Graphics and Applications, IEEE, Volume: 25, Issue: 6, pp. 38-46

Garmin. We'll Take You There.™, visited on October 3, 2007, Available:  
<http://www.garmin.com/garmin/cms/site/us>

Gelb, A, “Applied Optimal Estimation”, The M.I.T. Press, 1974, pp. 182-188

GlobalWave, GPS Asset Tracking, <http://www.globalwave.com/gps-asset-tracking.asp>,  
visited October 31<sup>st</sup>, 2008



Godha, S and Cannon, ME; “GPS/MEMS INS integrated system for navigation in urban areas”, Volume 11, Number 3 / July, 2007, pp. 193-203

GPS Business News, visited Oct 1, 2008

<http://www.gpsbusinessnews.com/index.php?action=article&numero=205>,

Grejner-Brzezinska, D.A., Toth, C.K., Moafipoor, S. (2007). Pedestrian Tracking and Navigation Using Adaptive Knowledge System Based on Neural Networks and Fuzzy Logic. Journal of Applied Geodesy. Vol. 1, No. 3, pp. 111-123

Grewal, MS; Weill, LR; Andrews, AP; “Global Positioning Systems, Inertial Navigation, and Integration”, John Wiley and Sons Inc., 2001, USA

Hide, C; Moore, T., Hill, C; and Park, D; “Low Cost, High Accuracy Positioning In Urban Environments”, THE JOURNAL OF NAVIGATION (2006), 59, pp. 365–379.

Hide, C; Moore, T; Smith, M; “Adaptive Kalman filtering for low cost GPS/IMU”; Journal of navigation 56 (1), January 2003, pp.143–152

Honeywell International Inc., DRM 4000, visited December 8<sup>th</sup>, 2008

<http://www.ssec.honeywell.com/magnetic/datasheets/DRM4000.pdf>

Hou H, 2004, “Modeling Inertial Sensors Errors Using Allan Variance”, UCGE Report 20201, Department of Geomatics Engineering, The University of Calgary, Alberta, Canada.

InvenSense Inc., <http://www.invensense.com/news/060516.html>, visited September 6, 2008

Jirawimut, R., Ptasinski, P., Garaj, V., Cecelja, F. and Balachandran, W., "A Method for Dead Reckoning Parameter Correction in Pedestrian Navigation Systems," presented at 18th IEEE Instrumentation and Measurement Conference, 2001, pp. 209 - 215.

Kappi, J, Syrjarinne, J, and Saarinen, J, “ MEMS-IMU Based Pedestrian Navigator for Handheld Devices”, Proceedings of the 14th International Technical Meeting of the Satellite Division of the Institute of Navigation ION GPS 2001, September 11 - 14, 2001, pp. 1369 - 1373

Kasameyer, PW., Hutchings, L., Ellis, MF., Gross, R., "MEMS-based INS Tracking of Personnel in a GPS-denied Environment", ION GNSS 18th International Technical Meeting of the Satellite Division, 13-16 September 2006, Long Beach, CA

Kim, J, W., Hwang, D, H., & Lee, S, J., (2006) A Deeply Coupled GPS/INS Integrated Kalman Filter Design Using a Linearized Correlator Output. PLANS 2006, California, 25-27 April, pp. 300-305

Knight, DT; “Rapid development of tightly-coupled GPS/INS systems”, Aerospace and Electronic Systems Magazine, IEEE, Vol. 12, Issue 2, February 1997, pp. 14-18.

Krakiwsky E J, 1990. The Method of Least Squares: A Synthesis of Advances, UCGE Report 10003, Department of Geomatics Engineering, The University of Calgary, Alberta, Canada.

Kwakkel, SP., Lachapelle G., and Cannon, M.E., "GNSS Aided In Situ Human Kinematics Studies During Running", ION GNSS, September 16-19, 2008, Savannah, Georgia

Ladetto, Q., "On Foot Navigation: Continuous Step Calibration Using Both Complementary Recursive Prediction and Adaptive Kalman Filtering," in presented at ION GPS 2000, Salt Lake City, Utah, 2000.

Lee, S.-W., and Mase, K., "Recognition of Walking Behaviors for Pedestrian Navigation," presented at Proceedings of 2001 IEEE Conference on Control Applications (CCA01), Mexico City, Mexico, 2001.

Levi, R.W., and Judd, T., "Dead Reckoning Navigational System using Accelerometers to Measure Foot Impacts.," vol. 5,583,776. United States, 1996.

MiTAC Intl, <http://www.mio.com/gps-navigation-products-a702-overview.htm>, visited October 1st, 2008

Mitra, SK; and Kaiser, JF; "Handbook for digital signal processing", John Wiley and Sons, New York, 1993

National Instruments, [www.ni.com](http://www.ni.com), visited November 27, 2007.

Navman In-Car & Personal Navigation, visited on October 3, 2007, Available: [http://www.navman.com/Navman/templates/BUHomepage\\_\\_\\_\\_6313.aspx](http://www.navman.com/Navman/templates/BUHomepage____6313.aspx)

Niu X, 2002. "Micromachined Attitude Measurement Unit with Application in Satellite TV Antenna Stabilization", PhD dissertation, Dept. of Precision Instruments and Machinery, Tsinghua University, Oct 2002.

Niu X, and El-Sheimy N, 2005. "The Development of a Low-cost MEMS IMU/GPS Navigation System for Land Vehicles Using Auxiliary Velocity Updates in the Body Frame ". Proceedings of ION GNSS 2005. September 13-16, Long Beach, CA, USA.

Niu, X, and Han, S, "Improving the Performance of Portable Navigation Devices by Using Partial IMU Based GPS/INS Integration Technology", ION GNSS 2008, Savannah Georgia

Noureldin, A; Sharaf, R; Osman, A and El-Sheimy, N; "A neuro-wavelet for multisensor system integration for vehicular navigation," Journal of measurement science and technology, Journal of Measurement Science and Technology, V15(2), pp. 404-412, London, UK, February 2004.

Ojeda, L and Borenstein, J, "Personal Dead-reckoning System for GPS-denied Environments", Proceedings of the 2007 IEEE, International Workshop on Safety, Security and Rescue Robotics, Rome, Italy, September 2007,

Peng, Y.K.; Golnaraghi, M.F., "A Vector-Based Gyro-Free Inertial Navigation System by Integrating Existing Accelerometer Network in a Passenger Vehicle" IEEE Position Location and Navigation Symposium 2004, Monterey, CA, April 26 to 29, 2004, pp. 234-

Schwarz, K.P. and Wei, M.: "INS/GPS Integration for Geodetic Applications". Lecture Notes ENGO623, Department of Geomatics Engineering, The University of Calgary, Canada, 2000.

Shin E-H, and El-Sheimy N, 2002. A new calibration method for strapdown inertial navigation systems. *Zeitschrift für Vermessungswesen*, 127(1), 1–10.

Shin, Eun-Hwan, 2001, "Accuracy Improvement of Low Cost INS/GPS for Land Application", M.Sc. thesis, Dec. 2001, Department of Geomatics Engineering, the University of Calgary, UCGE Report No. 20156.

Shin, S.H., and Hong, H.S., "MEMS Based Personal Navigator Equipped on User's Body," presented at ION GNSS 18th International Technical Meeting of the Satellite Division, Long Beach, CA, 2005, pp. 1998 - 2002

Sony: Personal navigation : UK, visited on Oct 3, 2007, Available: [http://www.sony.co.uk/view/ShowProductCategory.action?site=odw\\_en\\_GB&category=ICN+Personal+navigation](http://www.sony.co.uk/view/ShowProductCategory.action?site=odw_en_GB&category=ICN+Personal+navigation)

Syed, Z.F., Aggarwal, P, Goodall, C, Niu, X and El-Sheimy, N., "A new multi-position calibration method for MEMS inertial navigation systems", *Measurement Science and Technology* 18(2007-a) 1897-1907

Syed, Z., Aggarwal, P., Niu, X., El-Sheimy, N., "Economical and Robust Inertial Sensor Configuration for a Portable Navigation System" ION GNSS 2007, Fort Worth Texas, September 24-25, 2007-c.

Syed, Z.F., Aggarwal, P, Niu, X and El-Sheimy, N., "Civilian Vehicle Navigation: Required Alignment of the Inertial Sensors for Acceptable Navigation Accuracies", IEEE Transactions on Vehicular Technology, Vol. 57, No. 6, Nov 2008

Titterton, D.H., Weston, J.L., (1997) "Strapdown inertial navigation technology", Peter Peregrinus, London

TomTom, portable GPS car navigation systems, visited on October 3, 2007 Available: [www.tomtom.com](http://www.tomtom.com)

TomTom Go 920T In Depth Review, <http://www.pocketgpsworld.com/tomtom-go-920t-a2840.php>, visited October 31<sup>st</sup>, 2008

Wagenaar, R.C., and Beek, W.J., "Hemiplegic Gait: A Kinematic Analysis using Walking Speed as a Basis," Journal of Biomechanics, vol. 25, pp. 1007 - 1015, 1992.

Walchko, K., Nechyba, M., Schwartz, E., and Arroyo, A., "Embedded Low Cost Inertial Navigation System," Florida Conference on Recent Advances in Robotics, FAU, Dania Beach, FL, May 8-9, 2003.

Wang, X., and Shen, G., "A fast and accurate initial alignment method for strapdown inertial navigation system on stationary base", Journal of Control Theory and Applications, Vol (3), Number 2, 145-149







Wendel, J; Trommer, GF.; "Tightly coupled GPS/INS integration for missile applications", Aerospace Science and Technology, Vol. 8, Issue 7, October 2004, pp. 627-634

Yuchnovicz D, Burgess M, and Hammers W, 1999. An assessment of technical and production risks of candidate low-cost attitude/heading reference systems (AHRS).









NASA CR-1999-209096

## Appendix A

**Table 0-1: Example of available in-vehicle navigation systems**

Manufacturer	Product	Sensors		Picture
		GPS	Accel/Gyro	
Tom Tom	TomTom GO 920 T	X	x/x	
LG	LN730	X		
Navigon	2120 GPS Navigation System	X		
Garmin	Nuvi 760	X		
Sony	Nav u	X	x	
Garmin	GPSMAP® 5215	X		



Magellan	Maestro 4250	X		
Pharos	Pharos Drive GPS 250	X		
Cobra	GPSM 5000	X		
Fine Digital	FineDrive 350	X		
HP	Business iPaq 310 Travel Companion	X		
JVC	EXAD eAvinu KV-PX9SN	X		
Navman	Navman iCN 550	X		
Nokia	Nokia 330 Auto Navigation	X		

## **Appendix B**

Some preliminary results of DR implementation are discussed in this section. The first step is denoising of the accelerometer data and four different denoising methods were used. Next issue is to implement an appropriate step detection algorithm on the denoised accelerometer data. Two different methods for step detection were also implemented.

### **Denoising of the Data**

Five different denoising methods were used on the accelerometer data and the results are provided in Figure 0-1. The red line shows the filtered results and the blue line is the original dataset. The Butterworth, Moving average and elliptical filter provided similar results. In this case, the noise has been reduced but the actual data kinematics is preserved and therefore, any of these filters can be used. In this study an elliptical filter was used but a second order Butterworth filter can also be implemented. The wavelet filter is following the original waveform which indicates that level 2 decomposition of the data is not sufficient and a higher level decomposition is required. The Savitzky Golay filter on the other hand removes most of the signal dynamics and therefore cannot be used for DR.

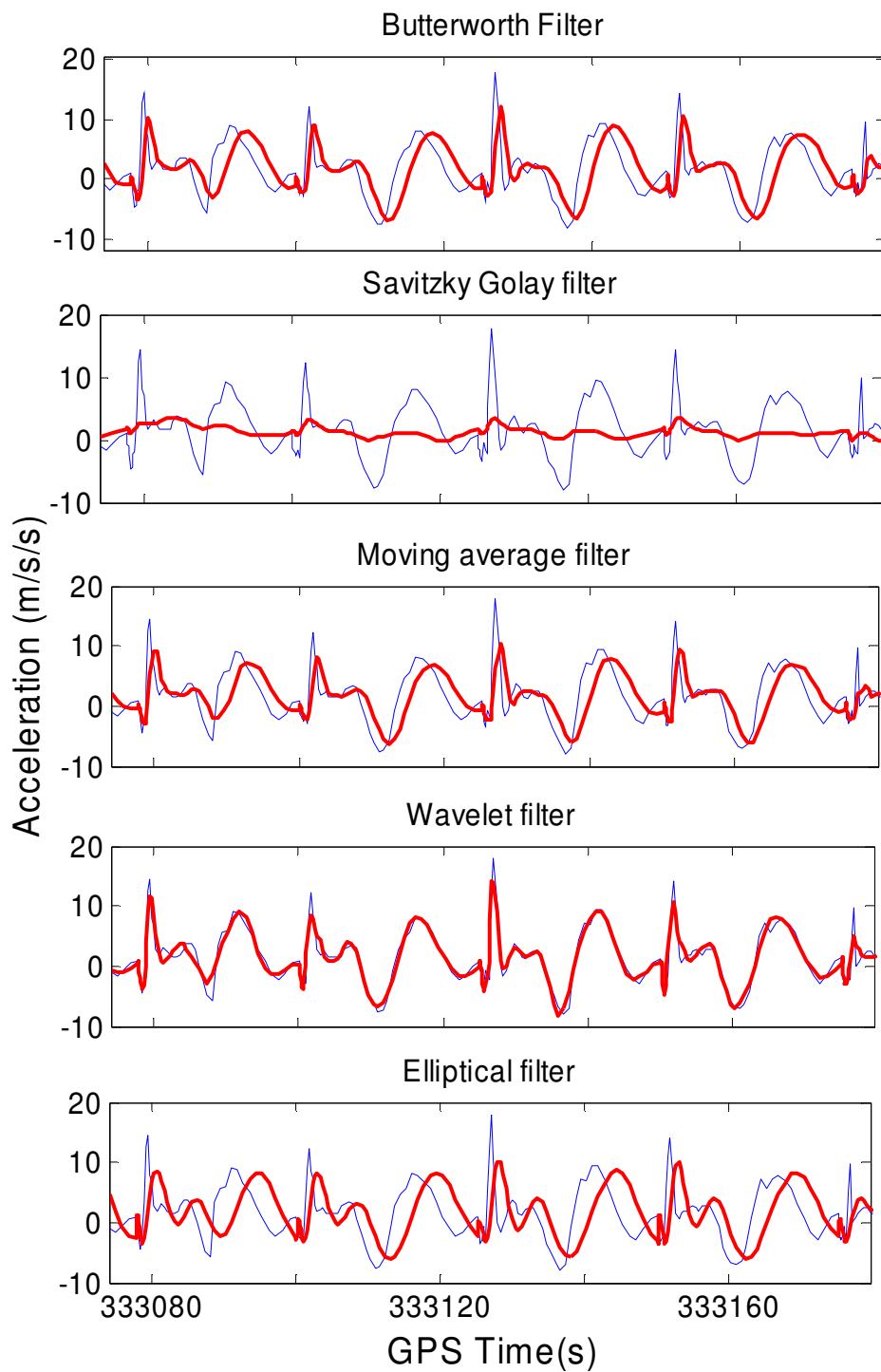


**Figure 0-1: Denoising results**

## Step Detection

Following are the two methods that were used to detect the number of steps in the dataset. There are other methods such as Fourier transform and pattern analysis that may be more useful and robust for this application. However, the search for a good DR algorithm is still ongoing for the PND.

### *Peak Identification via Differencing and Thresholds*

In this method, forward and downward accelerometer signals are used for the step detection. The two peaks are shifted in time but follow each other for every real step, i.e. each step (downward, or  $z$  accelerometer peak) will be followed by the forward acceleration ( $y$  accelerometer peak). After signal pre-processing, the two accelerometer signals were added together, and then the peaks were determined via differencing consecutive data points and utilizing a fixed absolute threshold of 0.2 times the gravity value. The threshold needs calibration as walking styles differ from person to person ([Ladetto, 2000](#)). A window size proportional to the data frequency was chosen to produce the results shown in Figure 0-2 as blue circles. There were total 200 steps but the algorithm detected 191 steps for this typical dataset.

### *Absolute Value, Peak to Peak Time and Correlation*

This algorithm for peak detection is provided in ([Lee and Mase, 2001](#)). A peak is considered if the following three criteria are met within the sliding window.

- 1) The absolute average value for the forward and downward peaks should be greater than 1.5 times the gravity.

- 2) The time between the two consecutive steps is more than a minimum threshold value (0.3s).
- 3) The correlation within the down accelerometer data points for one second data should be more than a pre-defined threshold value of 0.8. This is to ensure that only steps are detected and not some other sudden body movement.

The algorithm detected 199 steps and shown as black dots in Figure 0-2.

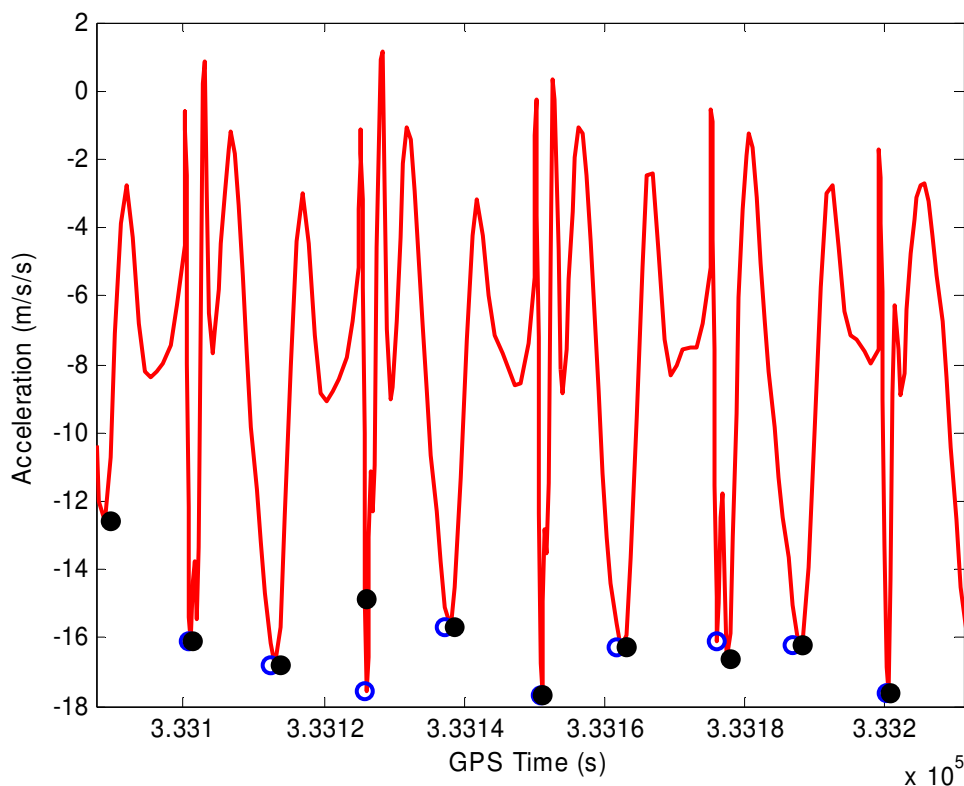


**Figure 0-2: Step Detection Results**

### **Comparison of DR Results with GPS Positions**

Using the step detection method by implementing “absolute value, peak to peak time and correlation” method along with the initial heading estimates as defined, a pure DR was

performed for the data set. The initial results are compared with the GPS only results. A KF is required to update the DR results similar to the one defined in section 2.5. The error states should include the sensor errors for magnetometer but the sensor errors for the accelerometer can be removed as they are not important. A constant step length was used but this is clearly not sufficient as shown from the dataset.

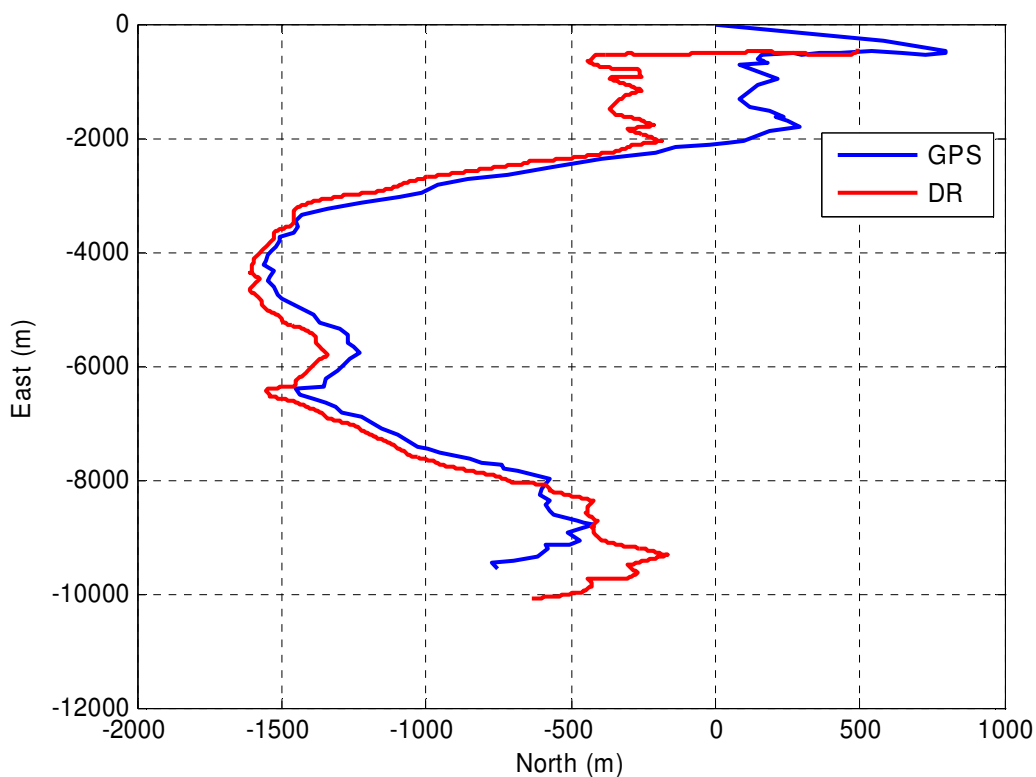


**Figure 0-3: Initial Dead Reckoning Results**